Washington University in St. Louis

What presolar grains tell us about stellar nucleosynthesis

Ernst Zinner
Washington University
St. Louis, MO

WE-Heraeus Summer School on Nuclear Astrophysics in the Cosmos

Our Stellar Origins: Some History

Observation of regularities in the abundance of the chemical elements in the Solar System

Harkins W. D. (1917) Am. Chem. Soc. 39, 856

Russell H. N. (1929) *Ap. J.* 70,11

Suess H. E. and Urey H. C. (1956). *Rev. Mod. Phys.* 28, 53-74.

Cameron A. G. W. (1973) *Space Sci. Rev.* 15, 121-146.

Anders E. and Ebihara M. (1982) *Geochim. Cosmochim. Acta* 46, 2363-2380.

Anders E. and Grevesse N. (1989) *Geochim. Cosmochim. Acta* **53**, 197-214.

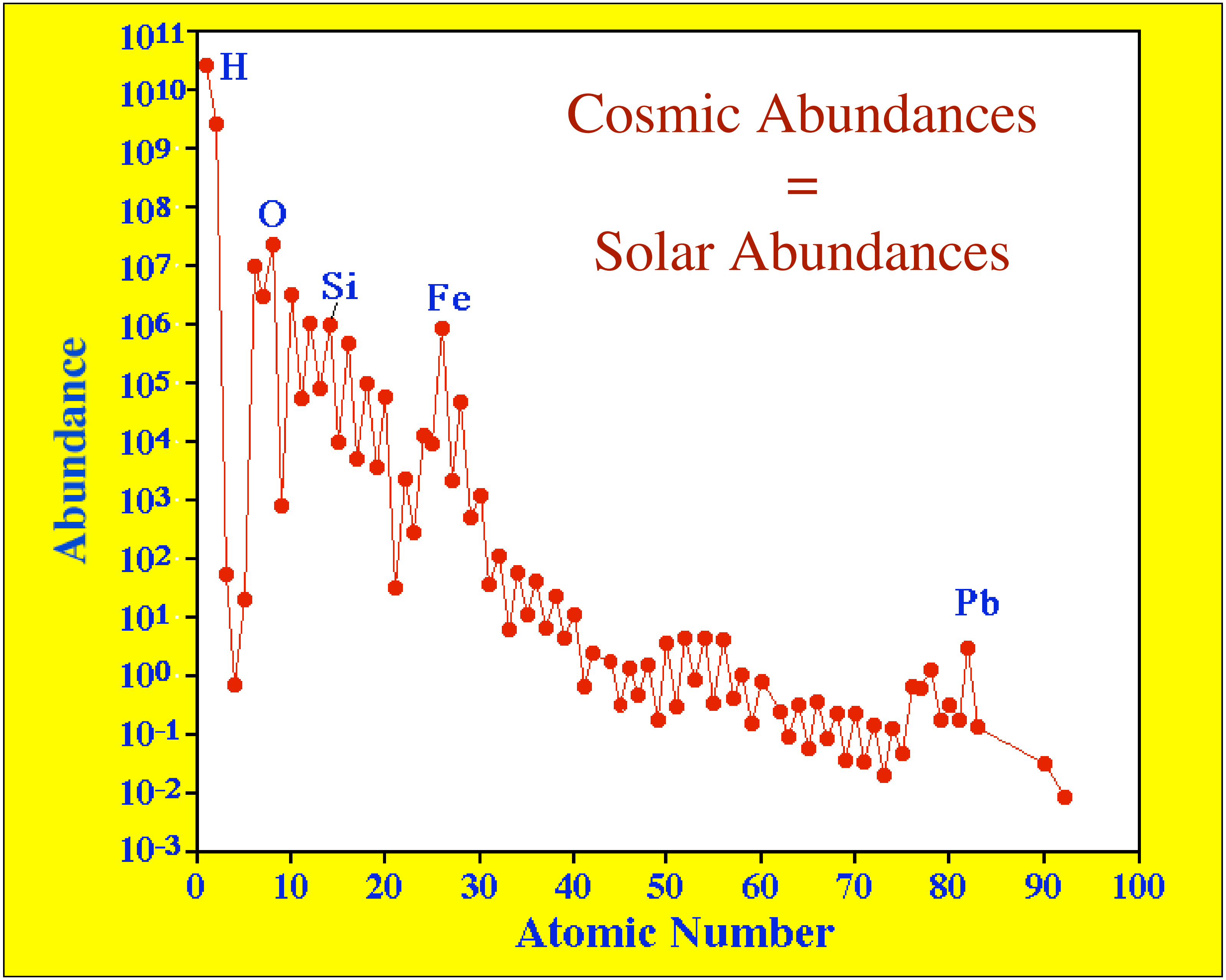

Abundance patterns reflect nuclear properties

Production of the Elements

Bethe H. A. (1939) No elements heavier than ^4He can be built up in ordinary stars.

Hoyle F. (1946, 1954) Stellar production of ^{12}C in Red Giant cores. Speculates on stellar synthesis of elements up to Fe.

Alpher R., Bethe H. A & Gamow G.- $\alpha\beta\gamma$ (1948) Nucleosynthesis in the early universe (Big Bang NS).

Fermi E. & Turkevich T. (1950) Only elements up to Li can be synthesized in the early universe.

Merrill P. W. (1952) Detection of unstable Tc in the spectra from S stars is evidence for stellar nucleosynthesis.

Burbidge G. & M., Fowler W. & Hoyle F. B^2FH (1957) and Cameron (1957) propose 8 processes in stars to produce the elements.

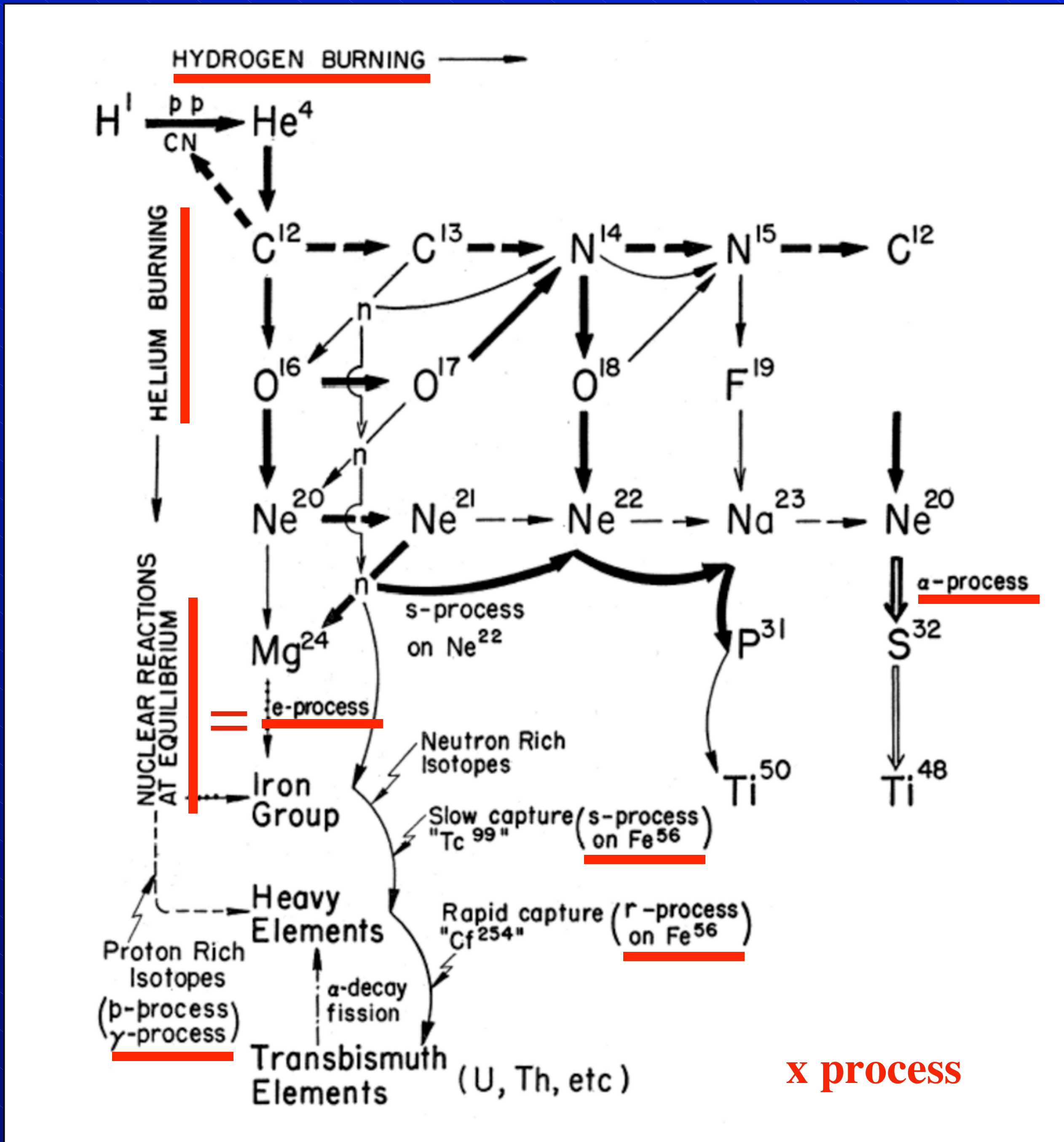

B^{2}FH proposed 8 different nucleosynthetic processes.

What stars produce and eject elements into the interstellar medium?

- Asymptotic Giant Branch (AGB) stars
- Type II (core-collapse) Supernovae

What is an AGB star?

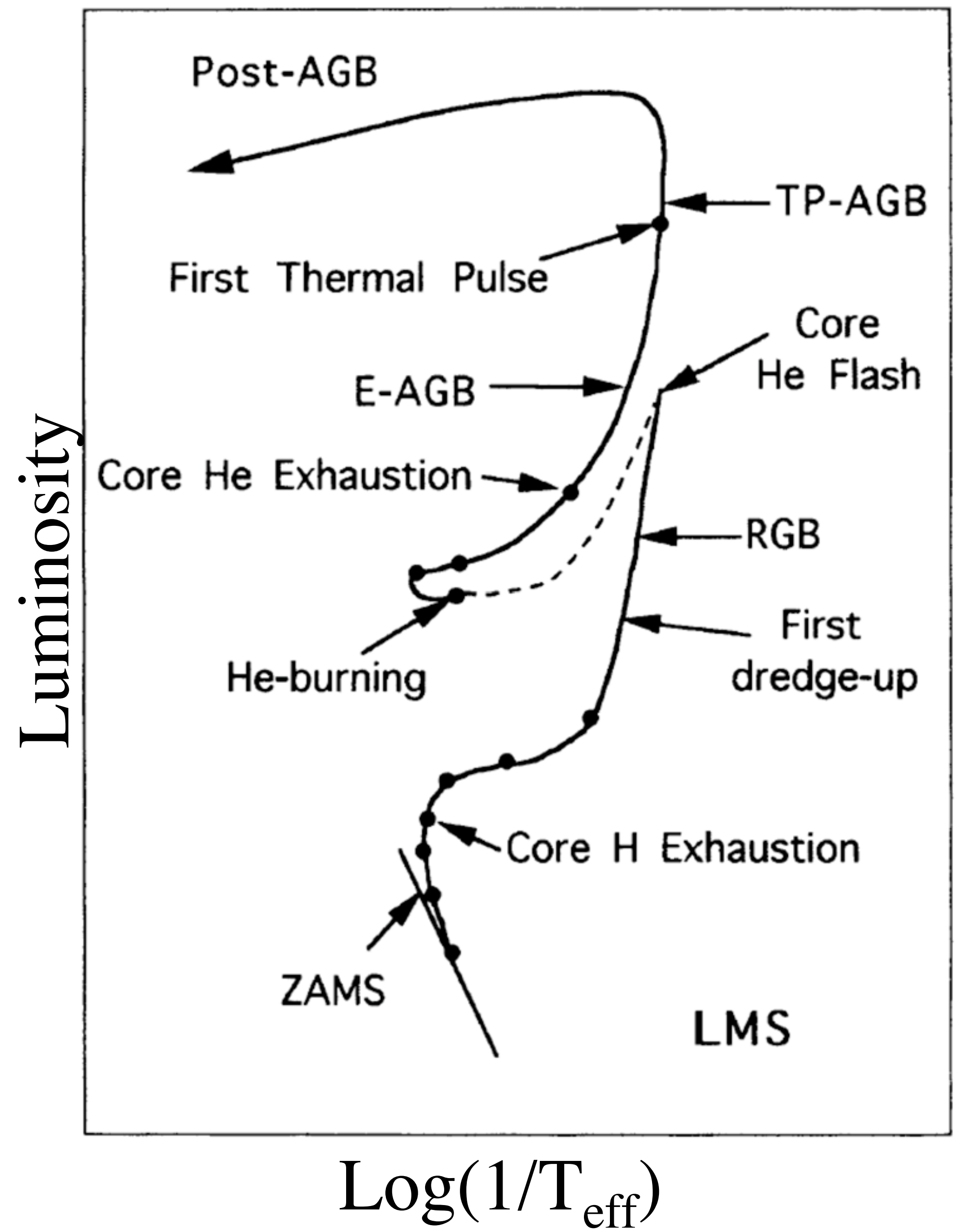

Busso et al., 1999

Evolution of a $1M_{\odot}$ star in the Hertzsprung-Russell diagram.

Schematic Structure of an AGB star

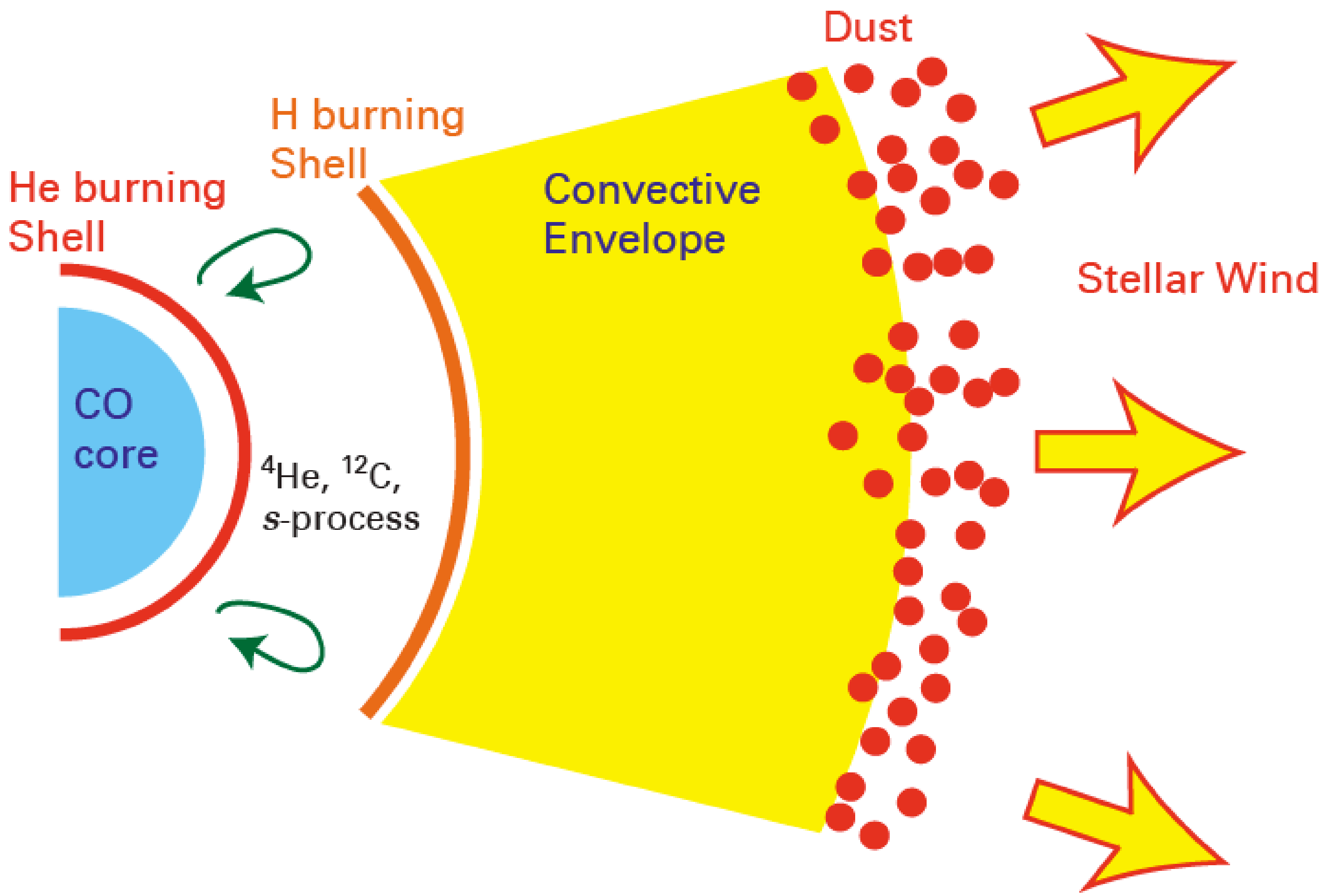

Cartoon by Larry Nittler

Planetary Nebulae

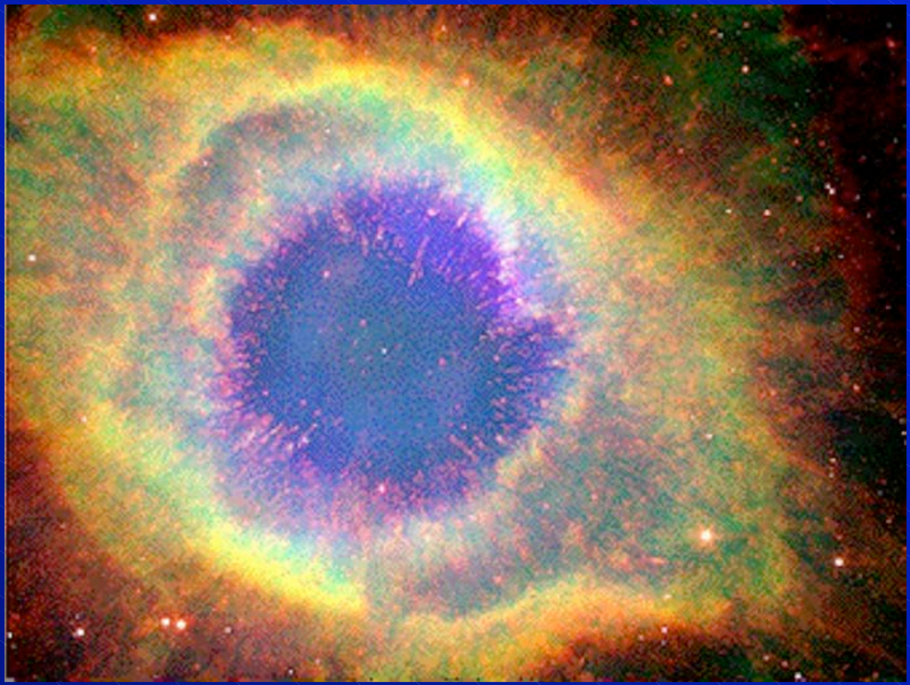

Helix Nebula

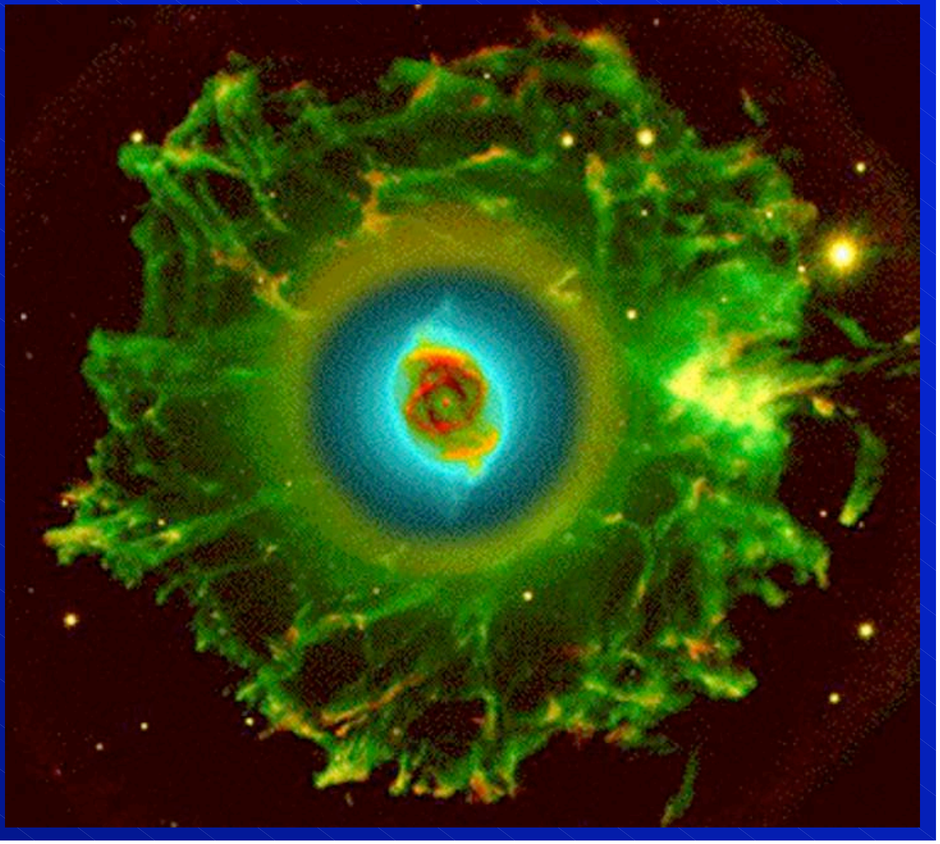

Cat Eye Nebula

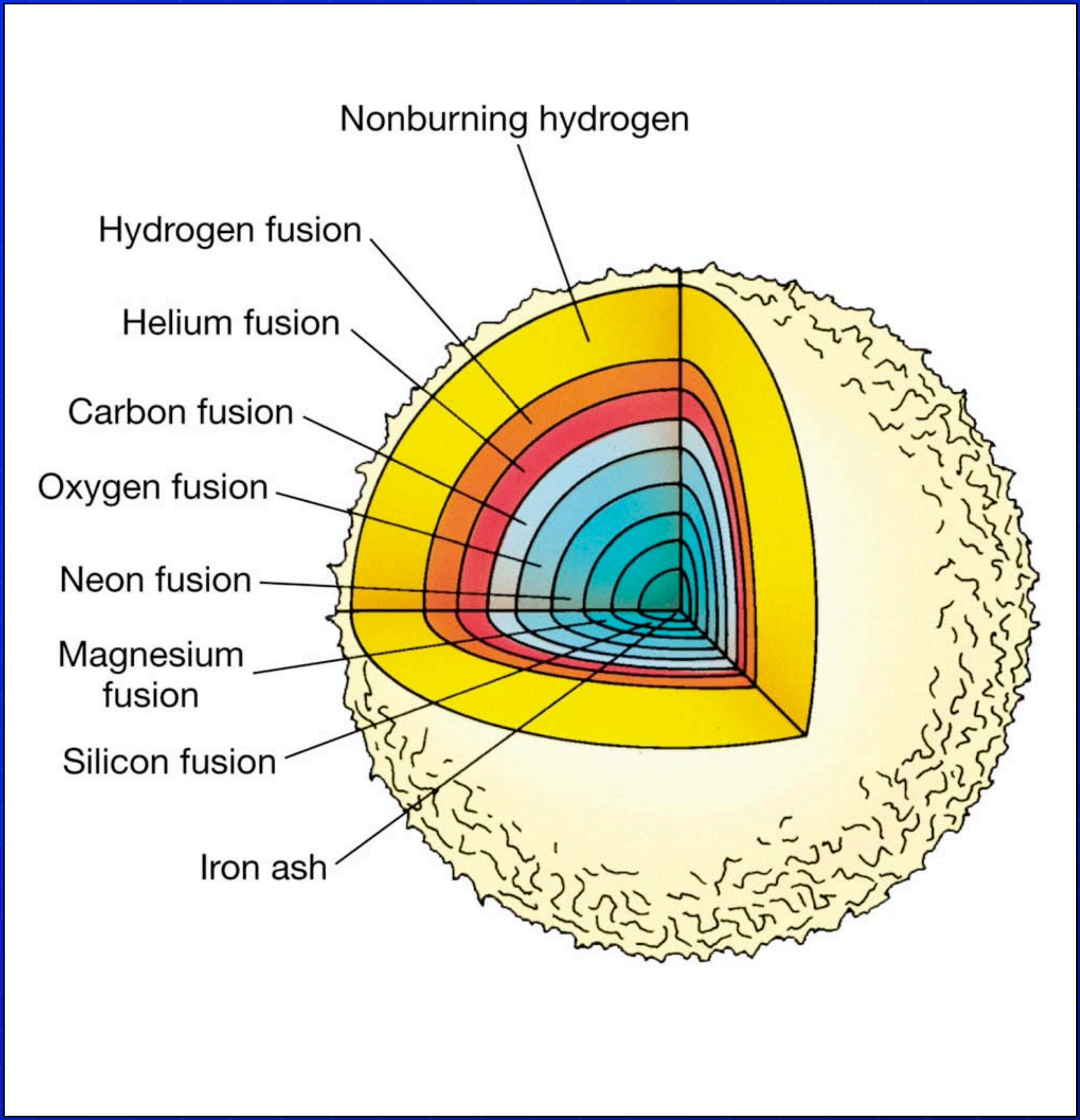

Structure of a massive star (mass > 10 $M_{\odot}$) before explosion as a supernova.

Supernova Remnants

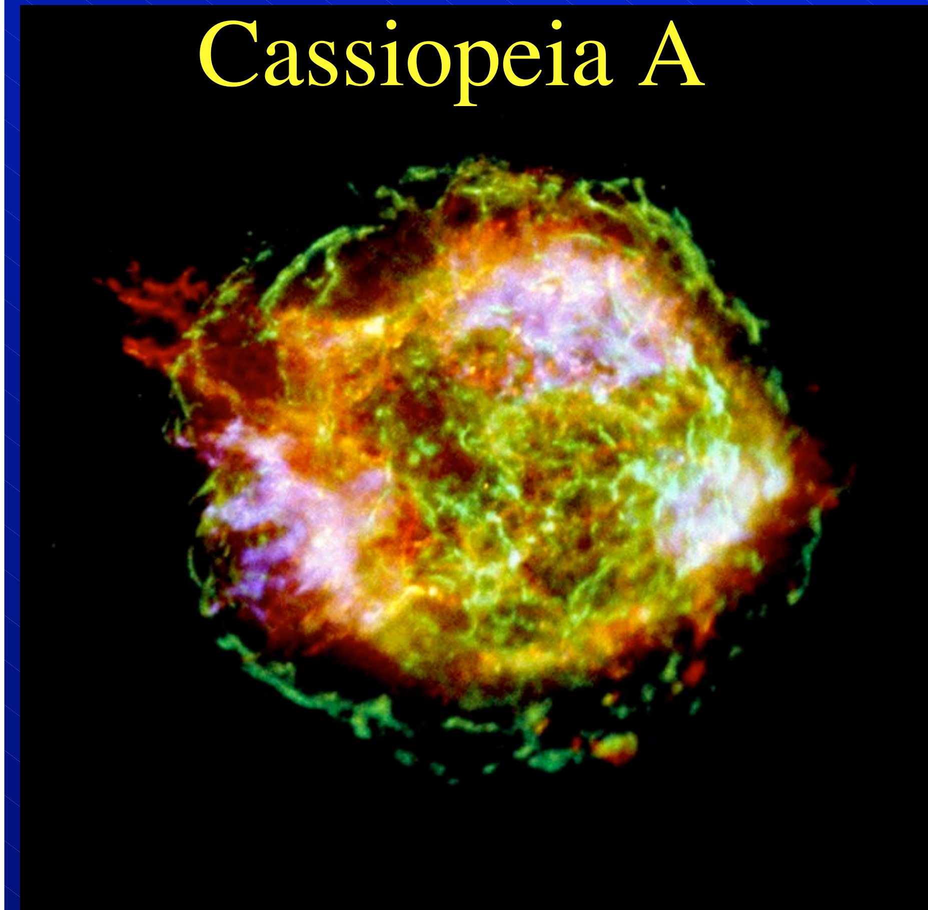

1680
3.4 kpc

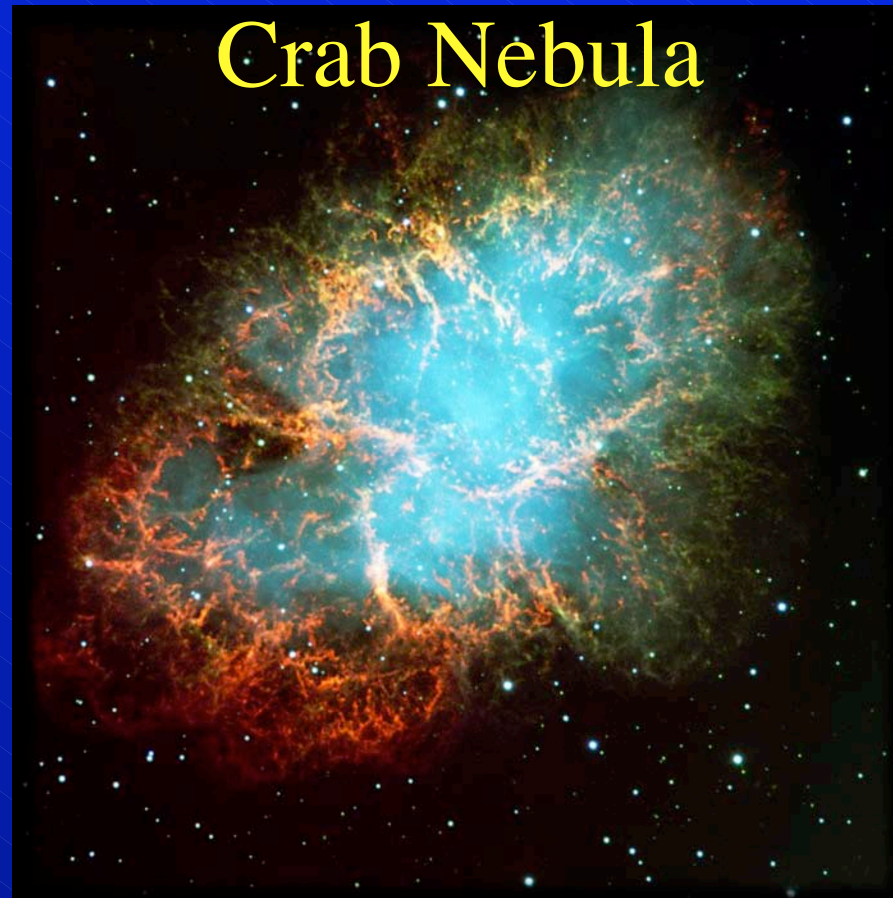

1054
2 kpc

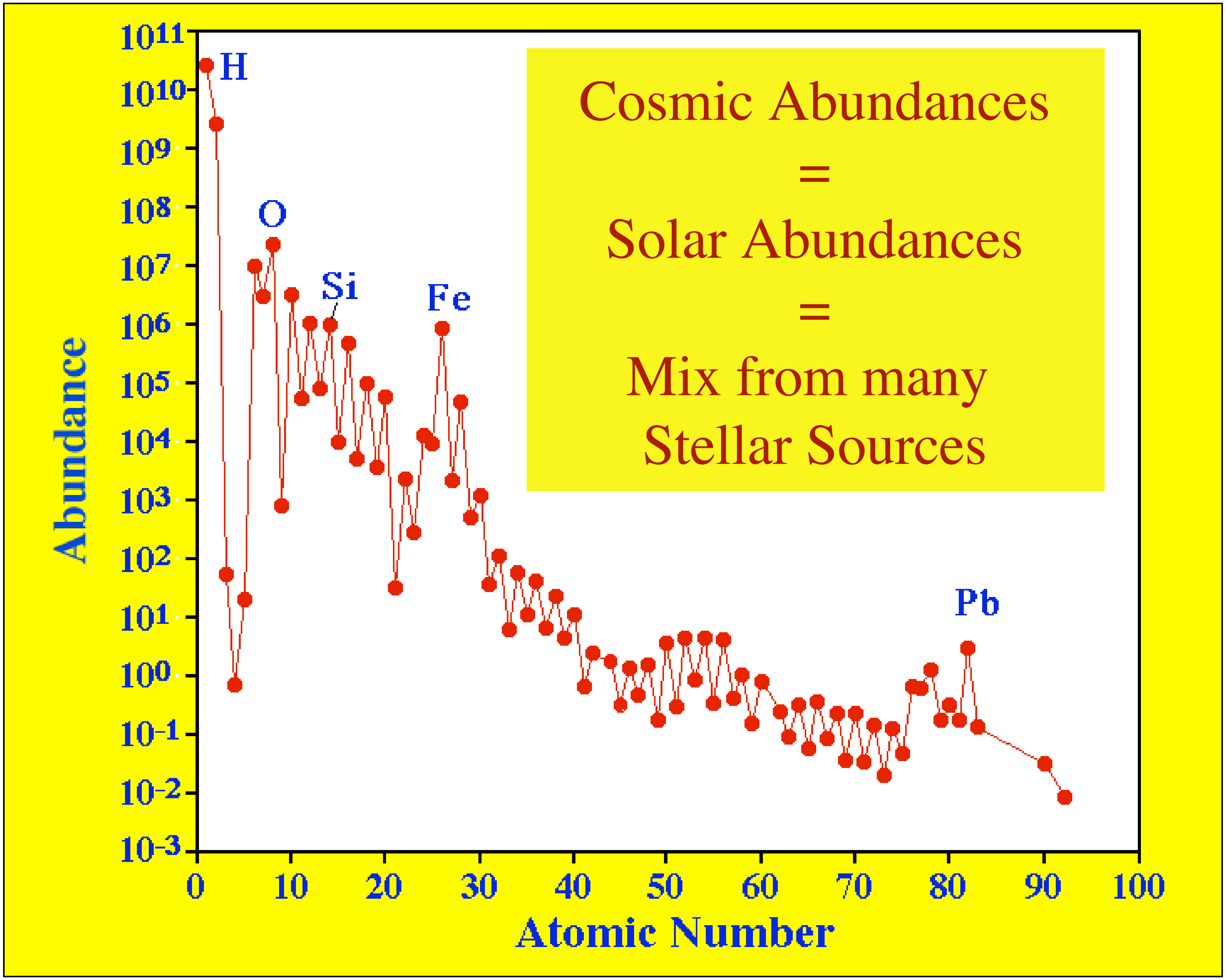

Cosmic Abundances
=
Solar Abundances
=
Mix from many
Stellar Sources
Abundance
Atomic Number
H
O
Si
Fe
Pb
10^{11}
10^{10}
10^{9}
10^{8}
10^{7}
10^{6}
10^{5}
10^{4}
10^{3}
10^{2}
10^{1}
10^{0}
10^{-1}
10^{-2}
10^{-3}
0
10
20
30
40
50
60
70
80
90
100

Data for checking nucleosynthesis theory

Cosmic abundances of the elements

An average of many stellar sources

Astronomical observations

Limited to certain stars. Isotopic data only for few elements

Stardust from primitive meteorites

The Allende meteorite, 4.6 Gyrs old, contains stardust

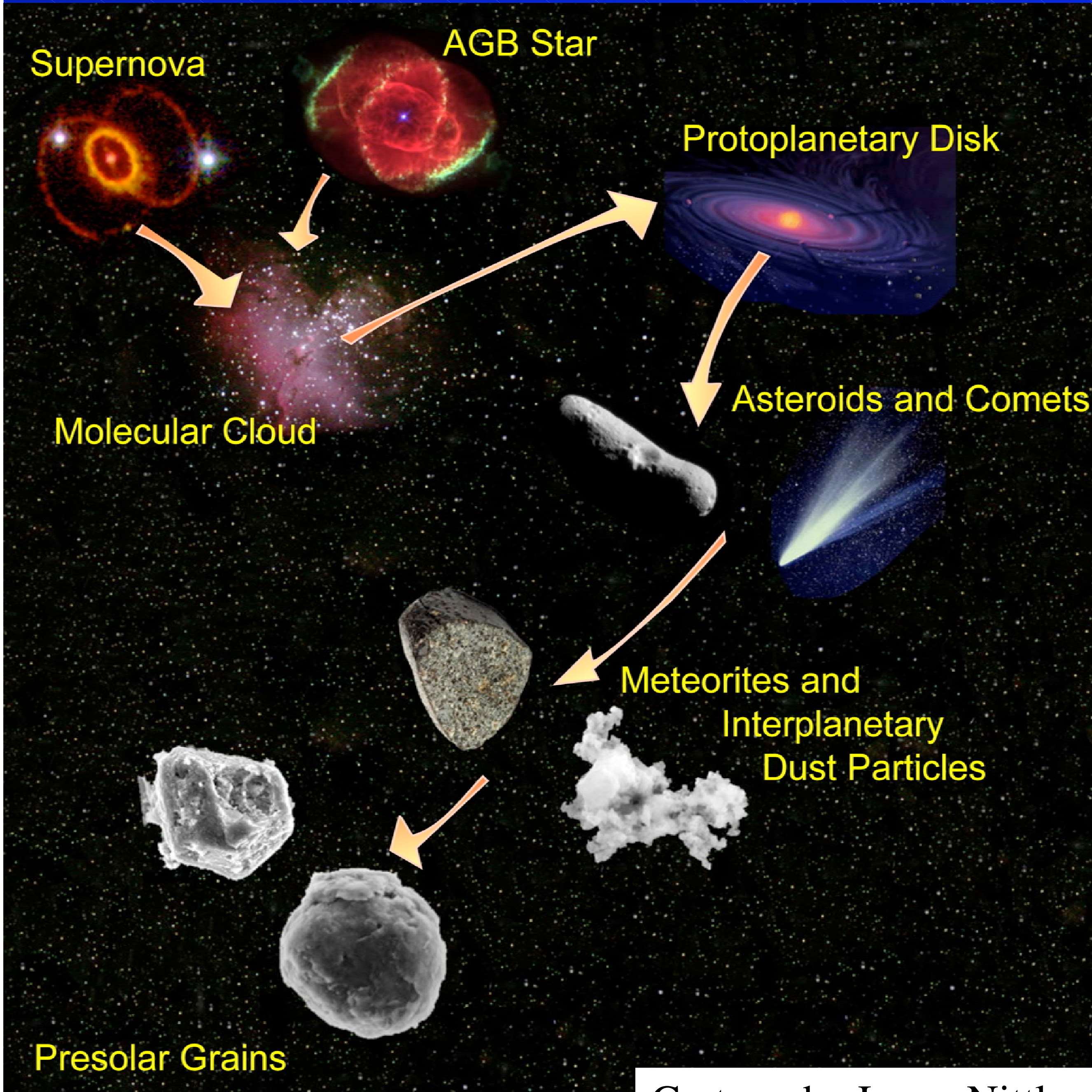

Cartoon by Larry Nittler

In the last 20 years a new source of information on isotopic abundances in stars has become available in the form of stardust preserved in primitive meteorites.

Grains from Red Giants or supernovae were included into the molecular cloud that collapsed into our Solar System.

Some of these grains are preserved in primitive meteorites, from which they can be extracted and studied in detail in the laboratory.

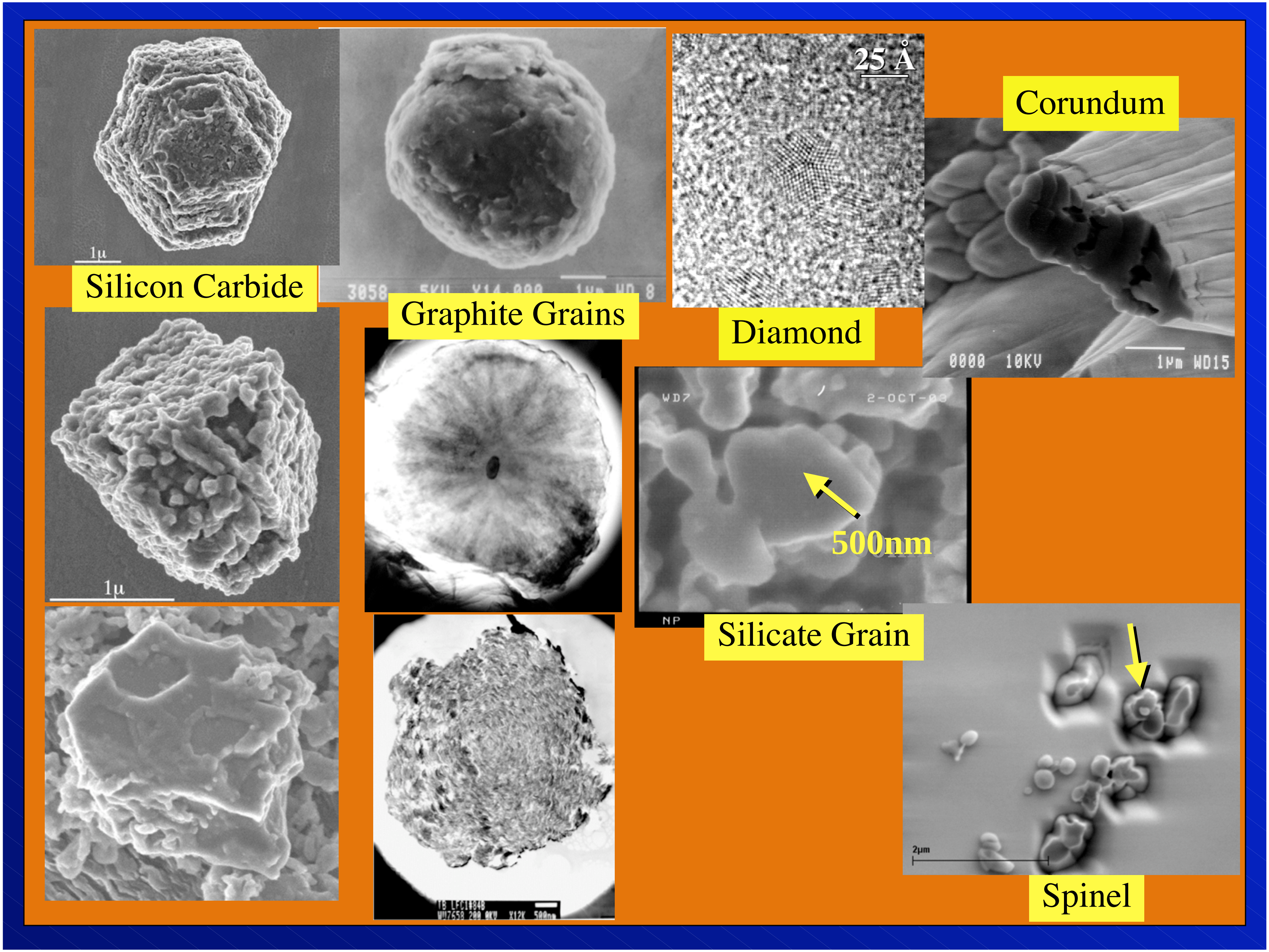

Silicon Carbide
1μ
Graphite Grains
Diamond
25 Å
Corundum
0000 10KV 1μm WD15
WD7
500nm
NP
Silicate Grain
Spinel
2μm

Some History

Some History

♣ Isotopically anomalous noble gases were found in meteorites in late 60s.

Ne-E(L): $^{20}Ne/^{22}Ne < 0.01$

(Solar $^{20}Ne/^{22}Ne = 9.8$)

close to pure ^{22}Ne (Black & Pepin)

♣ The huge isotopic anomalies in noble gases could be best explained by nucleosynthesis in stars, not by processes occurring in the solar system.

⇓

Stardust hidden in meteorites?

♣ Effort to isolate carriers of anomalous noble gases (Edward Anders, Roy S. Lewis and their coworkers)

Difficulities

Abundances of the carriers are low (<0.01%).

They are small (a few μm or less).

Anomalous noble gases served as tracers to isolate these minerals.

"Burn the haystack to find a needle" (Edward Anders)

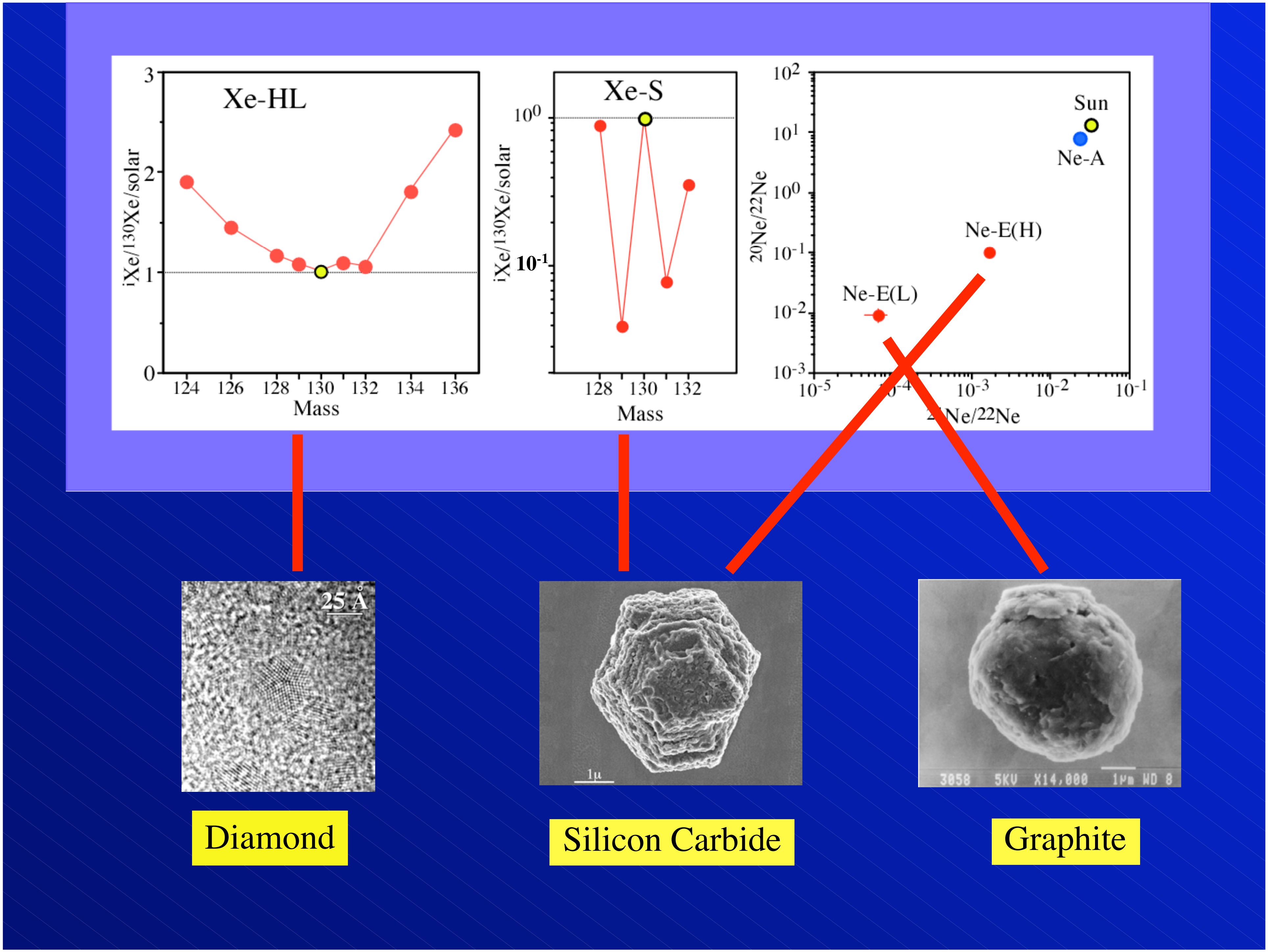
Xe-HL
iXe/130Xe/solar
Mass
Xe-S
iXe/130Xe/solar
Mass
20Ne/22Ne
21Ne/22Ne
Sun
Ne-A
Ne-E(H)
Ne-E(L)
25 Å
1μ
3058 5KV X14,000 1μm WD 8
Diamond
Silicon Carbide
Graphite

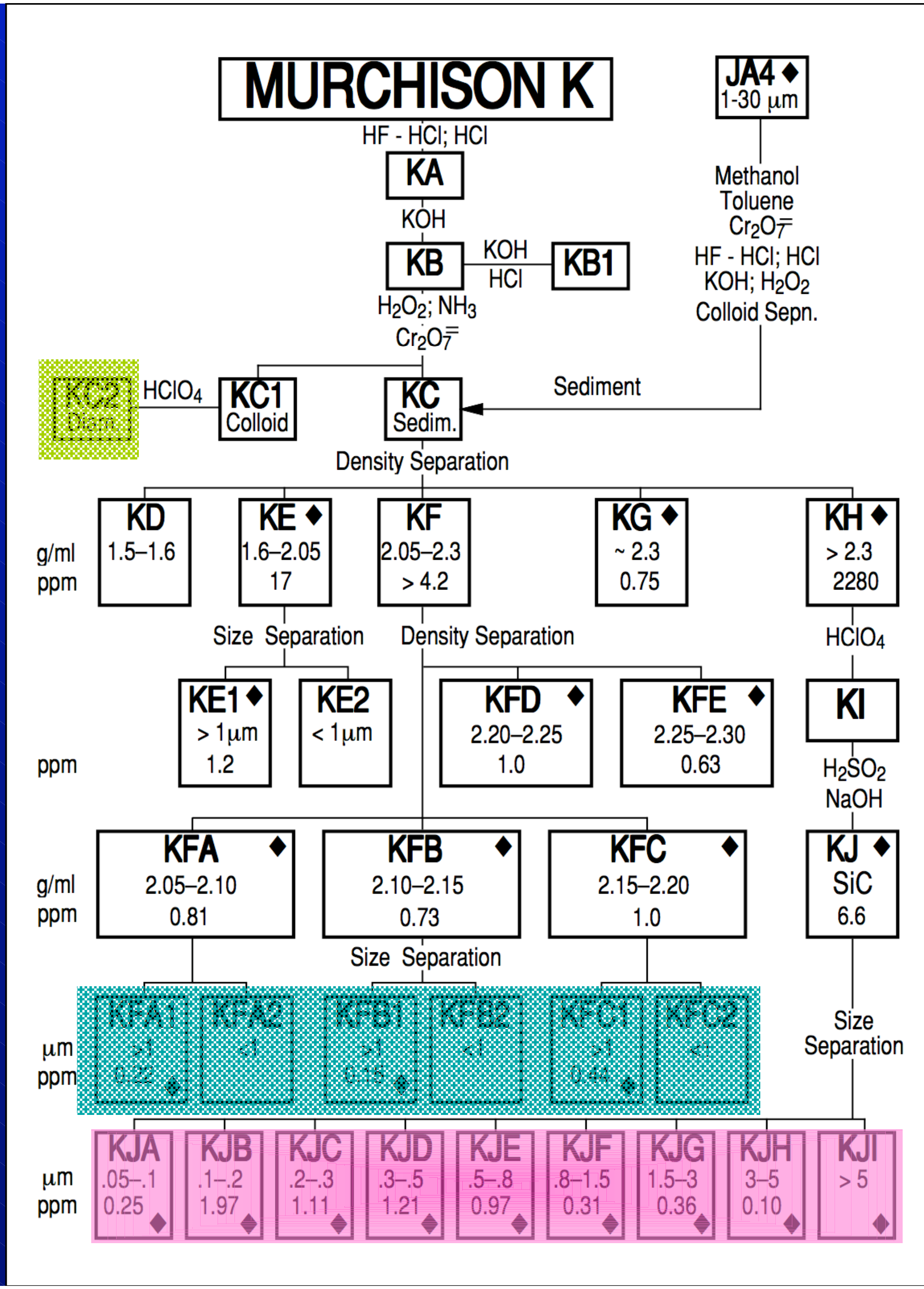

Many chemical and physical separation steps are necessary to “burn the haystack” and isolate presolar graphite and SiC grains.

Suspension of nanodiamonds.

Different layers of “graphite” grains of different densities in Na-polytungstate liquid. There is a density gradient in the liquid.

Presolar Grains
Stardust

Types: Silicon Carbide, Graphite, Oxides, Silicates

Size: 1 μm = 1/1000 mm

Mass: Picogram

One grains contains 10 billion atoms

They are older than the Solar System

How do we know the grains are stardust?

We measure their isotopic compositions and they are completely different from those of Solar System material.

ANALYSIS TECHNIQUES

1. "Bulk Analysis" (large number of grains)

TIMS and Gas Mass Spectrometry

Noble Gases, Sr, Ba, Nd, Sm
Separation by grain size, step-wise heating and/or combustion

Can measure trace elements but obtain only averages

2. Single Grain Analysis (SIMS, RIMS and Gas MS)

Find tremendous variations from grain to grain
Correlation on grain by grain basis: **Stellar Histories** of individual grains

Can identify and study **Rare Subpopulations** of grains

Locate **New Types** of circumstellar grains

Disadvantage: Limited amount of sample restricts analysis to major and minor elements

Ion Microprobe

Schematic of the SIMS instrument

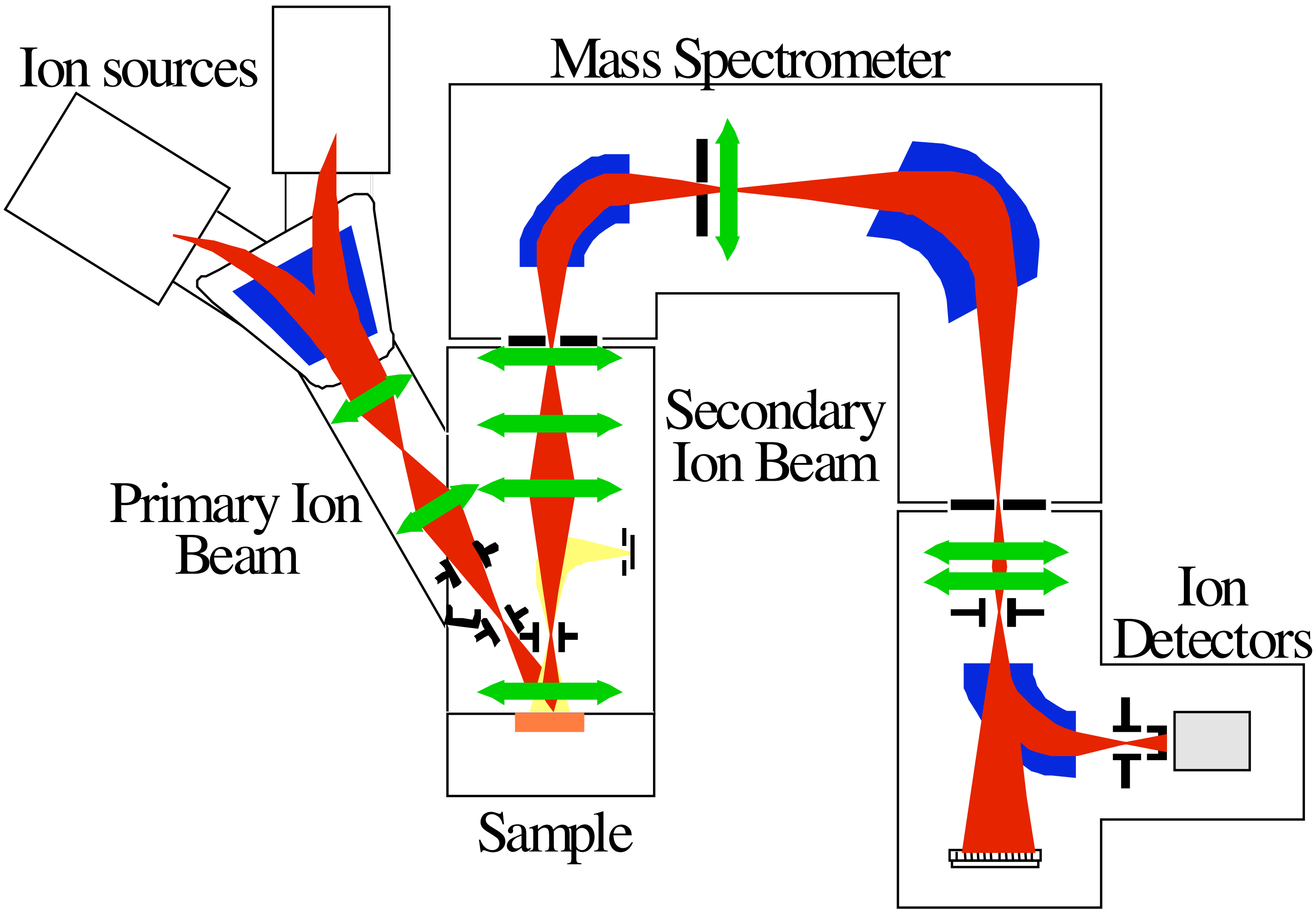

Schematic of the Cameca f-series ion microprobes.

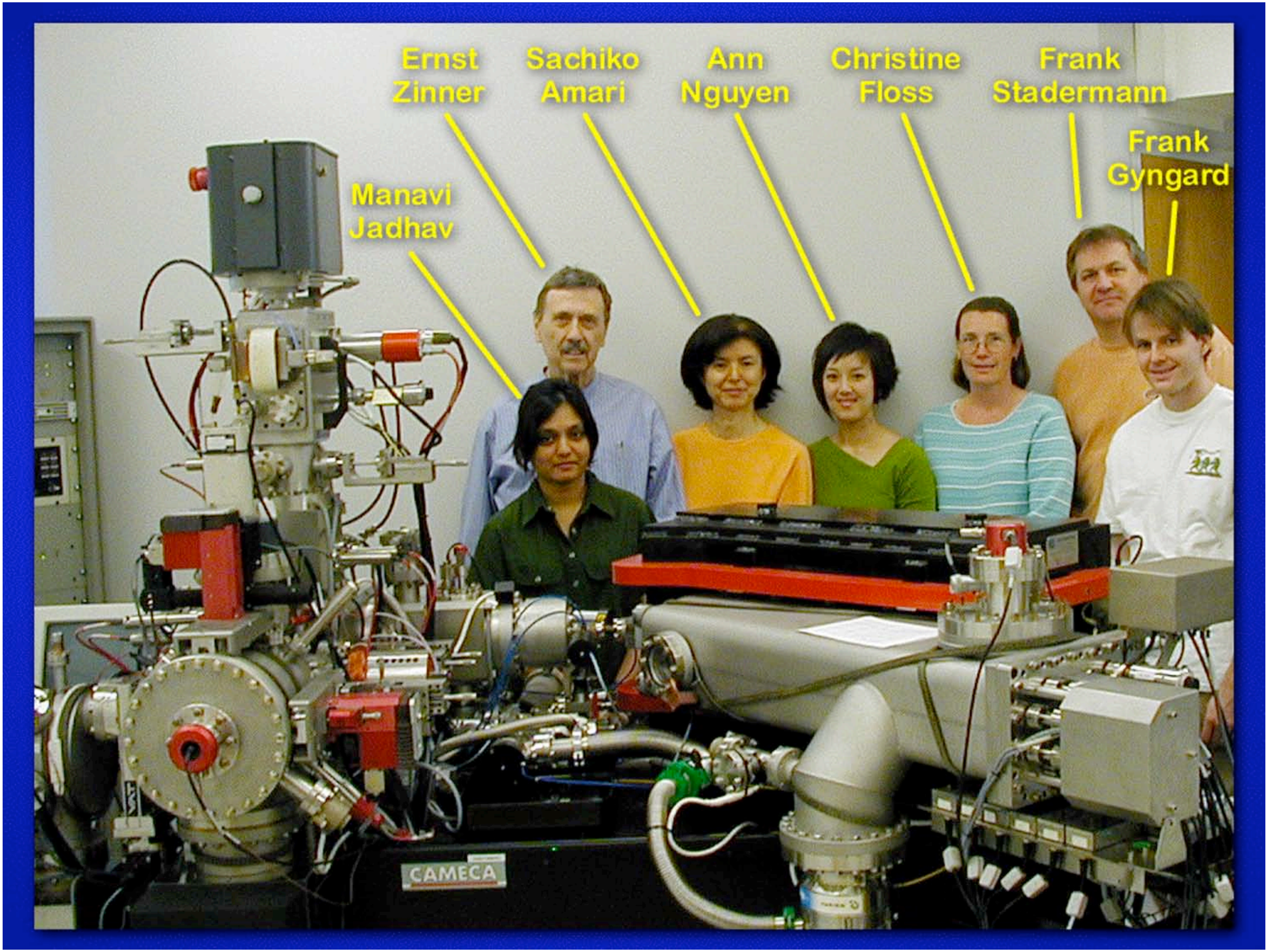
Ernst Zinner
Sachiko Amari
Ann Nguyen
Christine Floss
Frank Stadermann
Frank Gyngard
Manavi Jadhav
CAMECA

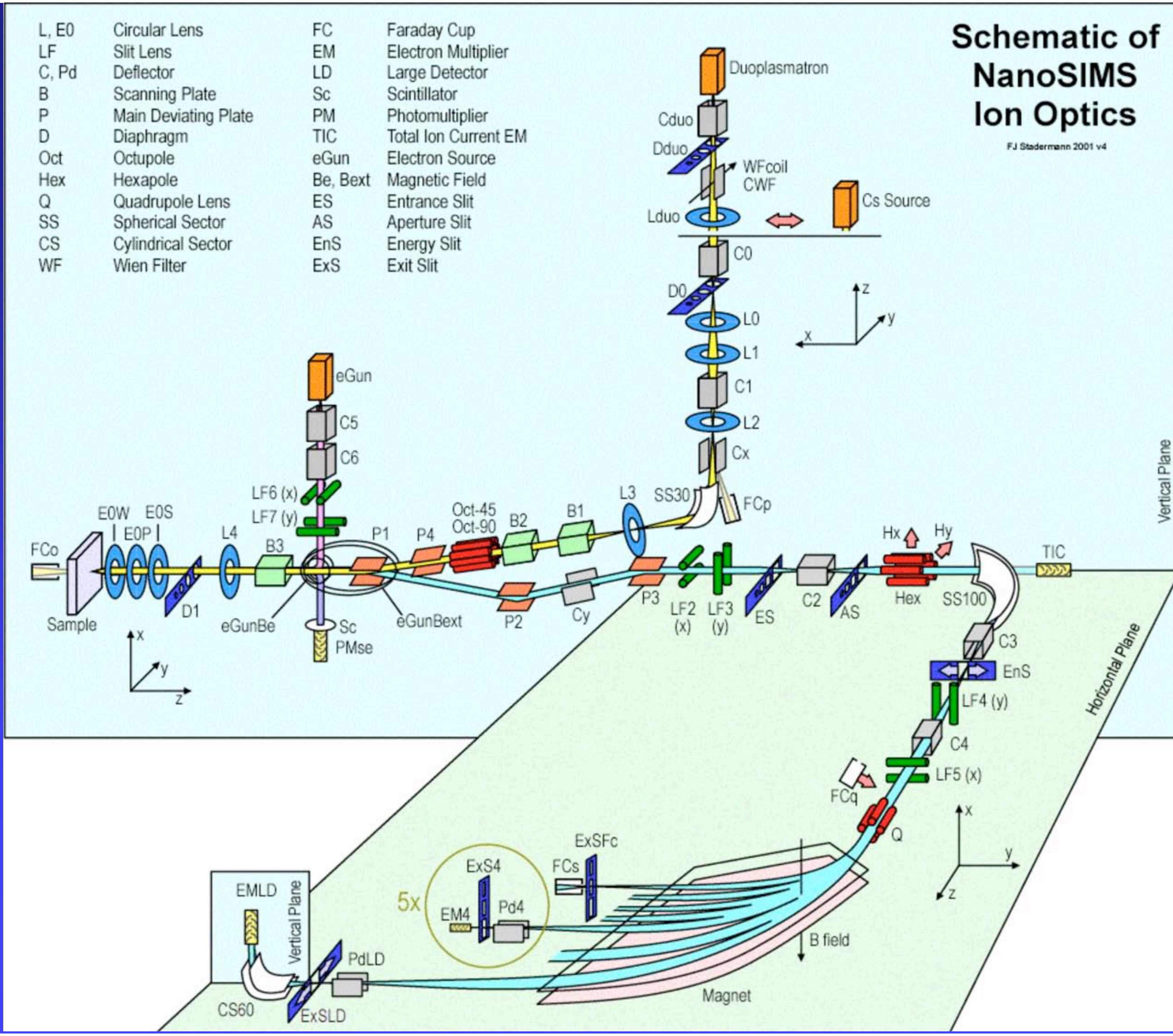

Schematic of NanoSIMS Ion Optics
FJ Stadermann 2001 v4
L, E0 Circular Lens
LF Slit Lens
C, Pd Deflector
B Scanning Plate
P Main Deviating Plate
D Diaphragm
Oct Octupole
Hex Hexapole
Q Quadrupole Lens
SS Spherical Sector
CS Cylindrical Sector
WF Wien Filter
FC Faraday Cup
EM Electron Multiplier
LD Large Detector
Sc Scintillator
PM Photomultiplier
TIC Total Ion Current EM
eGun Electron Source
Be, Bext Magnetic Field
ES Entrance Slit
AS Aperture Slit
EnS Energy Slit
ExS Exit Slit
Duoplasmatron
Cduo
Dduo
WFcoil
CWF
Cs Source
Lduo
C0
D0
L0
L1
C1
L2
Cx
SS30
FCp
L3
eGun
C5
C6
LF6 (x)
LF7 (y)
Oct-45
Oct-90
B2
B1
E0W
E0S
E0P
L4
B3
P1
P4
FCo
Sample
D1
eGunBe
Sc
PMse
eGunBext
P2
Cy
P3
LF2 (x)
LF3 (y)
ES
C2
AS
Hx
Hy
Hex
SS100
TIC
Vertical Plane
Horizontal Plane
C3
EnS
LF4 (y)
C4
LF5 (x)
FCq
Q
ExSFc
FCs
ExS4
5x
EM4
Pd4
B field
EMLD
Vertical Plane
PdLD
CS60
ExSLD
Magnet

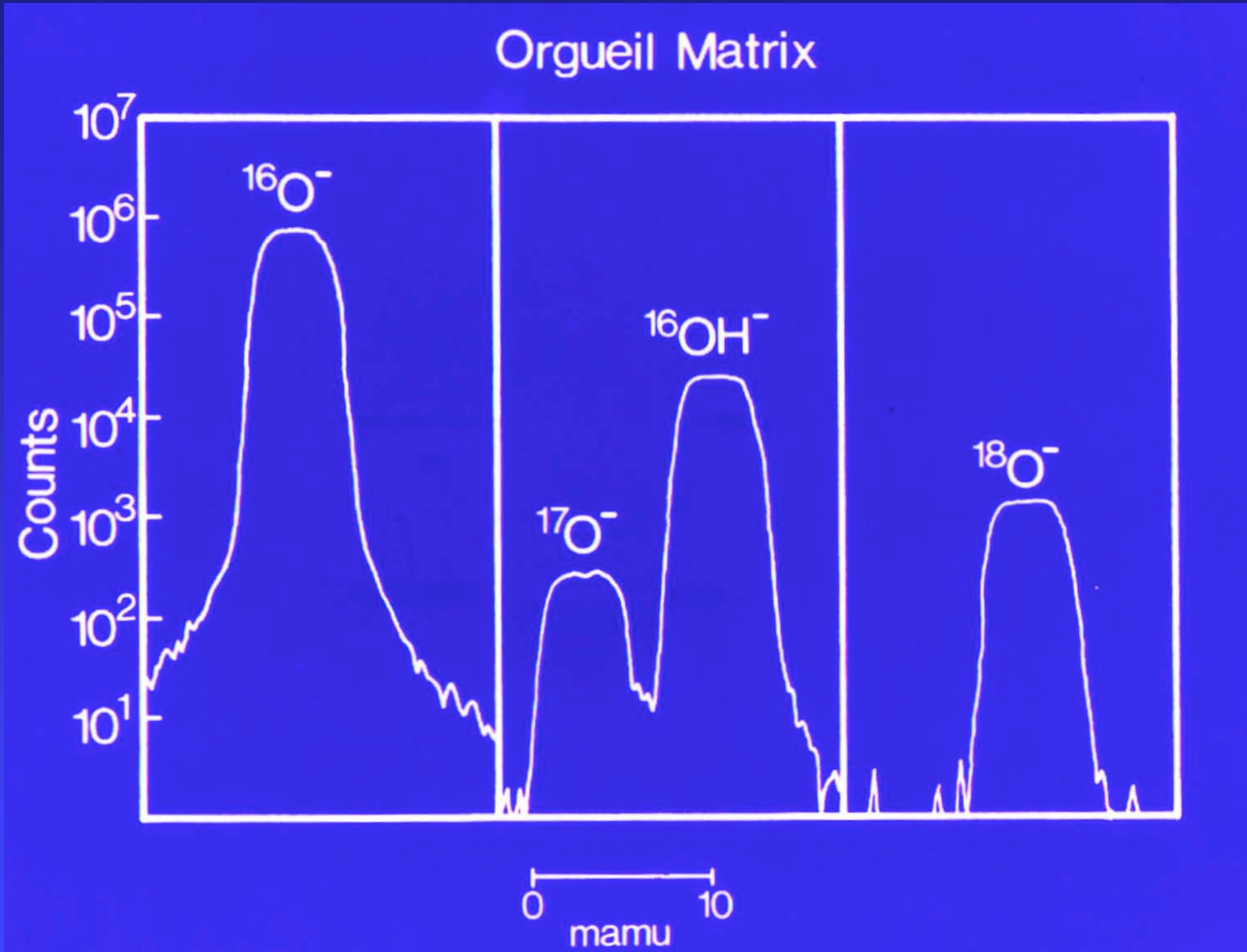

High mass resolation is necessary to separate atomic ions from molecular interferences.

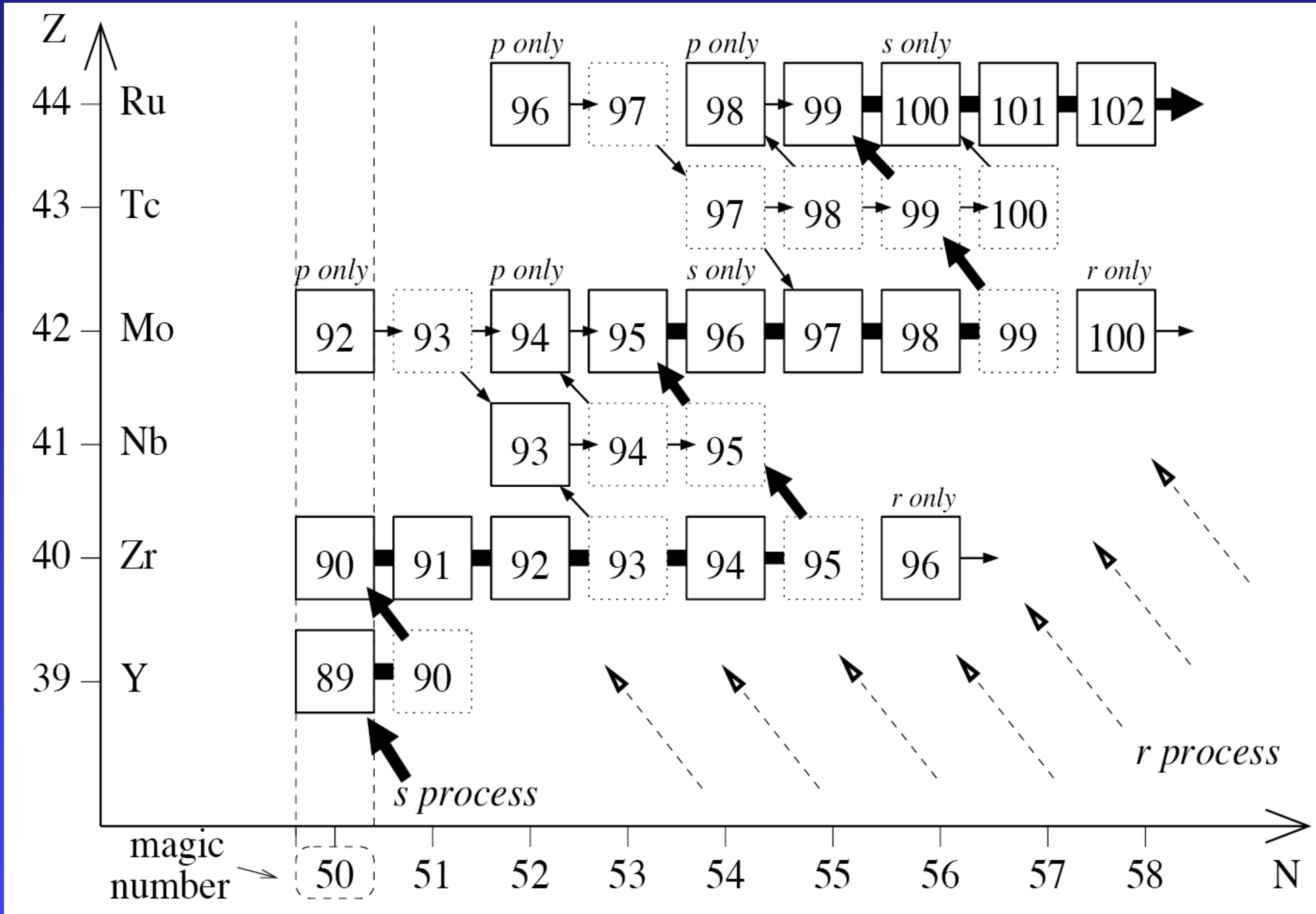

Isobaric isotopes (e.g., ^{94}Zr and ^{94}Mo) cannot be separated in the mass spectrometer. RIMS makes analysis of only one element possible.

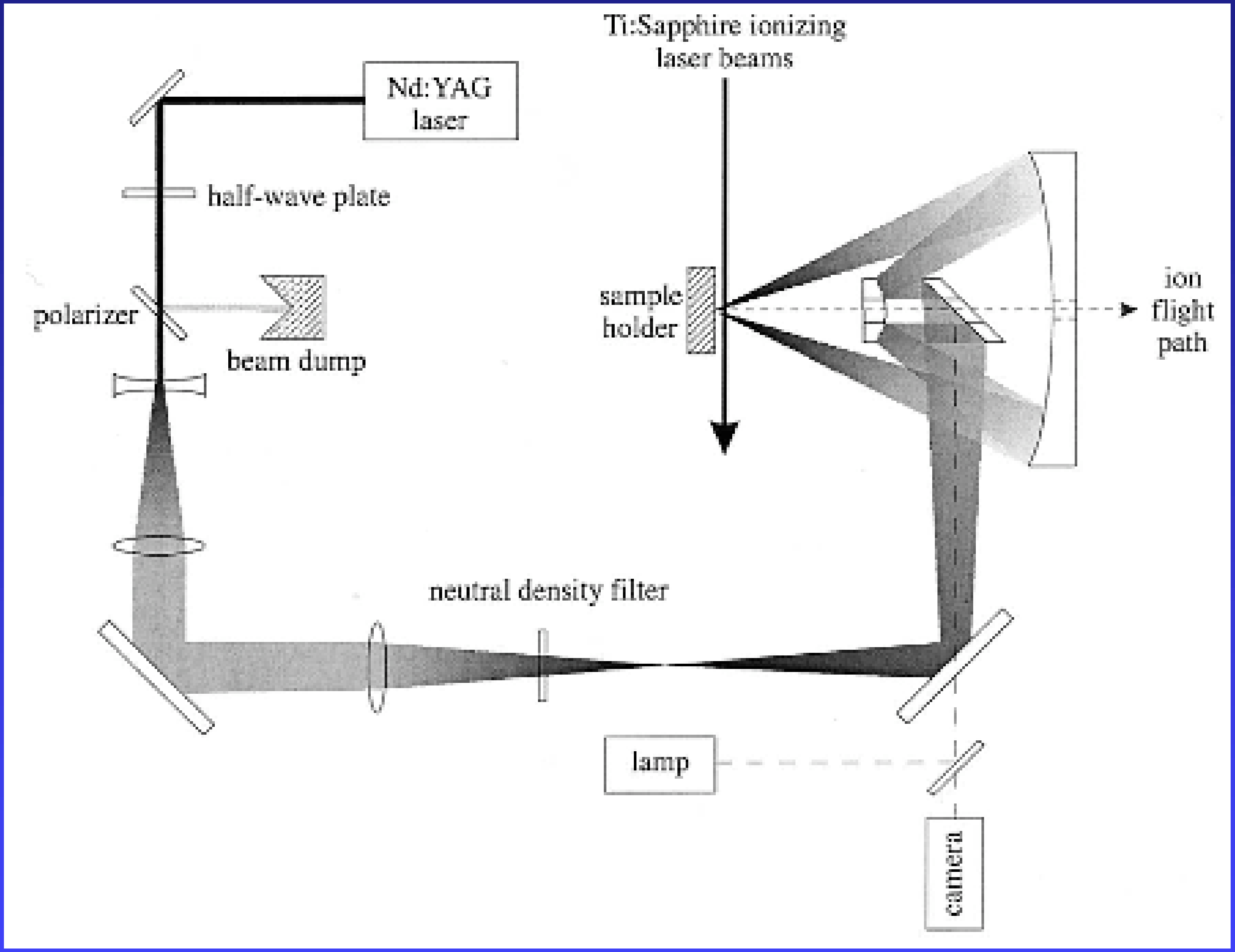

Schematic of a Resonance Ionization Mass Spectrometer (RIMS).

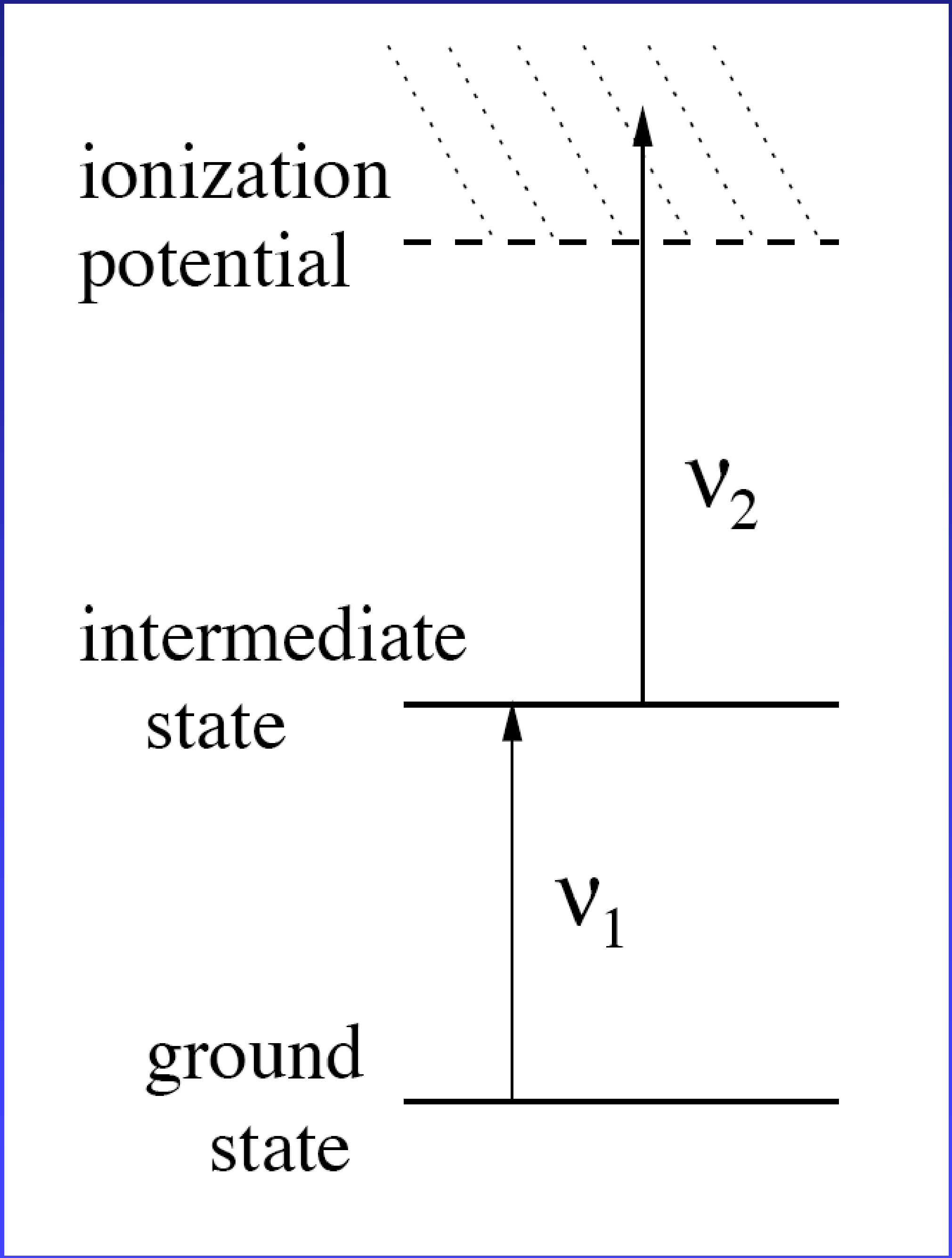

Irradiation with well-tuned laser light ionizes only a given element.

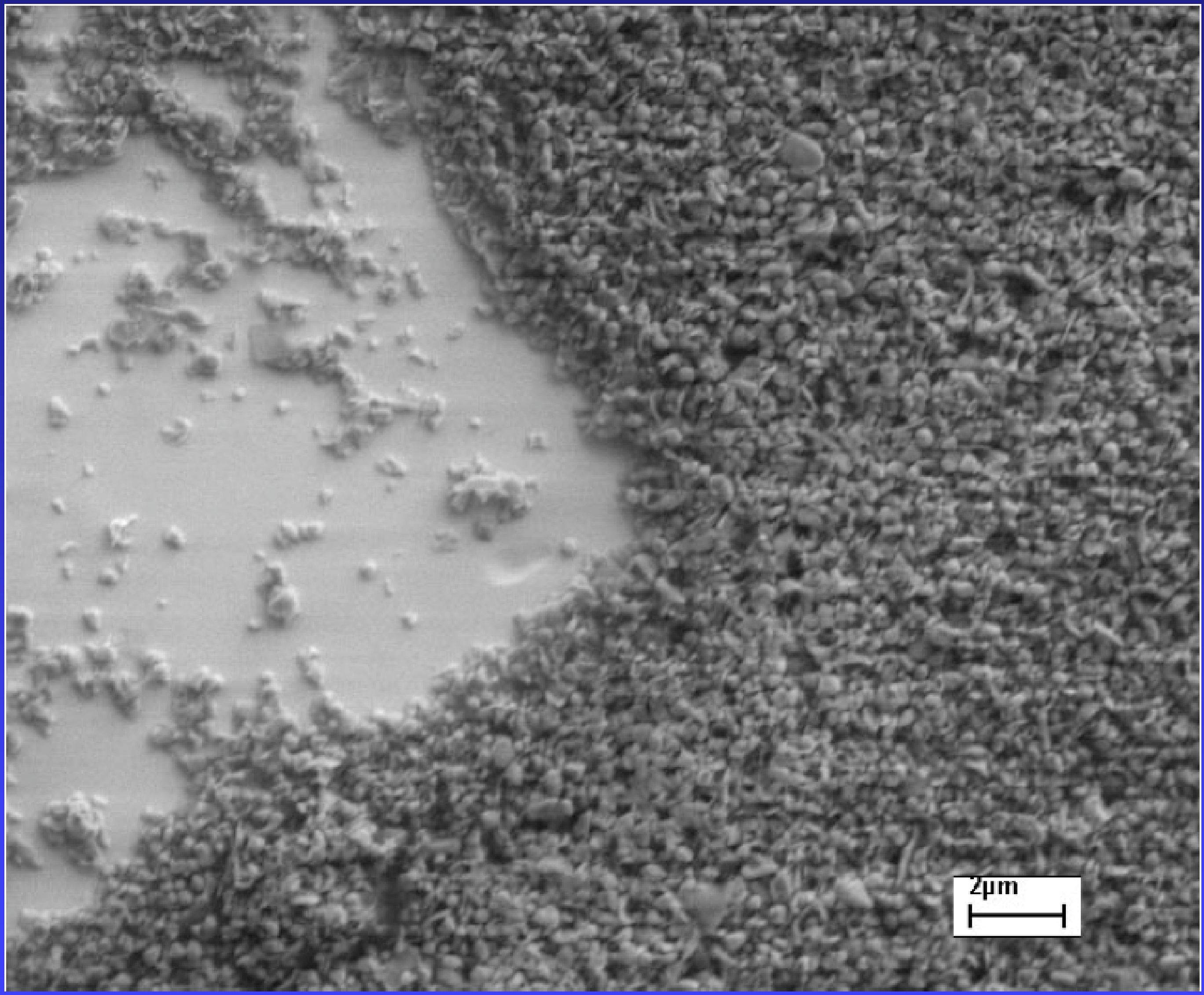

Deposit of 0.5 μm spinel grains on a gold foil for NanoSIMS analysis.

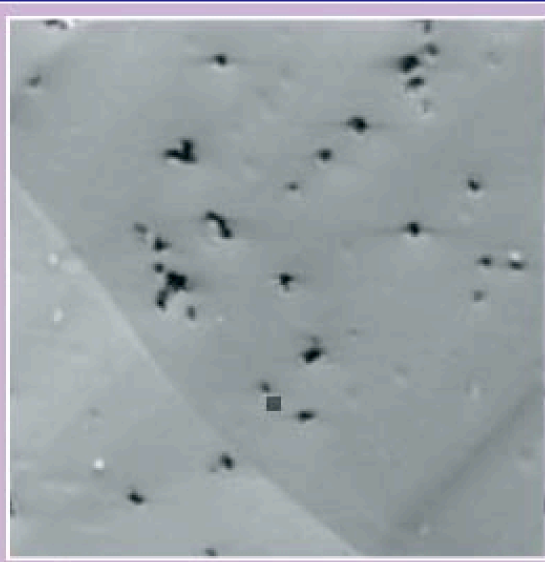

Sec. electron image

$^{16}O^-$ image

SEM image after

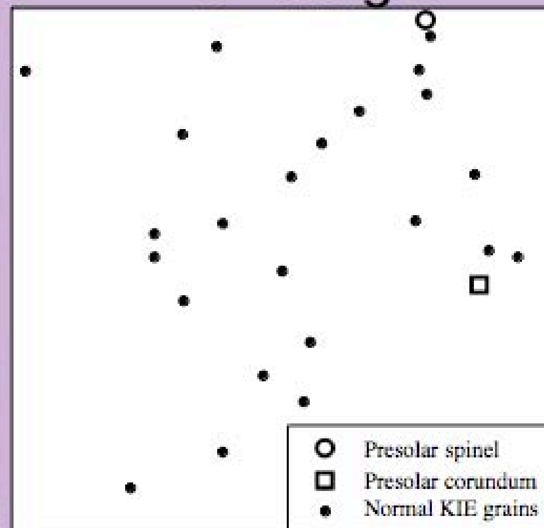

Analyzed grains

Murchison
KIE grains

20x20 μm^2

Analysis of well-separated grains.

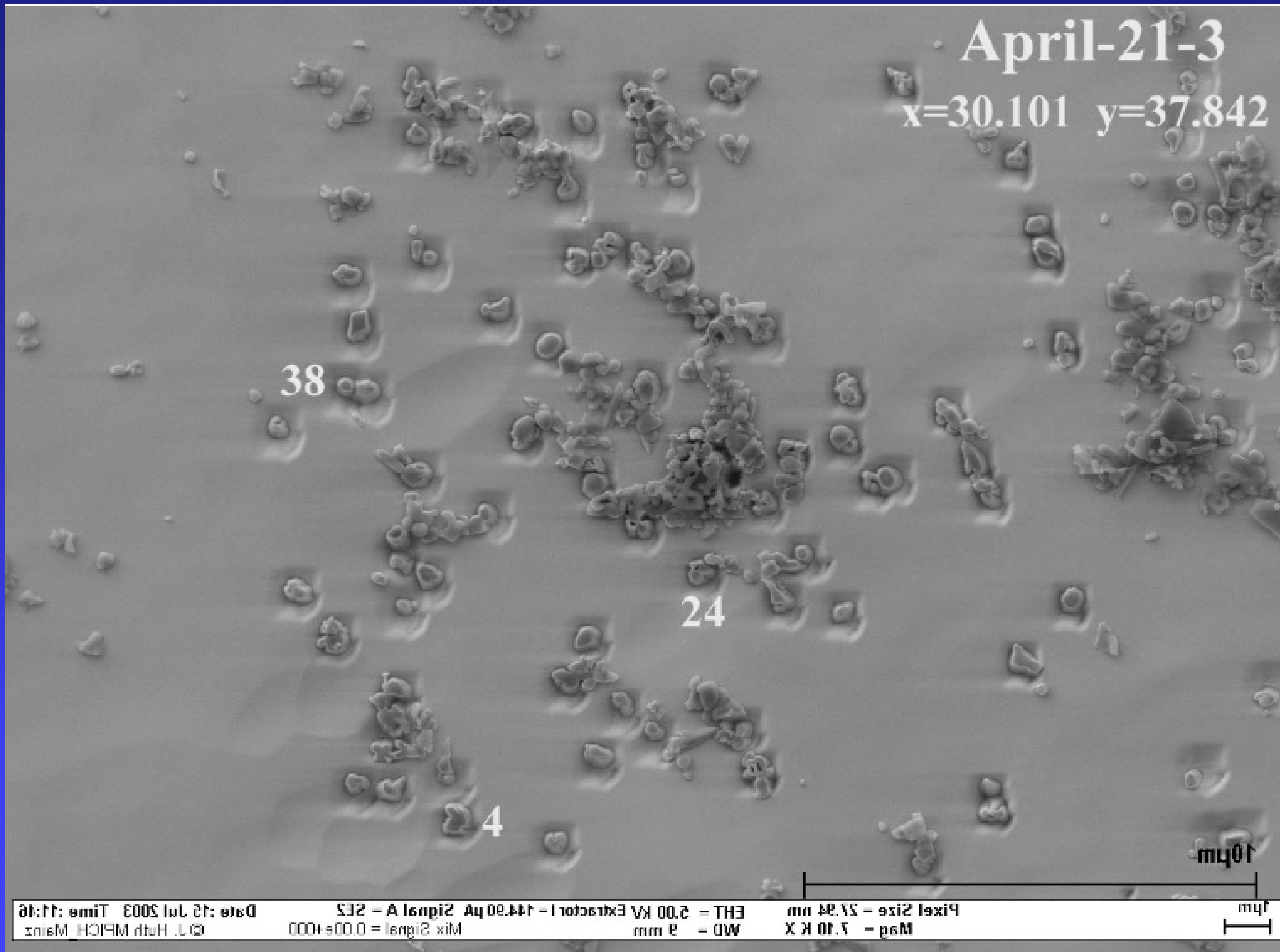

Another example of individual grain isotopic analysis in the NanoSIMS. Shown is an SEM image after ion probe analysis.

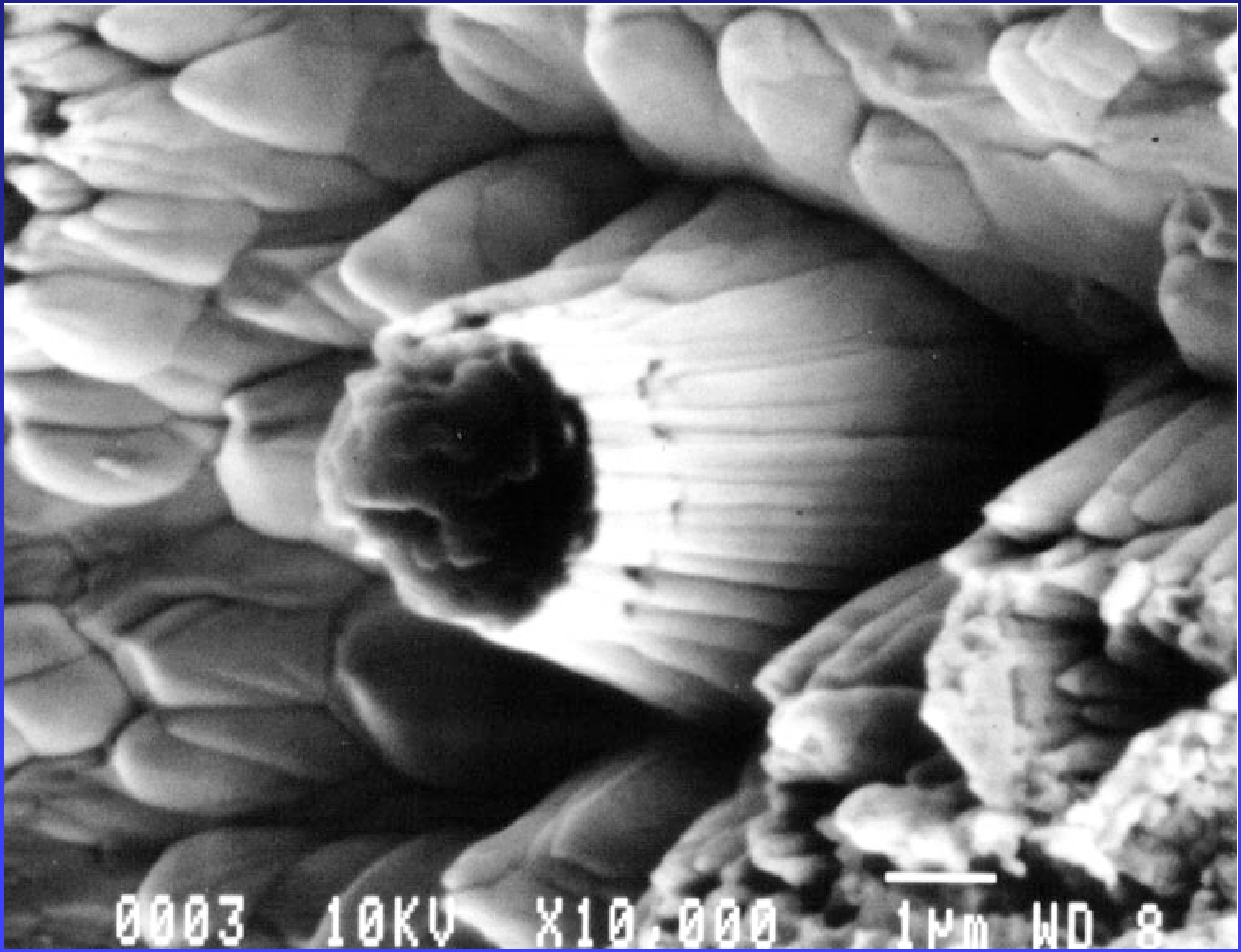

Effects of sputtering by the primary ion beam.

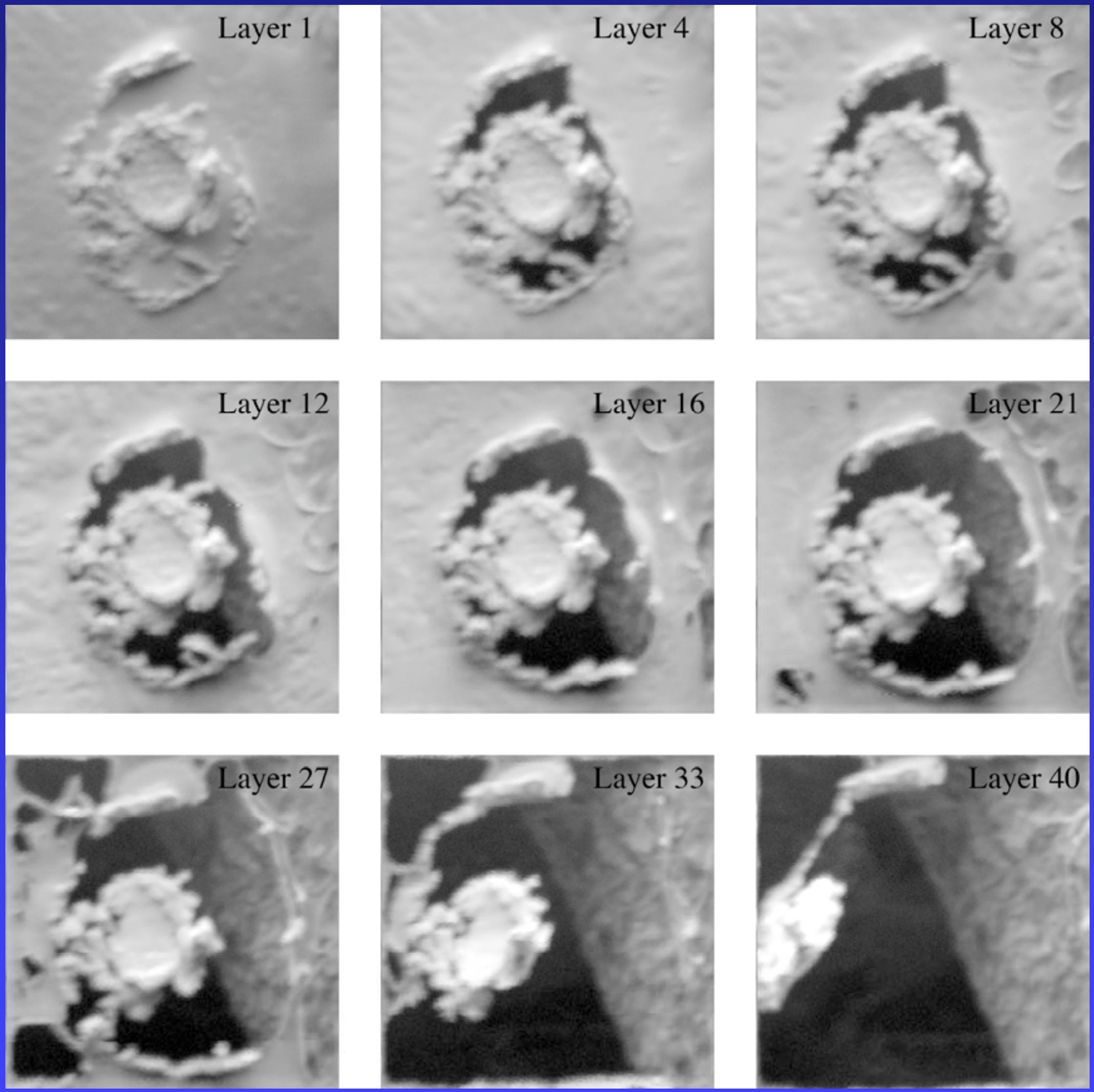

NanoSIMS analysis of an ultratome section of a presolar graphite grain.

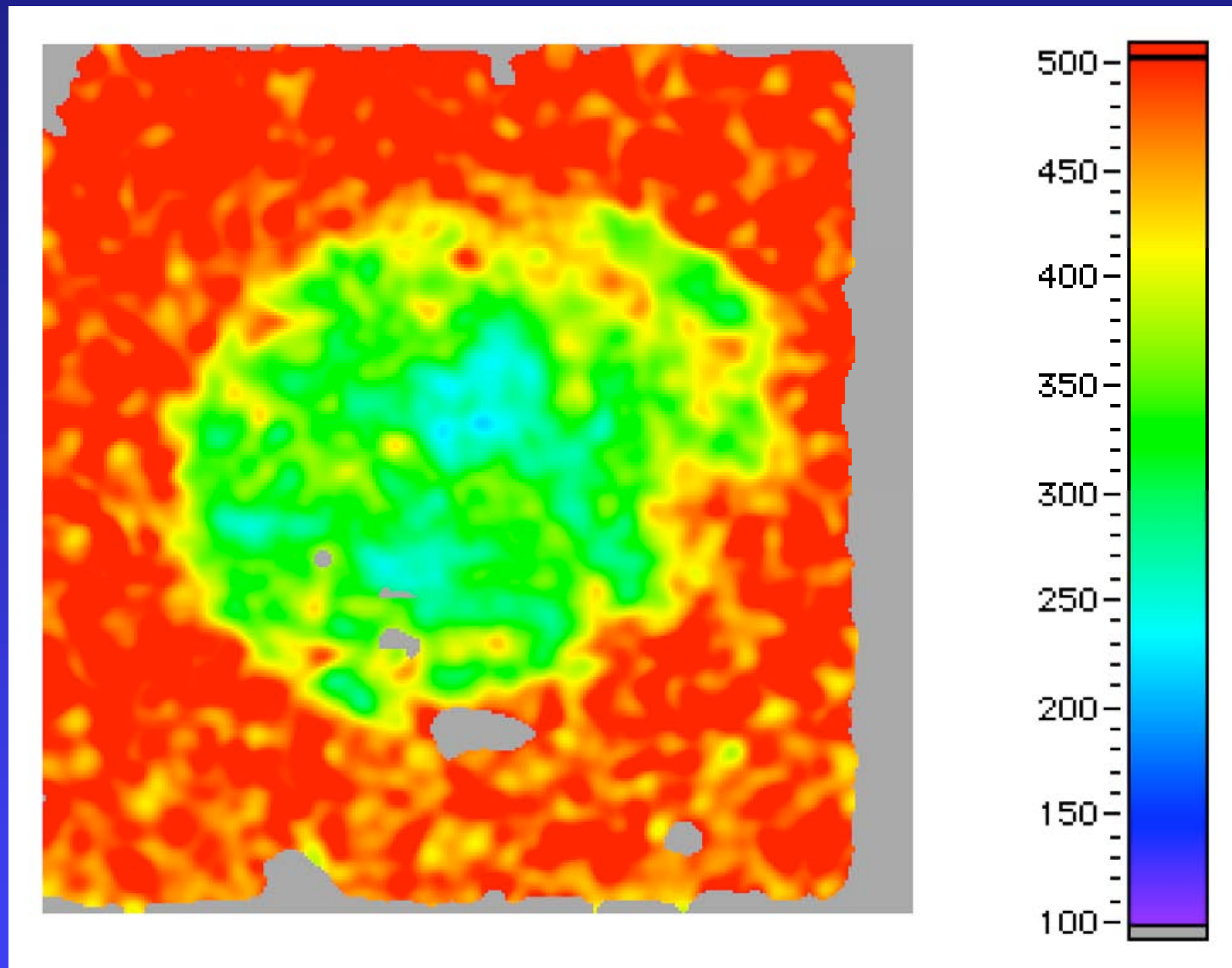

Isotopic ratio image of $^{16}O/^{18}O$ inside a presolar graphite grain. The grain has a large ^{18}O excess. The solar ratio is 500.

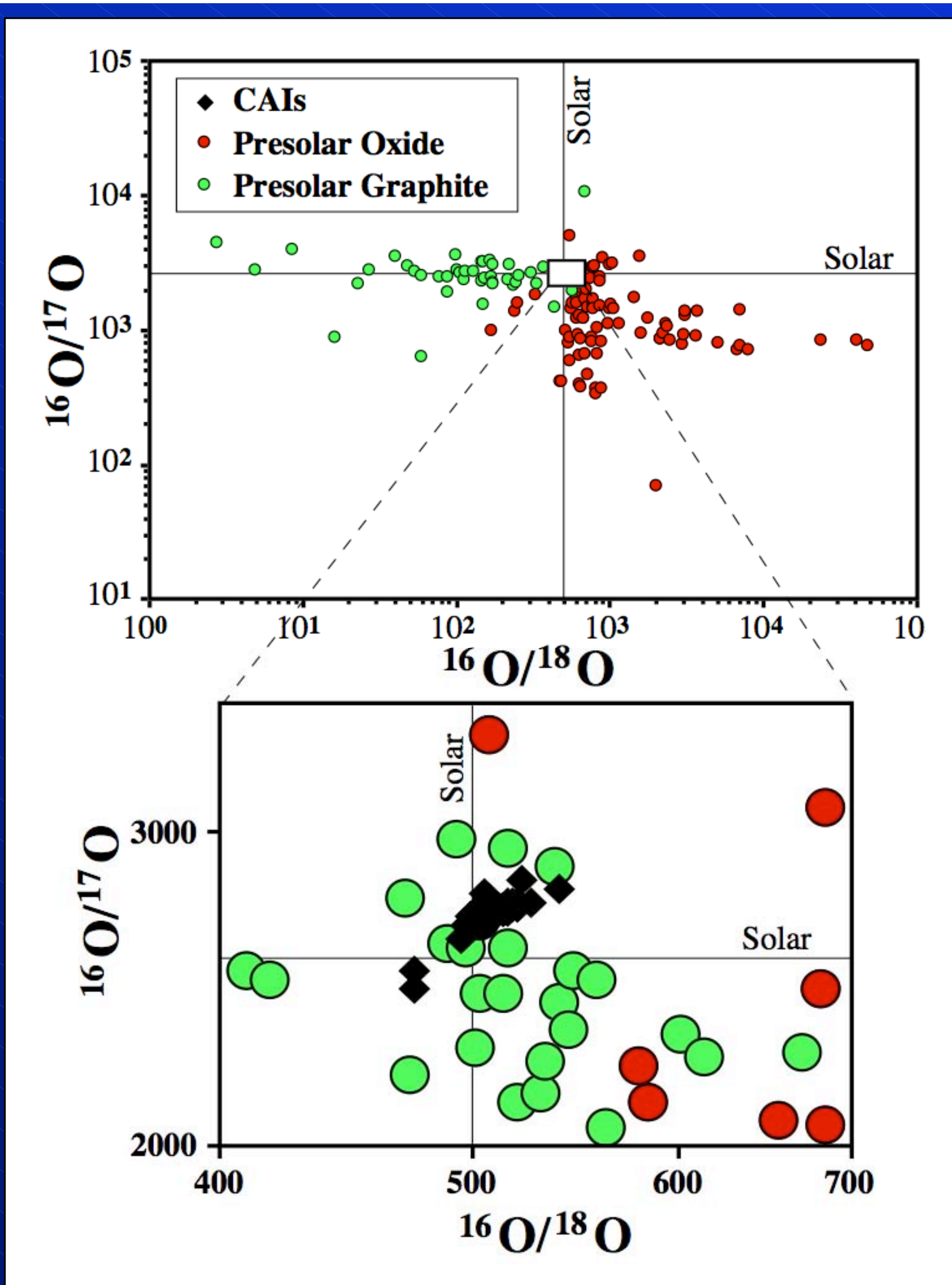

Isotopic anomalies in presolar grains are orders of magnitude larger than variations in solar system materials.

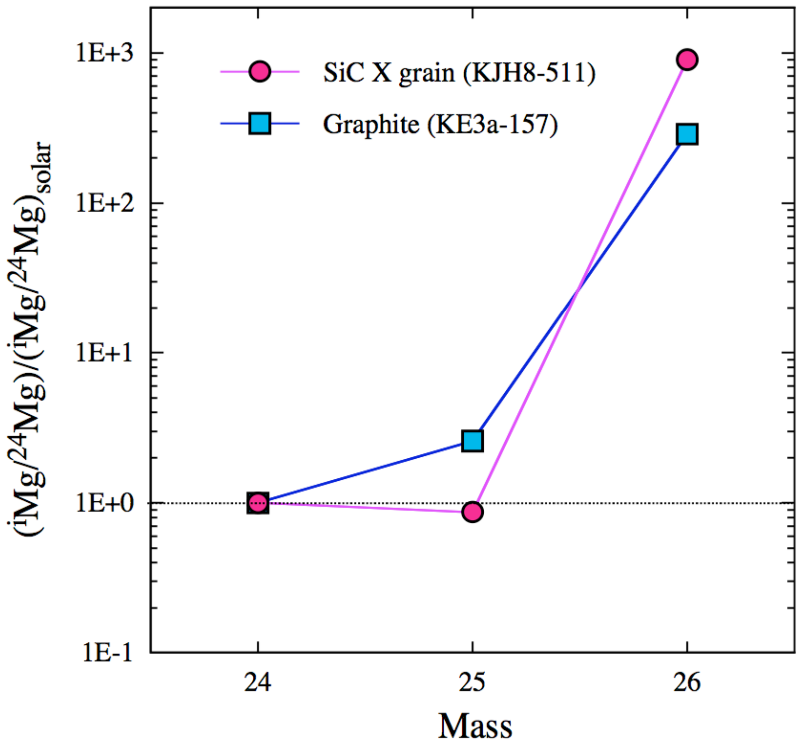

SiC X

$^{25}Mg/^{24}Mg$: ~ solar

$^{26}Mg/^{24}Mg$: ×899 solar

Excess ^{26}Mg: from the decay of ^{26}Al

Graphite

$^{25}Mg/^{24}Mg$: ×3 solar

$^{26}Mg/^{24}Mg$: ×288 solar

Excess ^{26}Mg: ^{26}Mg from neutron capture is negligible;the decay of ^{26}Al still dominates.

In some grains Mg is dominated by radiogenic ^{26}Mg.

“Extinct” isotopes

^{26}**Al** $(T_{1/2} = 7.3 \times 10^5 a) \Rightarrow$ ^{26}**Mg**
^{41}**Ca** $(T_{1/2} = 1.0 \times 10^5 a) \Rightarrow$ ^{41}**K**
^{44}**Ti** $(T_{1/2} = 60a) \Rightarrow$ ^{44}**Ca**

Since meteorites formed 4.5×10^9 years ago and presolar grains, which are extracted from meteorites, are older than meteorites,

^{26}Al, ^{41}Ca and ^{44}Ti can be inferred from their daughter isotopes (^{26}Mg, ^{41}K, ^{44}Ca).

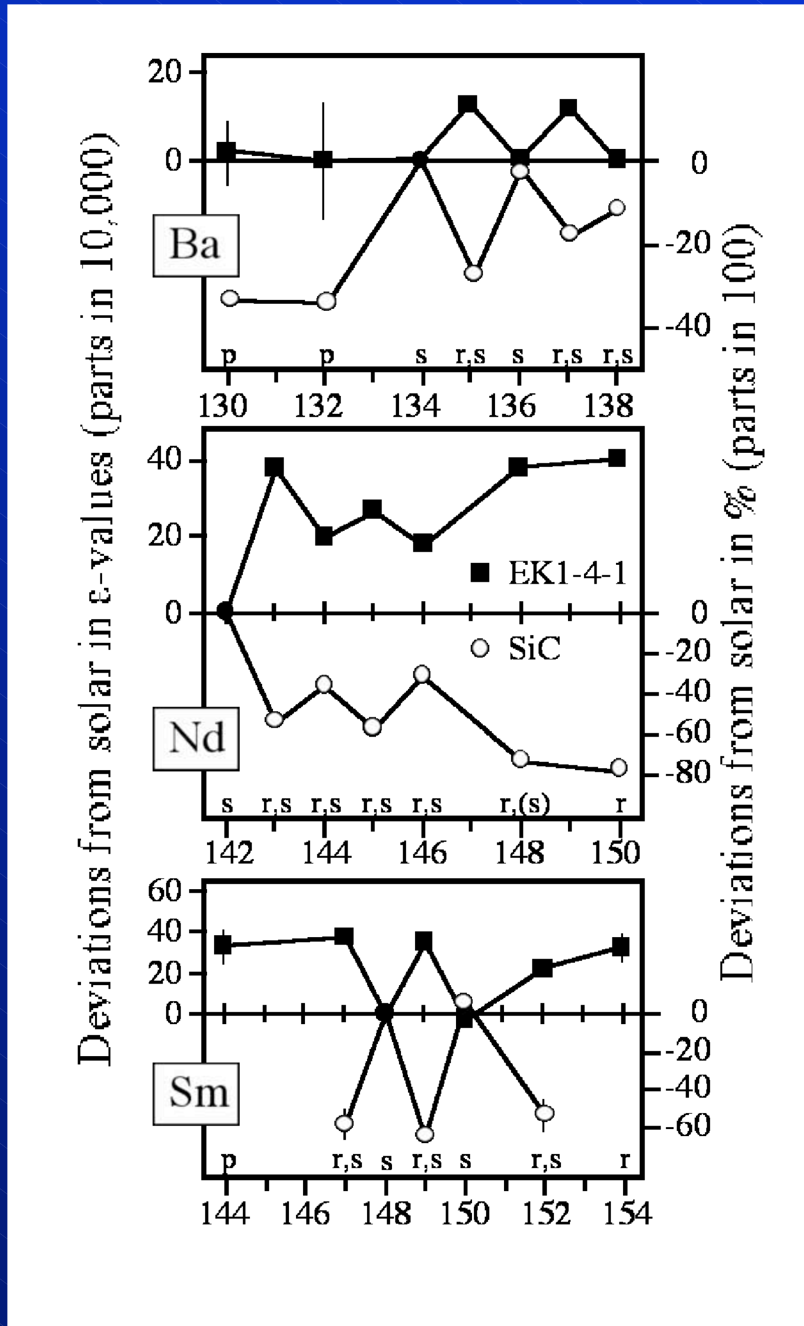

Figure 2

Another example that isotopic anomalies in presolar grains are much larger than those in SS materials.

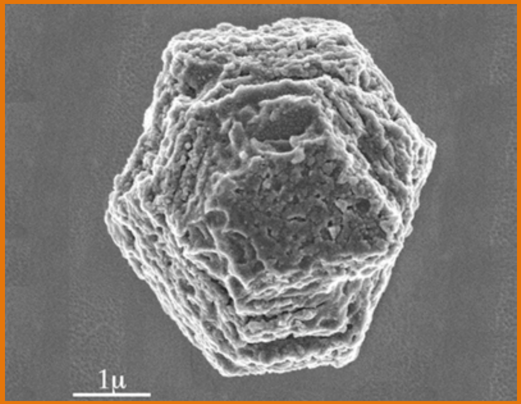

Silicon carbide grains: all are of stellar origin

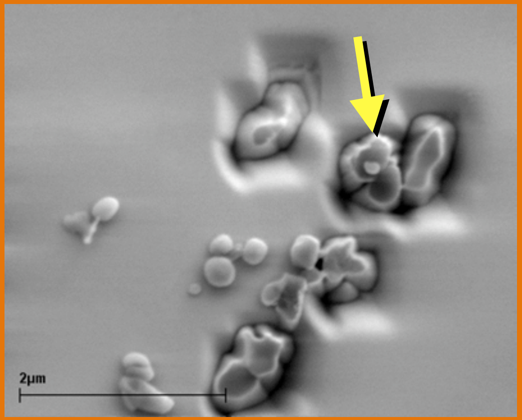

Spinel grains: only ~2% are of stellar origin

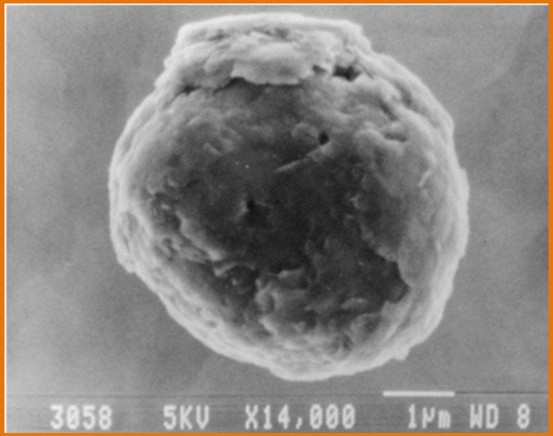

Graphite grains: approximately half of them are of stellar origin

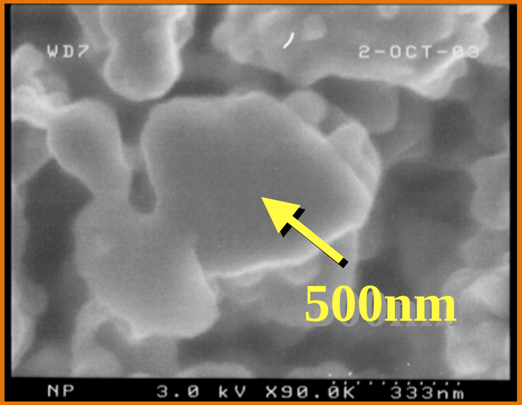

Silicate grains: only 0.001-0.02% are of stellar origin

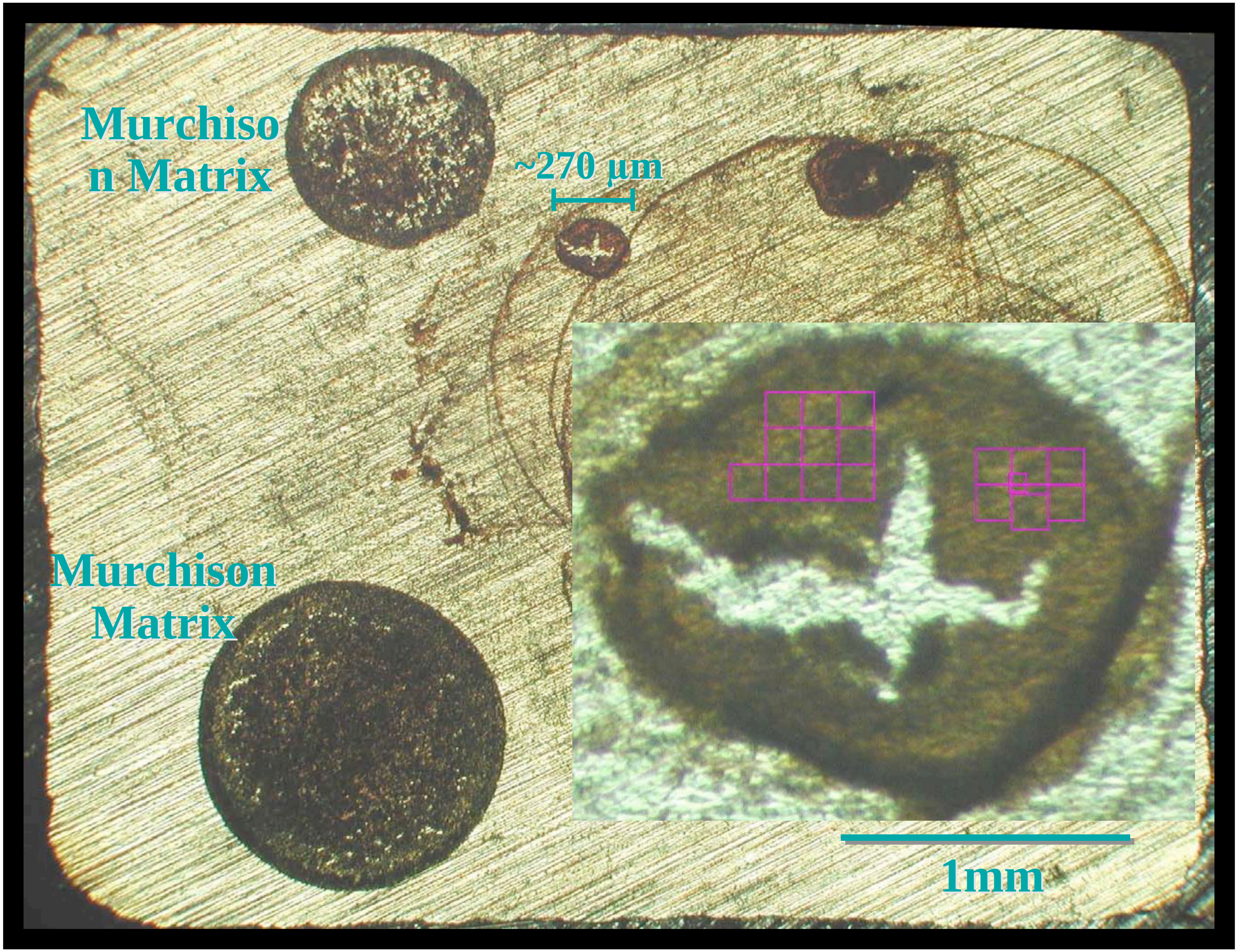

Deposit of small matrix grains from the primitive meteorite Acfer 094 for isotopic imaging to detect anomalous grains.

$10x10\ \mu m^2$

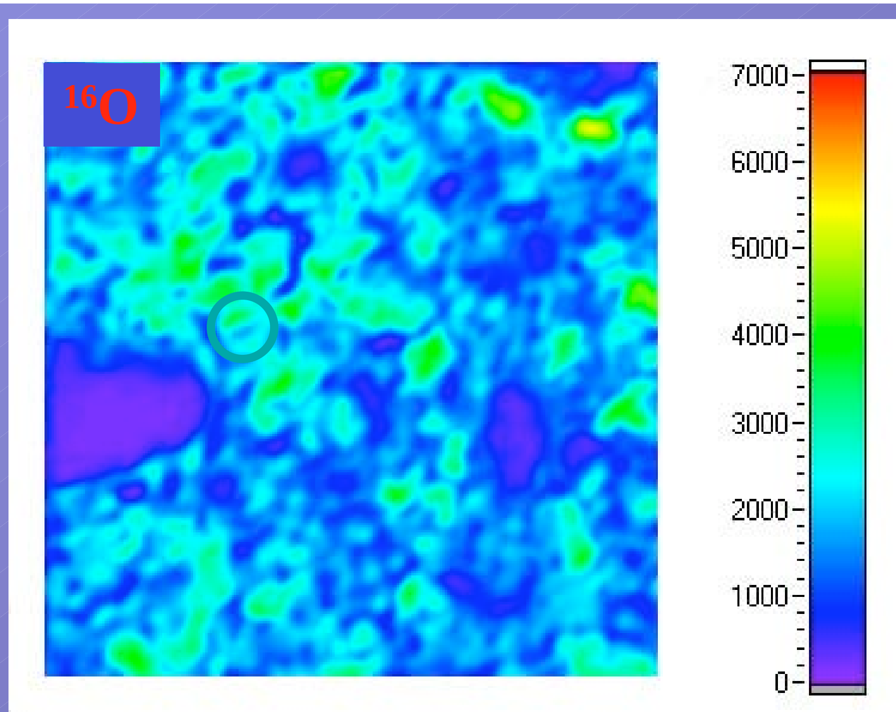

O Isotopic images of a $10\mu m x 10\mu m$ area.

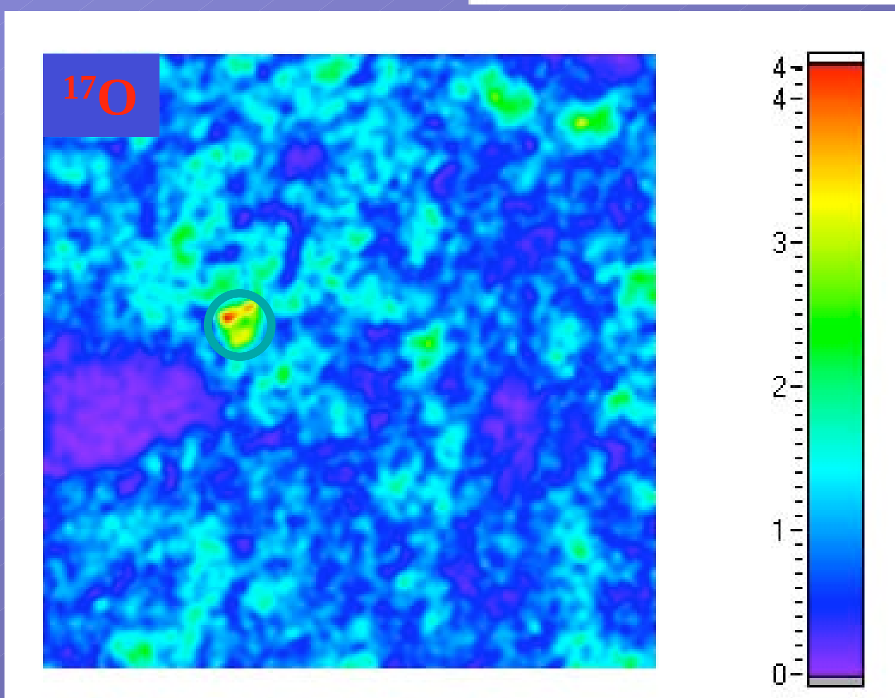

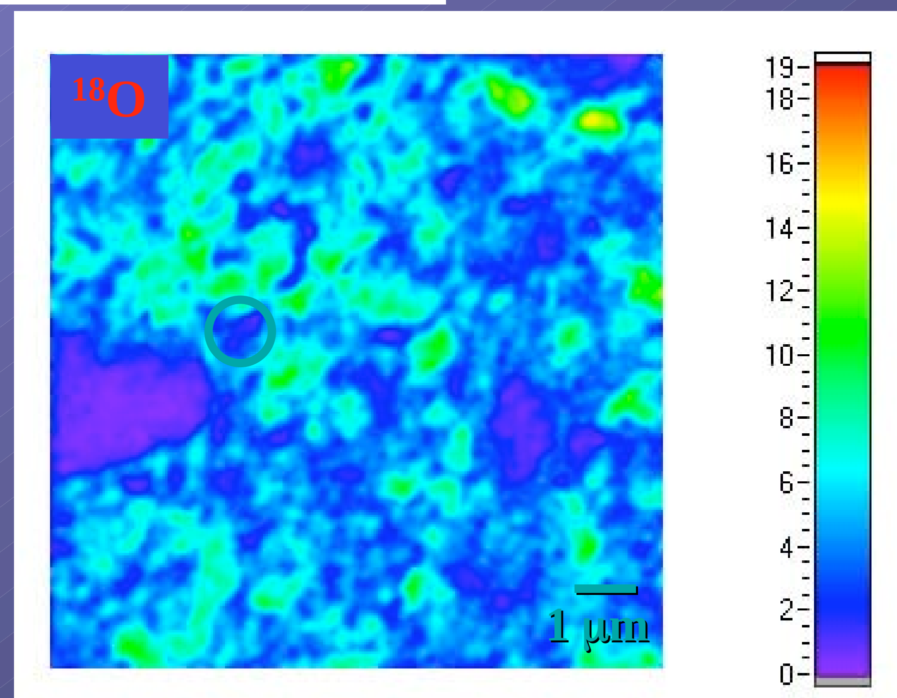

$\delta^{17}O/^{16}O$

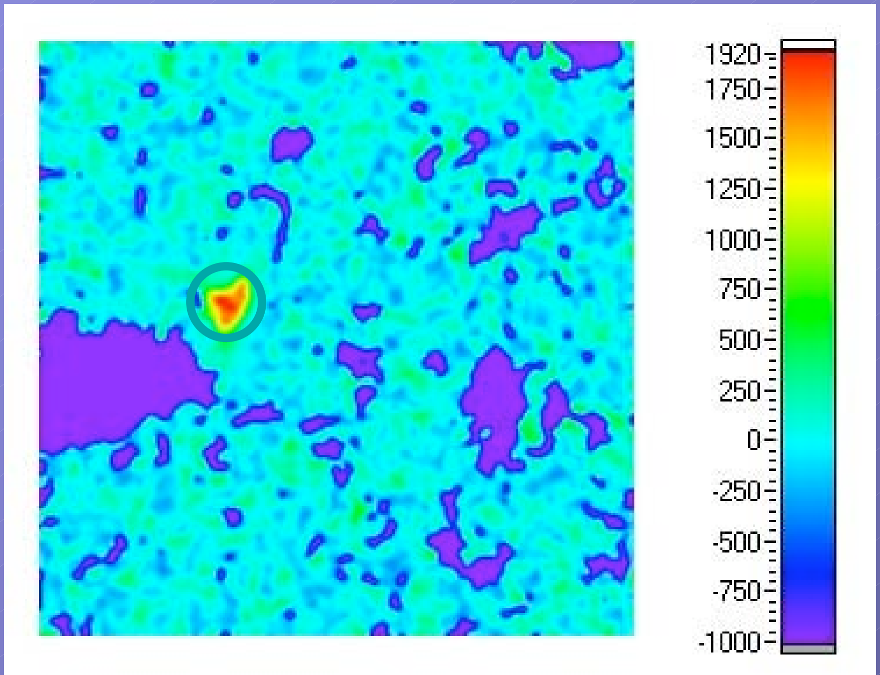

$\delta^{18}O/^{16}O$

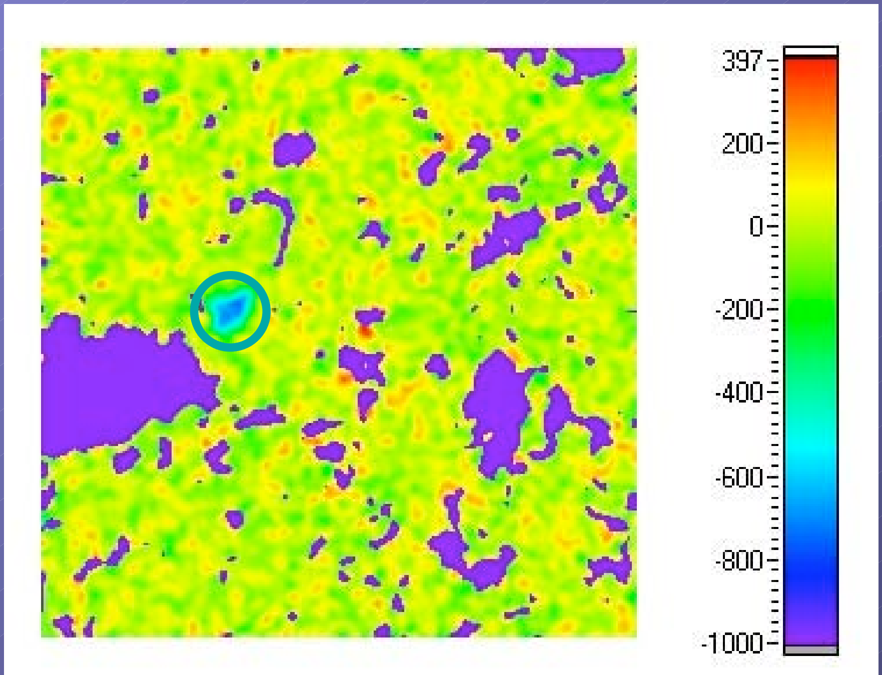

$10x10\ \mu m^2$

$^{24}Mg^{16}O$

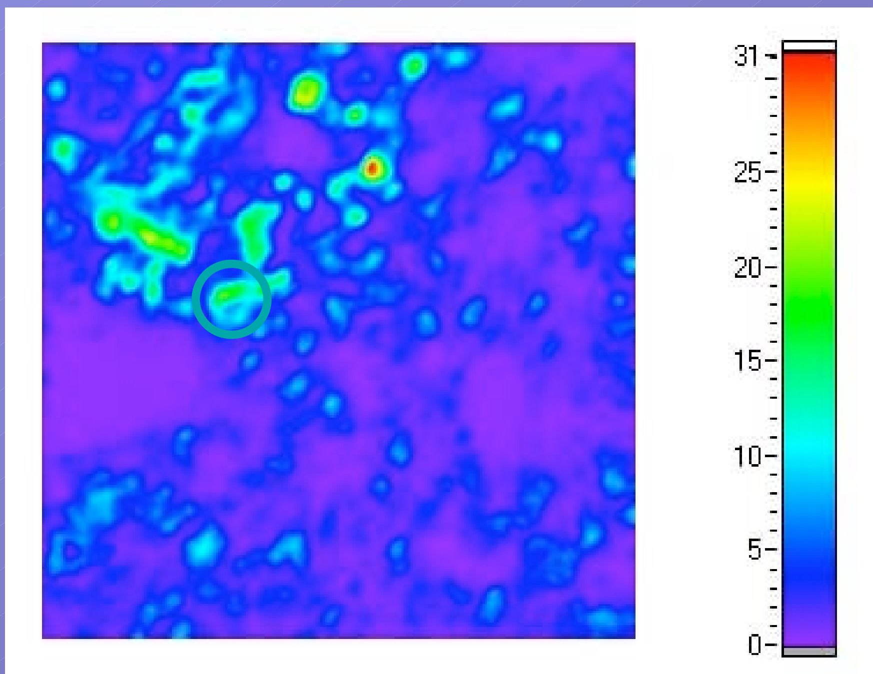

^{28}Si

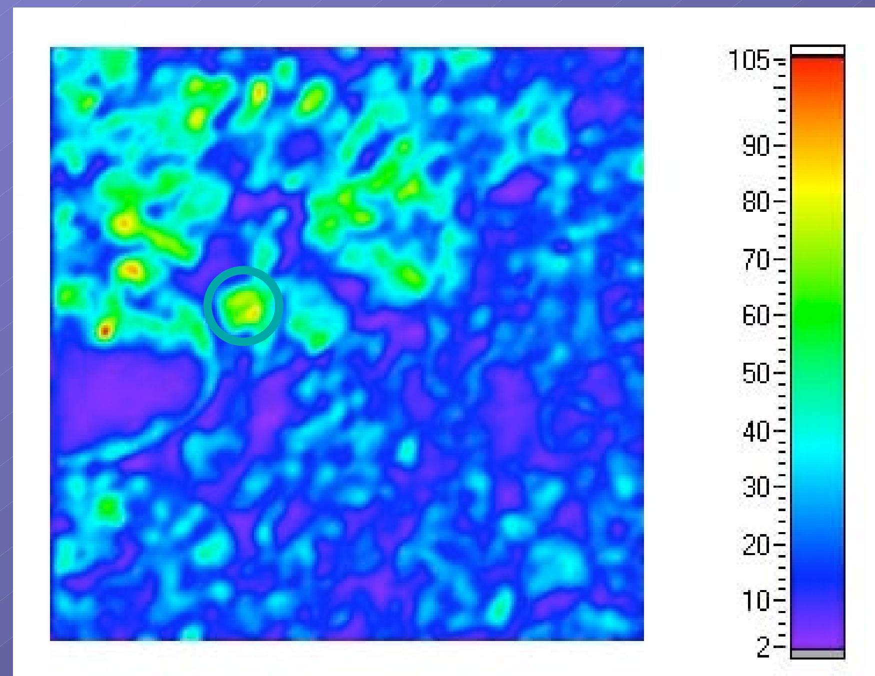

10x10 μm^2

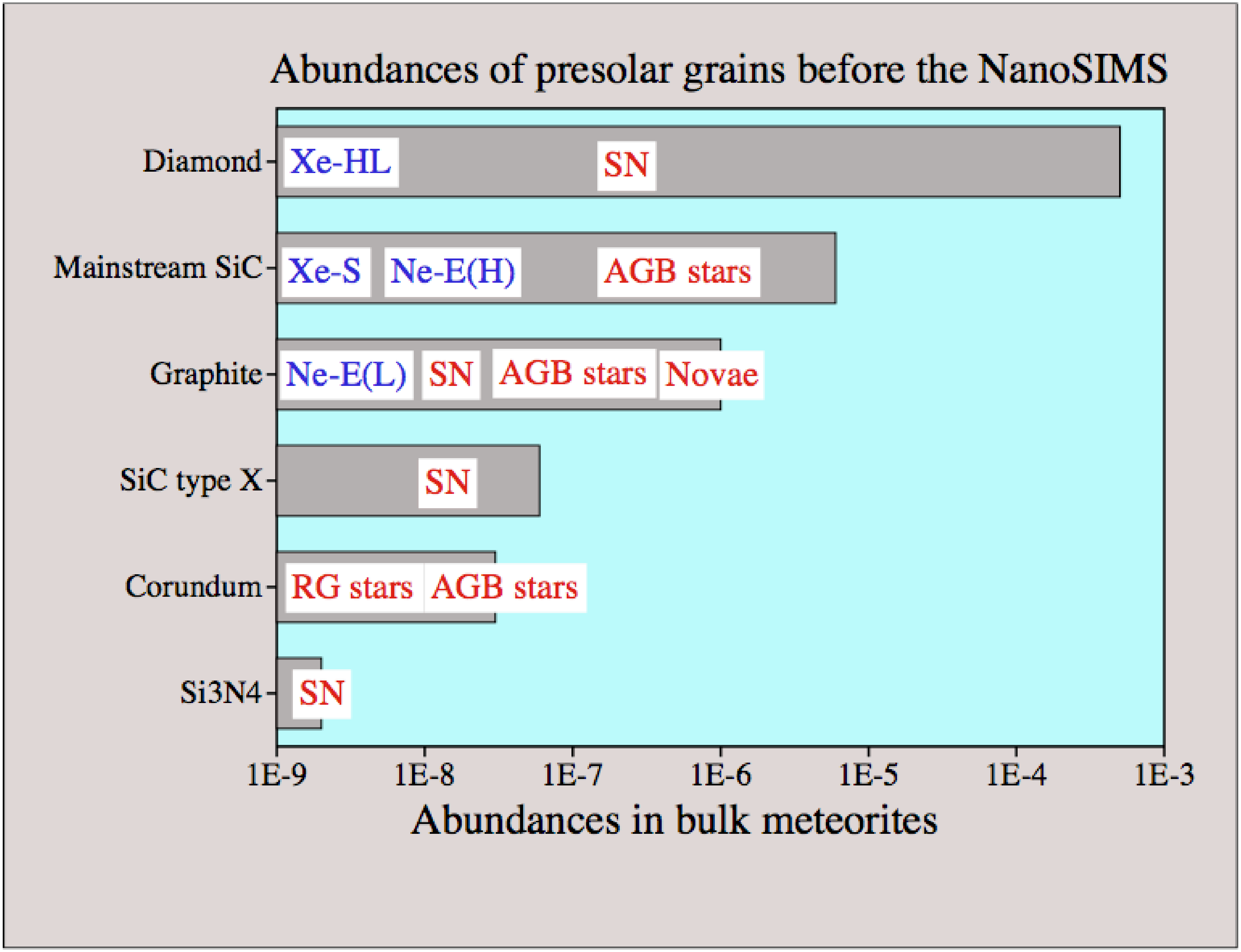
Abundances of presolar grains before the NanoSIMS
Diamond
Xe-HL
SN
Mainstream SiC
Xe-S
Ne-E(H)
AGB stars
Graphite
Ne-E(L)
SN
AGB stars
Novae
SiC type X
SN
Corundum
RG stars
AGB stars
Si3N4
SN
1E-9
1E-8
1E-7
1E-6
1E-5
1E-4
1E-3
Abundances in bulk meteorites

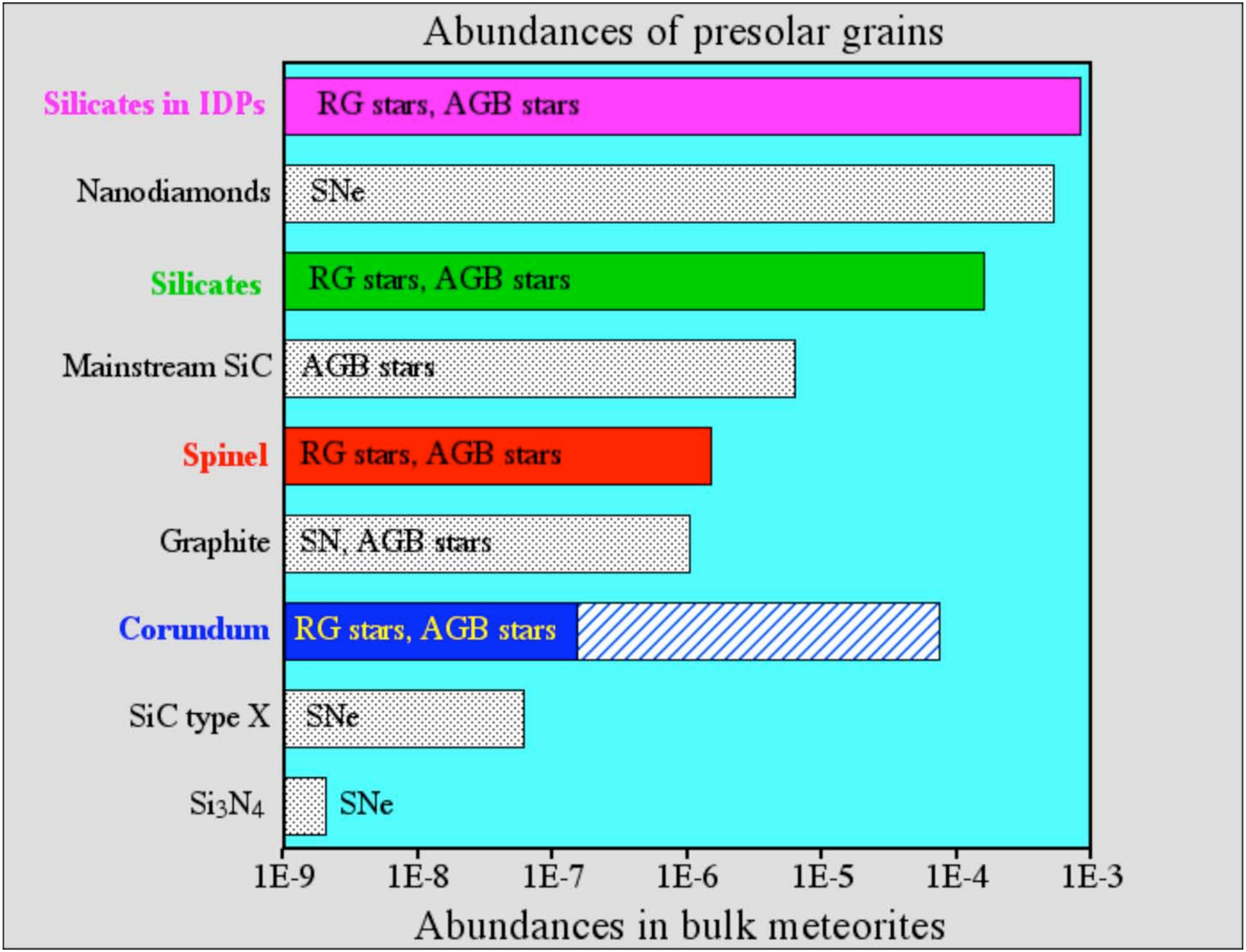

Abundances of presolar grains
Silicates in IDPs
RG stars, AGB stars
Nanodiamonds
SNe
Silicates
RG stars, AGB stars
Mainstream SiC
AGB stars
Spinel
RG stars, AGB stars
Graphite
SN, AGB stars
Corundum
RG stars, AGB stars
SiC type X
SNe
Si_3N_4
SNe
1E-9
1E-8
1E-7
1E-6
1E-5
1E-4
1E-3
Abundances in bulk meteorites

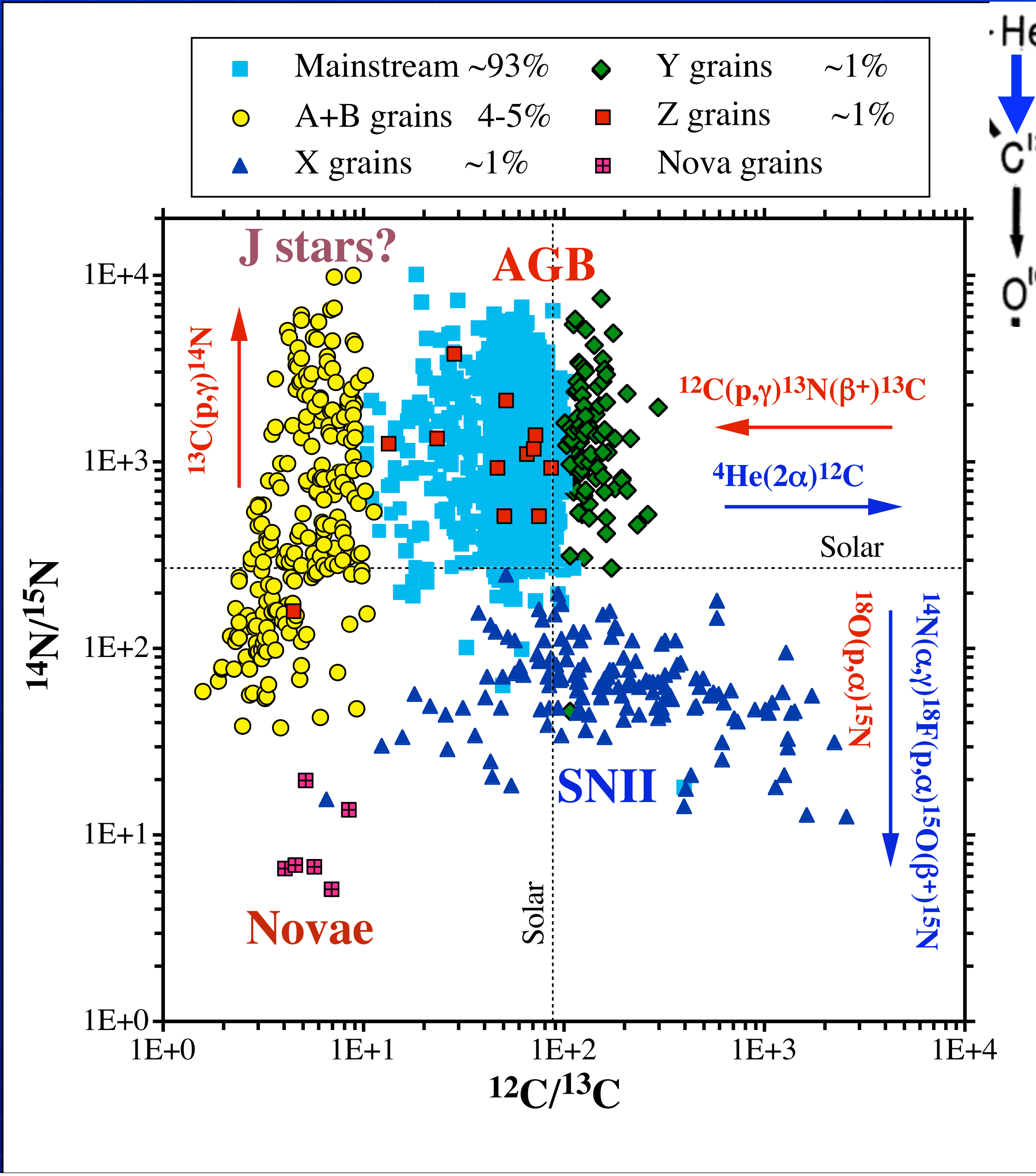

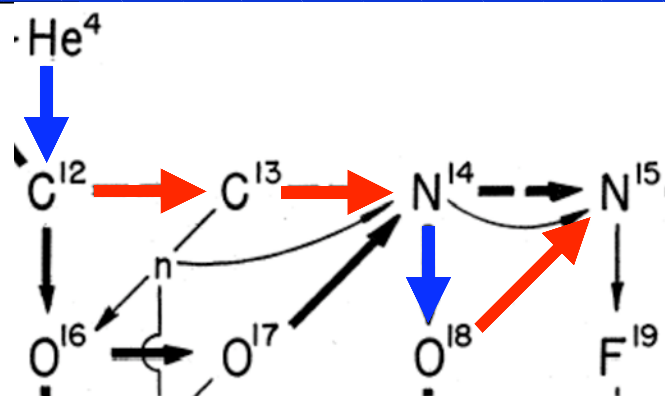

Signatures of H and He burning are shown by presolar SiC grains.

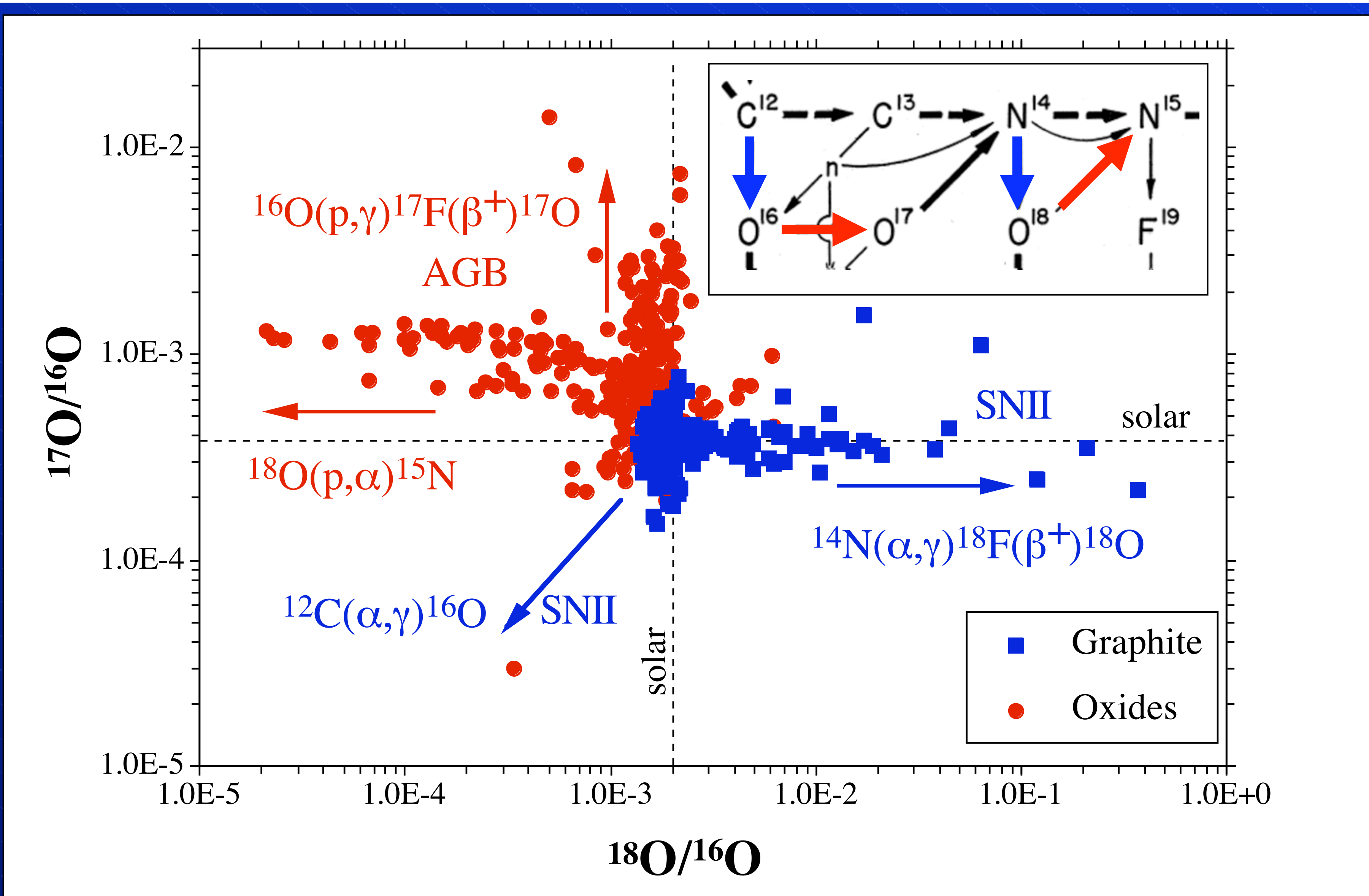

Signatures of Hydrogen and Helium burning are shown by presolar oxide and graphite grains.

Grains from AGB stars

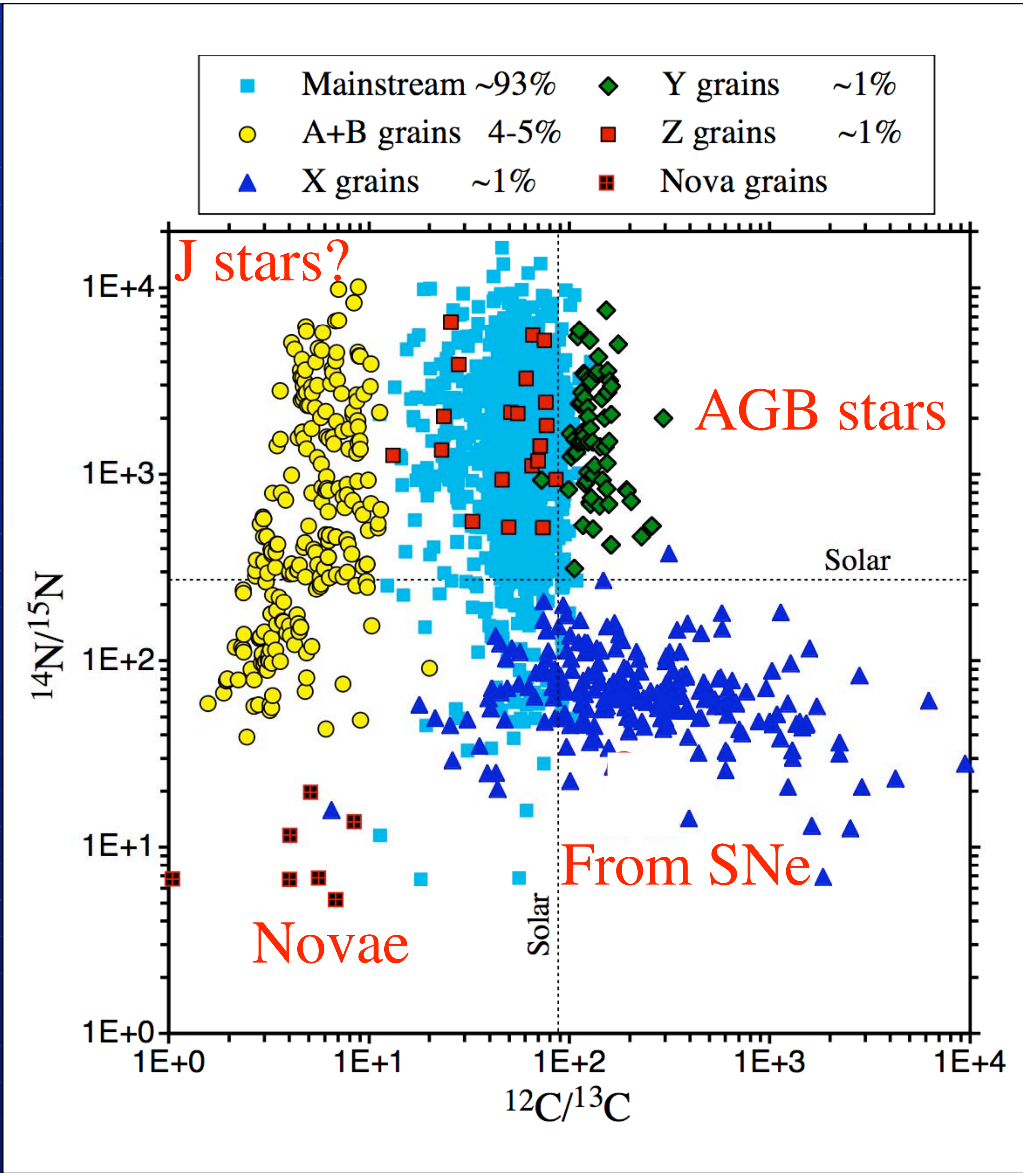

SiC grains come from different stellar sources

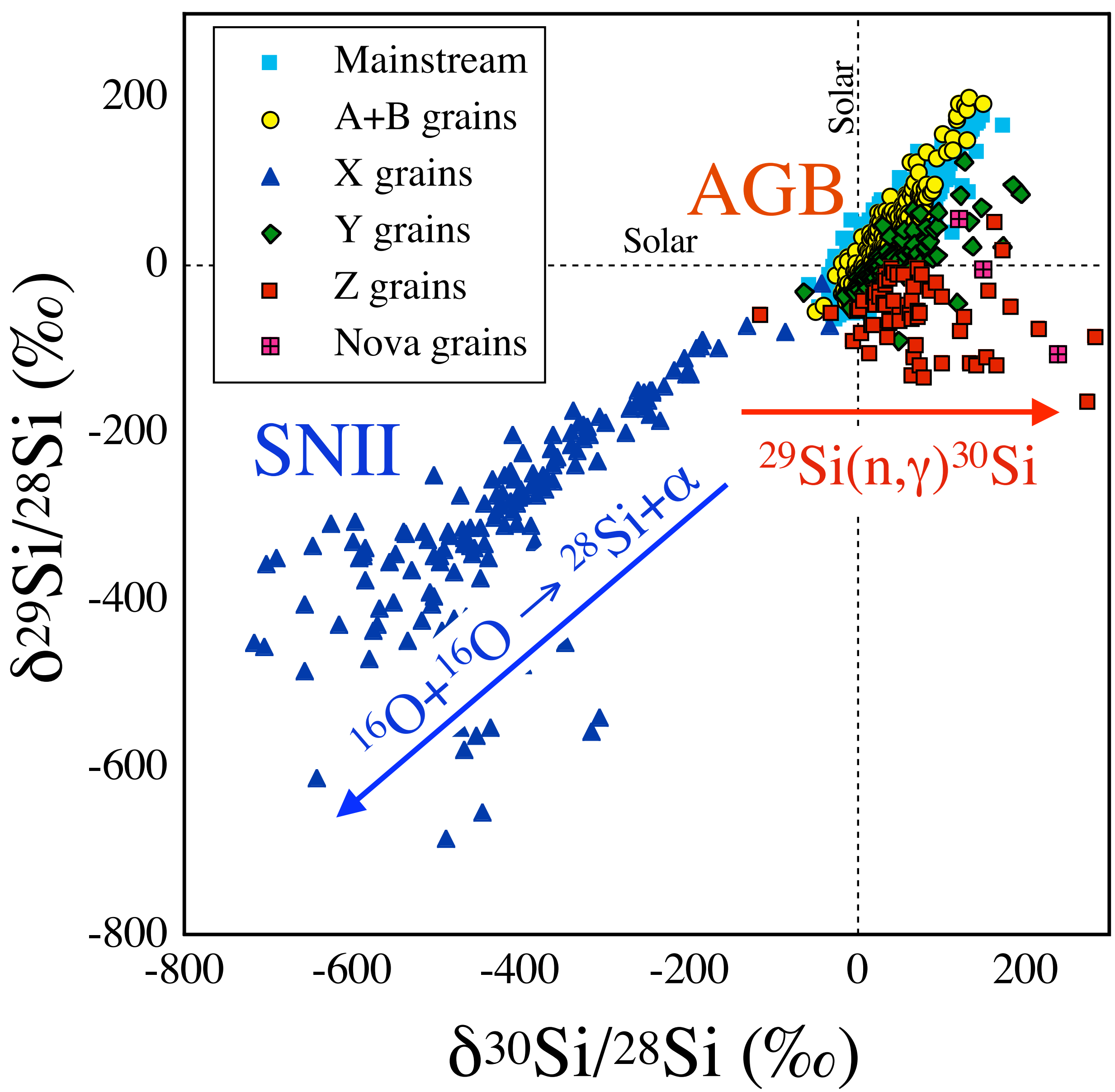

α process

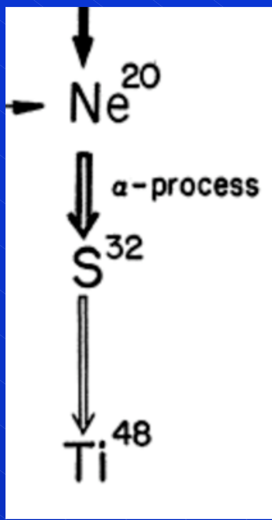

Si isotopes show the signatures of O burning and of neutron capture (s-process)

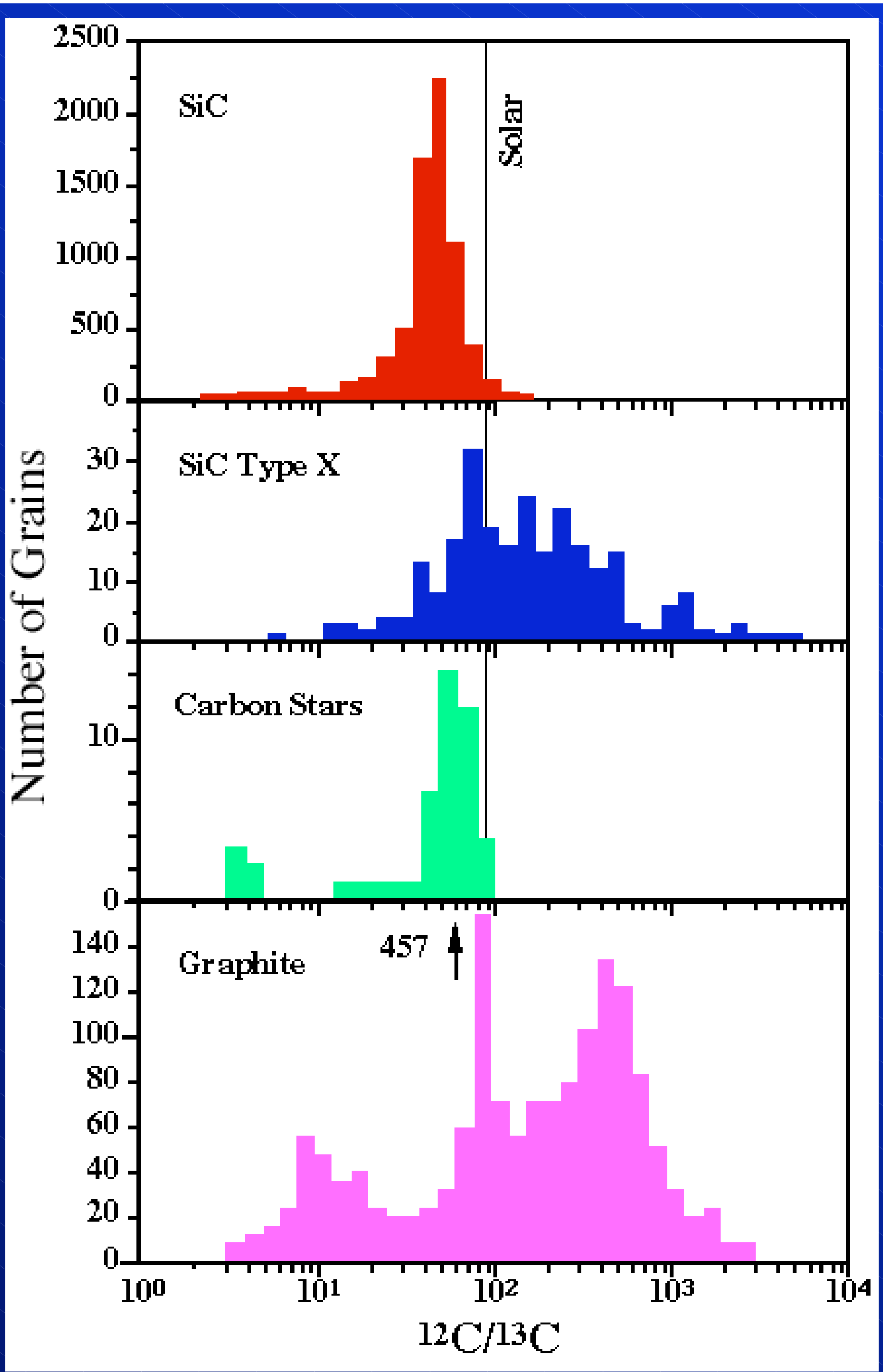

The distribution of carbon isotopic ratios in graphite grains is different from those of mainstream and SN SiC grains, indicating distinct stellar sources.

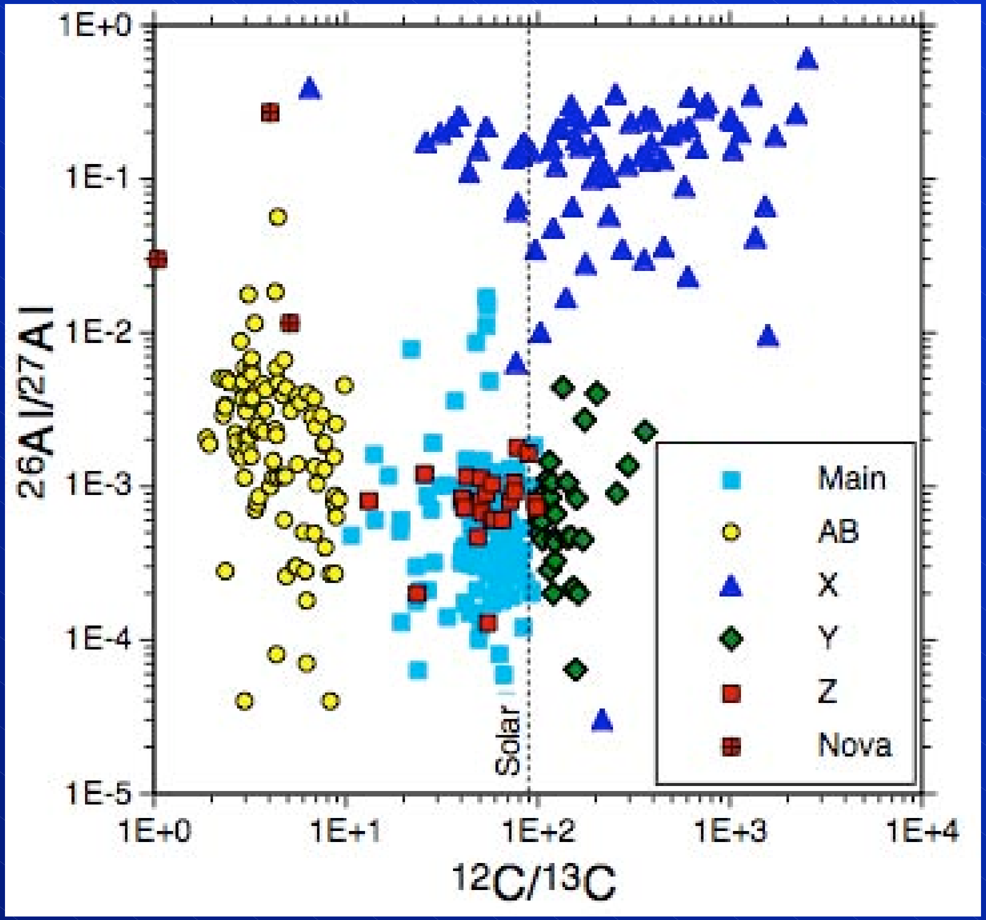

Also the inferred $^{26}Al/^{27}Al$ ratios are greatly different between X (SN) grains and other grains.

AGB stars

ess
yy
elements.

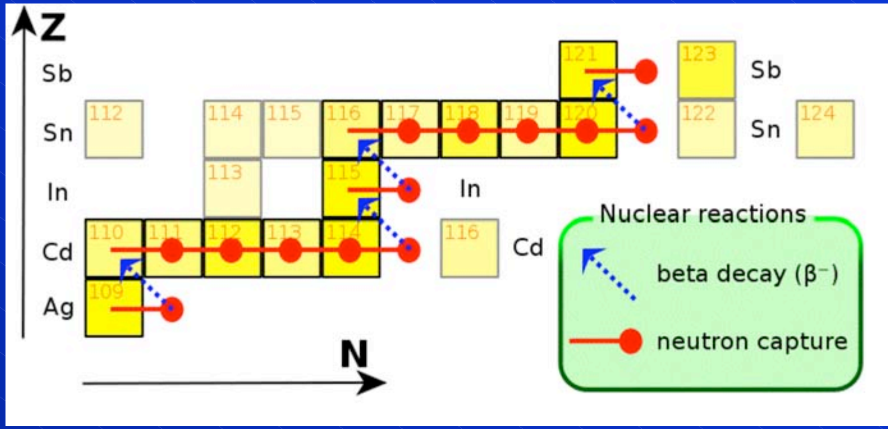

Z
Sb
Sn
In
Cd
Ag
N
112
114
115
116
117
118
119
120
121
123
122
124
113
115
110
111
112
113
114
116
109
Sb
Sn
In
Cd
Nuclear reactions
beta decay (β⁻)
neutron capture

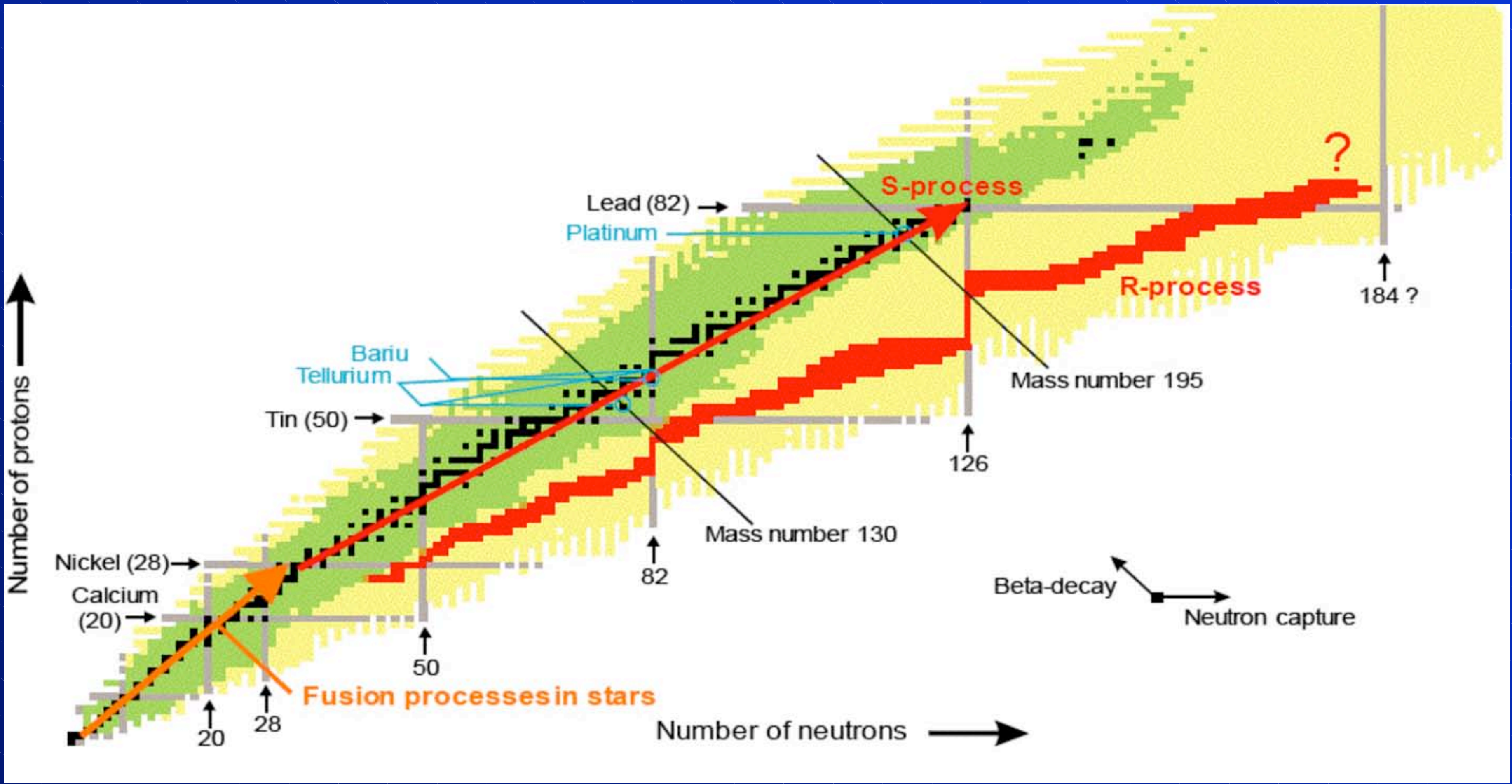

Lead (82)
Platinum
Bariu
Tellurium
Tin (50)
Nickel (28)
Calcium
(20)
S-process
R-process
?
184 ?
Mass number 195
126
Mass number 130
82
50
20
28
Fusion processes in stars
Beta-decay
Neutron capture
Number of protons
Number of neutrons

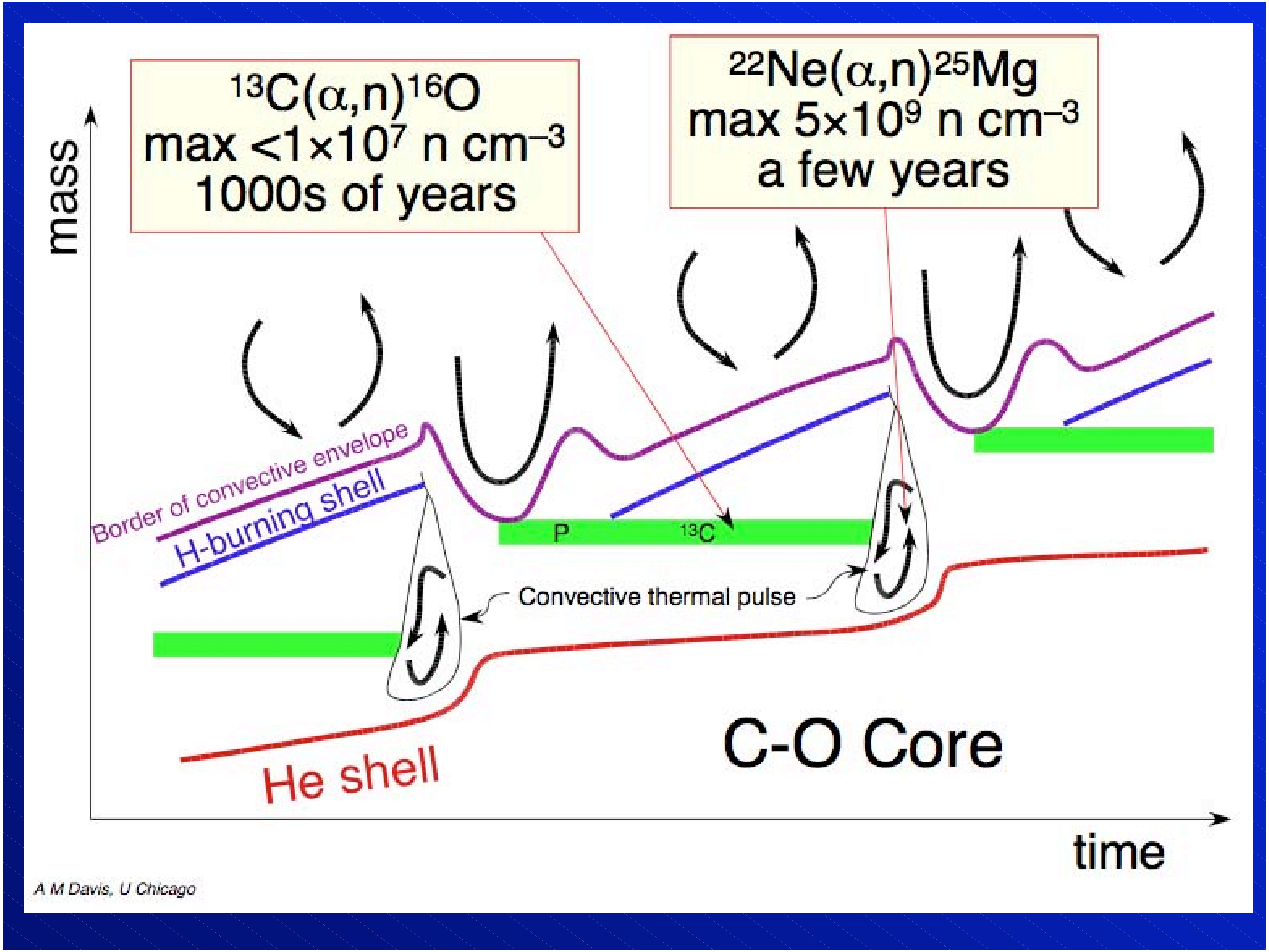

$^{13}C(\alpha,n)^{16}O$
max $<1\times10^{7}$ n cm^{-3}
1000s of years
$^{22}Ne(\alpha,n)^{25}Mg$
max 5×10^{9} n cm^{-3}
a few years
mass
Border of convective envelope
H-burning shell
P
^{13}C
Convective thermal pulse
He shell
C-O Core
time
A M Davis, U Chicago

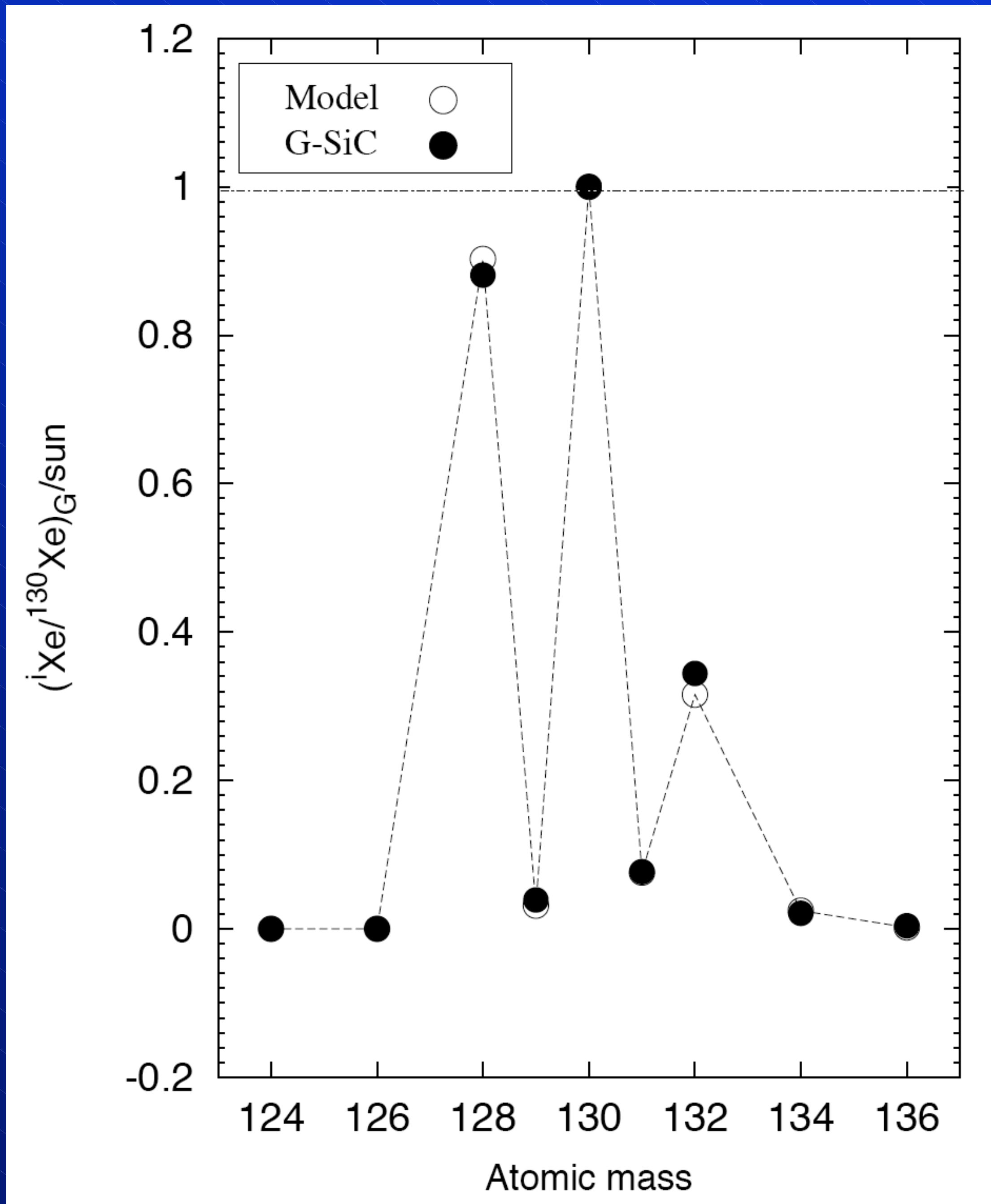

There is very good agreement between SiC data and AGB models.

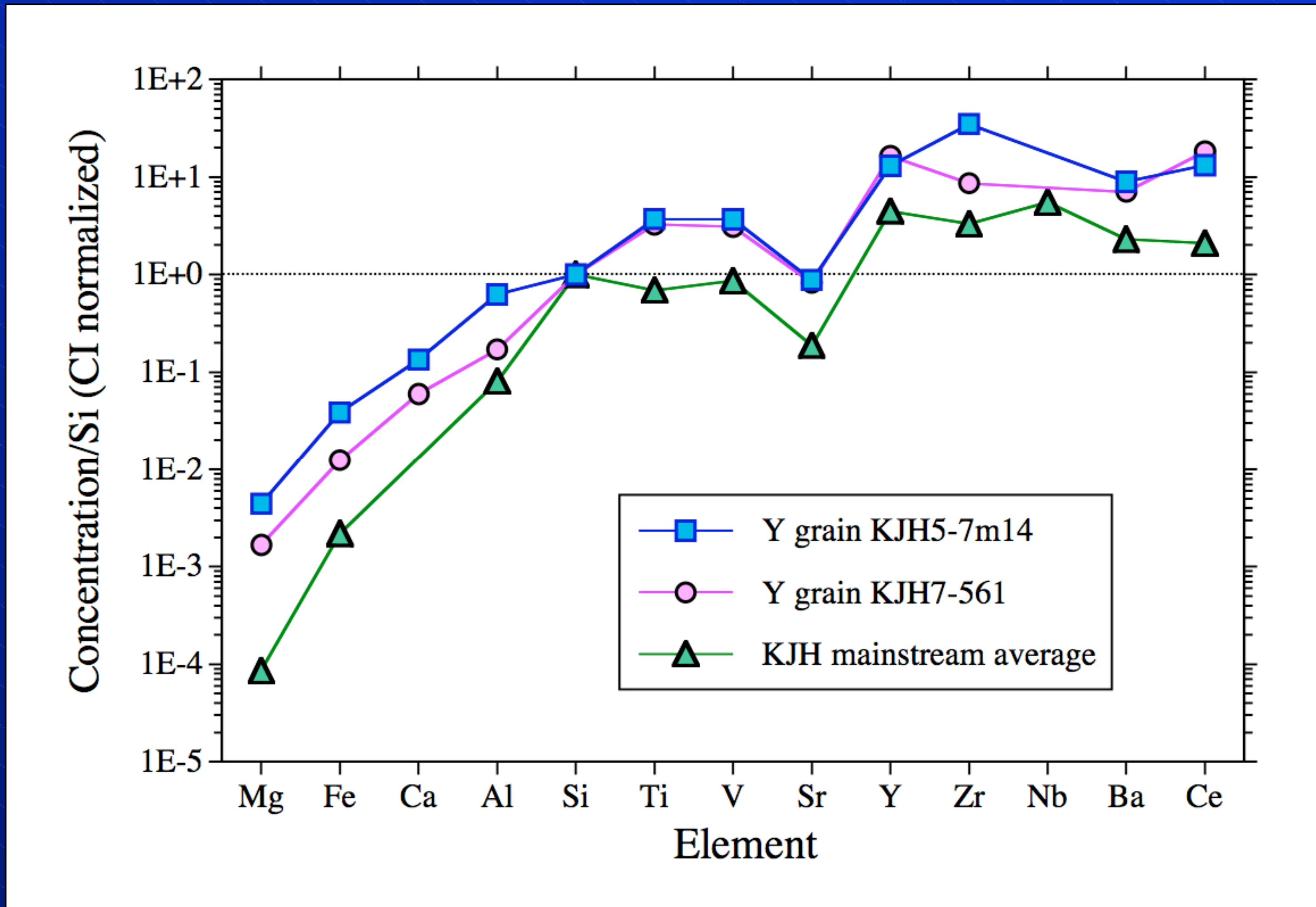

Abundance enhancements of s-process elements are another piece of evidence for an AGB origin of most SiC grains.

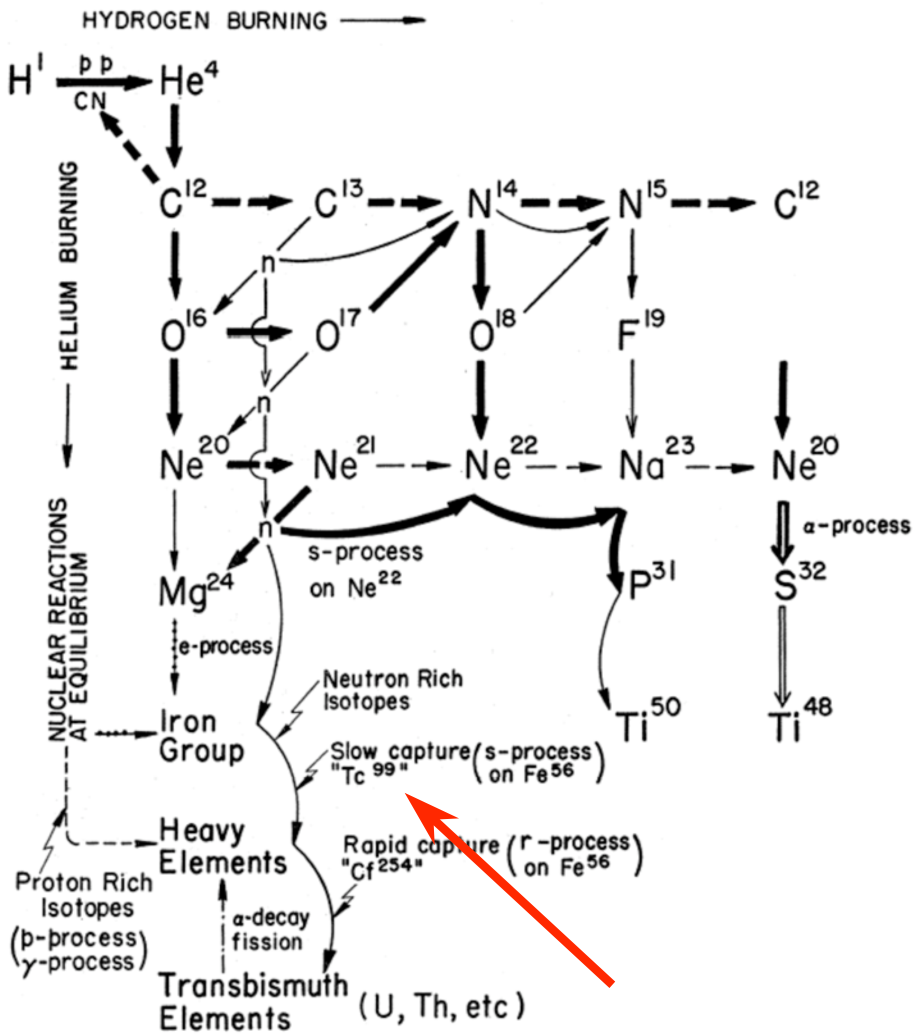

Savina et al. 2004

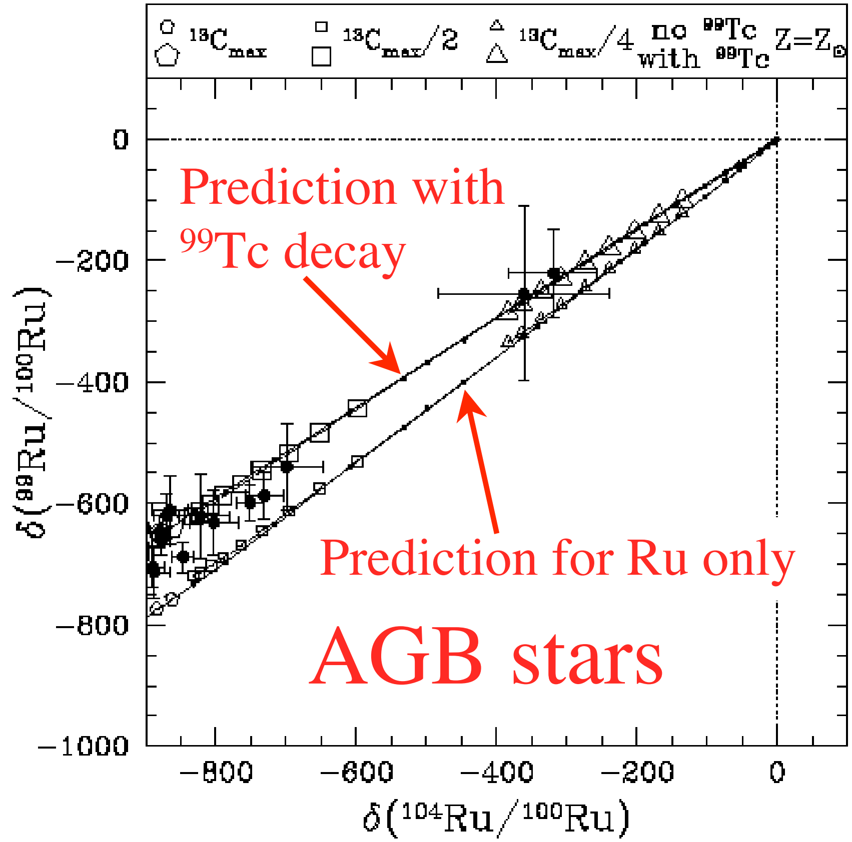

s process

Excesses of ^{99}Ru in presolar SiC above theoretical predictions for AGB stars are evidence for the initial presence of ^{99}Tc.

Two important pieces of information on s-process obtained from grains.

1) ^{96}Zr is extremely depleted, implying that the ^{22}Ne neutron source is not activated and grains do not come from intermediate mass stars.

2) The Ba isotopic ratios indicate that the "^{13}C-pocket" is within the standard pocket within a factor of less than two.

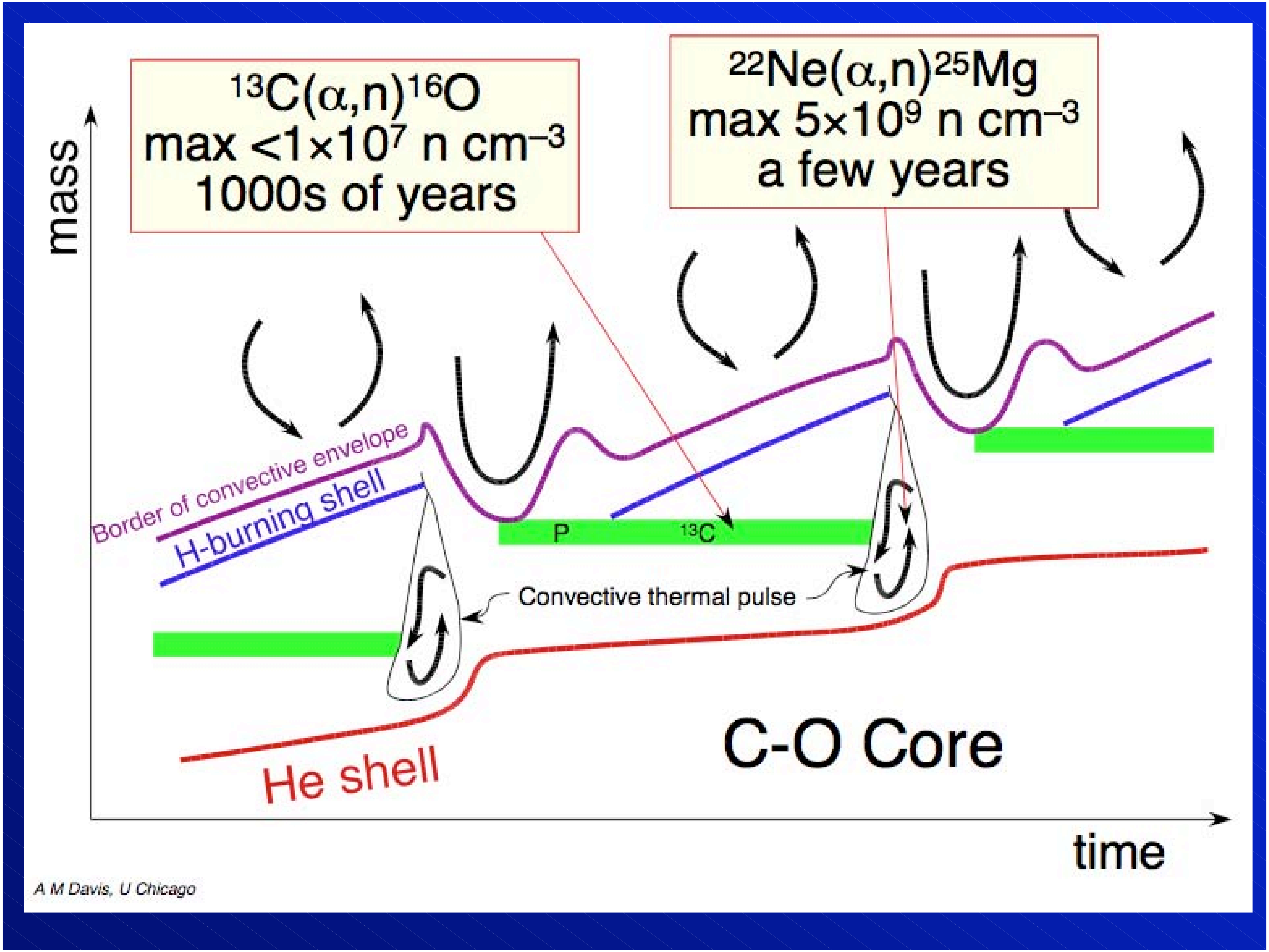

$^{13}C(\alpha,n)^{16}O$
max $<1\times10^{7}$ n cm^{-3}
1000s of years
$^{22}Ne(\alpha,n)^{25}Mg$
max 5×10^{9} n cm^{-3}
a few years
mass
Border of convective envelope
H-burning shell
P
^{13}C
Convective thermal pulse
C-O Core
He shell
time
A M Davis, U Chicago

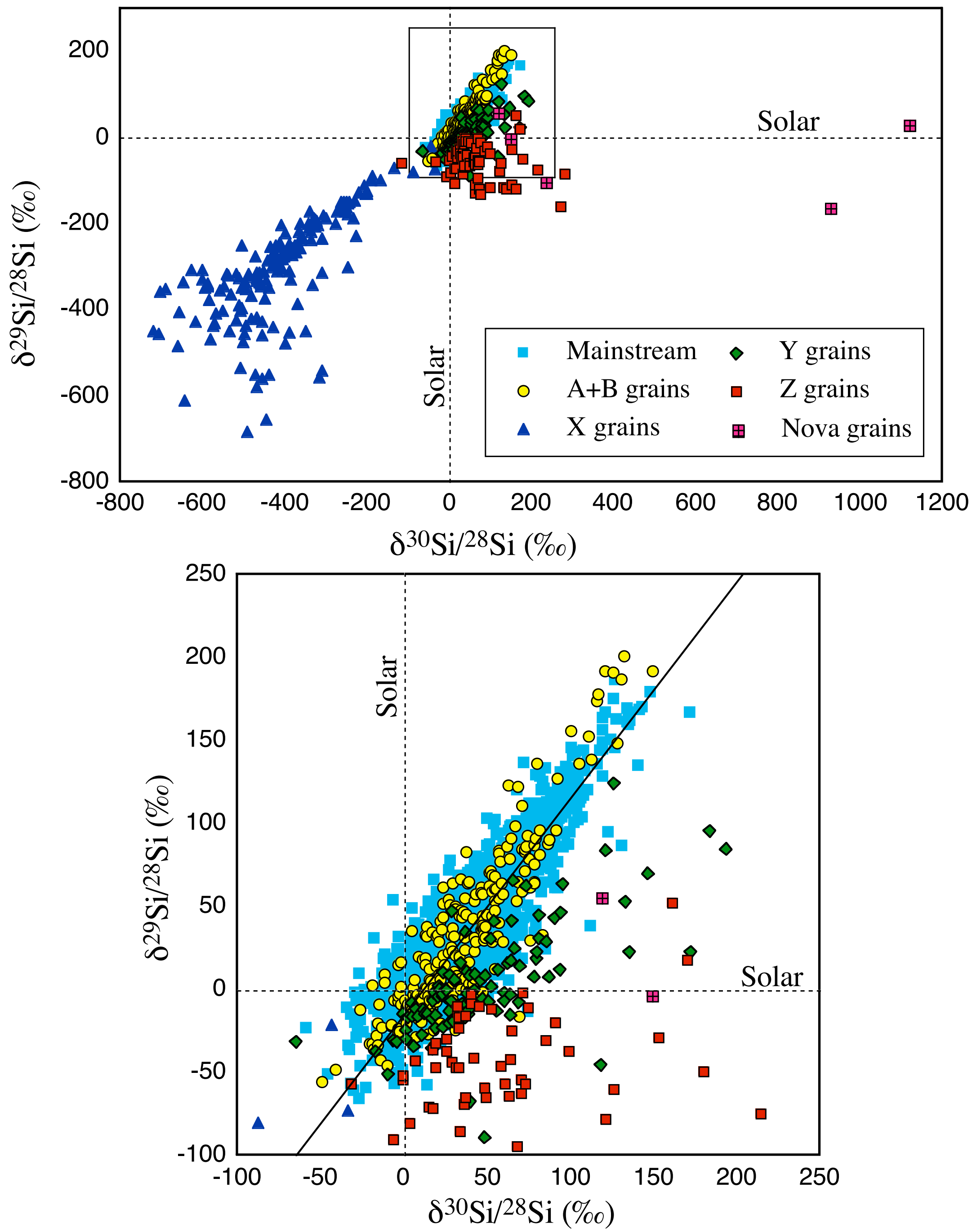

Different types of presolar SiC grains are defined by their C, N, and Si isotopic ratios.

The $^{29,30}Si$ excesses in presolar SiC grains are a problem.

Whereas the isotopic ratios of C, N, and the heavy elements (Sr, Zr, Mo, etc.) in SiC from AGB stars are completely dominated by stellar nucleosynthesis, the elements Si and Ti carry the signatures of both Galactic evolution (original compositions of the parent stars) and AGB nucleosynthesis (neutron capture).

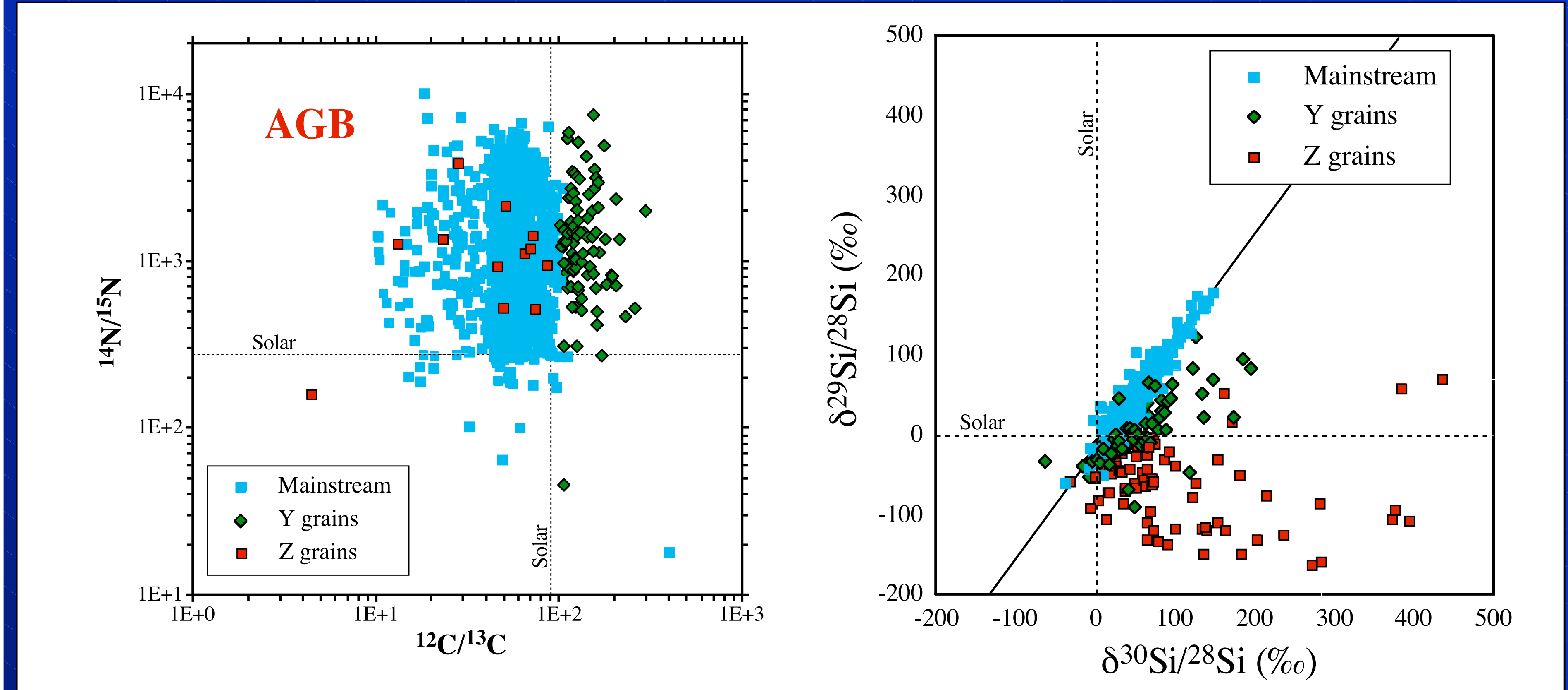

Mainstream, Y and Z grains are believed to have originated in C-rich AGB stars of varying metallicities.

Structure of AGB star

Busso et al. (1999)

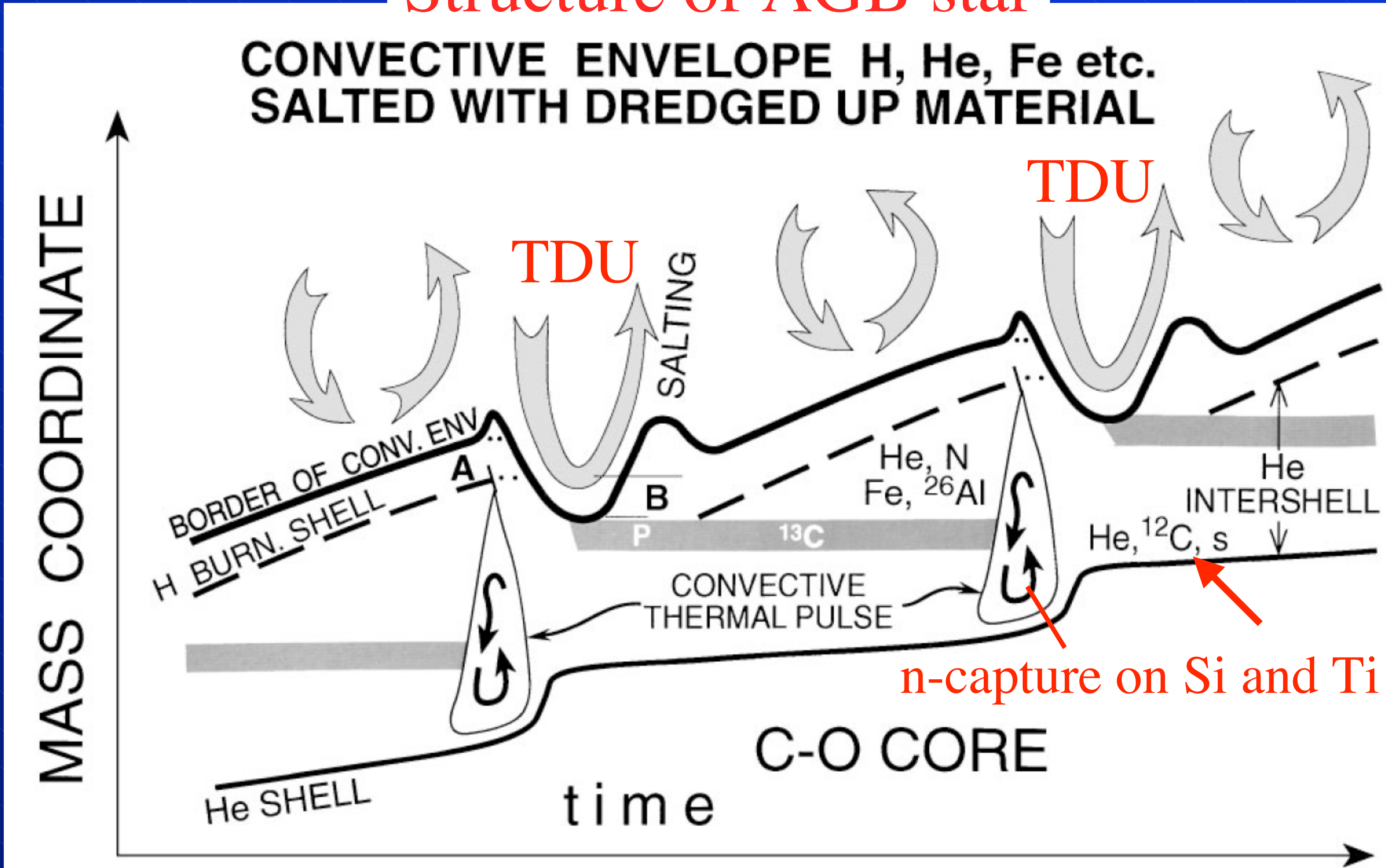

1. Dredge-up of ^{12}C turns the star into a C-star and increases the $^{12}C/^{13}C$ ratio
2. n capture on Si increases the $^{30}Si/^{28}Si$ ratio

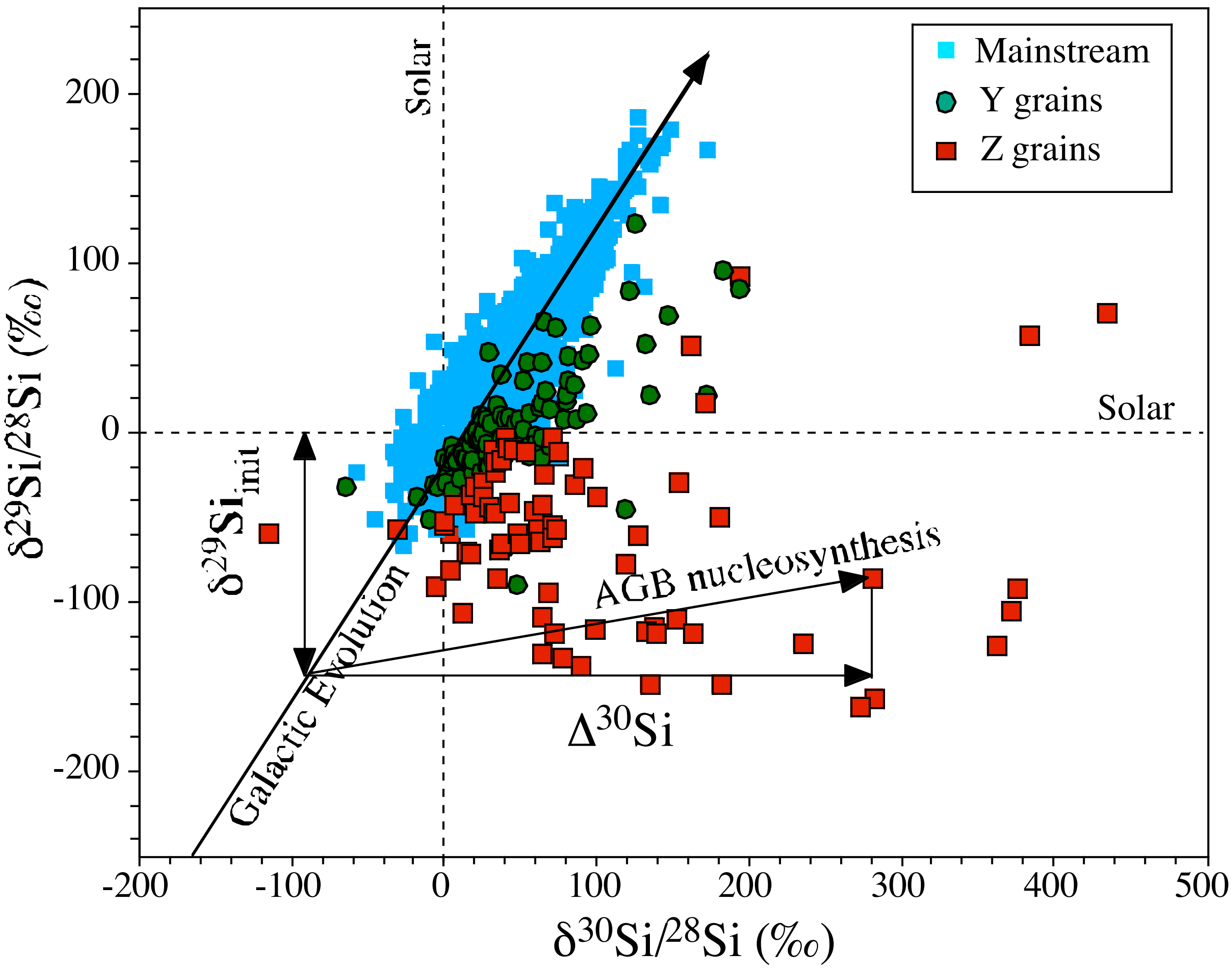

Deconvolve the Si isotopic composition of a given grain into a Galactic component $\delta^{29}Si_{init}$ and an AGB component $\Delta^{30}Si$.

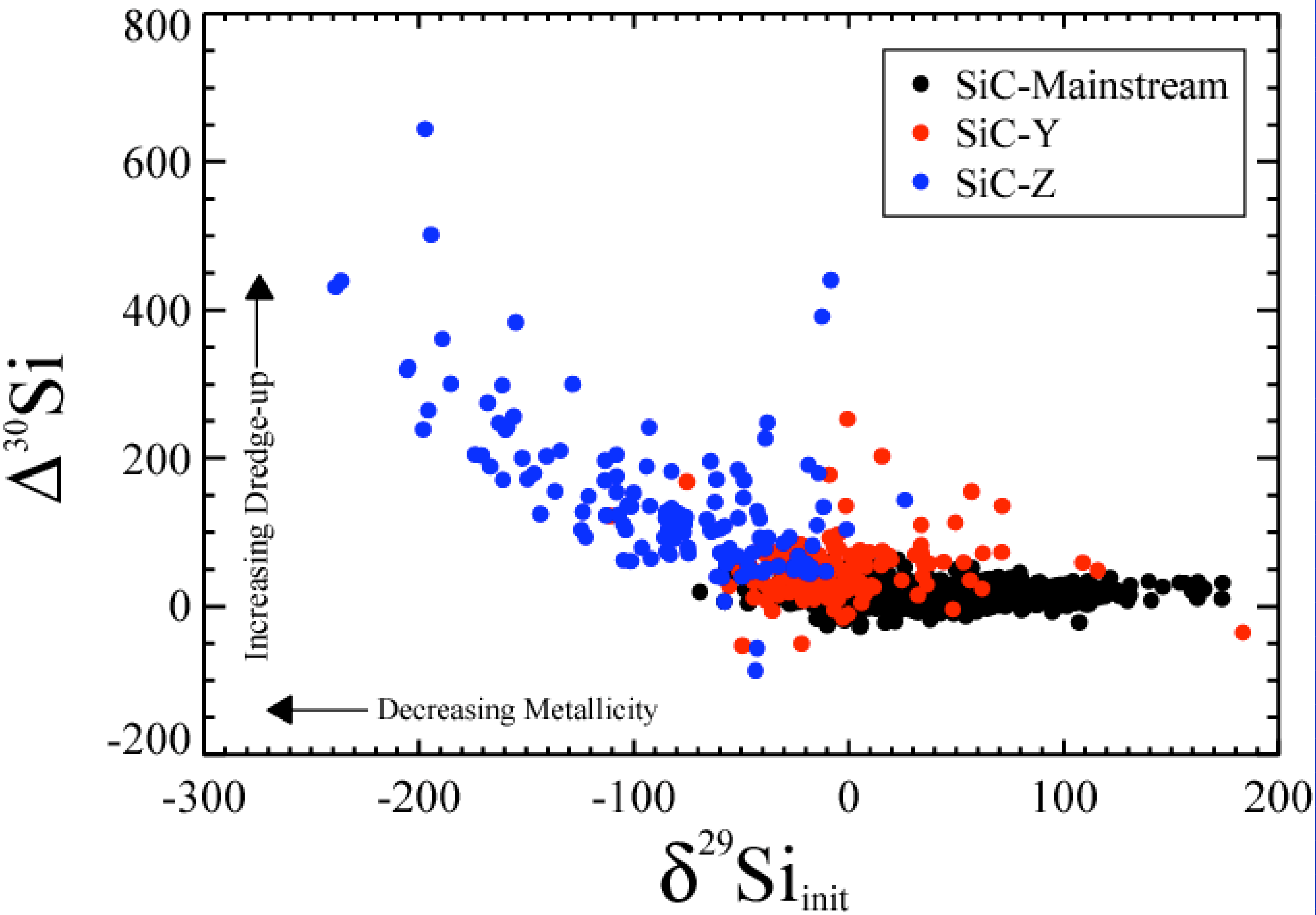

SiC-Mainstream
SiC-Y
SiC-Z
Increasing Dredge-up
Decreasing Metallicity
$\Delta^{30}Si$
$\delta^{29}Si_{init}$
800
600
400
200
0
-200
-300
-200
-100
0
100
200

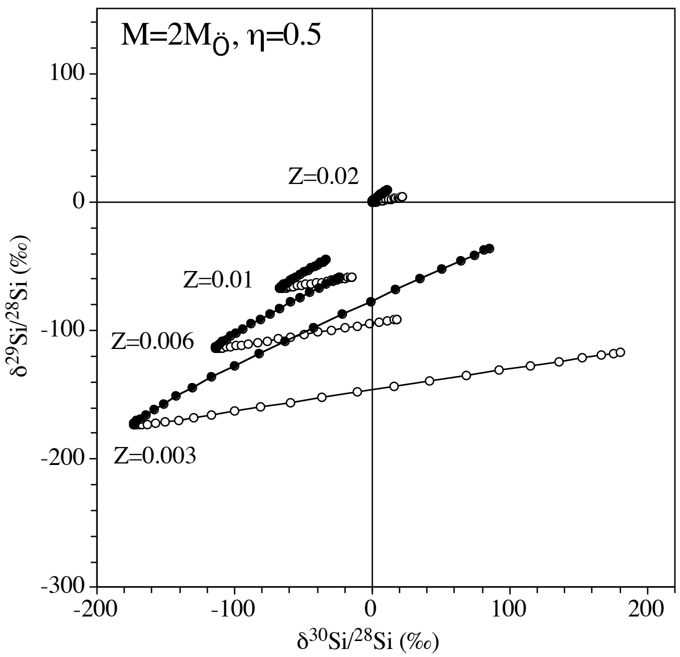

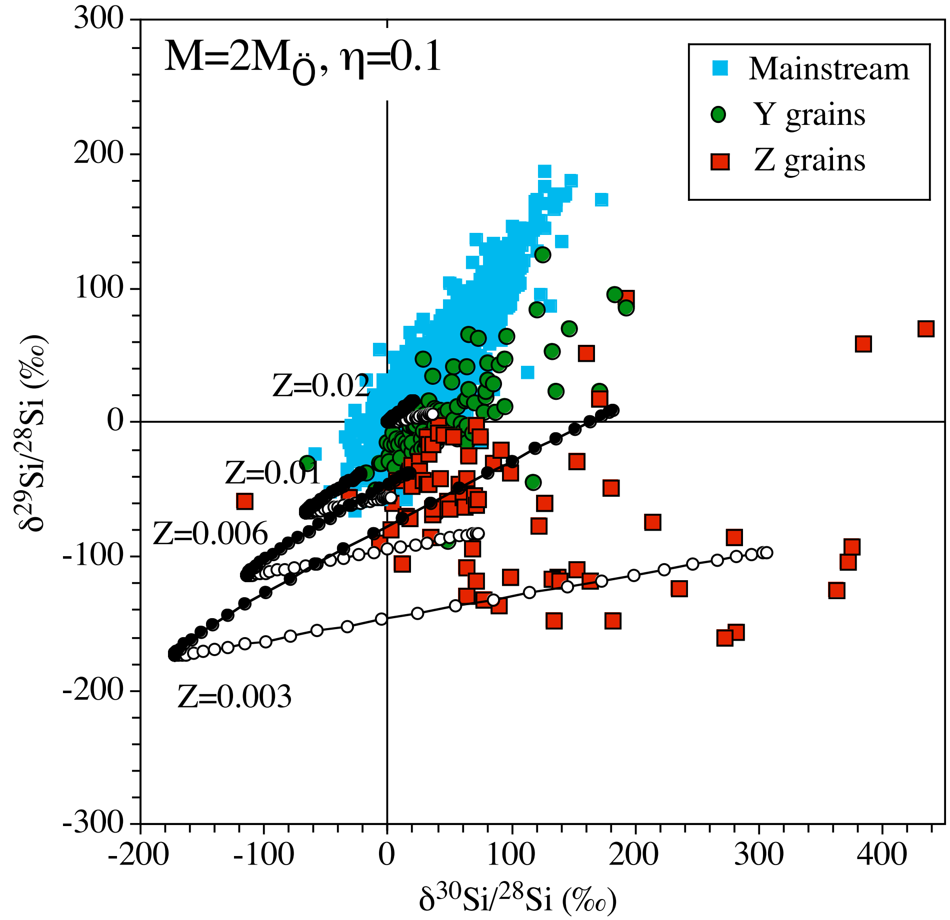

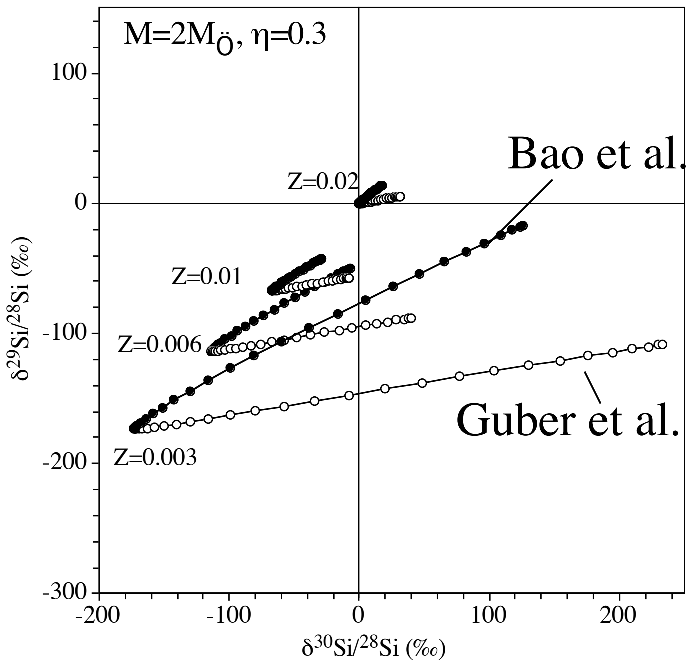

Models of AGB stars predict Si isotopic shifts for different masses, metallicities and mass loss. The Guber et al. cross sections account better for the isotopic ratios of the Z grains.

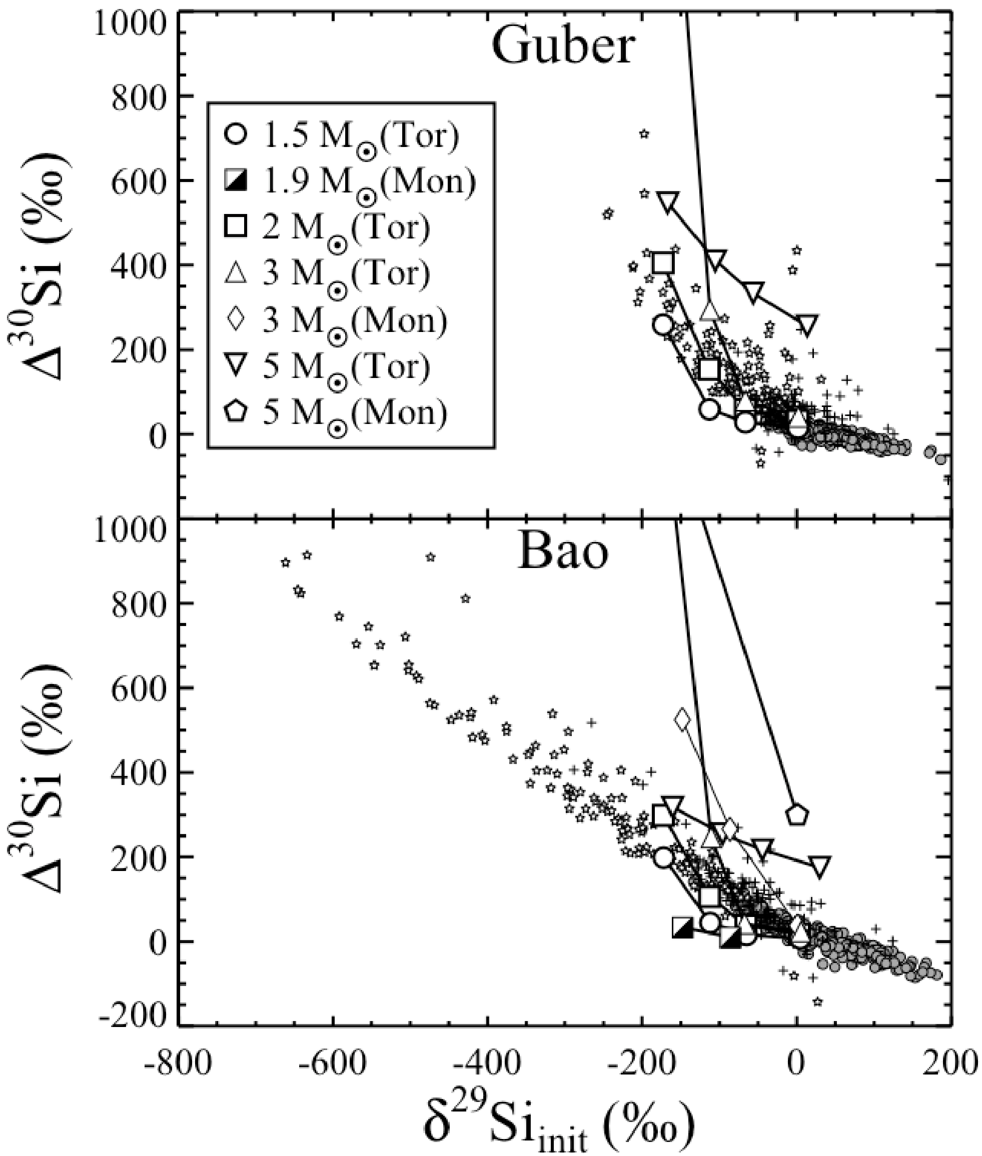

As expected, the data show a correlation between the Galactic component $\delta^{29}Si_{init}$ and the ABG component $\Delta^{30}Si$. Models with the Guber cross sections give a better fit to the data.

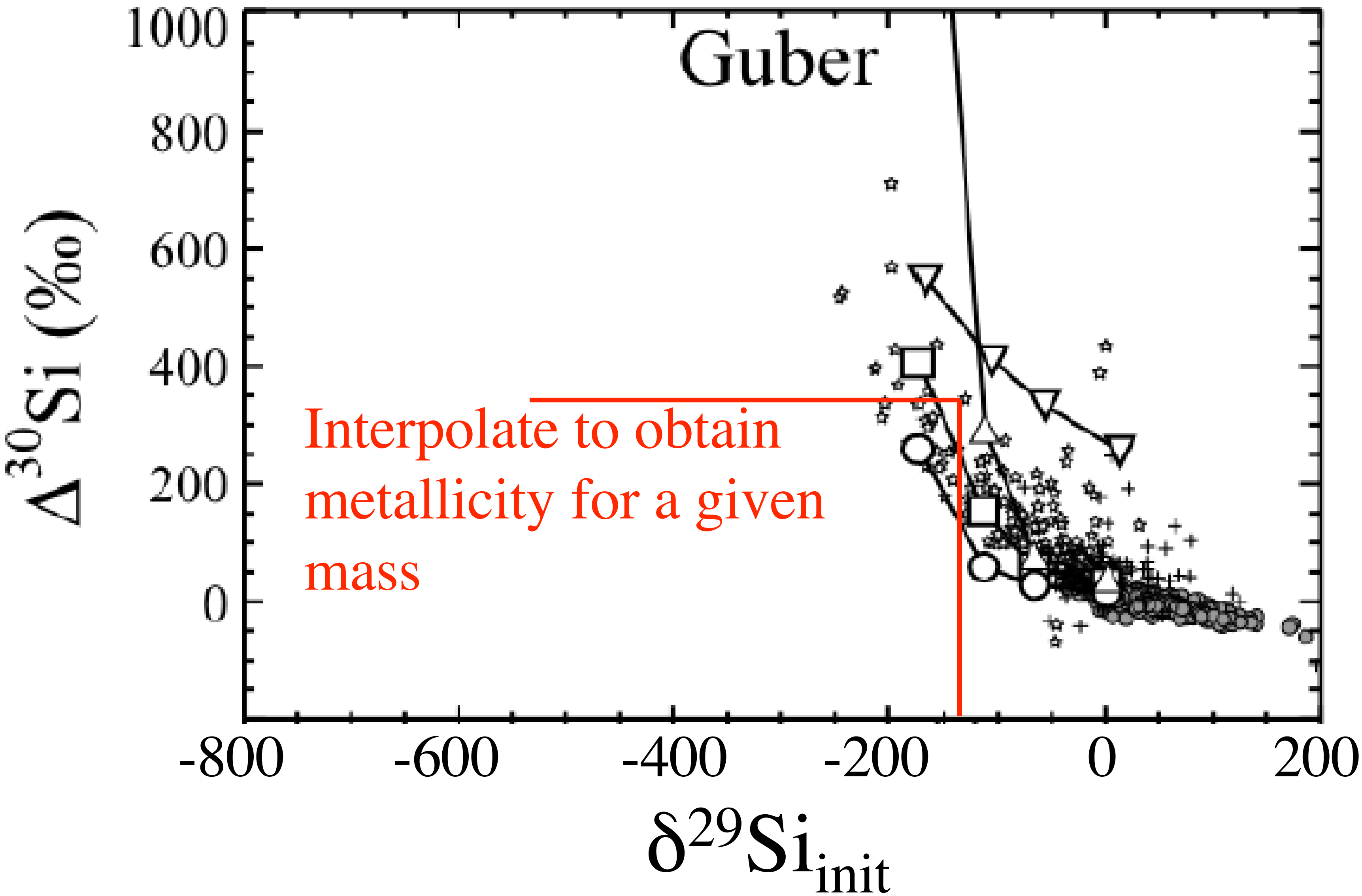

Guber
Interpolate to obtain metallicity for a given mass
1000
800
600
400
200
0
-800
-600
-400
-200
0
200
$\Delta^{30}Si$ (‰)
$\delta^{29}Si_{init}$

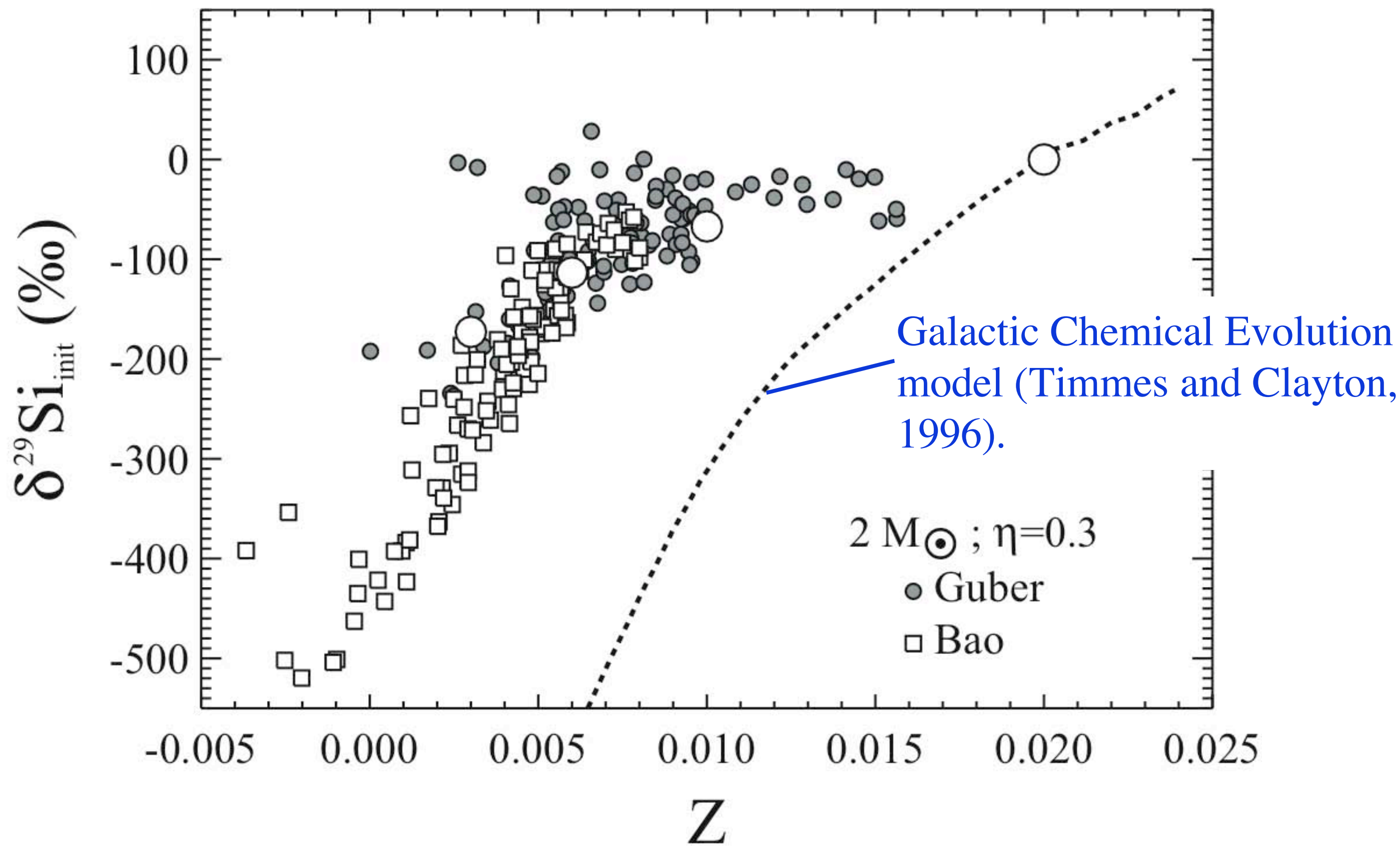

The grains' Δ^{30}Si values and the models can be used to infer the metallicity Z of each grain. Thus it is possible to determine $\delta^{29}Si_{init}$ as function of Z, i.e., the Galactic evolution of the Si isotopic ratios. The grain data indicate that Si ratios rise much faster than predicted by SNII-based GCE models.

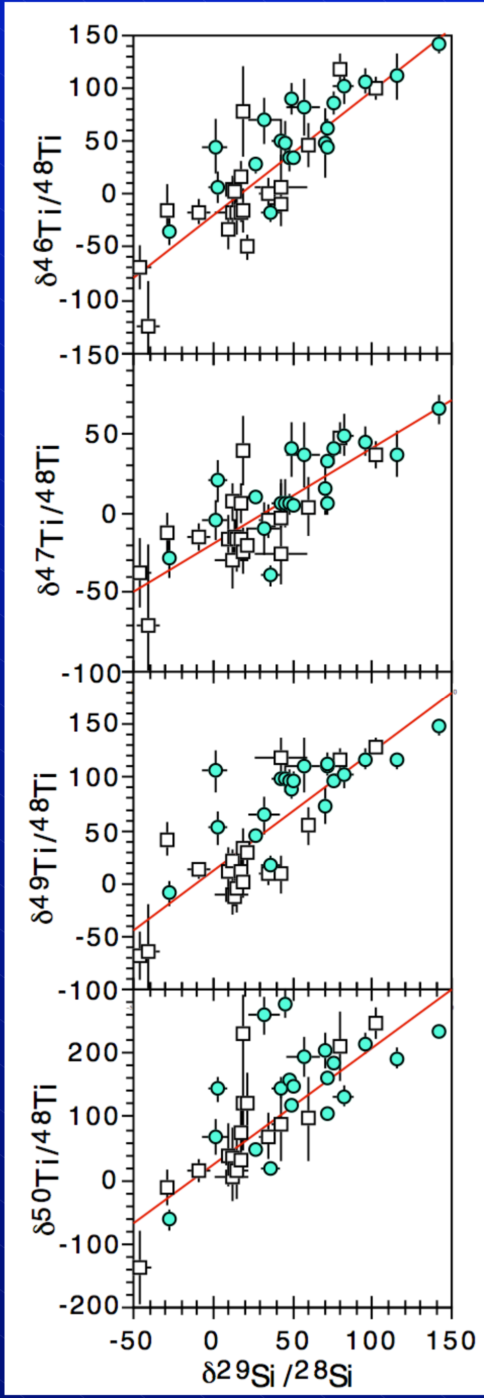

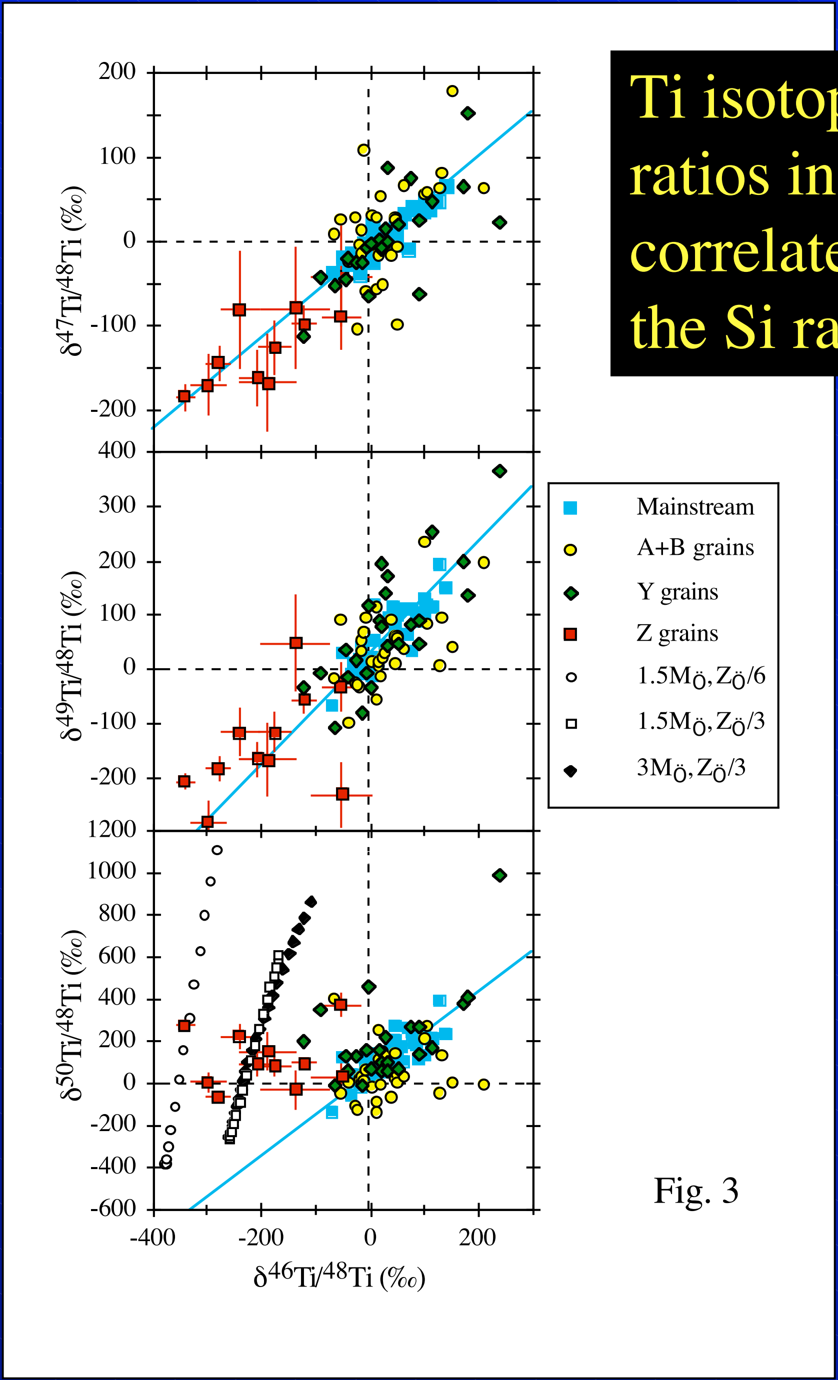

Ti isotopic ratios in SiC are correlated with the Si ratios.

Fig. 3

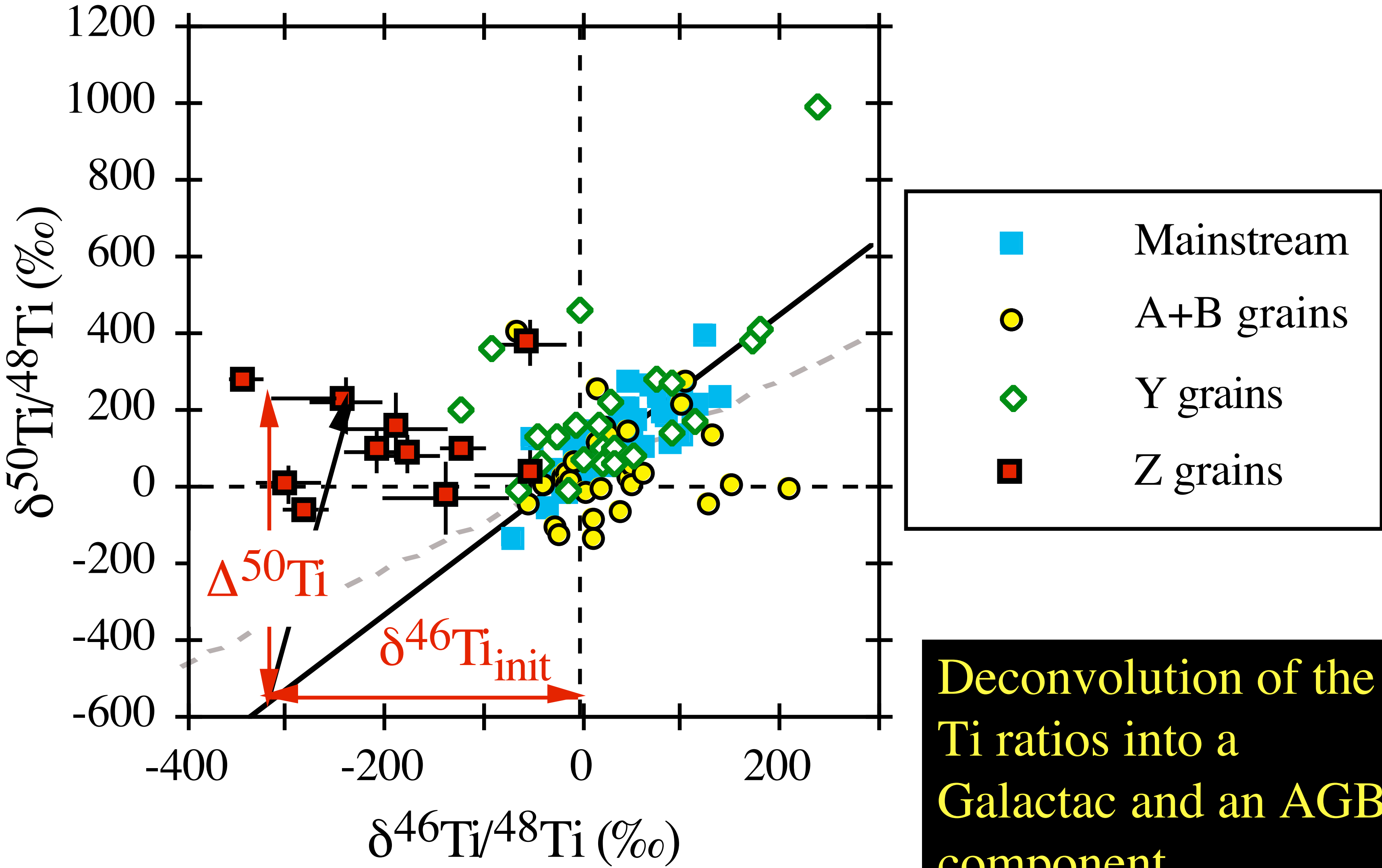

Deconvolution of the Ti ratios into a Galactac and an AGB component.

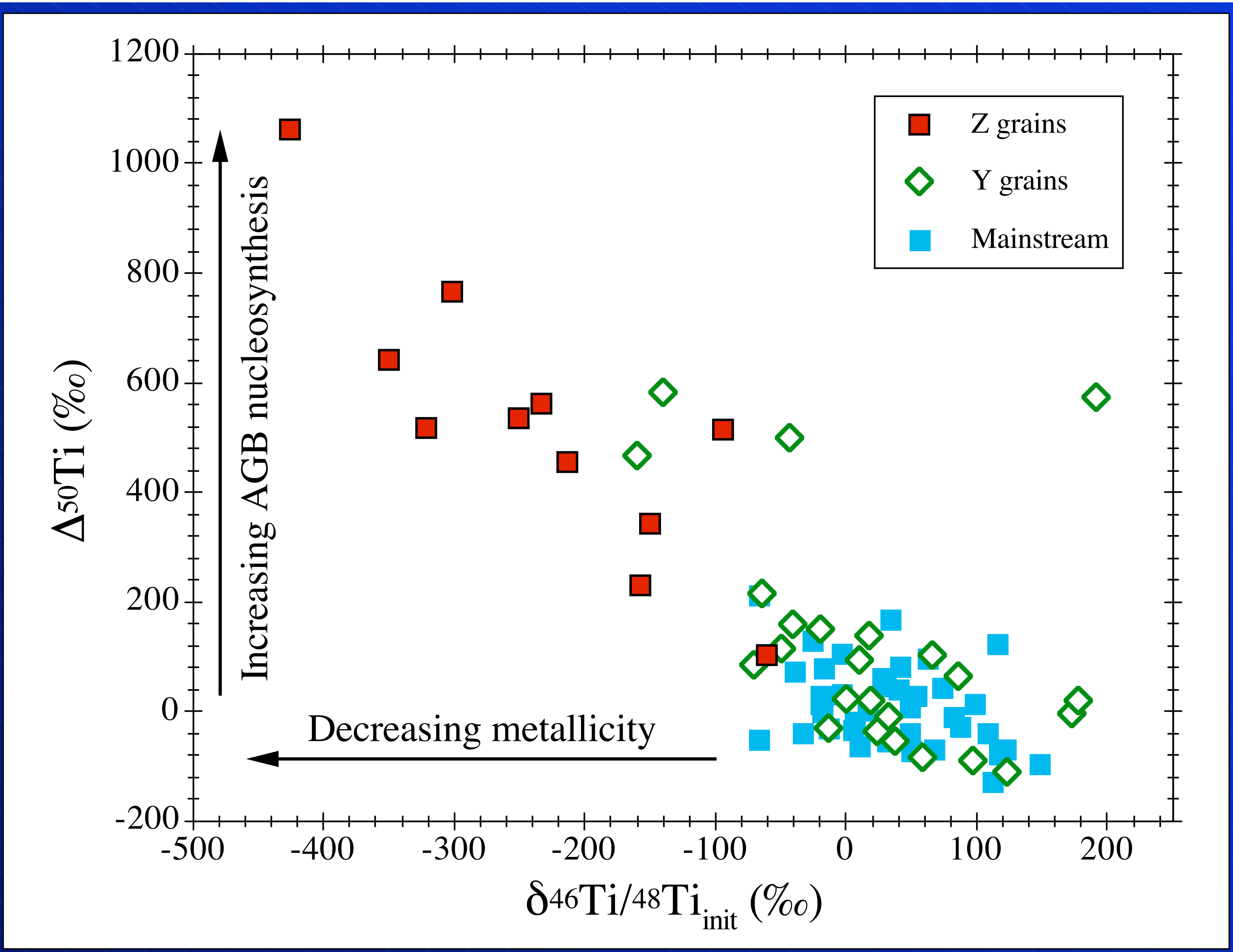

Z grains
Y grains
Mainstream
Increasing AGB nucleosynthesis
Decreasing metallicity
Δ^{50}Ti (‰)
$\delta^{46}Ti/^{48}Ti_{init}$ (‰)
1200
1000
800
600
400
200
0
-200
-500
-400
-300
-200
-100
0
100
200

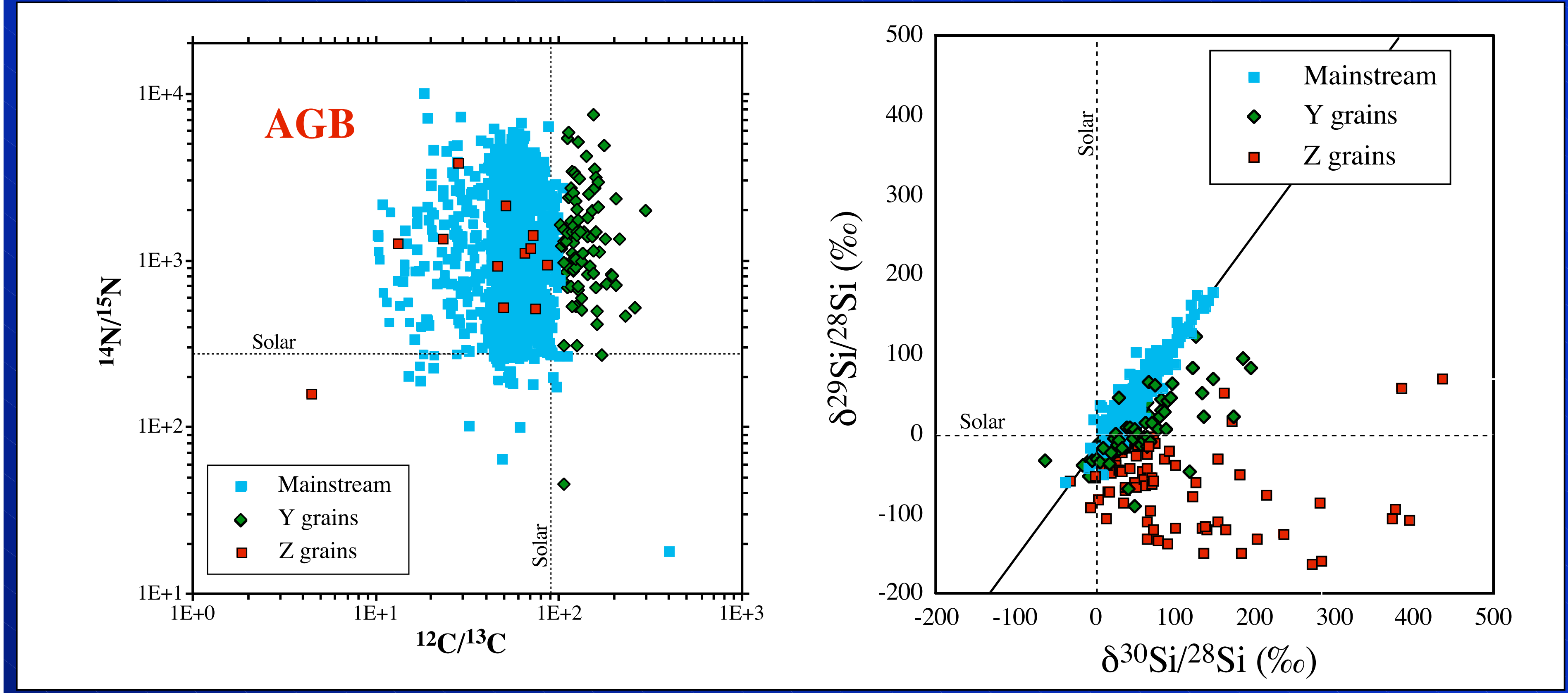

Mainstream, Y and Z grains are believed to have originated in C-rich AGB stars of varying metallicities.

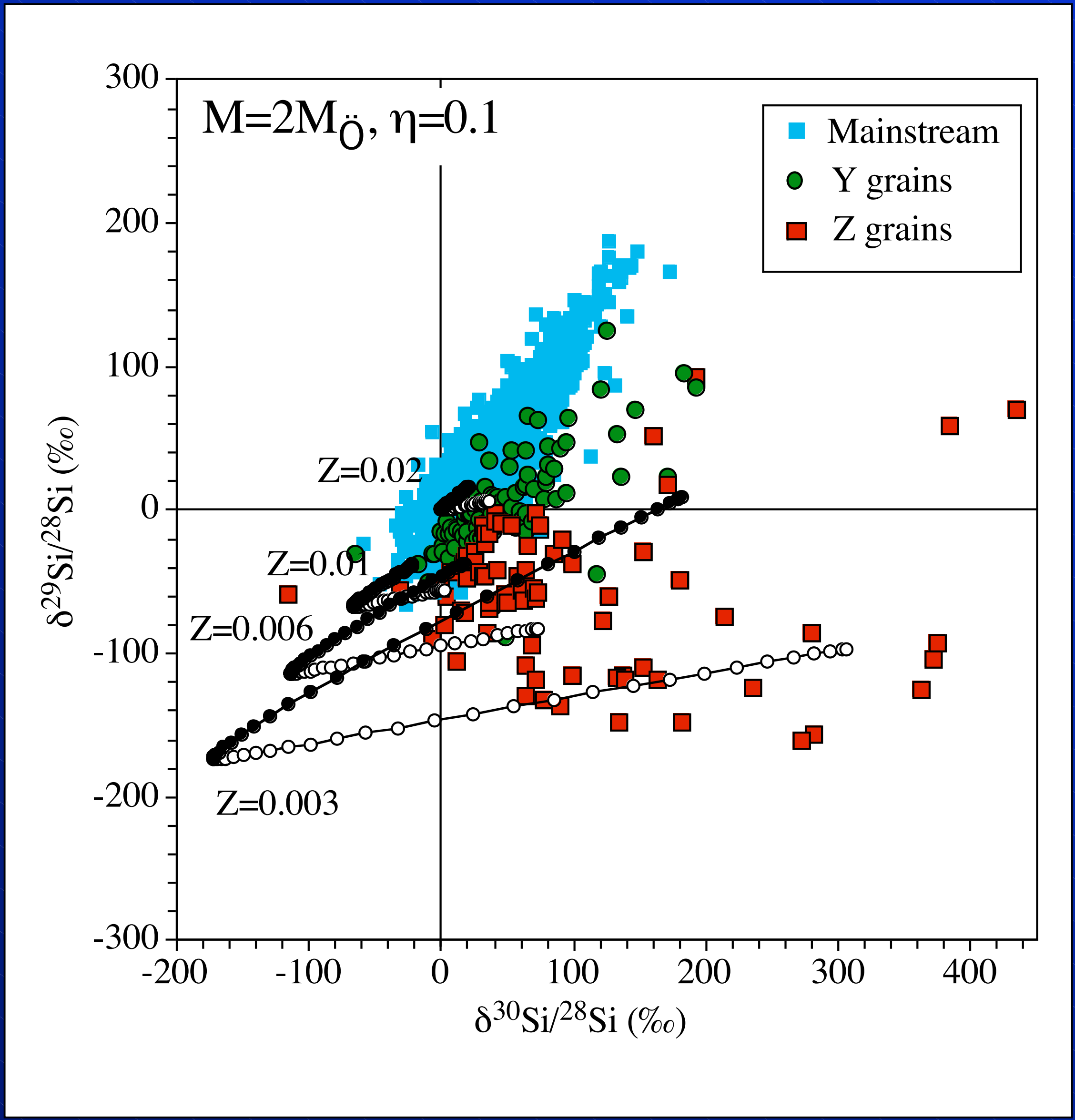

Models of AGB stars predict Si isotopic shifts for different masses, metallicities and mass loss. The Guber et al. cross sections account better for the isotopic ratios of the Z grains.

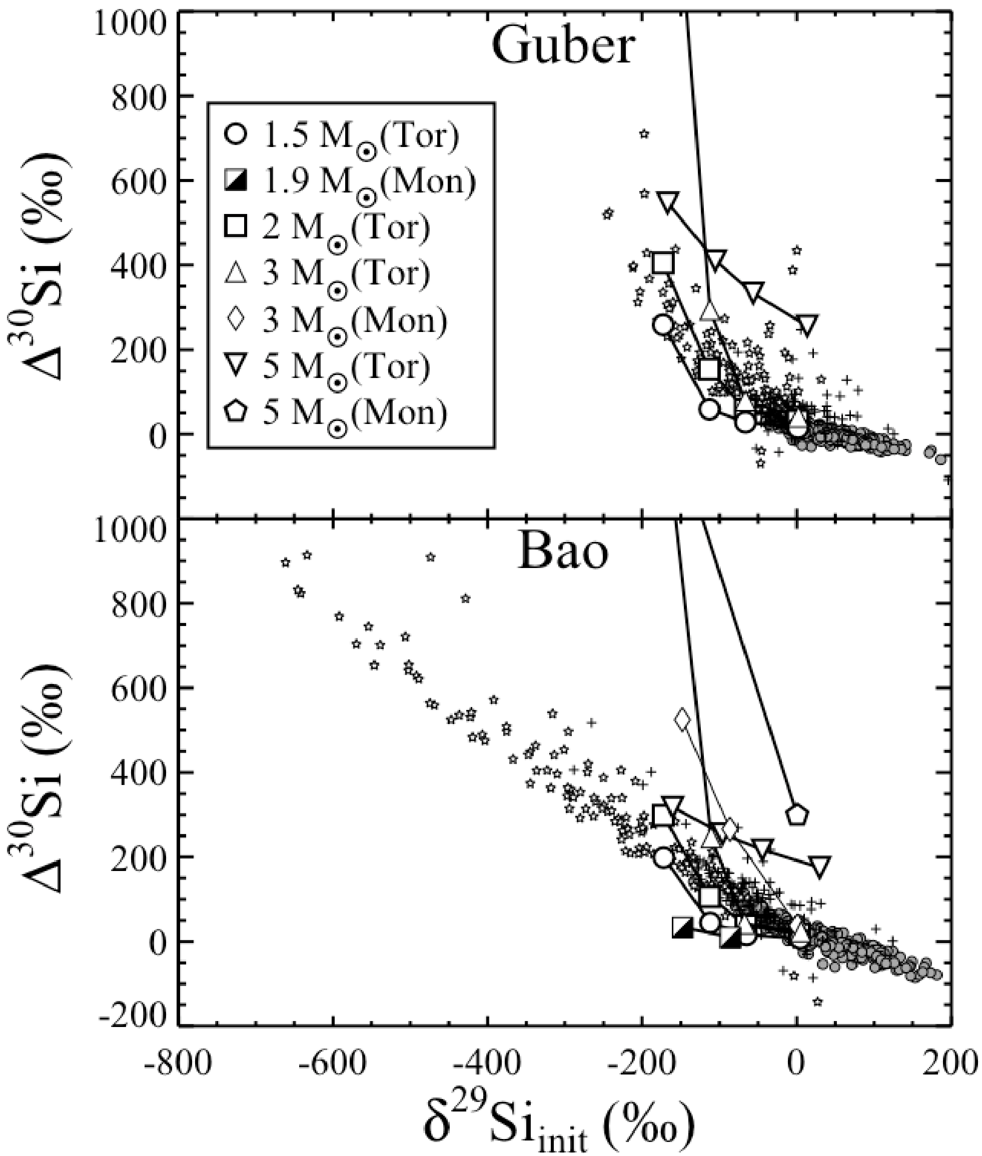

As expected, the data show a correlation between the Galactic component $\delta^{29}Si_{init}$ and the ABG component $\Delta^{30}Si$. Models with the Guber cross sections give a better fit to the data.

Start with an intial $^{12}C/^{13}C$ ratio of 5, assumed to result from Cool Bottom Processing (CBP) on the RGB

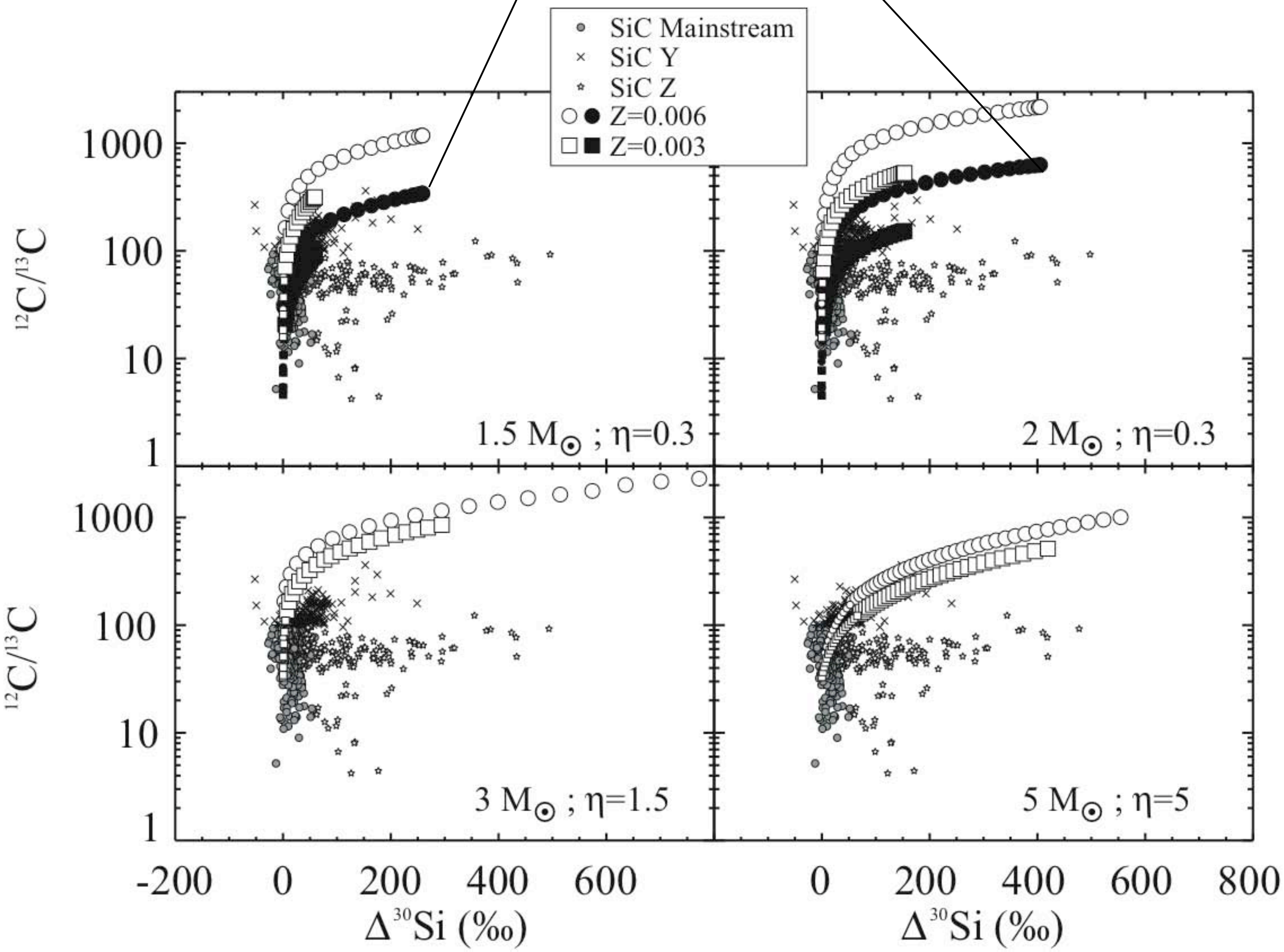

For all low-metallicity models, required to explain the Si shifts, the $^{12}C/^{13}C$ ratios are much higher than these ratios are in grains.

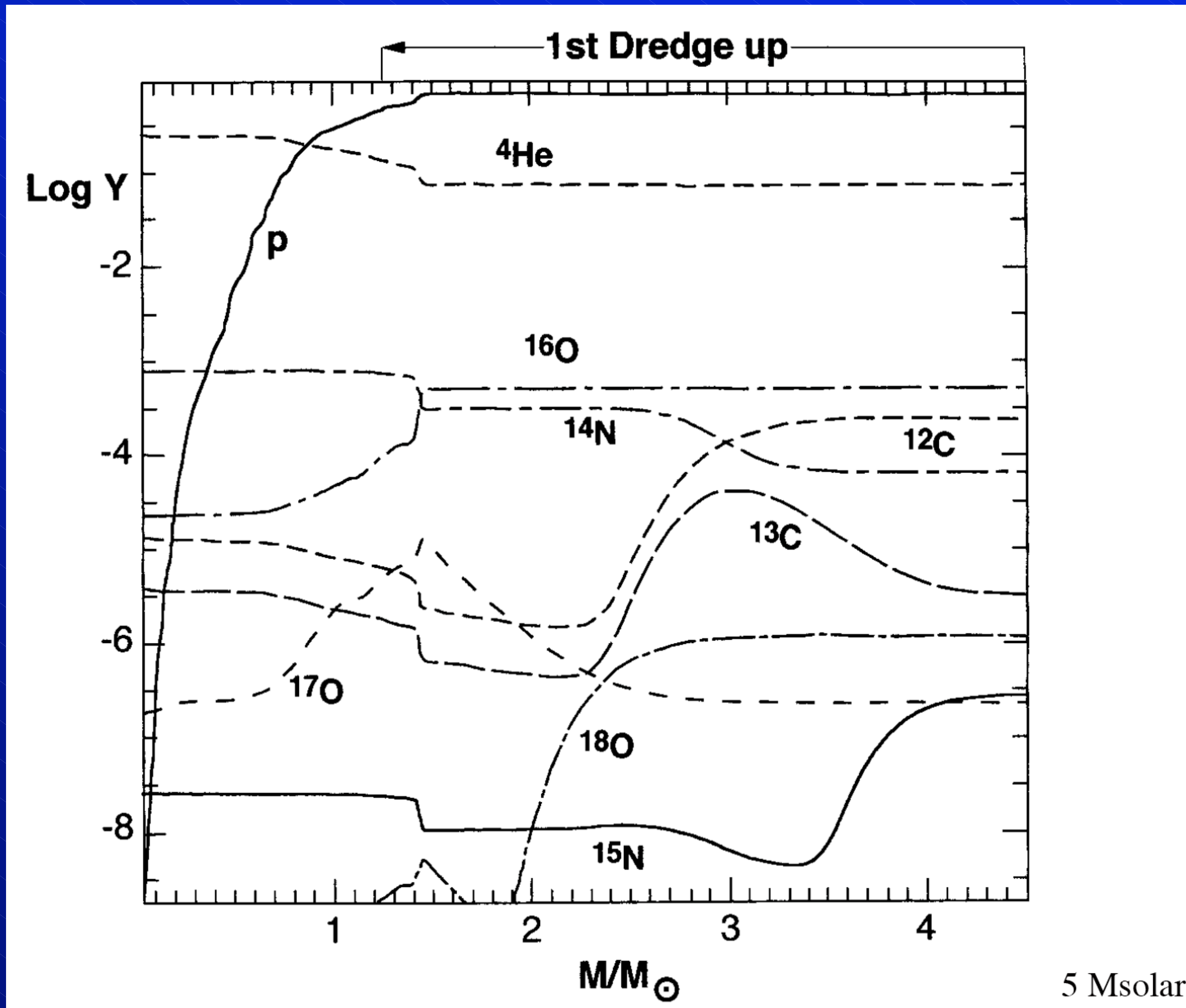

Model compositions of a 5 $M_\odot$ star after H exhaustion in the core. After the 1st dredge-up the surface is enriched in ^{13}C.

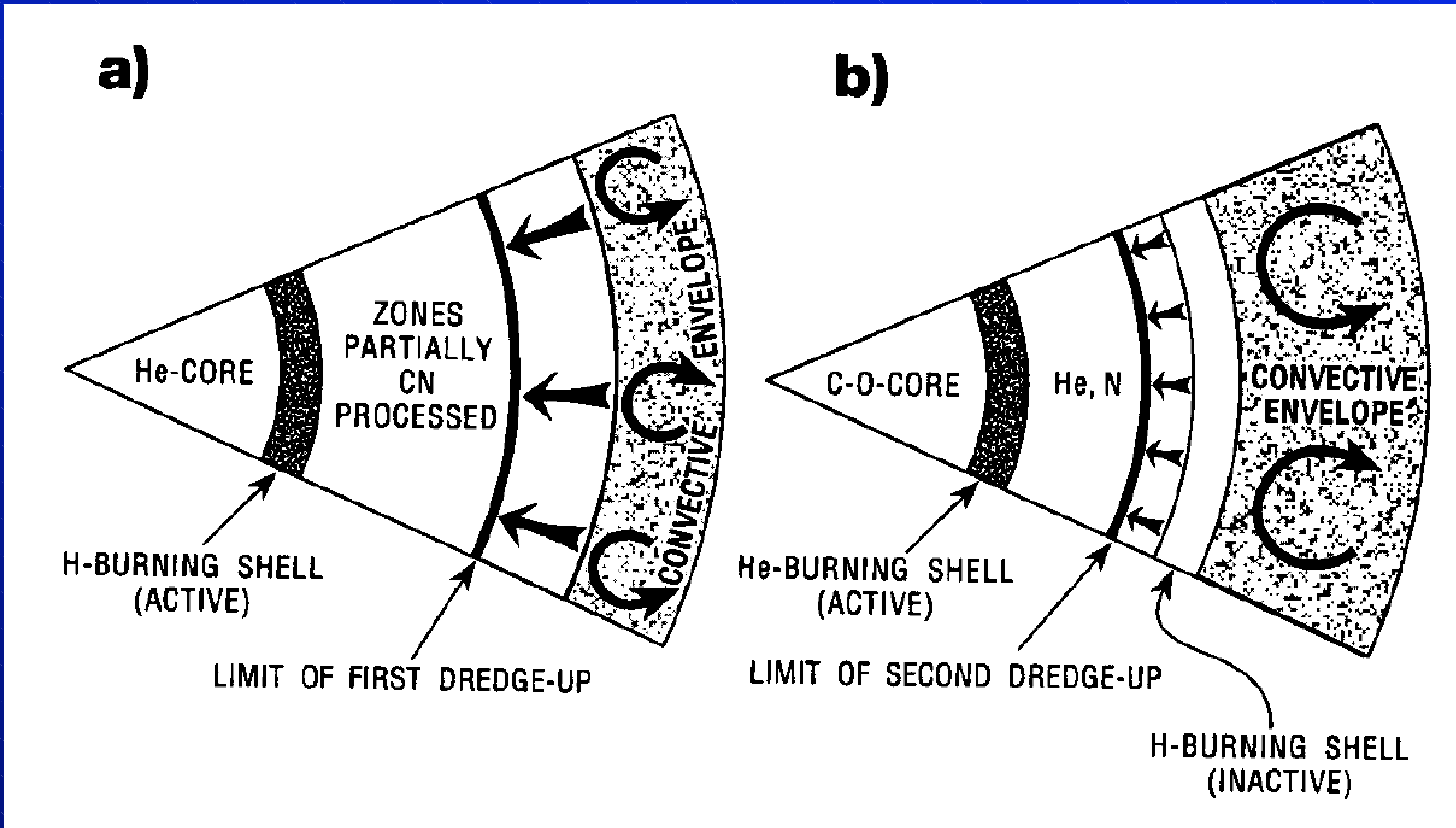

a)
He-CORE
ZONES
PARTIALLY
CN
PROCESSED
CONVECTIVE ENVELOPE
H-BURNING SHELL
(ACTIVE)
LIMIT OF FIRST DREDGE-UP
b)
C-O-CORE
He, N
CONVECTIVE
ENVELOPE
He-BURNING SHELL
(ACTIVE)
LIMIT OF SECOND DREDGE-UP
H-BURNING SHELL
(INACTIVE)

Start with an intial $^{12}C/^{13}C$ ratio of 5, assumed to result from Cool Bottom Processing (CBP) on the RGB

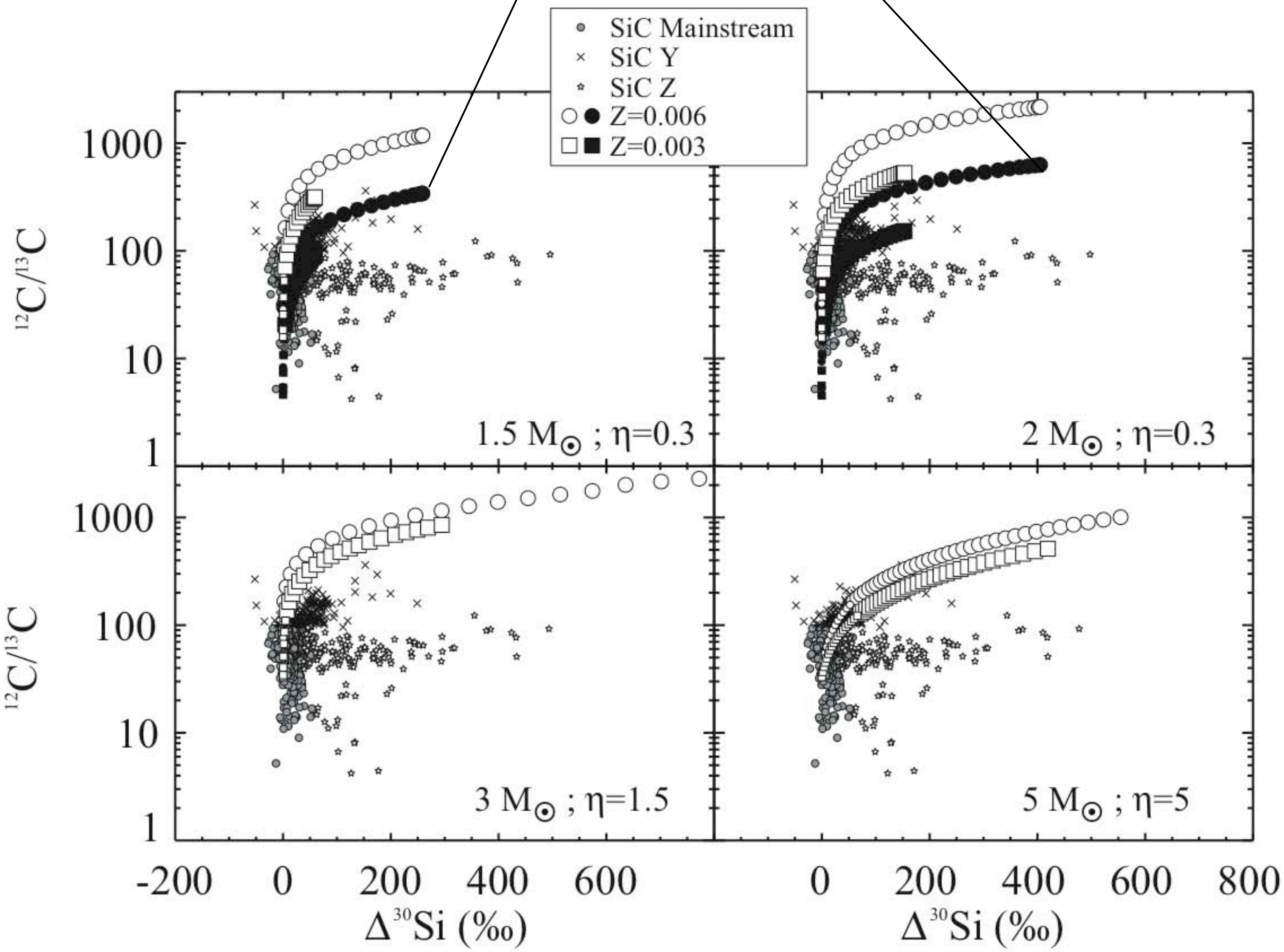

For all low-metallicity models, required to explain the Si shifts, the $^{12}C/^{13}C$ ratios are much higher than these ratios are in grains.

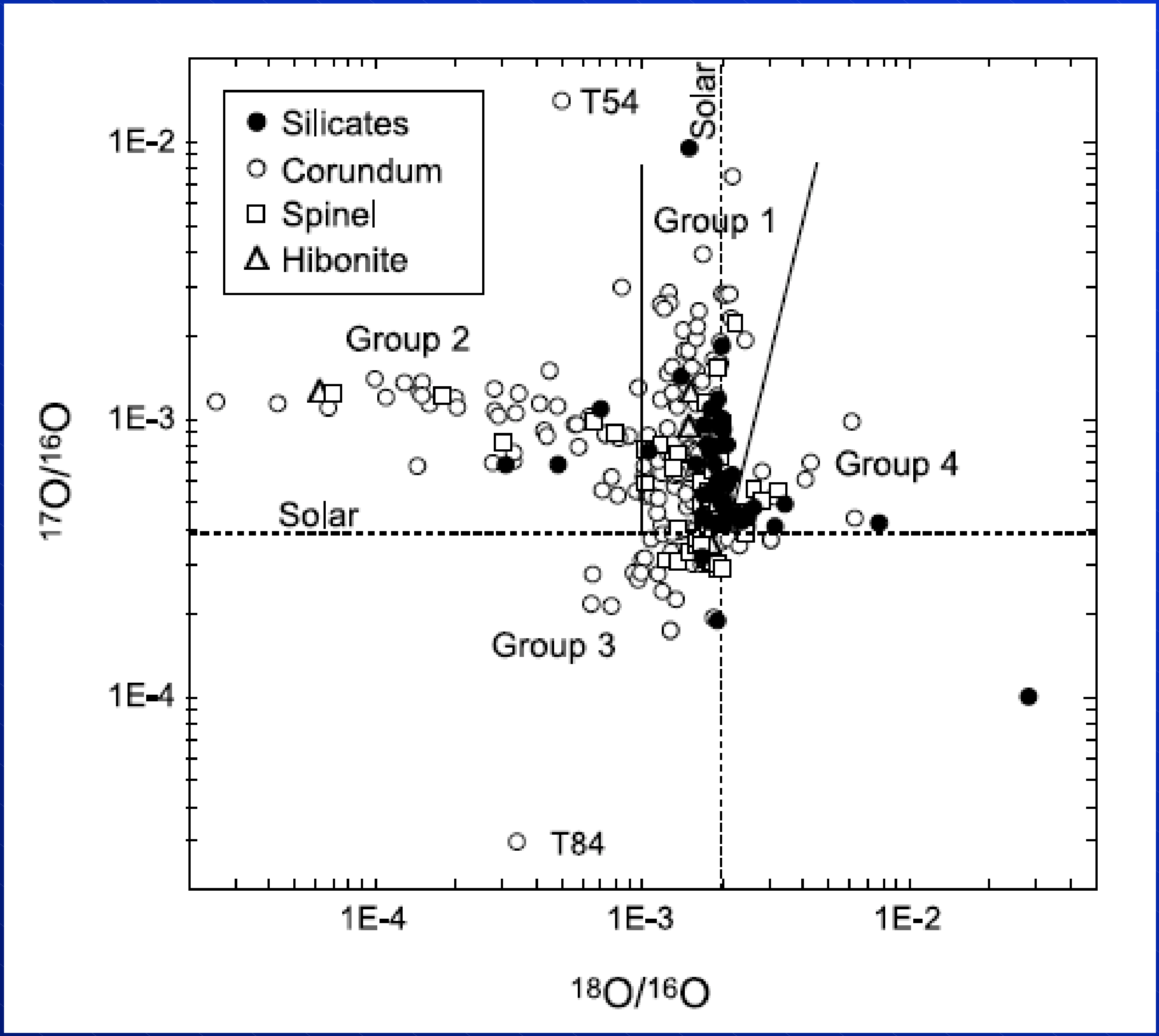

Nittler et al. (1997) distinguished four groups of O-rich presolar grains. The O isotopic ratios of group 1 grains can be explained by first dredge-up, but not those of group 2 grains.

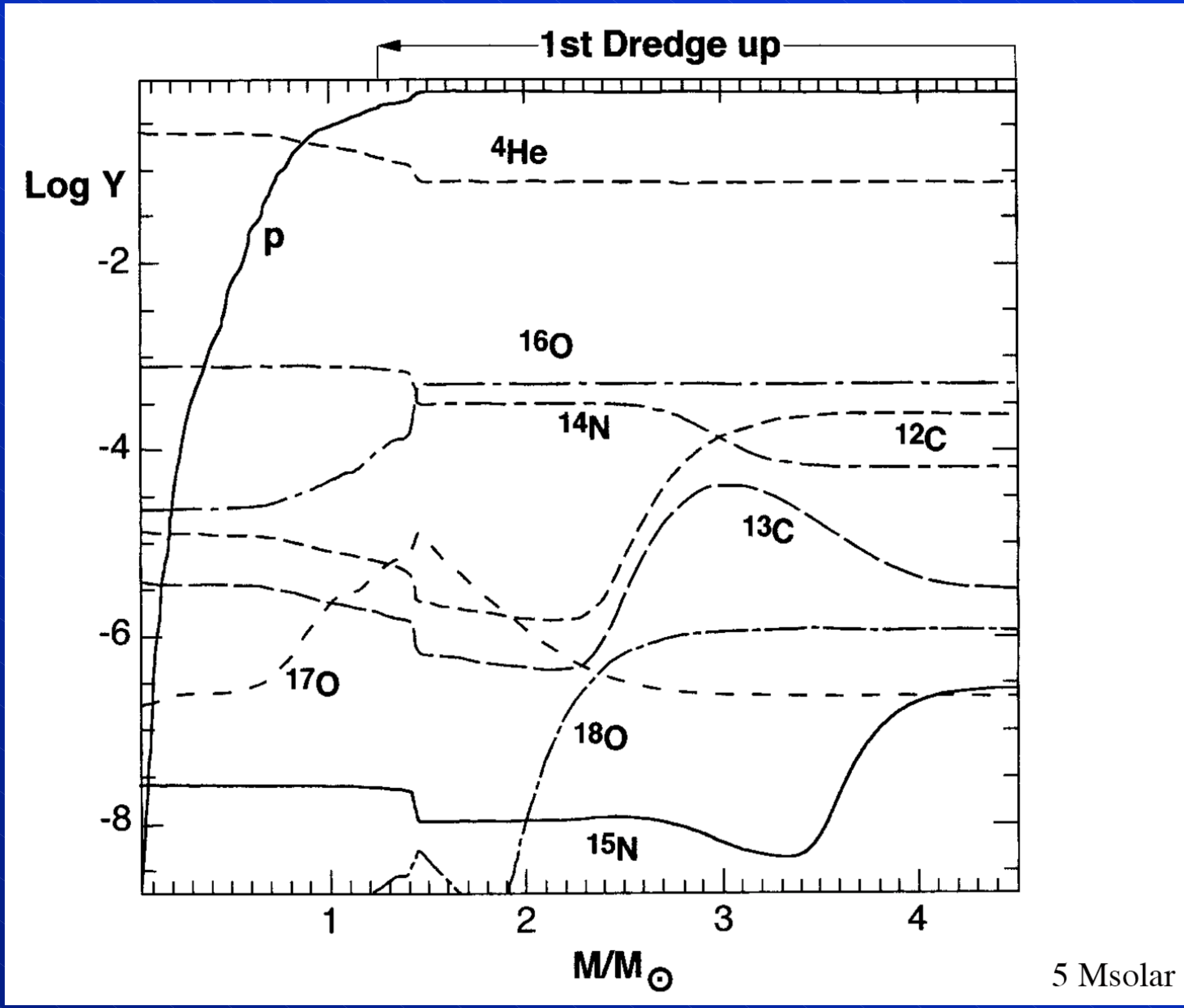

The 1st dredge-up also enriches the surface in ^{17}O and depletes it in ^{18}O.

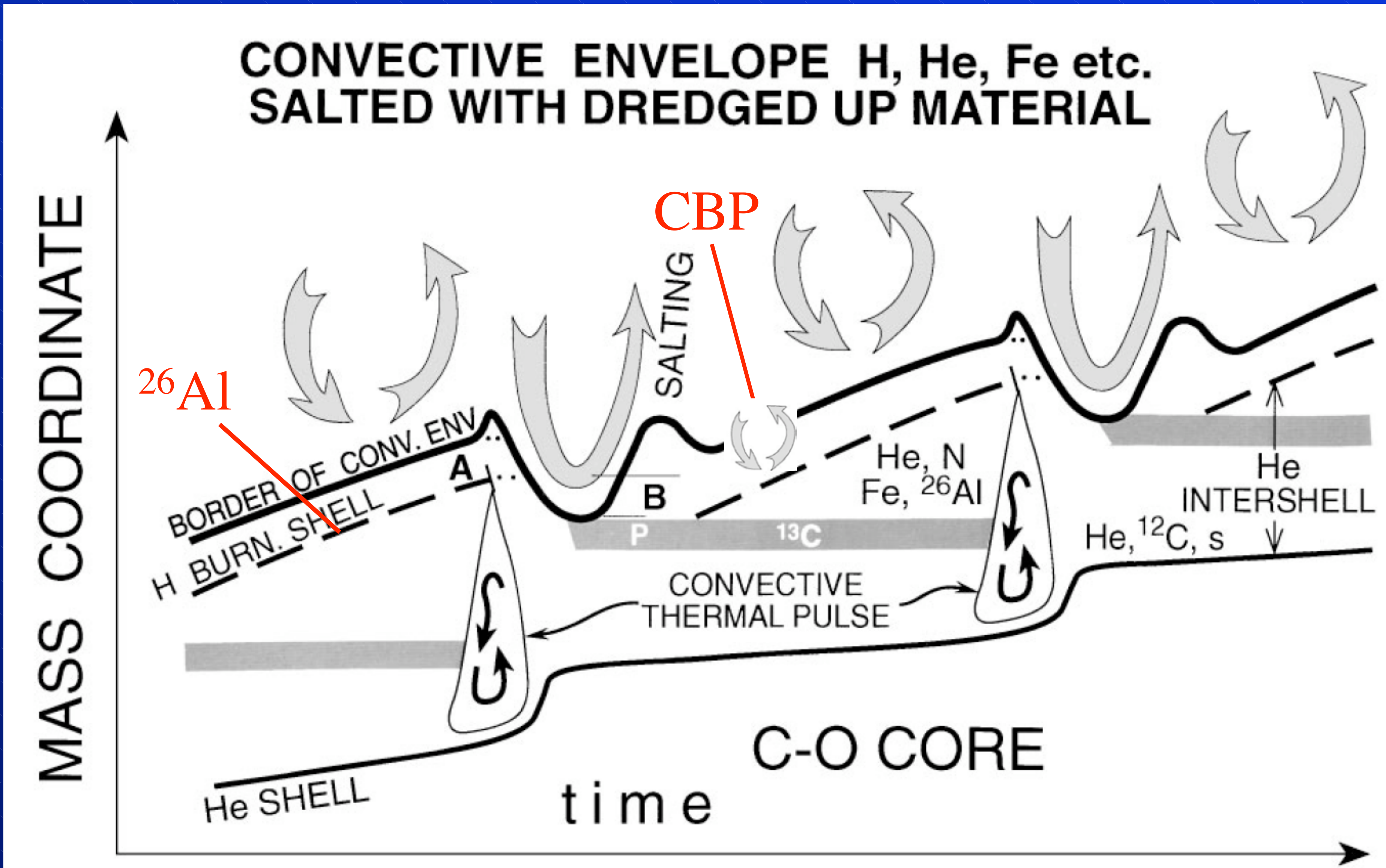

Busso et al. (1999)

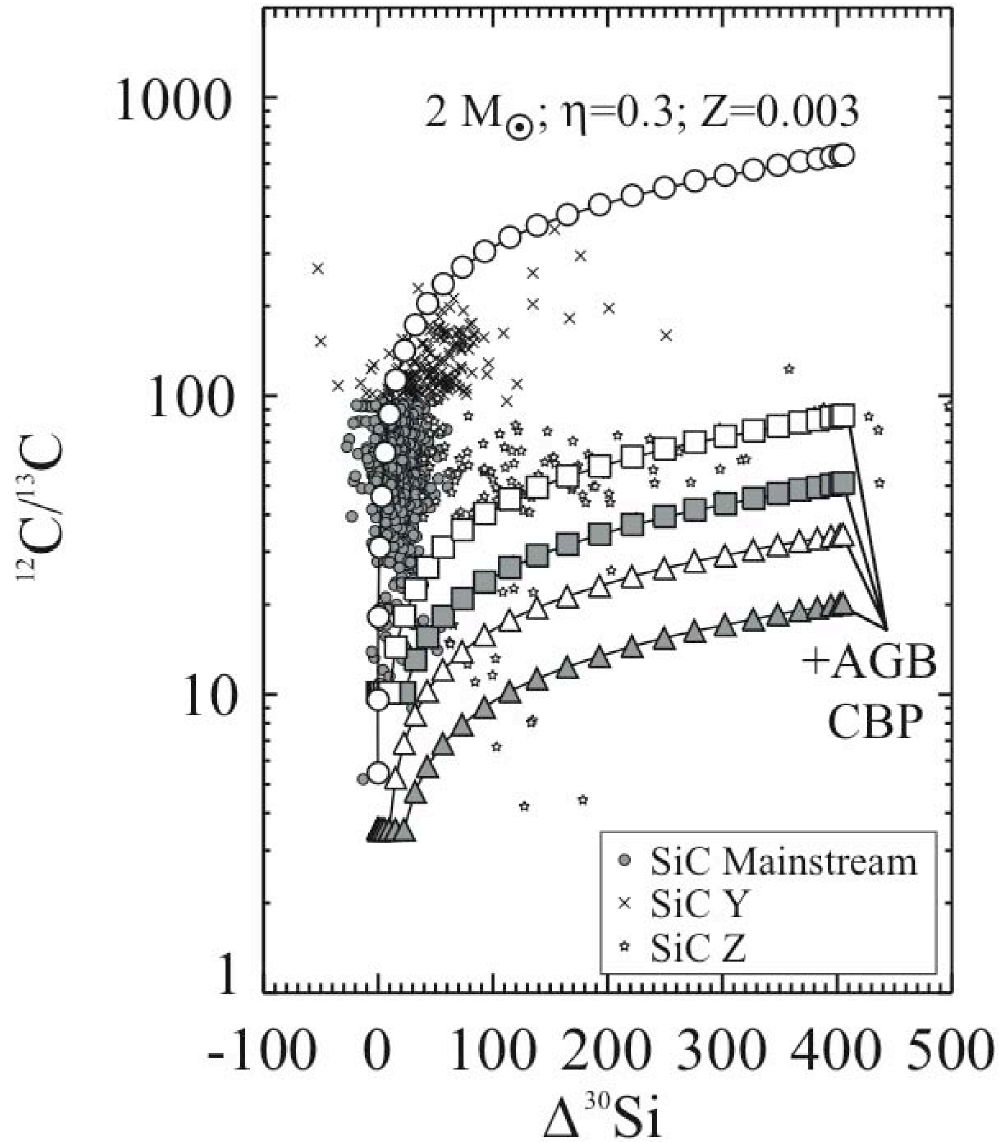

If it is assumed that cool bottom processing occurs also during the AGB phase, low enough $^{12}C/^{13}C$ ratios can be achieved to reproduce the Z grain data.

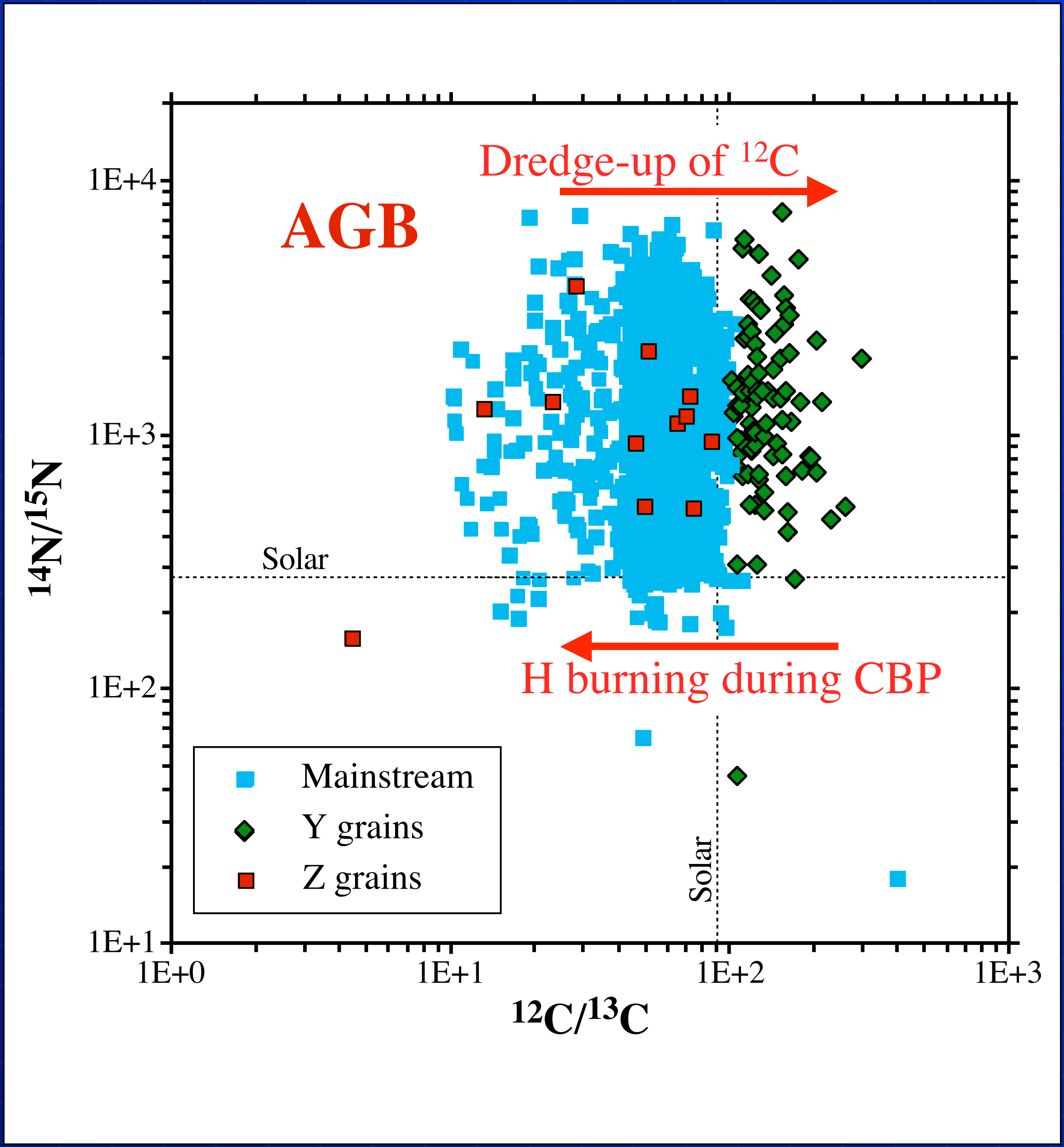

While he $^{12}C/^{13}C$ ratio increases from mainstream to Y grains, Z grains have smaller $^{12}C/^{13}C$ ratios, in contrast to theoretical models. Extra mixing (Cool Bottom Processing) has been invoked as an explanation.

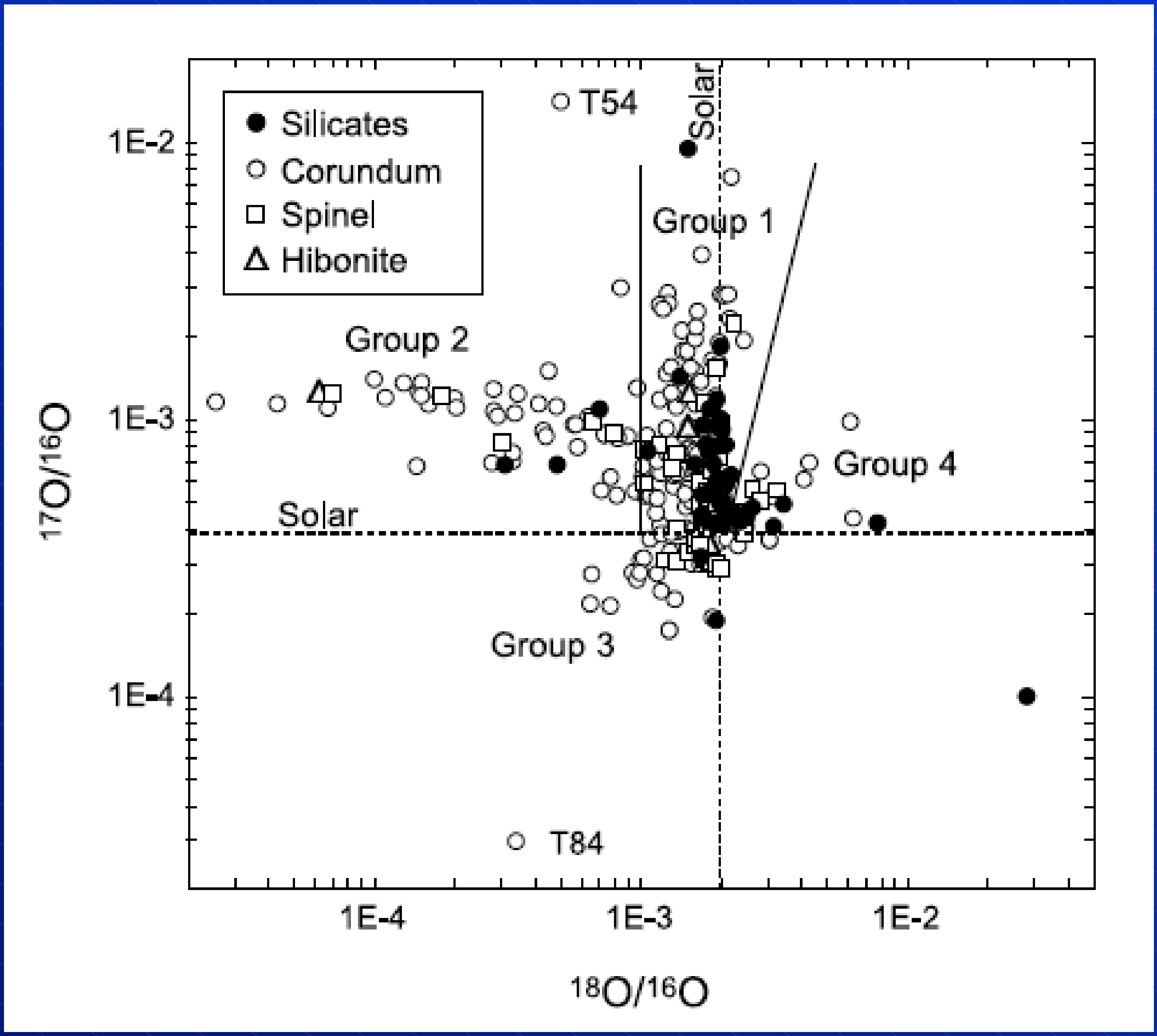

Nittler et al. (1997) distinguished four groups of O-rich presolar grains. The O isotopic ratios of group 1 grains can be explained by first dredge-up, but not those of group 2 grains.

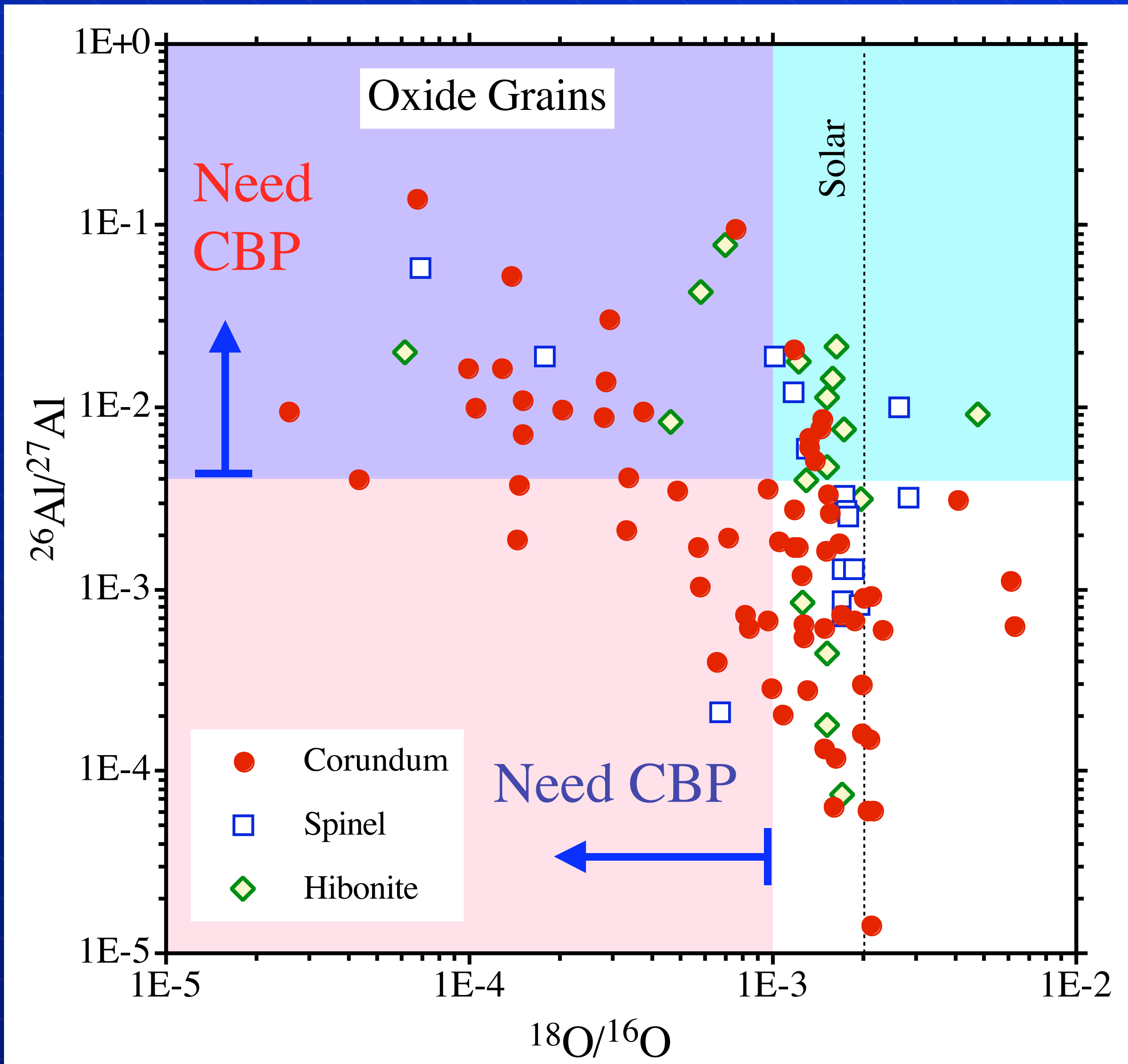

In AGB stars, ^{26}Al/^{27}Al ratios > 4×10^{-3} and ^{18}O/^{16}O ratios < 10^{-3} cannot be explained by "normal" shell H burning and "cool bottom processing" has been invoked to explain these ratios.

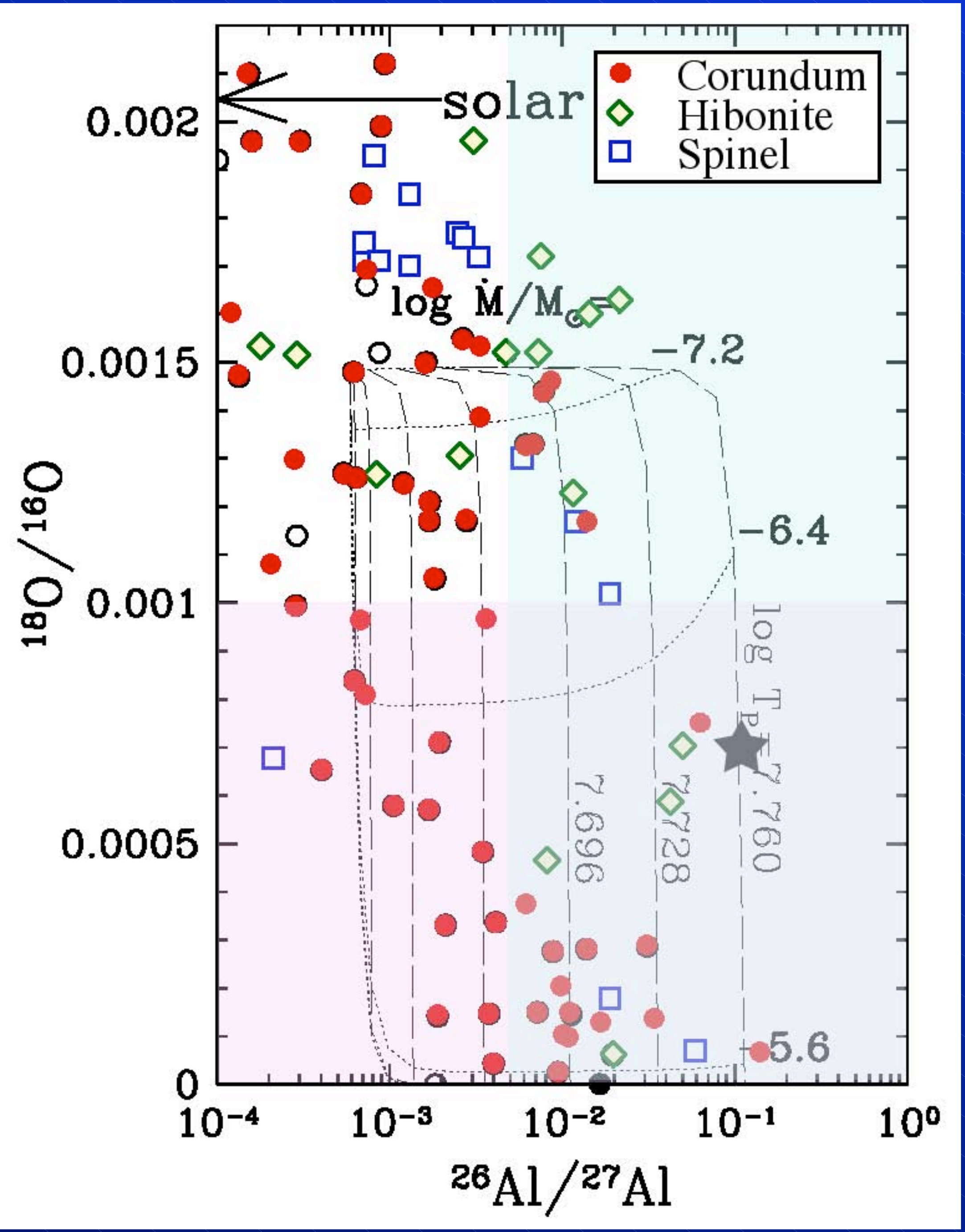

Cool bottom processing is an assumed mixing process in which material from the convective envelope is circulated to hot regions close to the H-burning shell. Nollett et al. (2003) developed a parametric theory. They introduced two parameters, the circulation rate dM/dt and the maximum temperature T_p reached by the circulating material.

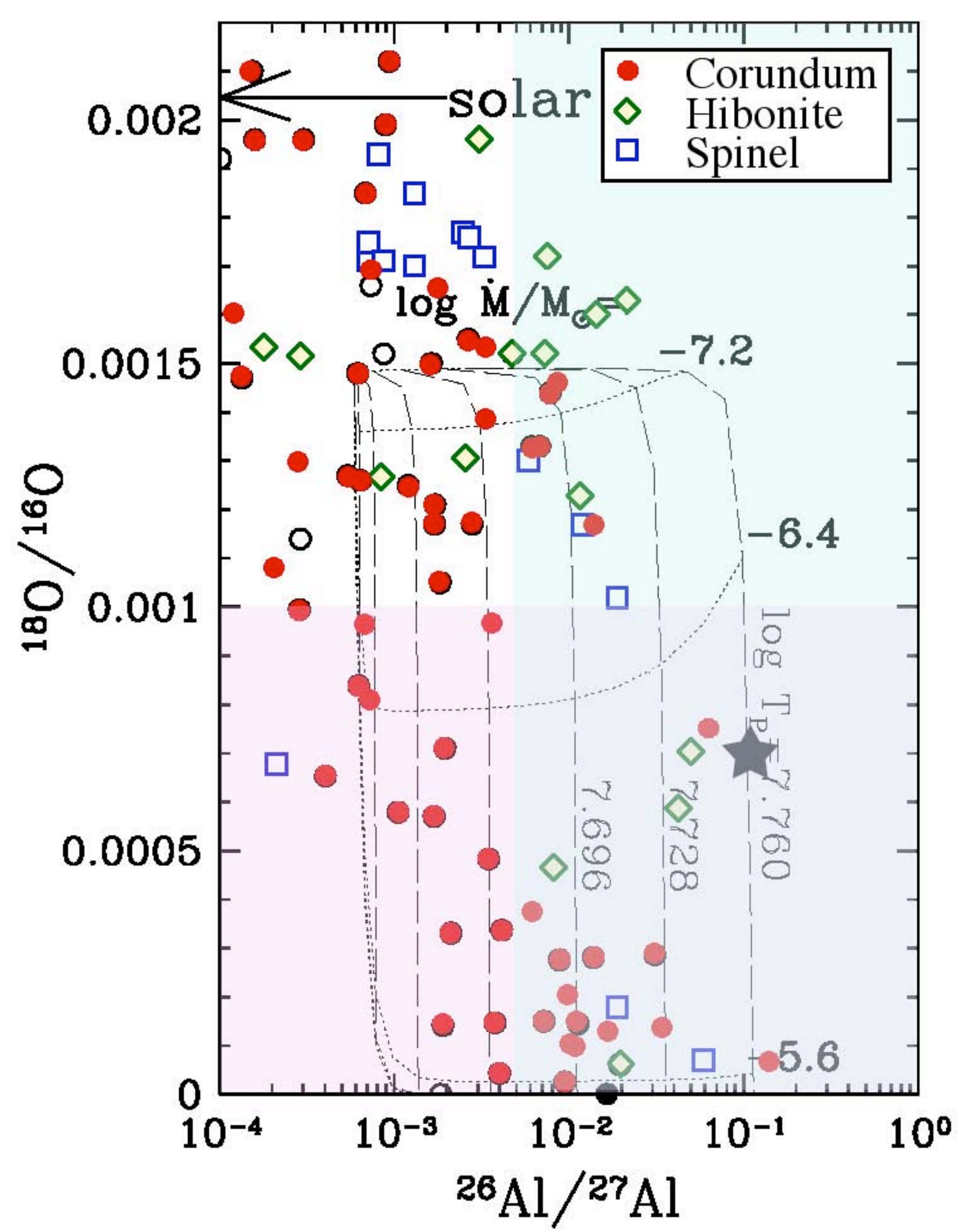

dM/dt mostly affects the destruction of ^{18}O (and the production of ^{13}C from ^{12}C), the maximum temperature T_p reached by the circulating material affects the production of ^{26}Al.

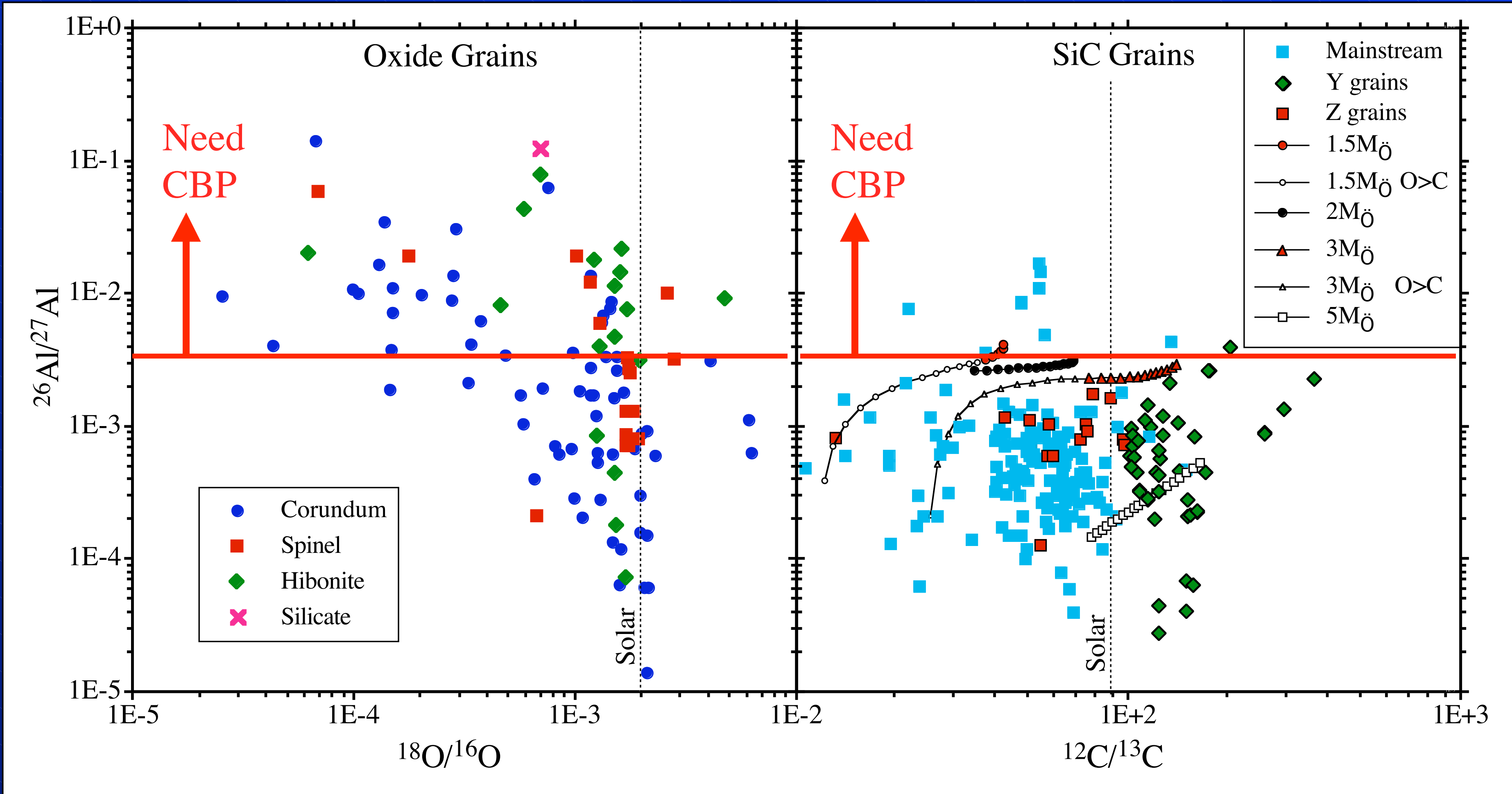

Upper limits of $^{26}Al/^{27}Al$ ratios in SiC grains from AGB stars generally agree with model predictions of shell H burning. In contrast, $^{26}Al/^{27}Al$ ratios in oxide grains are much higher. Cool bottom processing at high temperature apparently does not occur in the parent stars of SiC grains, although low-temperature CBP accounts for $^{12}C/^{13}C$ ratios in Z grains.

Does CBP prevent AGB stars from becoming carbon stars?

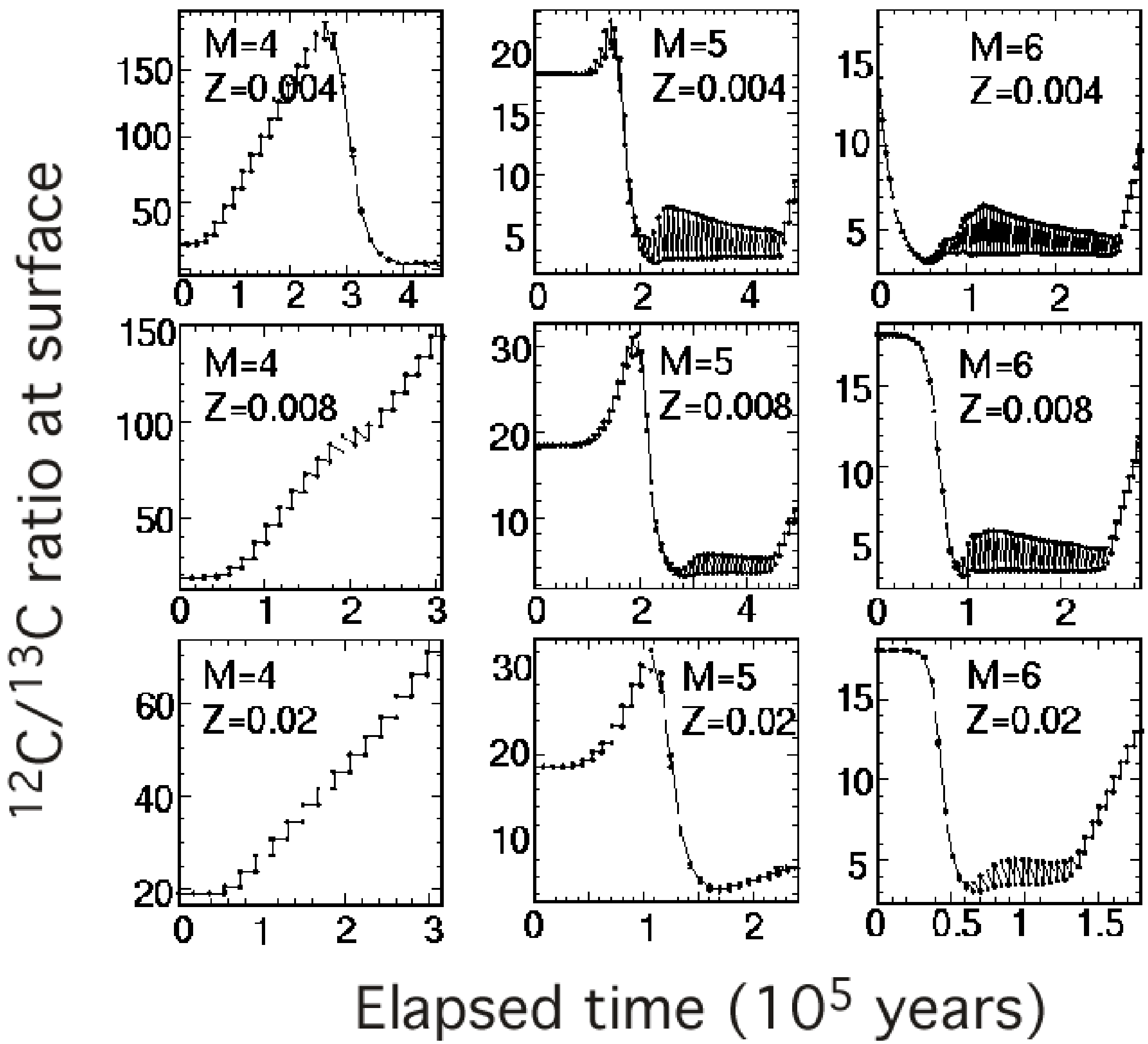

Lattanzio and Forestini

Grains from Supernovae

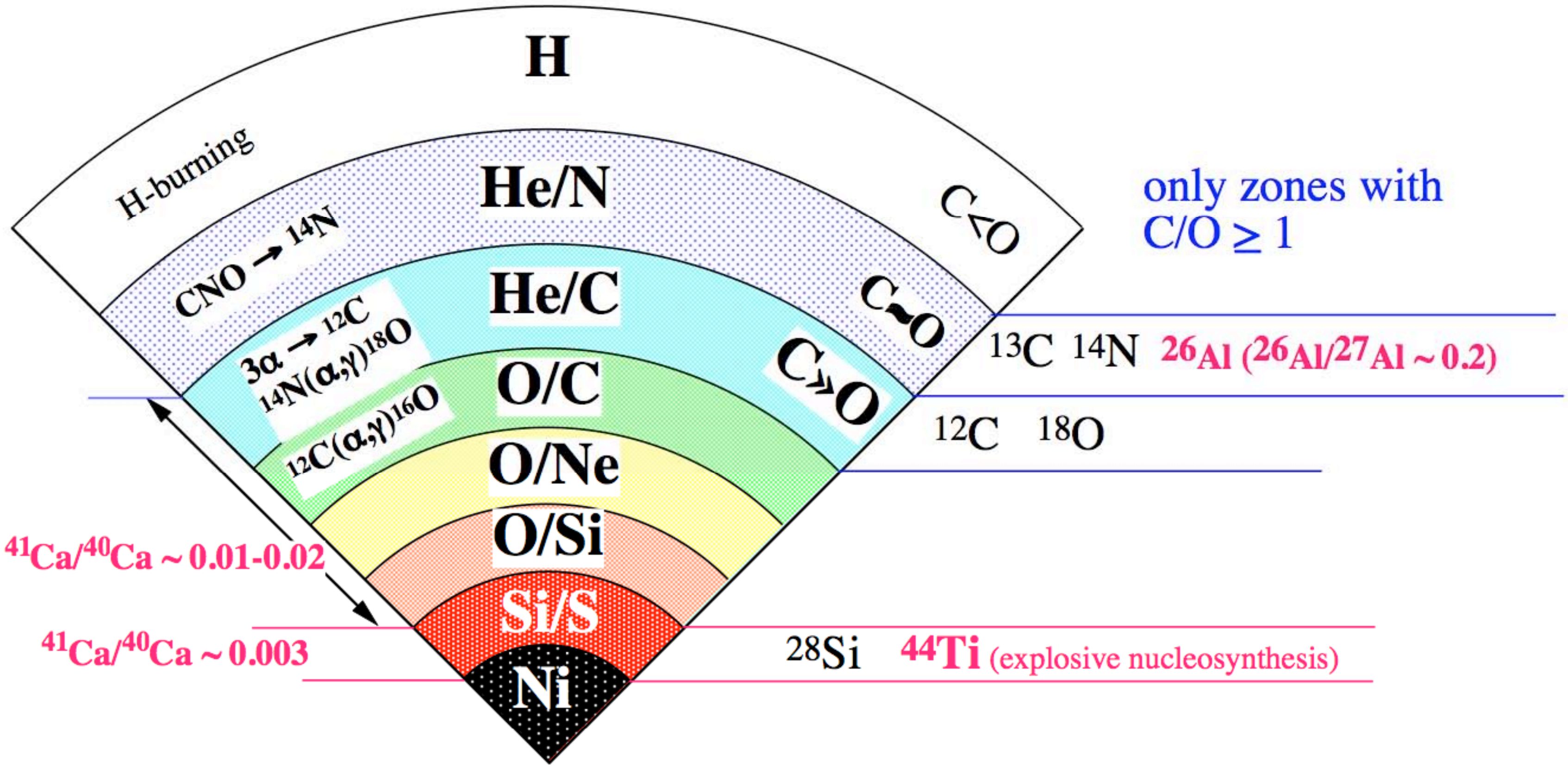

Schematic Structure of 15M$_\odot$ Star Before Explosion

(Meyer et al., 1995)

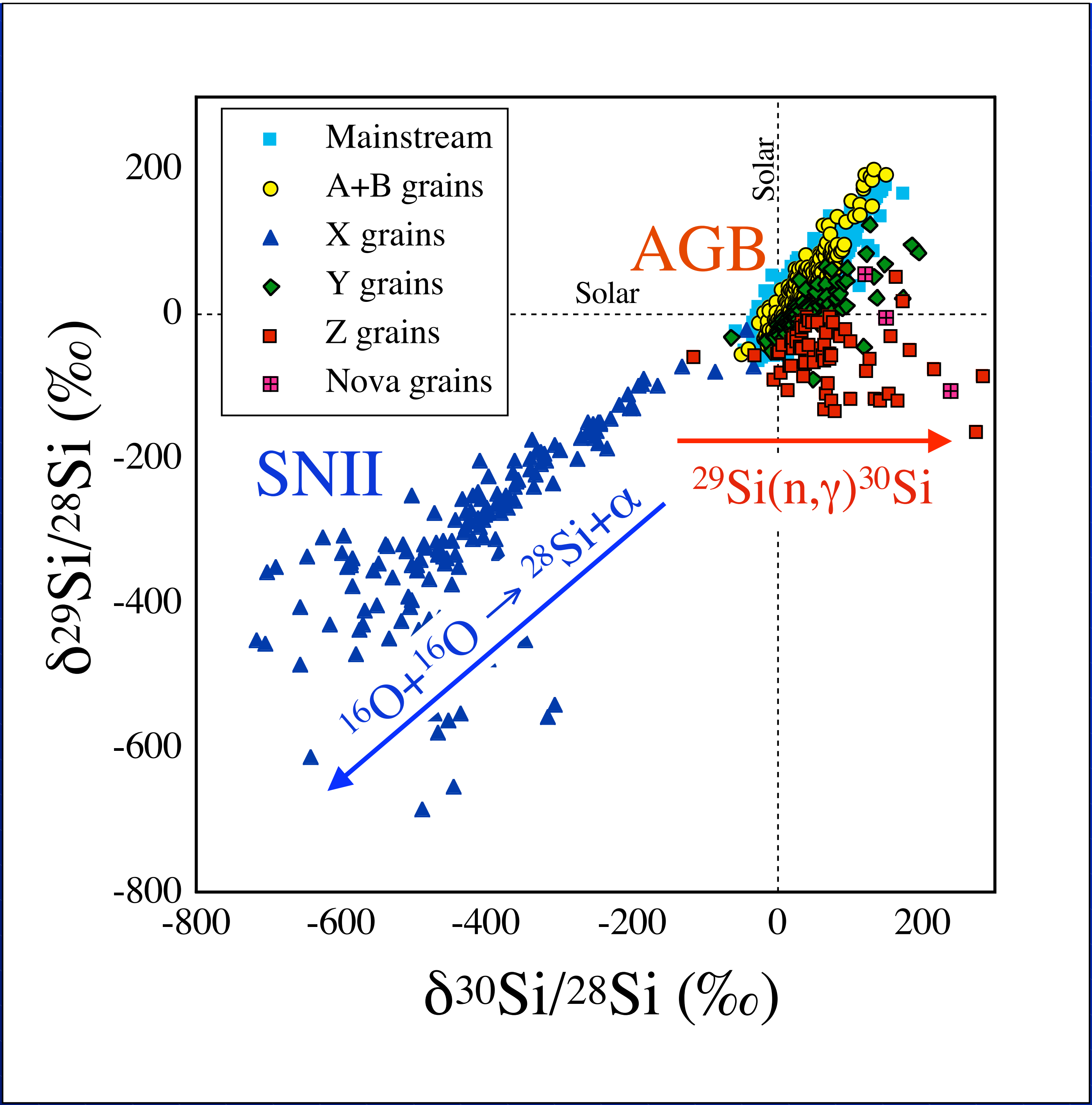

Si isotopes show the signatures of O burning.

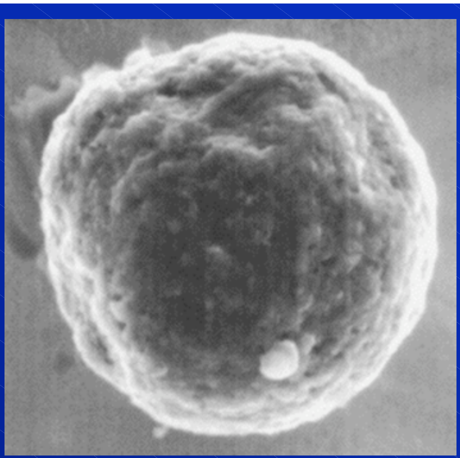

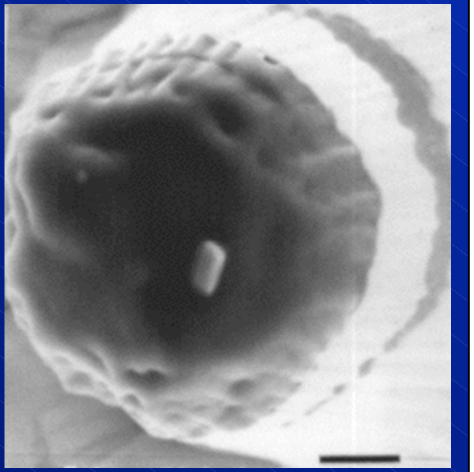

Graphite grain KFA1-302 with TiC sub-grain

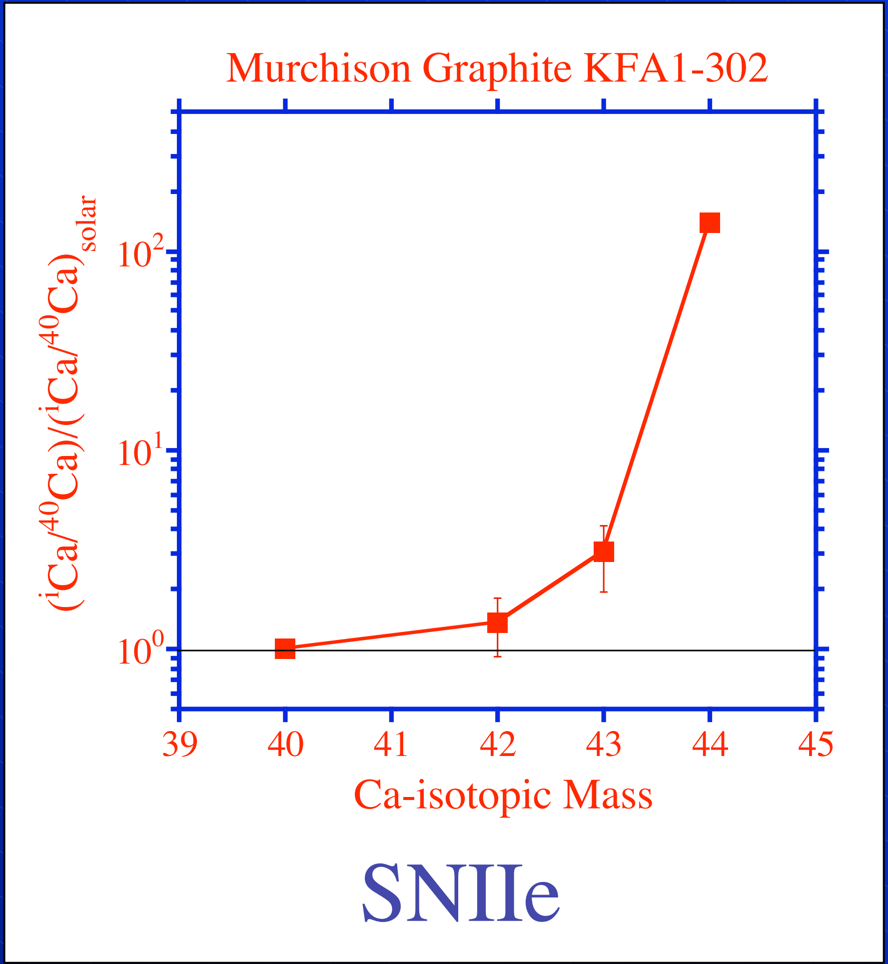

e process

X-type SiC grains and low-density graphite grains show evidence for ^{44}Ti, produced by α-rich freeze-out from QSE burning in SNeII.

^{44}Ti is radioactive and decays into ^{44}Ca.
Presolar grains preserve evidence for “live” ^{44}Ti,
thus they are considered to be
Stellar Fossils.

Bonanza Grain

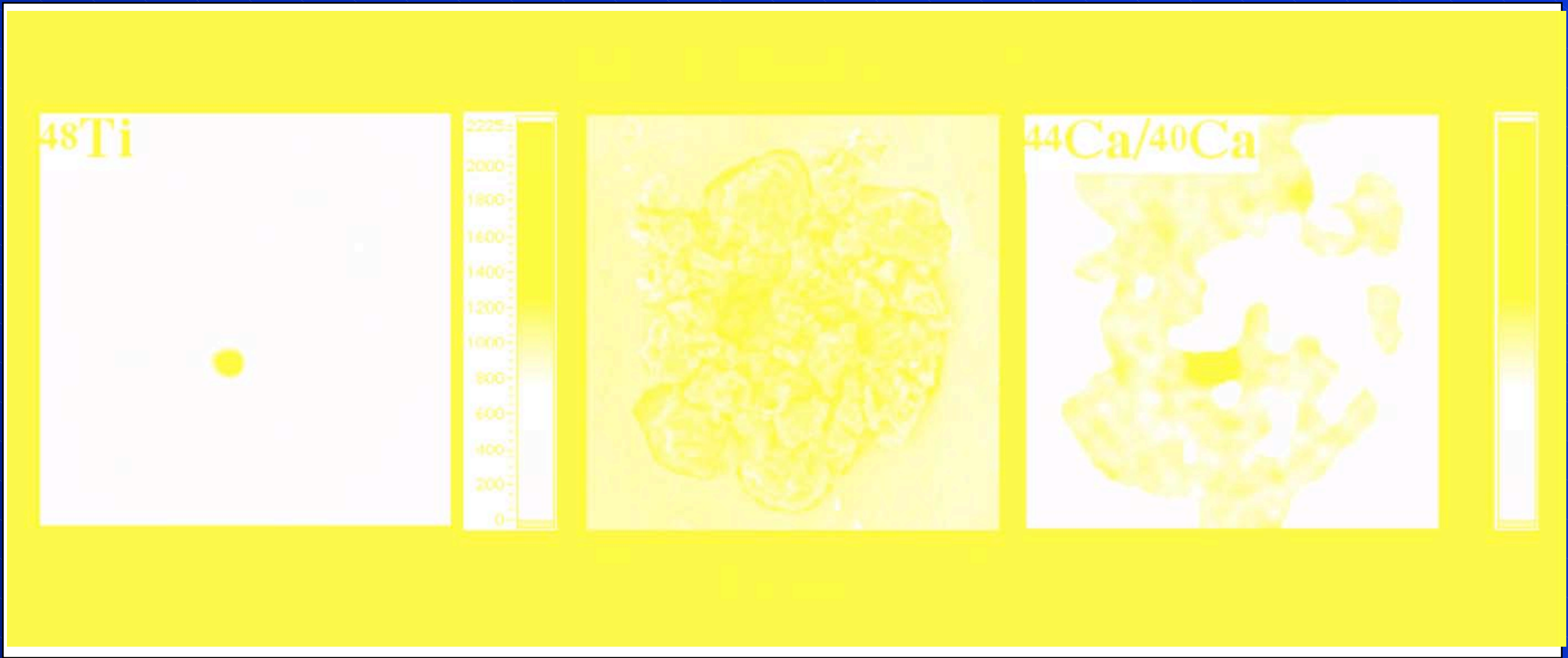

$^{12}C/^{13}C = 190$
$^{14}N/^{15}N = 28$
$\delta^{29}Si/^{28}Si = -282$
$\delta^{30}Si/^{28}Si = -442$
$^{26}Al/^{27}Al = 0.6\text{-}0.9$

^{44}Ca excess is associated with a Ti-rich subgrain, thus it originates from the decay of ^{44}Ti ($T_{1/2}$ = 60 yrs).

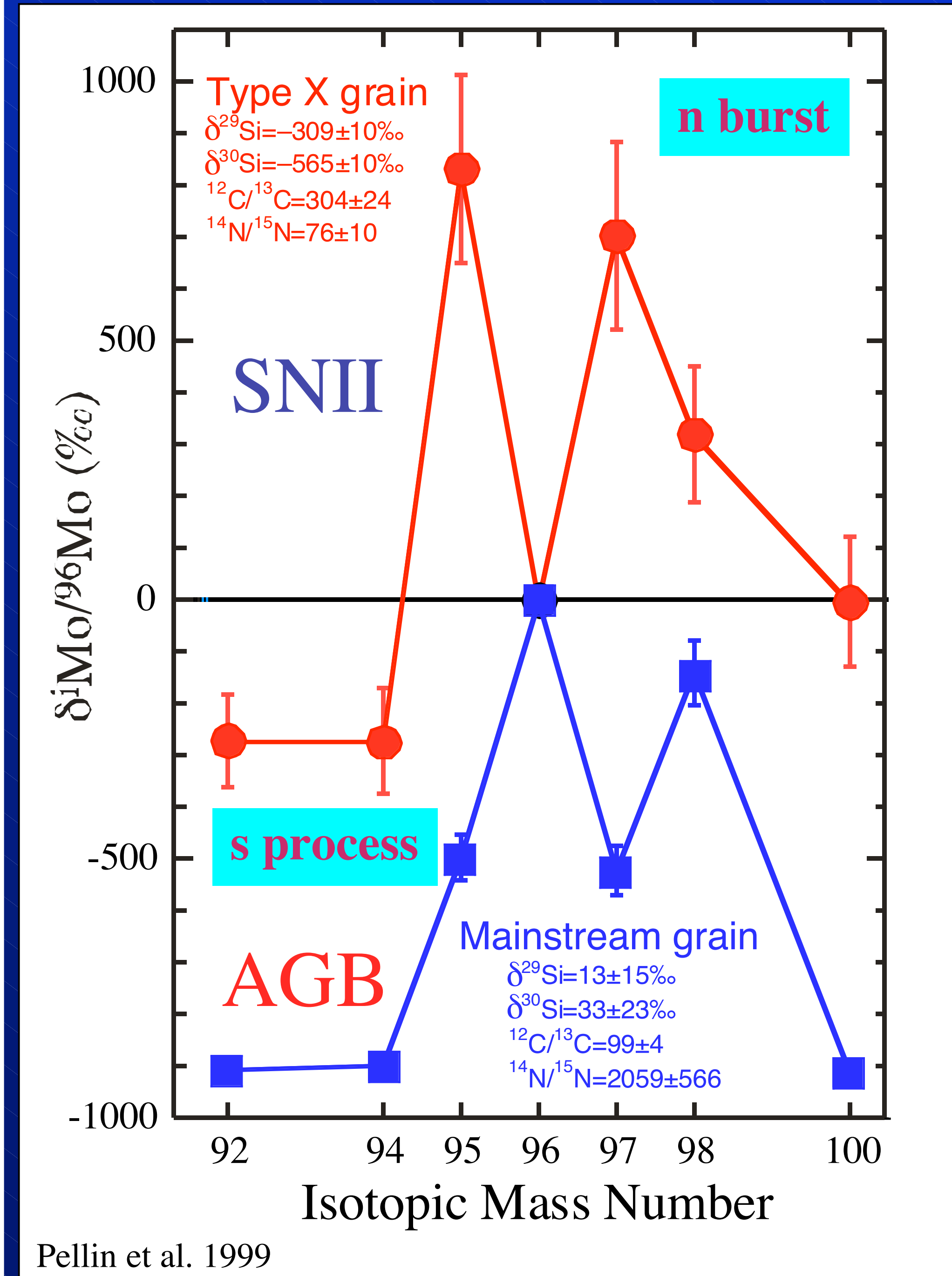

r process

No evidence for the r-process has been found to date in presolar grains. SiC grains from SNIIe show an isotopic pattern in Mo that can be explained by a short intense neutron burst.

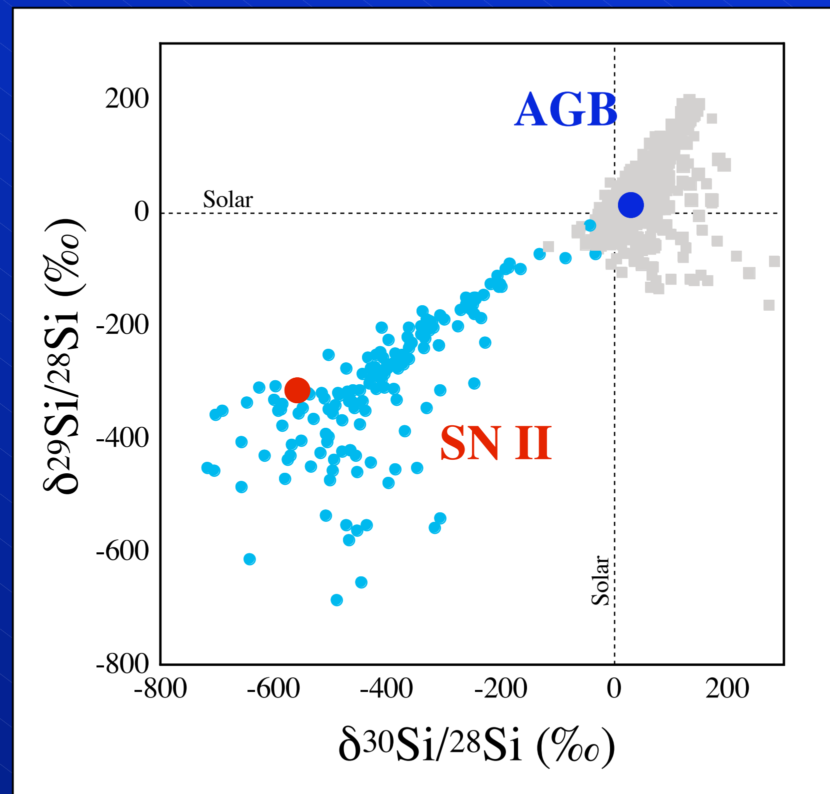

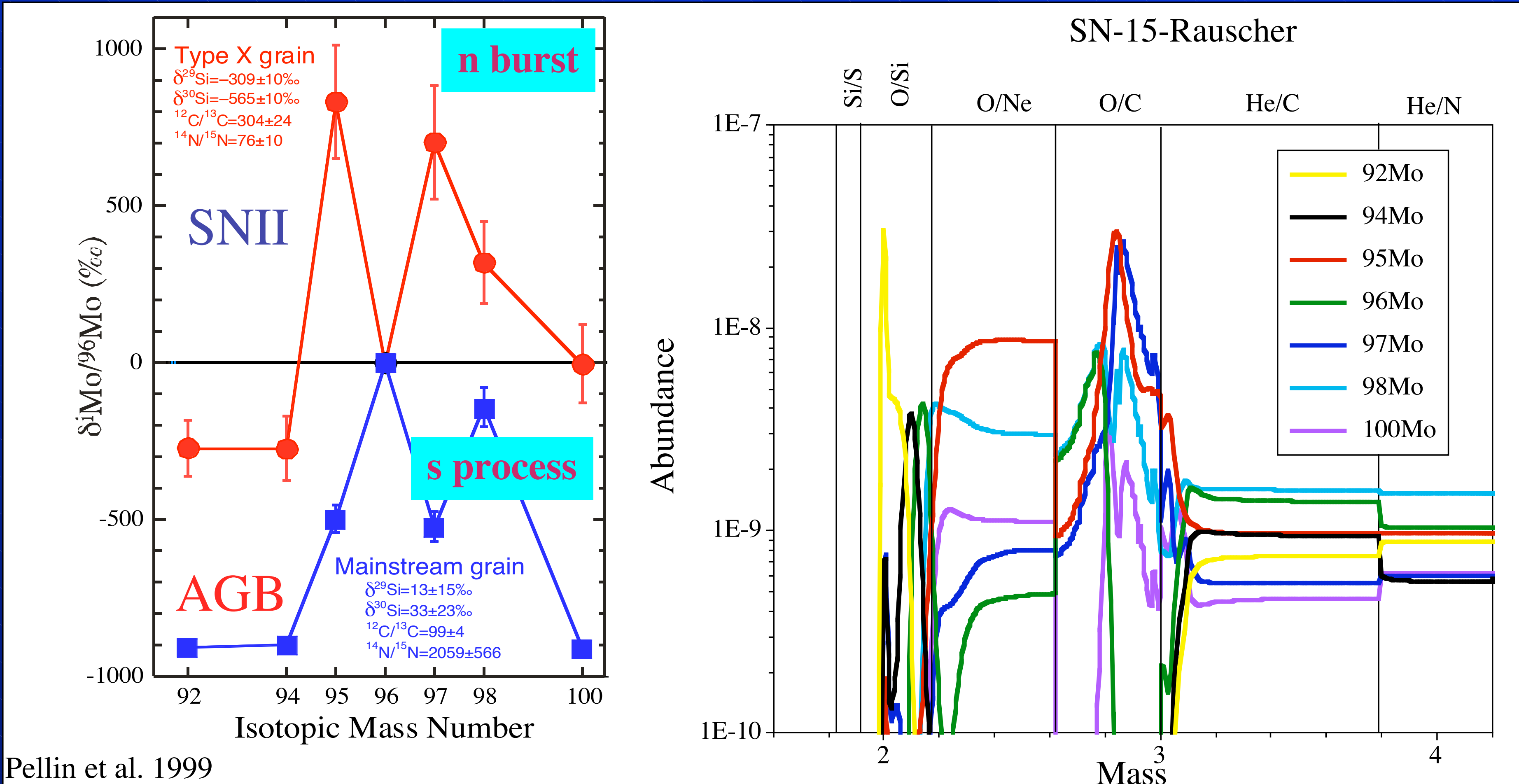

Pellin et al. 1999

SiC X grains from SNIIe show an isotopic pattern in Mo that can be explained by a short intense neutron burst.

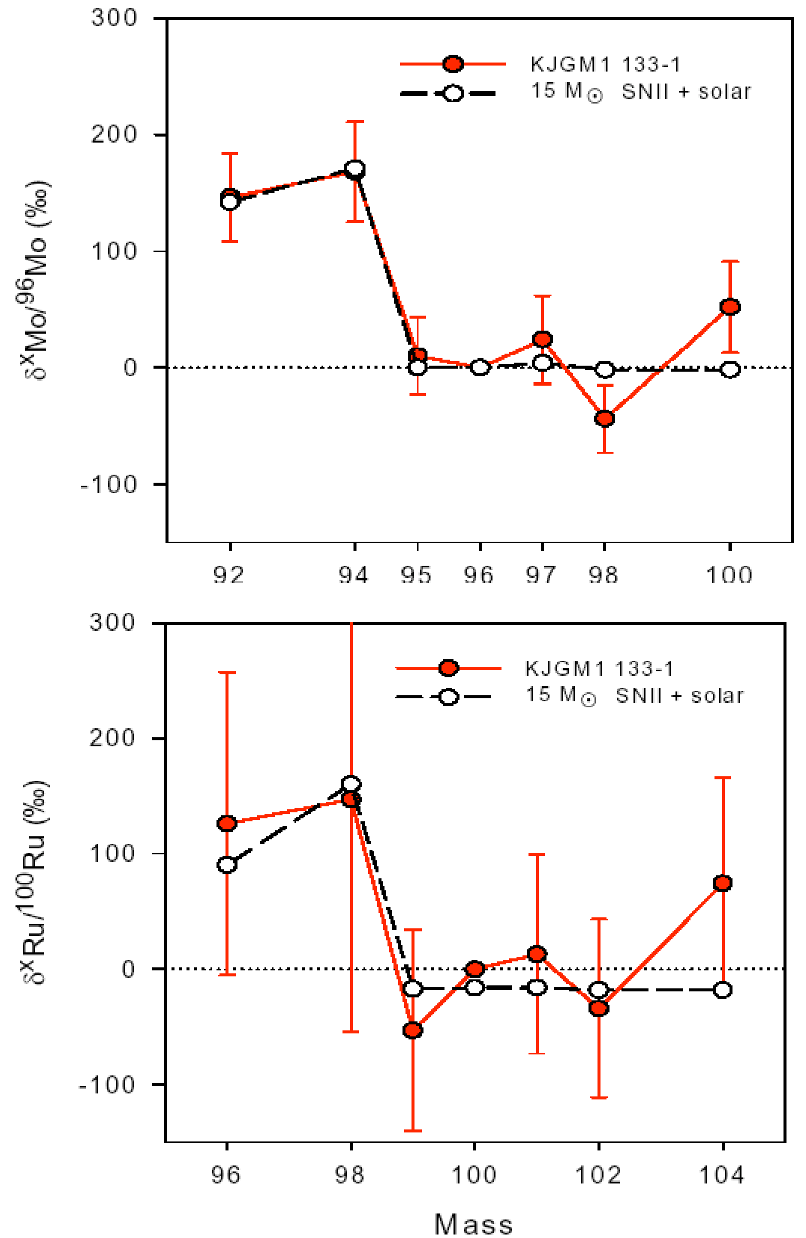

Savina et al., 2007

p process
γ process

A SiC grain of type A+B ($^{12}C/^{13}C$=4.5) has excesses in the p-process isotopes ^{92}Mo, ^{94}Mo, ^{96}Ru, and ^{98}Ru. Large excesses are predicted for inner zones of Type II SNe (model fits).

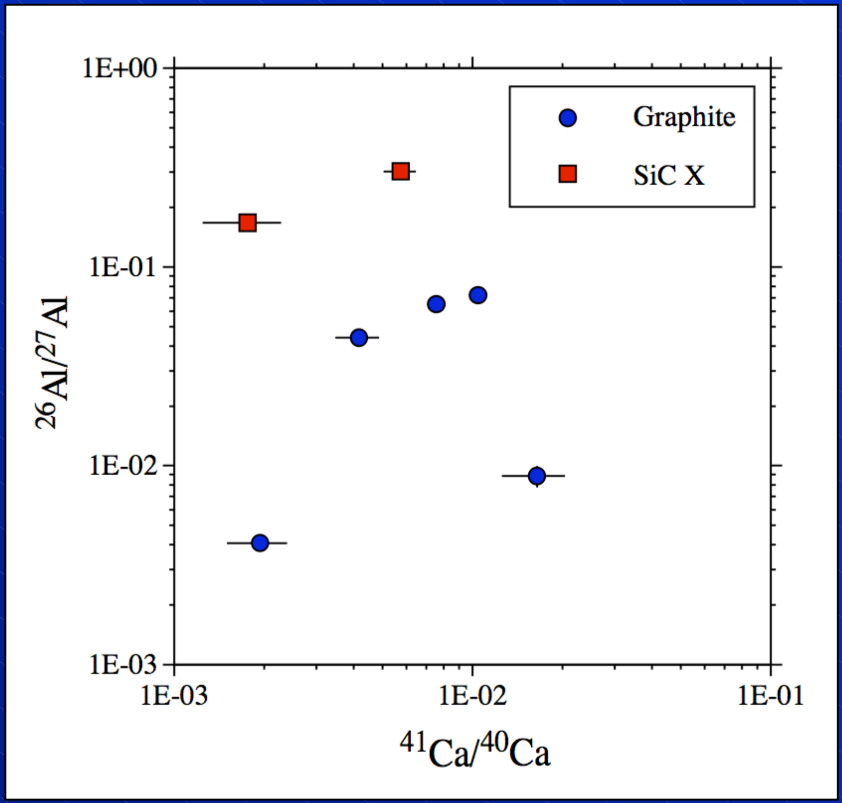

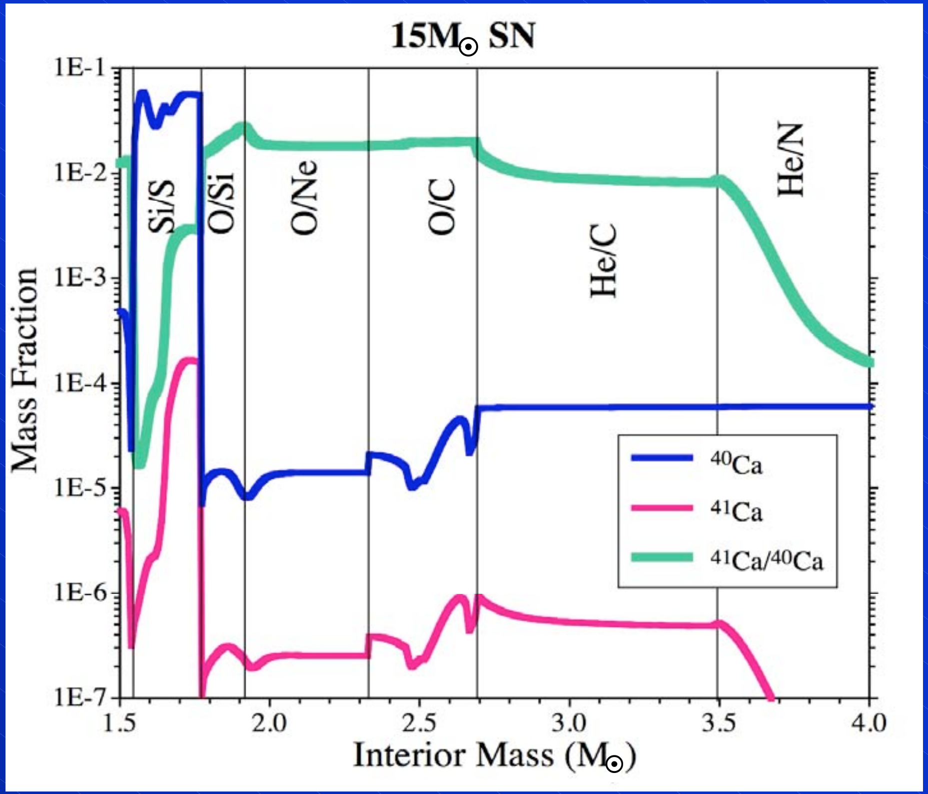

The initial presence of ^{41}Ca (from ^{41}K excesses) is evidence for a SN origin.

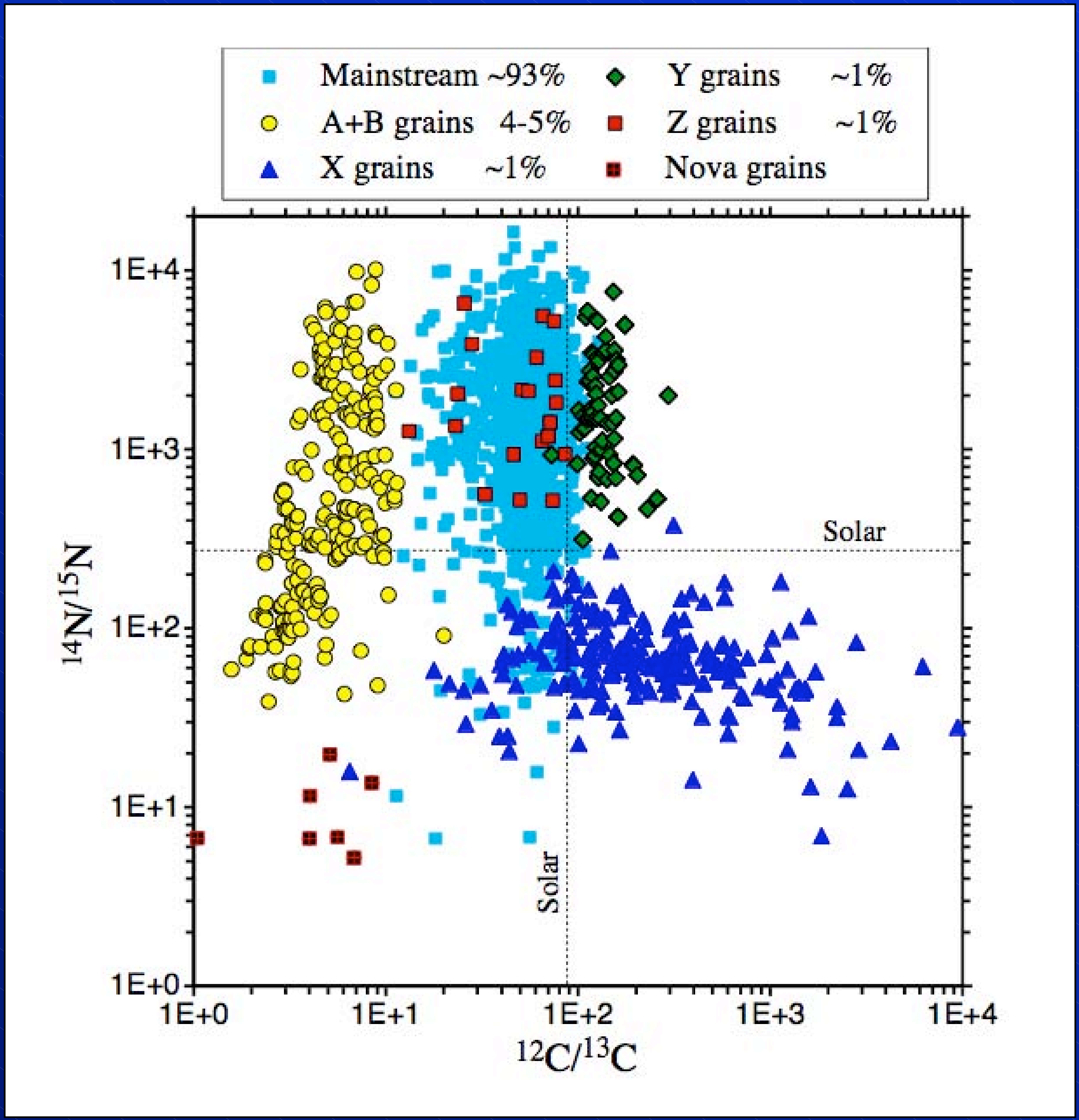

X grains have (mostly) ^{12}C excesses and ^{15}N excesses.

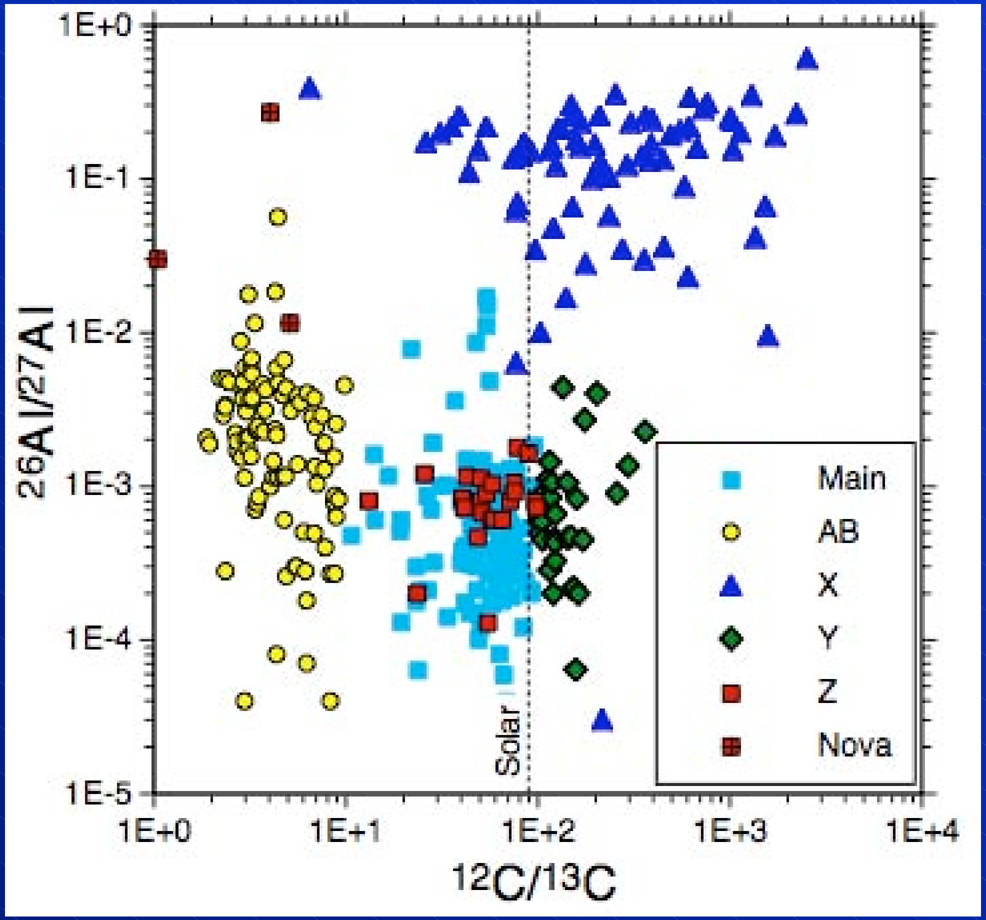

Also the inferred $^{26}Al/^{27}Al$ ratios are greatly different between X (SN) grains and other grains.

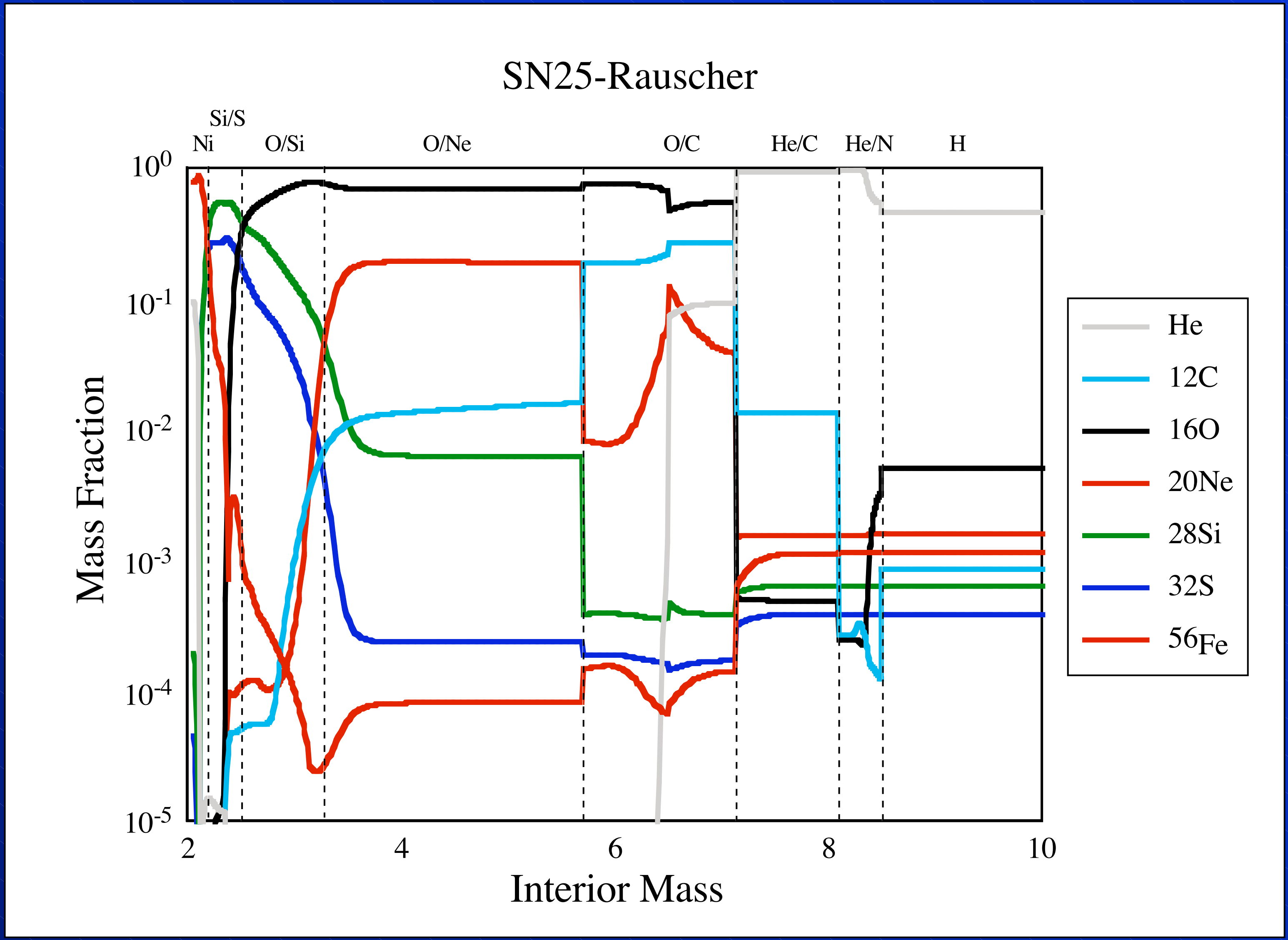

Compare grain data with SN models.

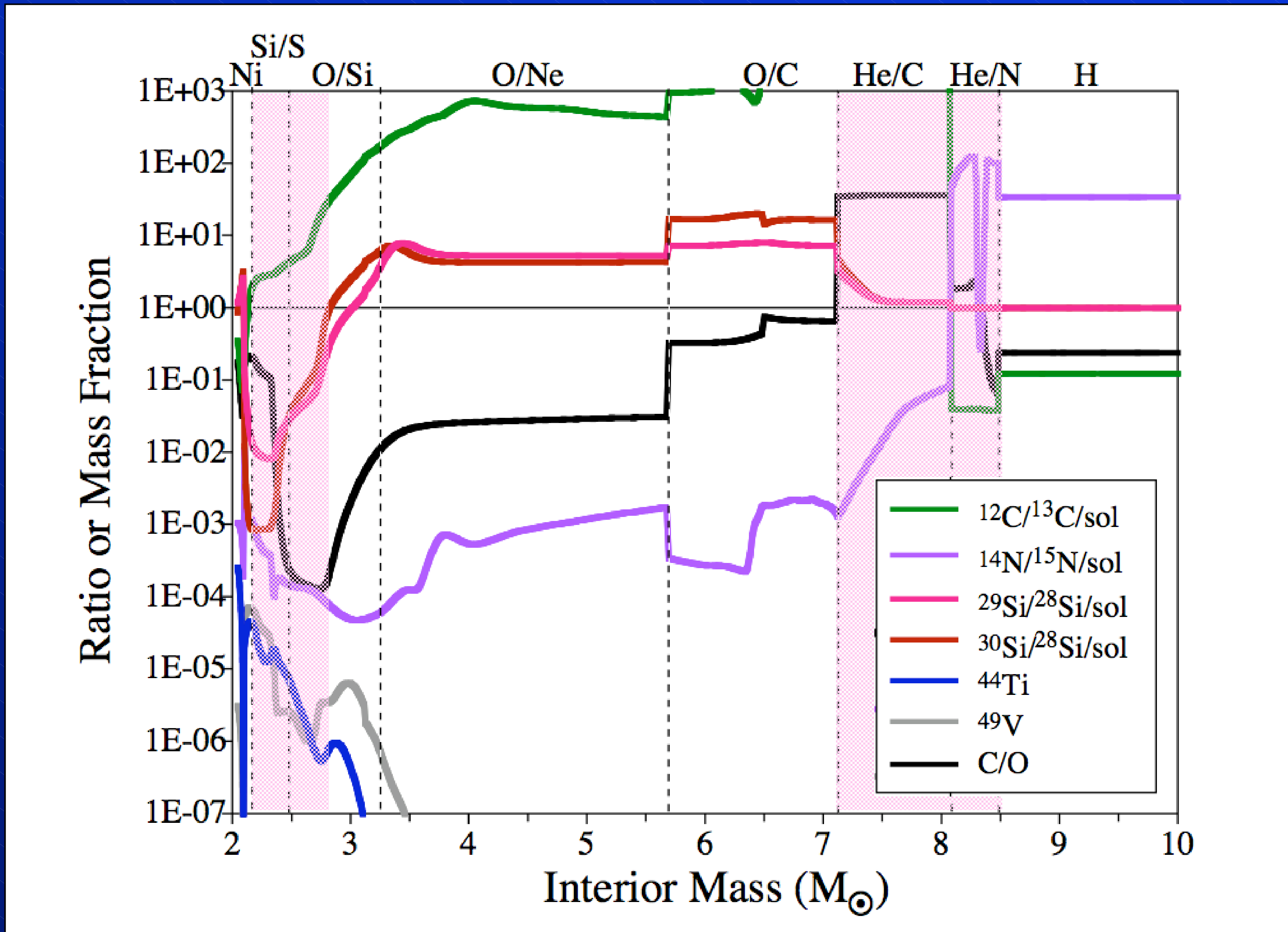

The He/N and He/C zones are the only zones with C>O. ^{28}Si, ^{44}Ti, and ^{49}V are produced in the inner Si/S and O/Si zones.

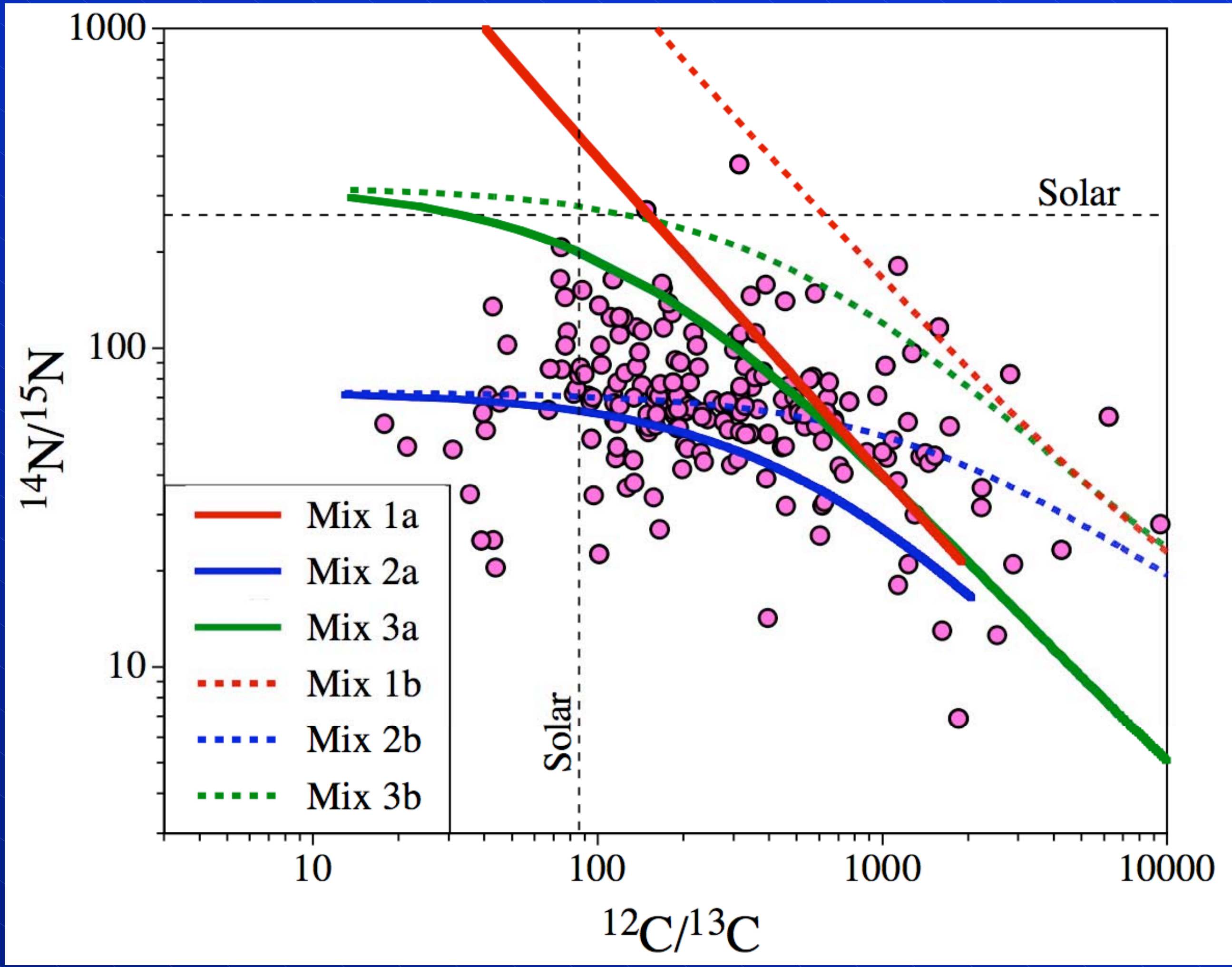

Can cover the N and C ratios of X grains but need the ^{15}N spike.

The 15 and 20 $M_{\odot}$ SN models by Limongi and Chieffi don't have ^{15}N excesses anywhere in the star.

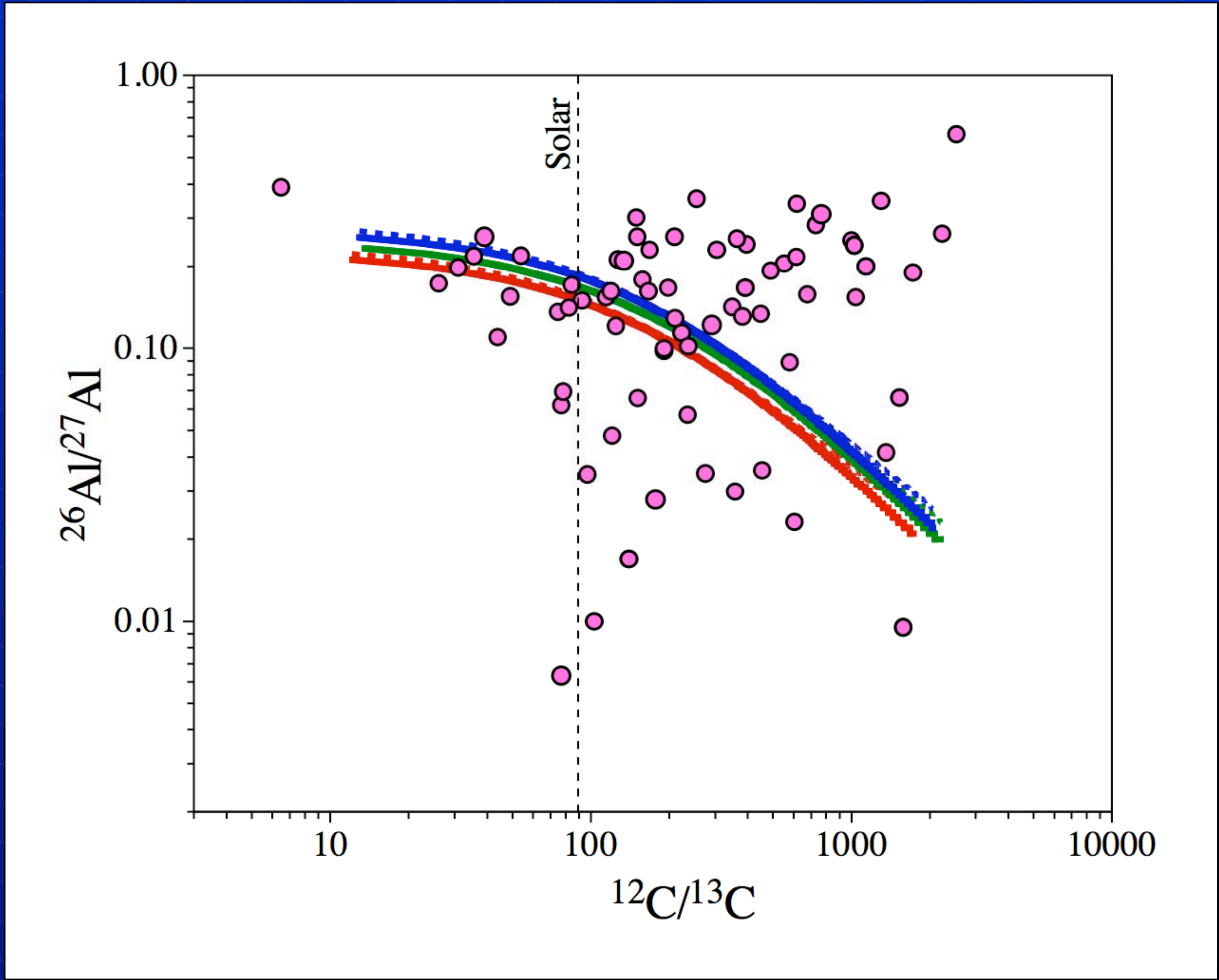

The C and Al isotopic ratios in X grains cannot be explained by SN mixing models.

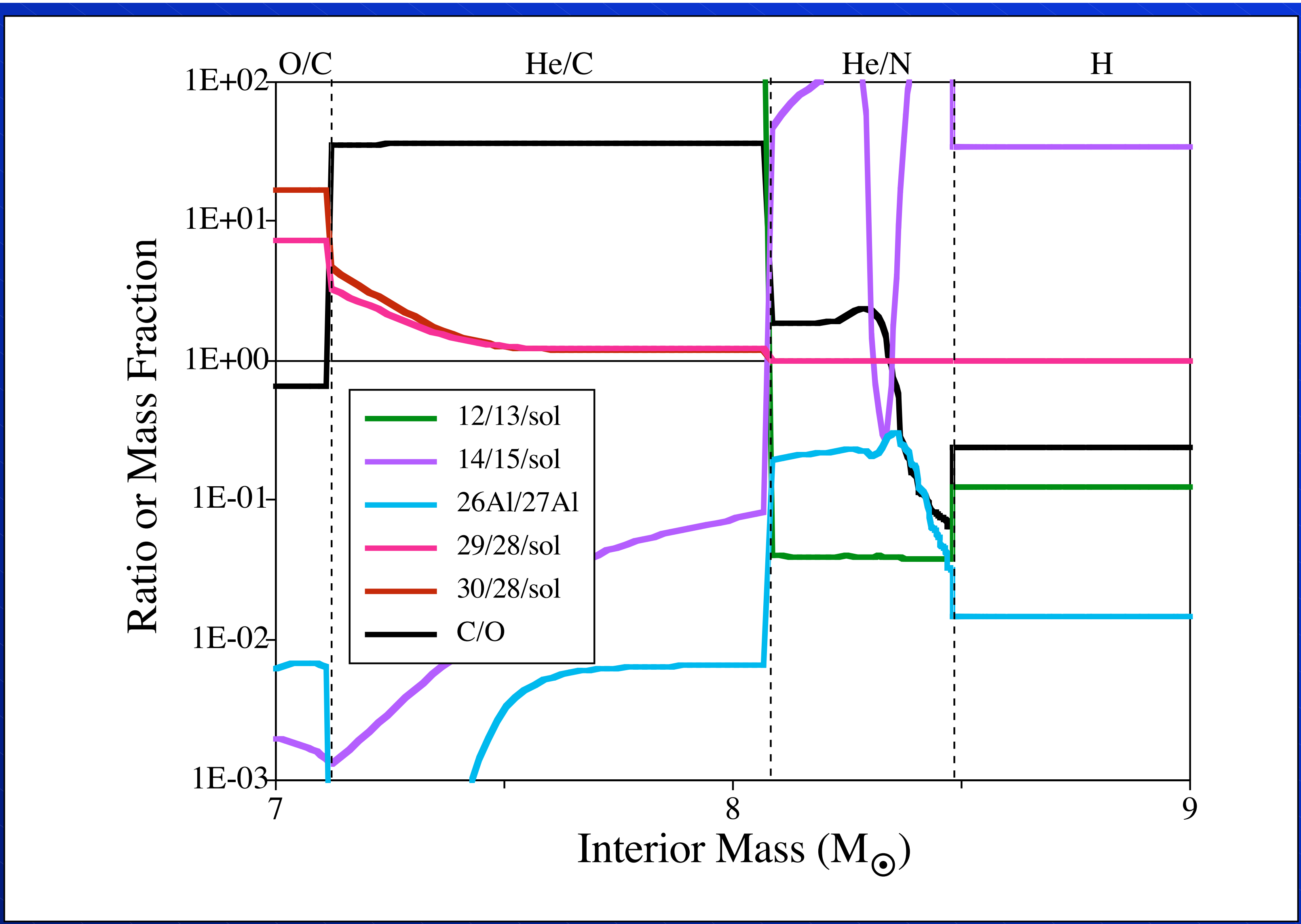

The $^{12}C/^{13}C$ ratio is high in the He/C zone and low in the He/N zone. The $^{26}Al/^{27}Al$ ratio behaves in the opposite way.

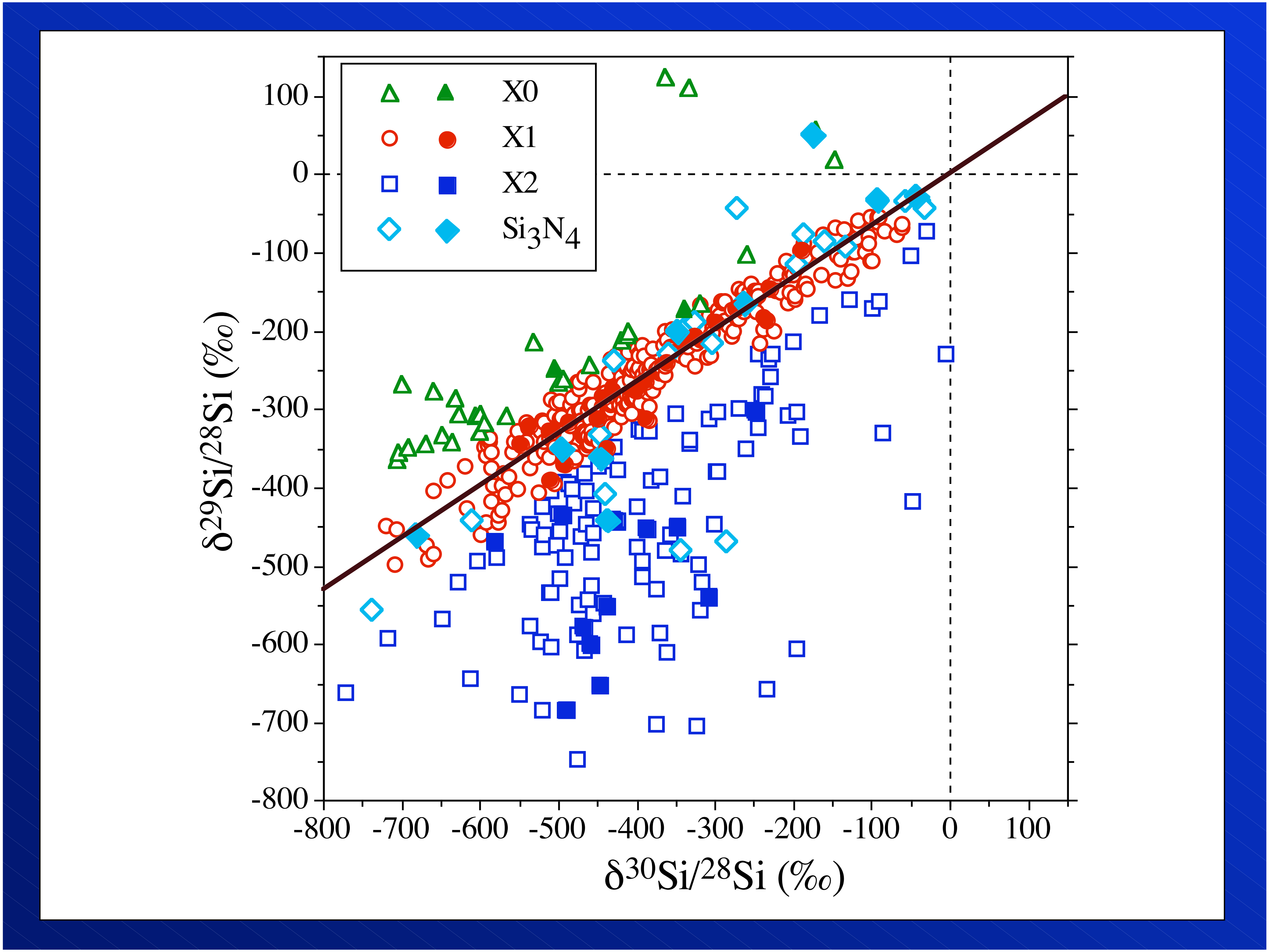

X0
X1
X2
Si_3N_4
$\delta^{29}Si/^{28}Si$ (‰)
$\delta^{30}Si/^{28}Si$ (‰)
100
0
-100
-200
-300
-400
-500
-600
-700
-800
-800
-700
-600
-500
-400
-300
-200
-100
0
100

The most interesting cases are when grain data do NOT agree with theoretical models.
The Si isotopic ratios of X grains are another example.

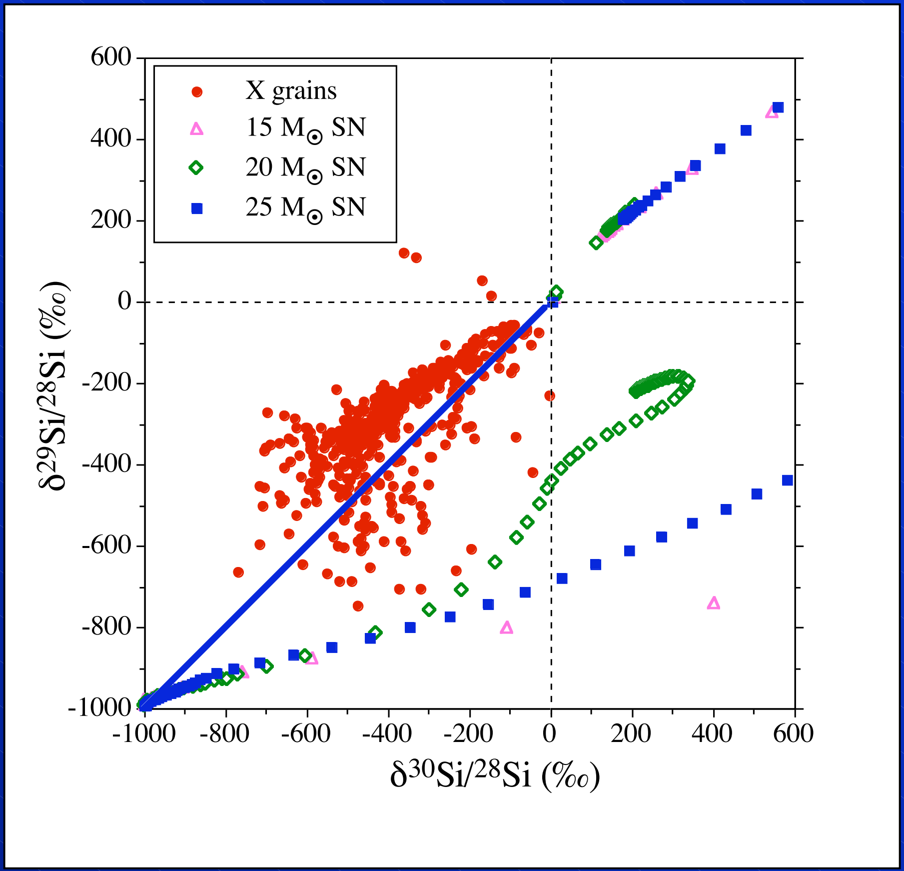

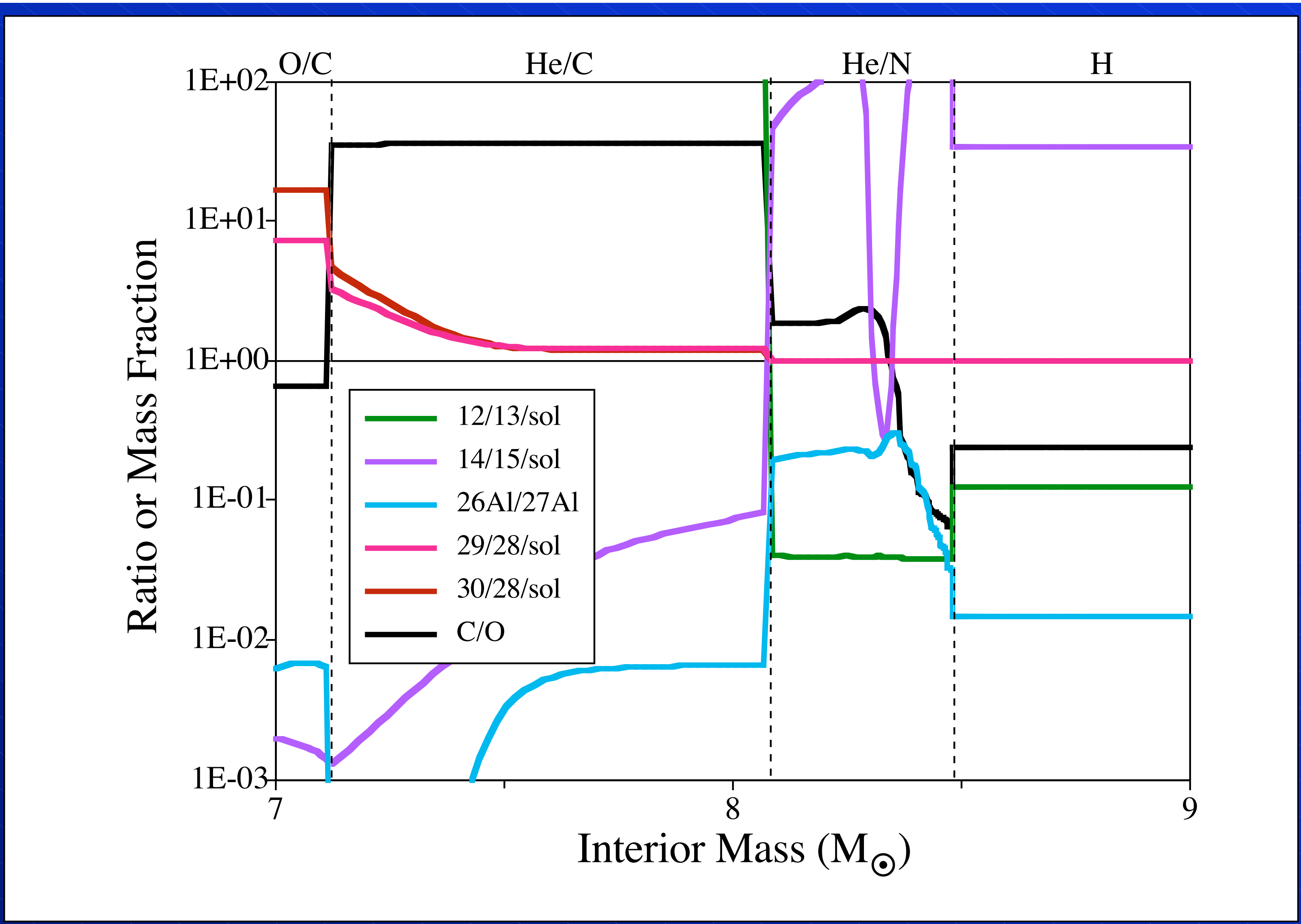

A He/N-He/C mix has ^{29}Si and ^{30}Si excesses.

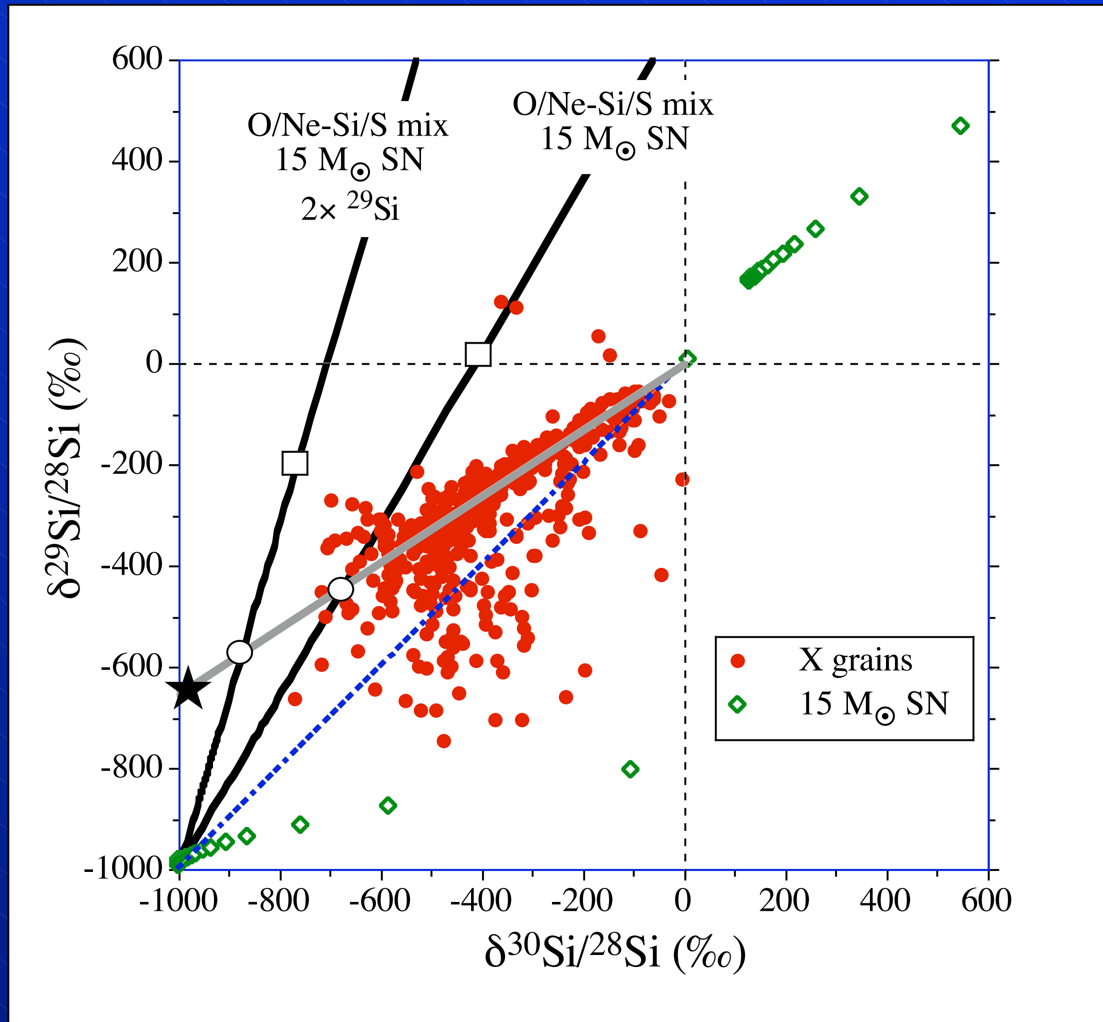

Hoppe et al. proposed a contribution from the O/Ne zone to explain the composition of a grain with an ^{29}Si excess and ^{30}Si deficit.

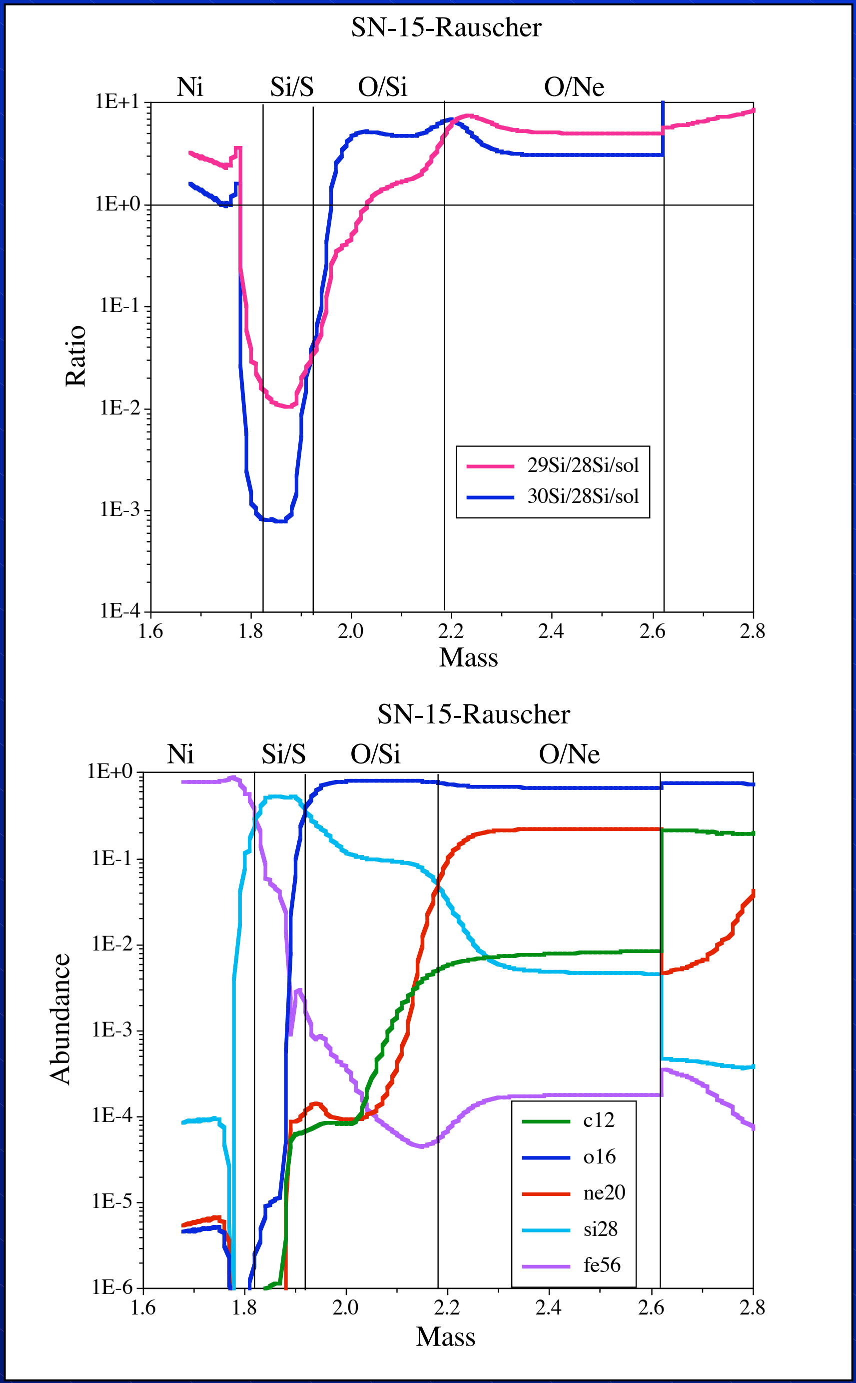

The O/Si zone is rich in ^{30}Si and has much more Si than the O/Ne zone.

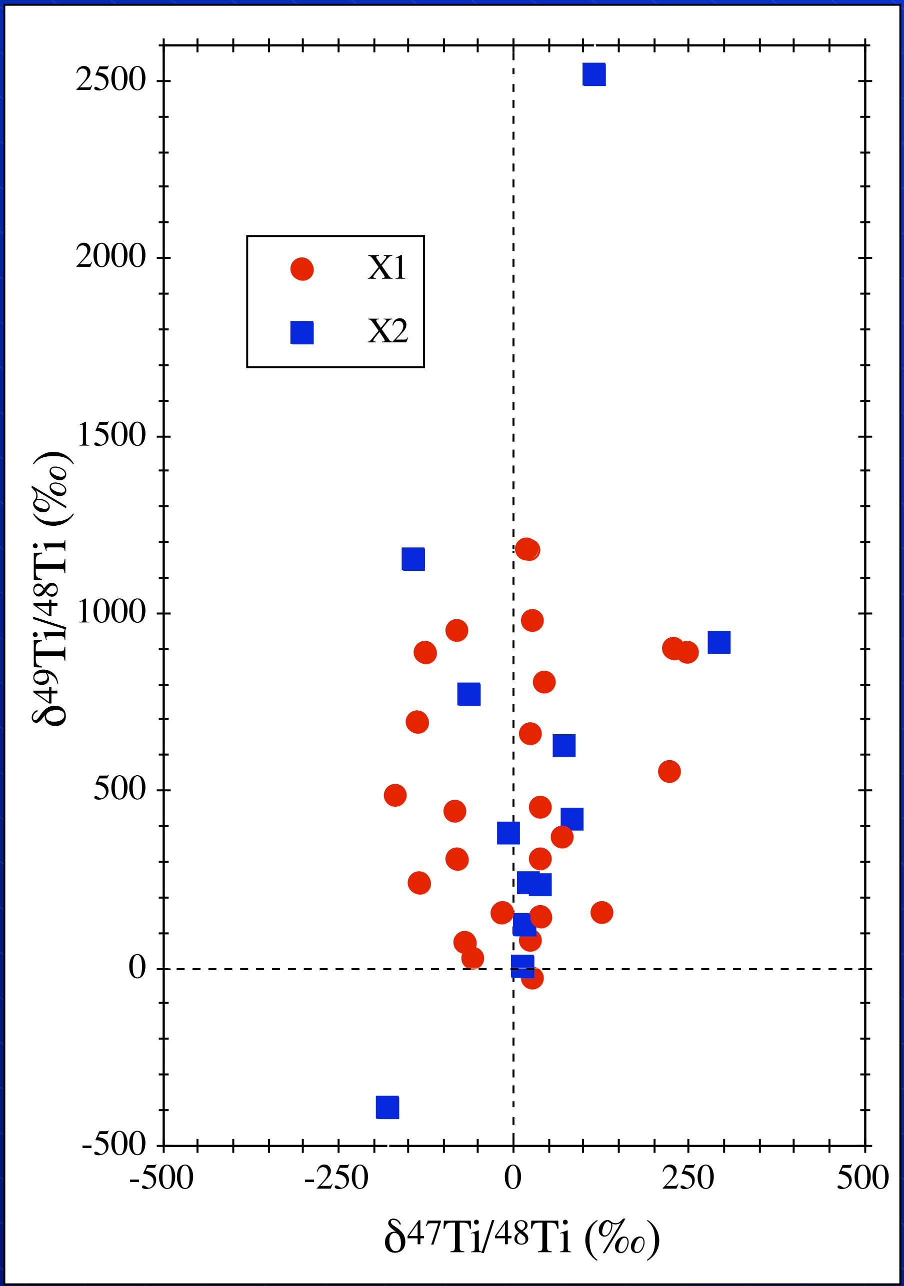

X grains also have large ^{49}Ti excesses, possibly from the decay of ^{49}V ($T_{1/2}$ = 336d).

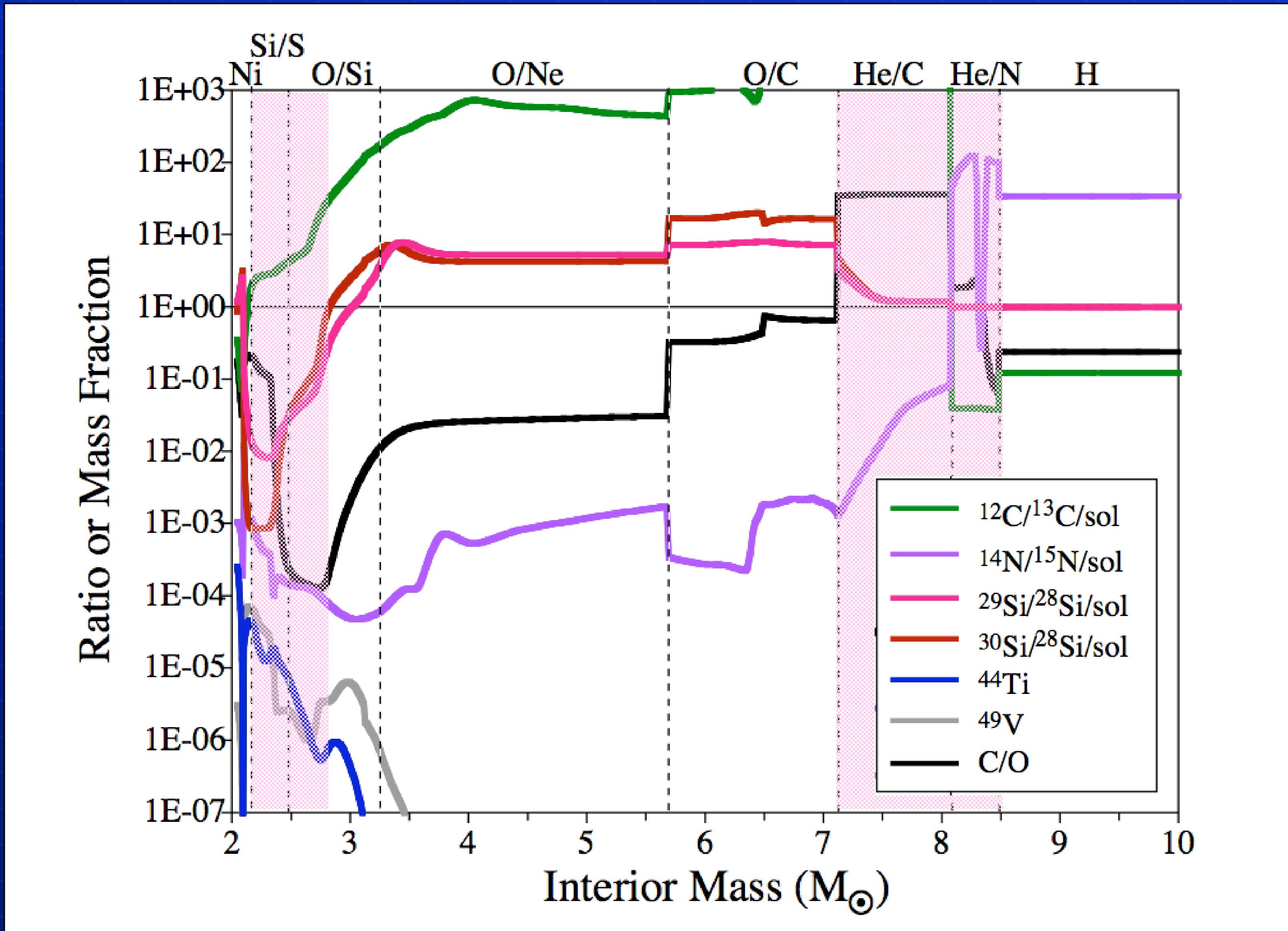

The He/N and He/C zones are the only zones with C>O. ^{28}Si, ^{44}Ti, and ^{49}V are produced in the inner Si/S and O/Si zones.

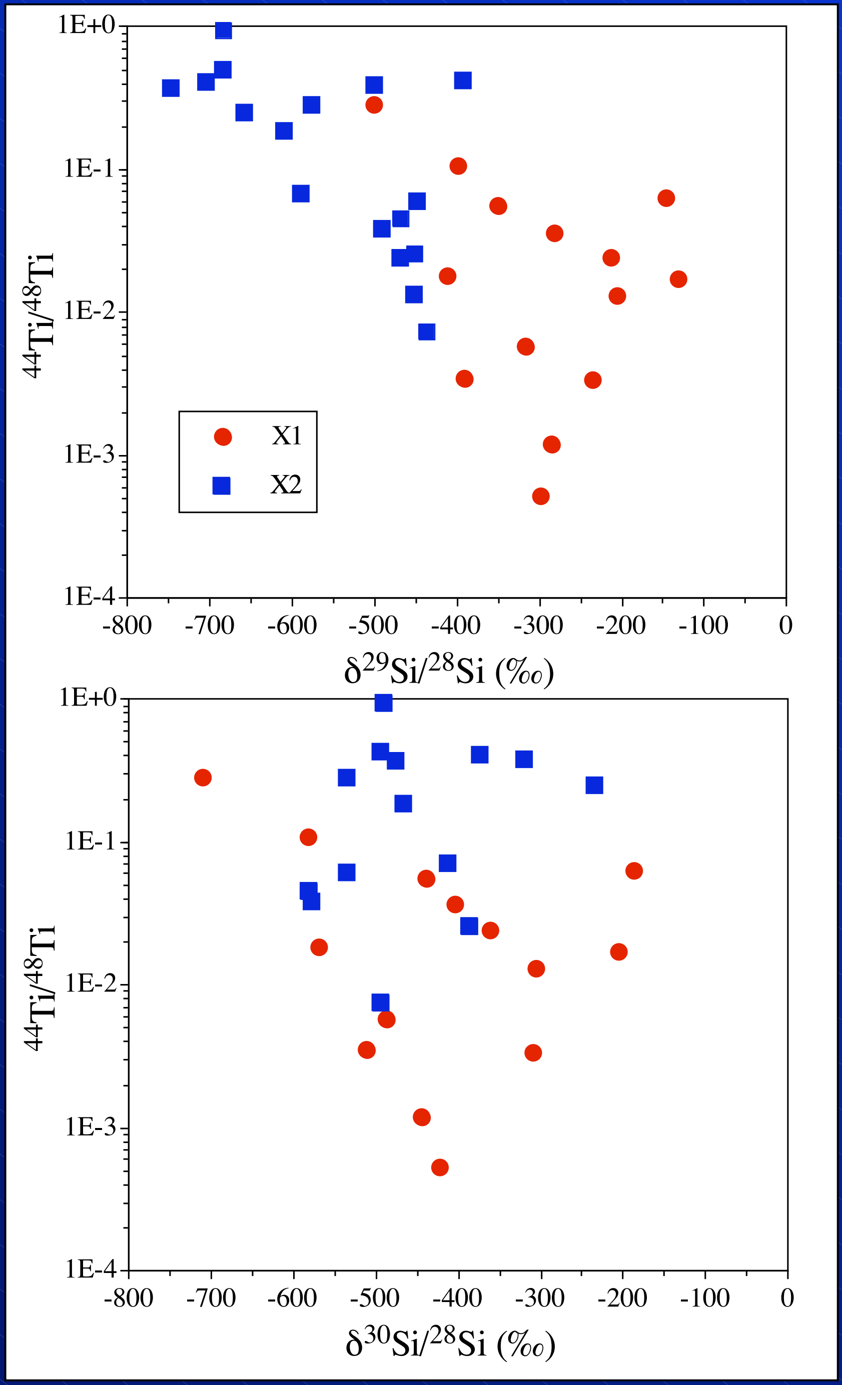

$^{44}Ti/^{48}Ti$ ratios are higher in X2 grains and there is a correlation with $\delta^{29}Si/^{28}Si$.

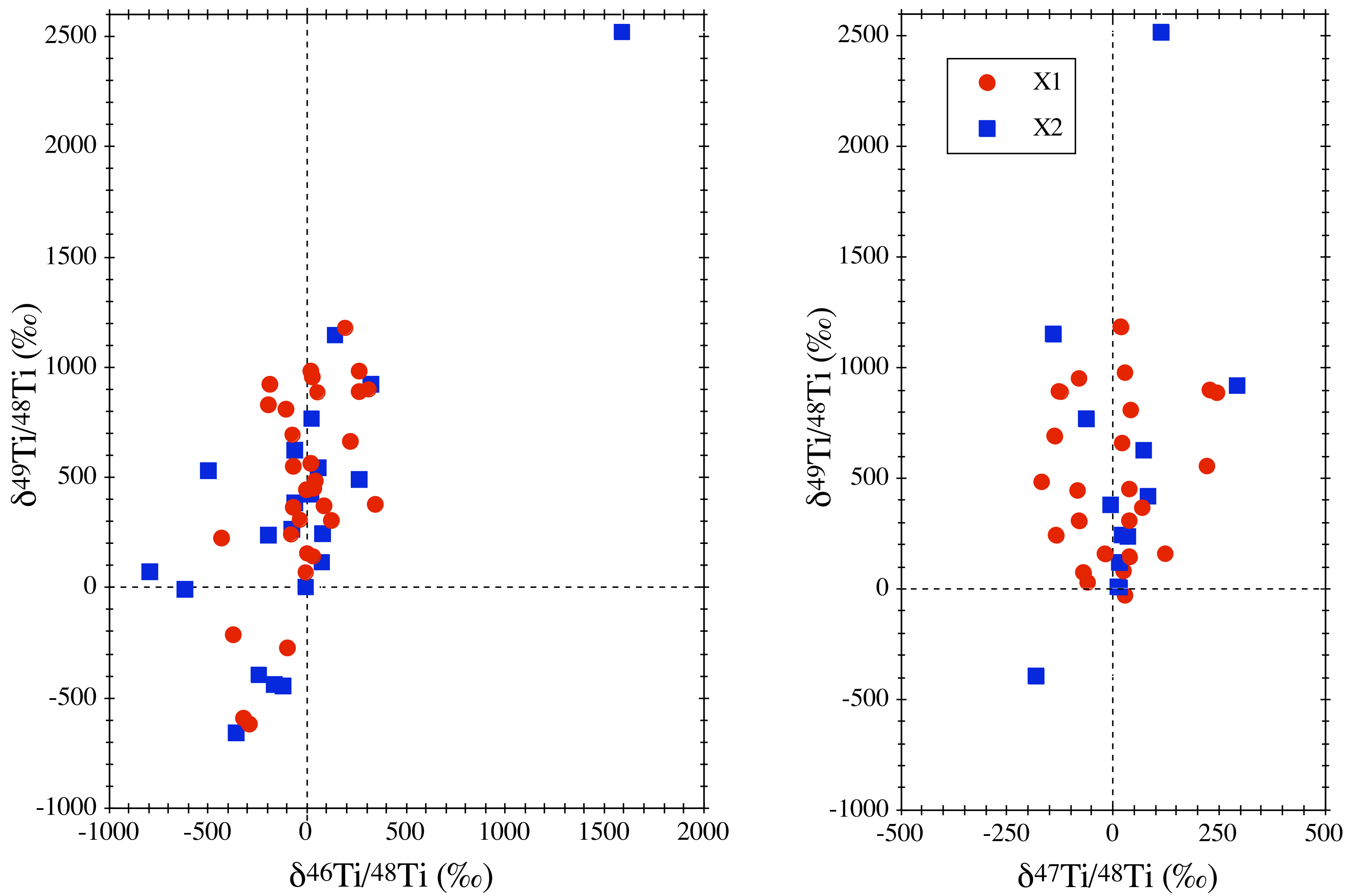

^{46}Ti and ^{49}Ti also show some deficits.

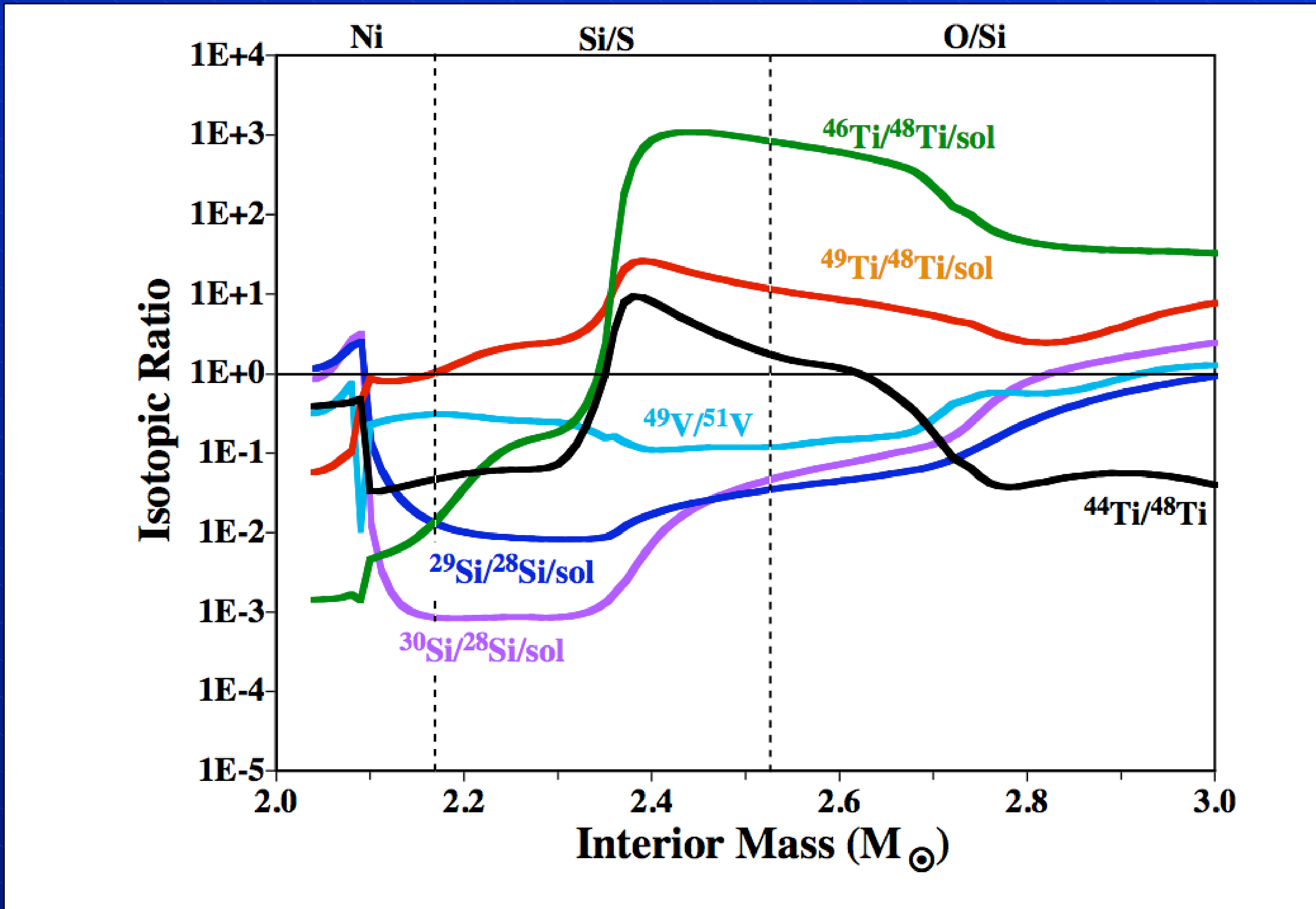

Mix He/N-He/C mix (with $^{12}C/^{13}C=100$) with different layers from Si/S and O/Si zones.

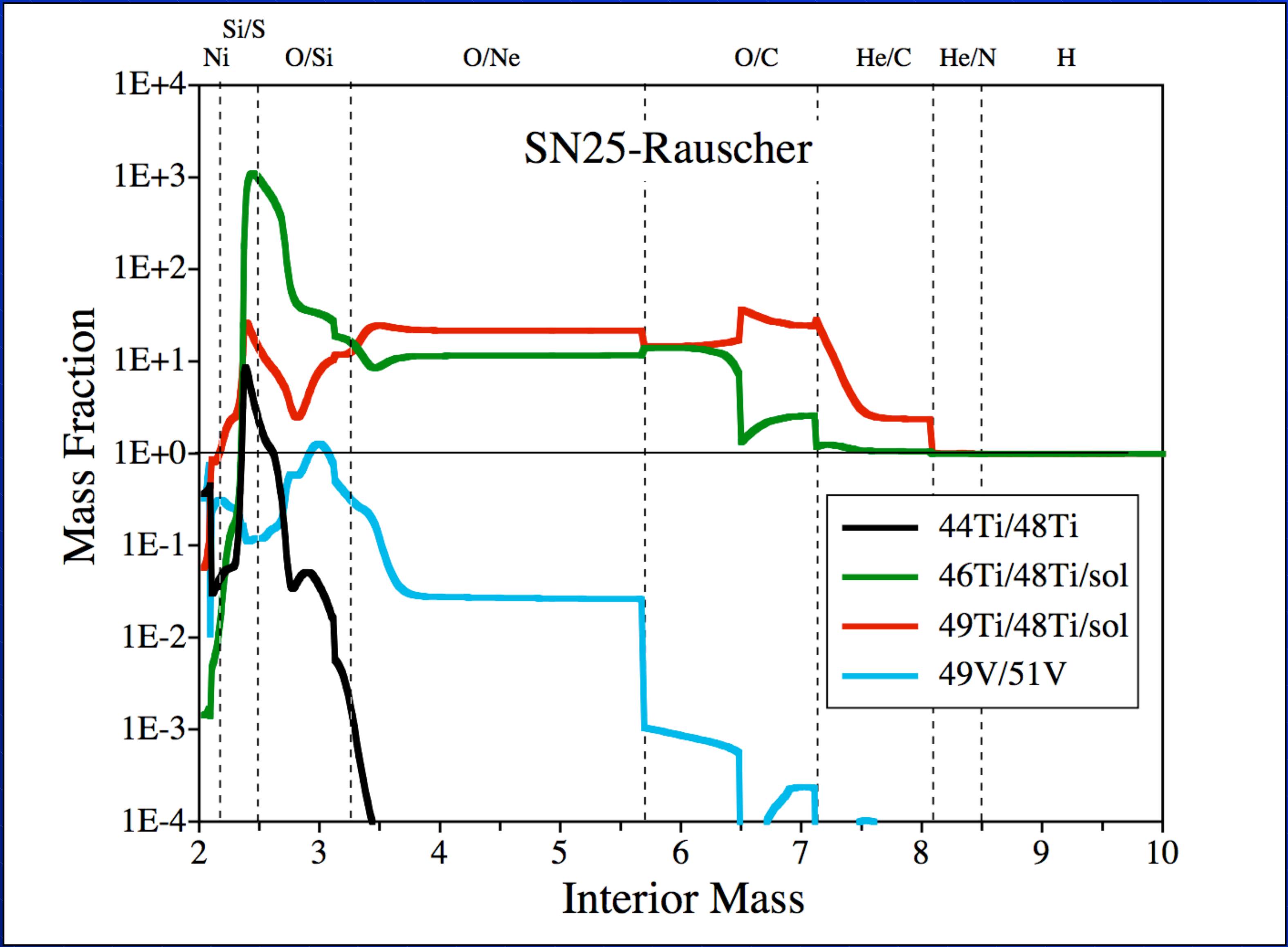

Large ^{49}Ti excesses from n-capture are in the He/C and O/C zones.

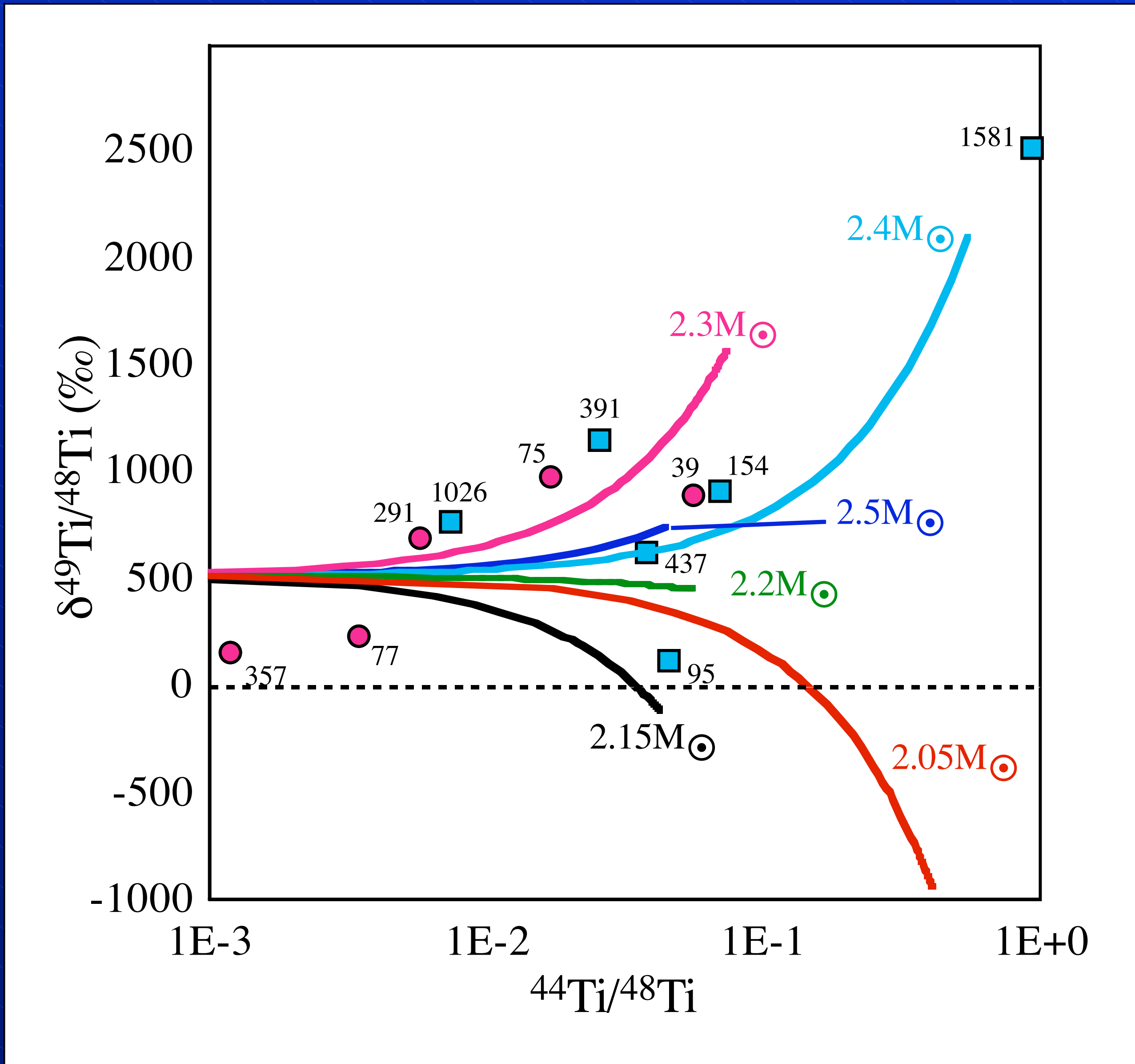

In the He/N-He/C mix with $^{12}C/^{13}C=100$, $\delta^{49}Ti/^{48}Ti=522$.

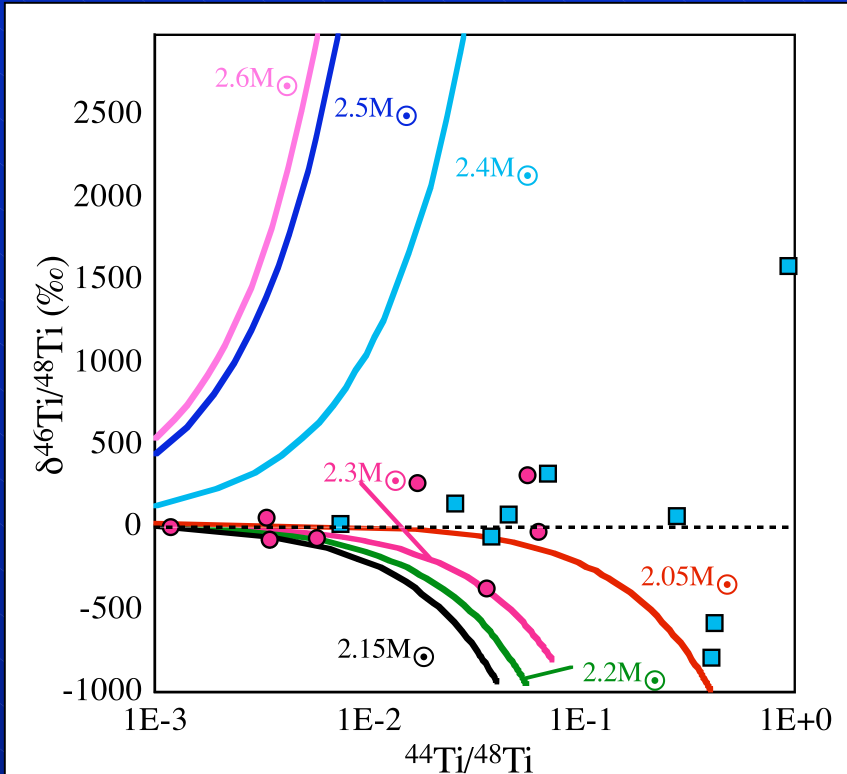

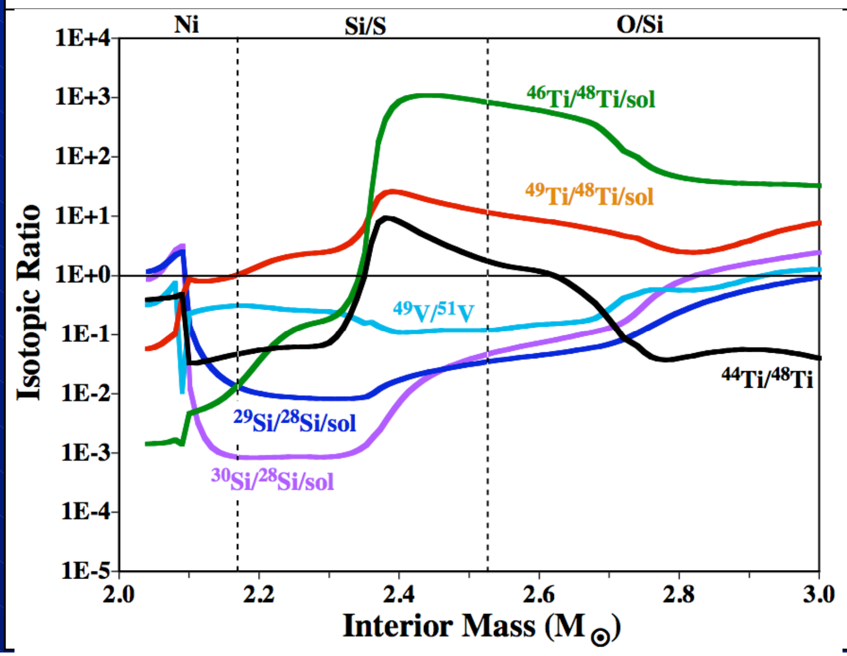

A few X2 grains with large $^{44}Ti/^{48}Ti$ ratios show ^{46}Ti deficits, indicating contributions from the inner Si/S zone. There is no indication for contributions from the outer Si/S and the O/Si zone. A similar conclusion has been made from Fe isotopic ratios in X grains.

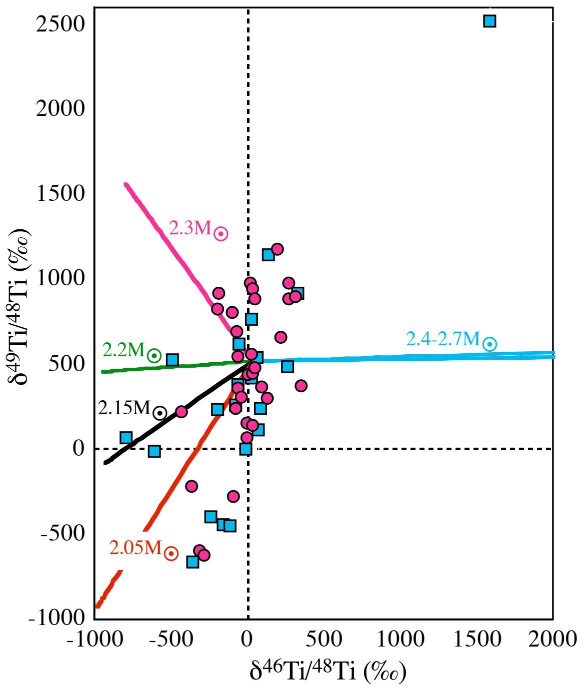

Deficits in ^{49}Ti and ^{46}Ti can be achieved by mixing with the Ni core.

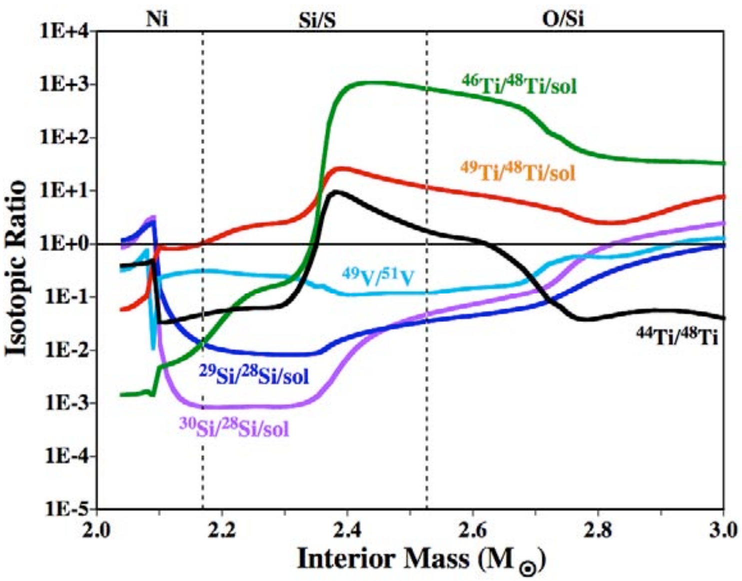

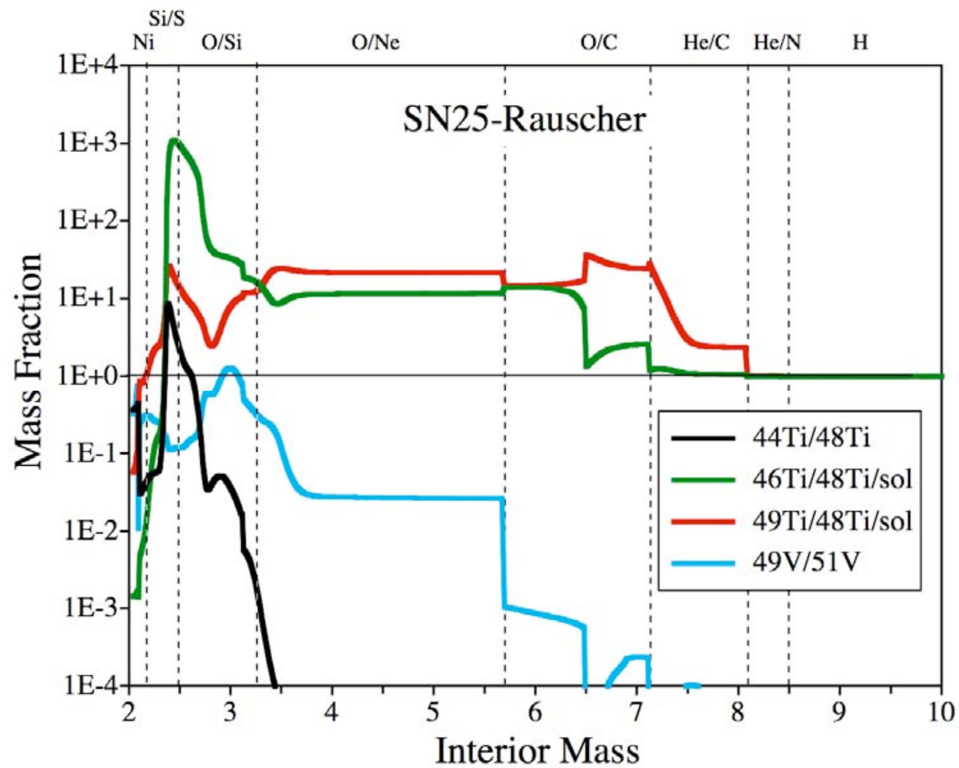

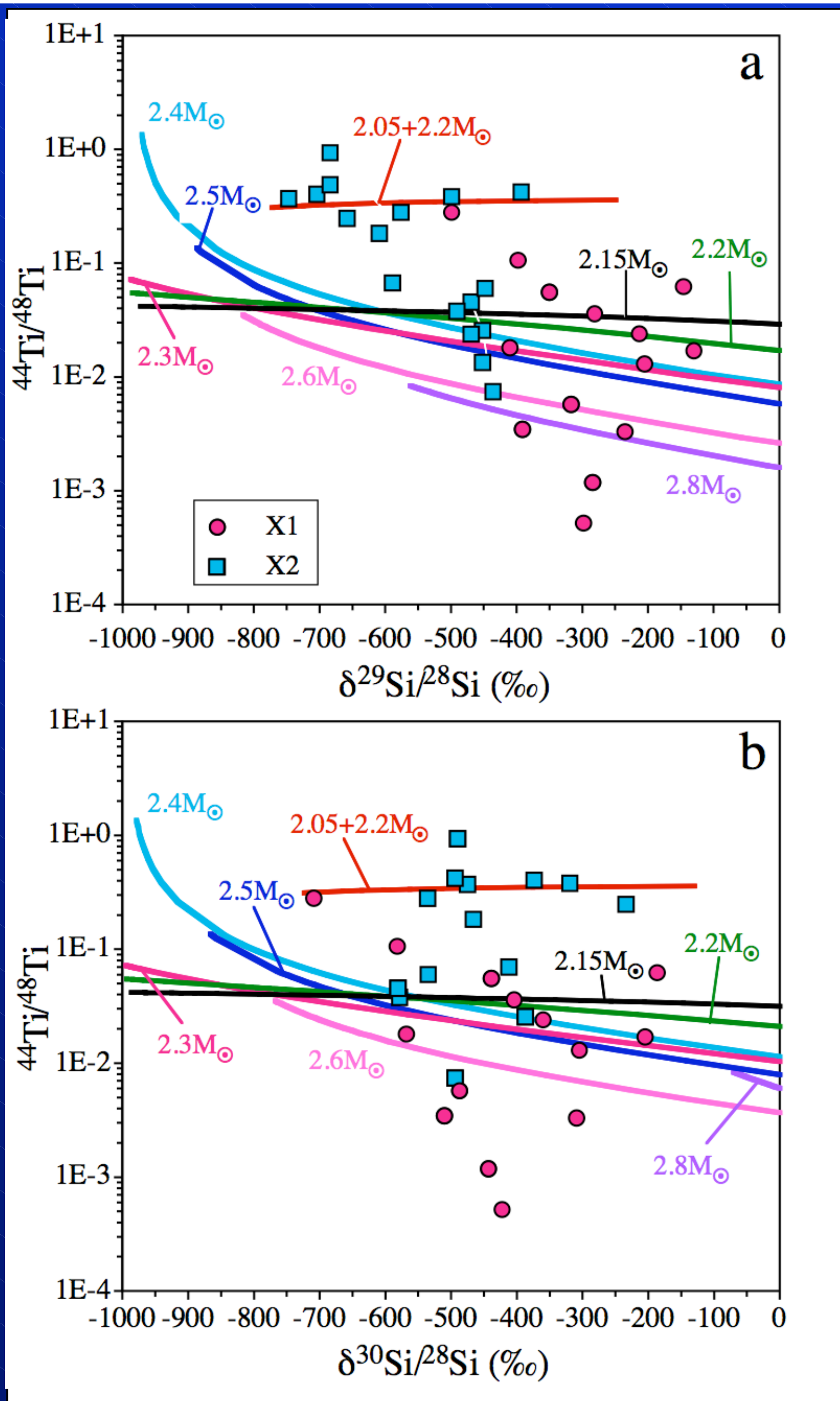

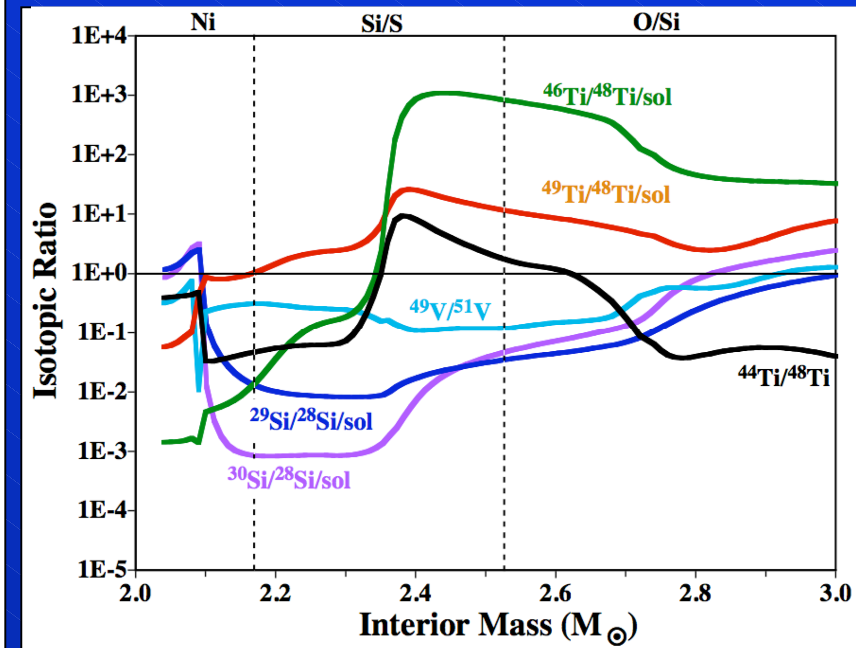

SN mixes show the same sign of the correlation between ^{44}Ti/^{48}Ti and ^{29}Si/^{28}Si. X2 grains data lie outside of the region spanned by mixing curves and require contributions from the Ni core.

ANOTHER CHALLENGE

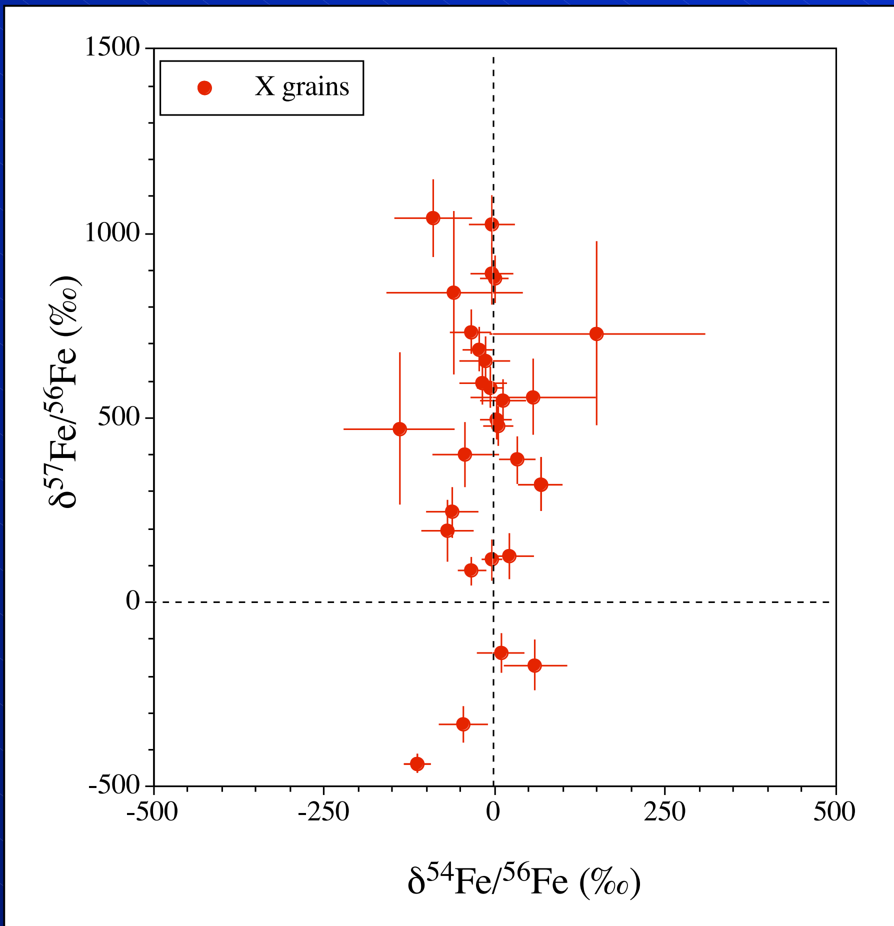

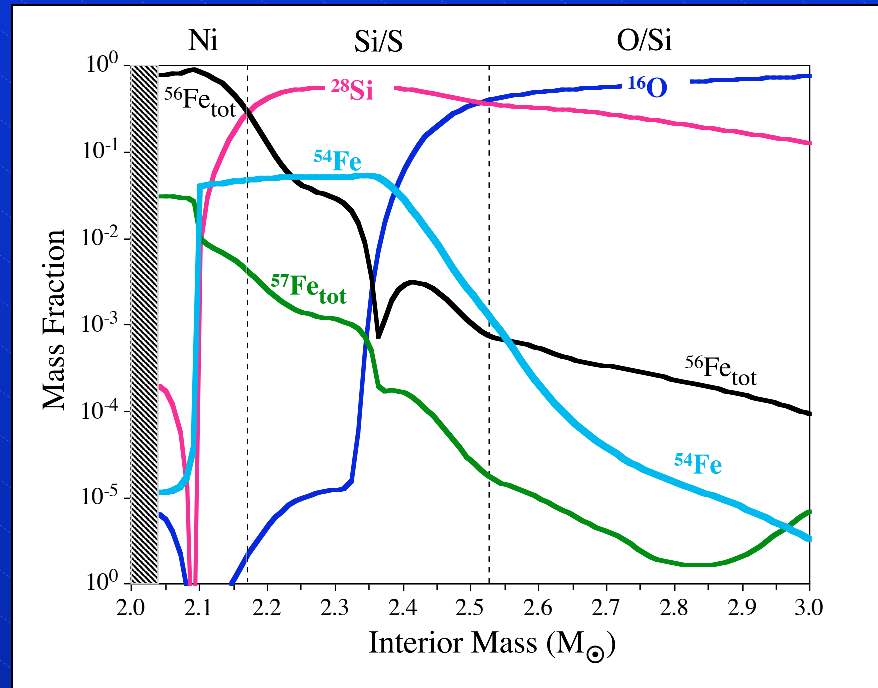

No significant ^{54}Fe excesses are seen in X grains, although the Si/S zone has a very high ^{54}Fe abundance.

A+B grains

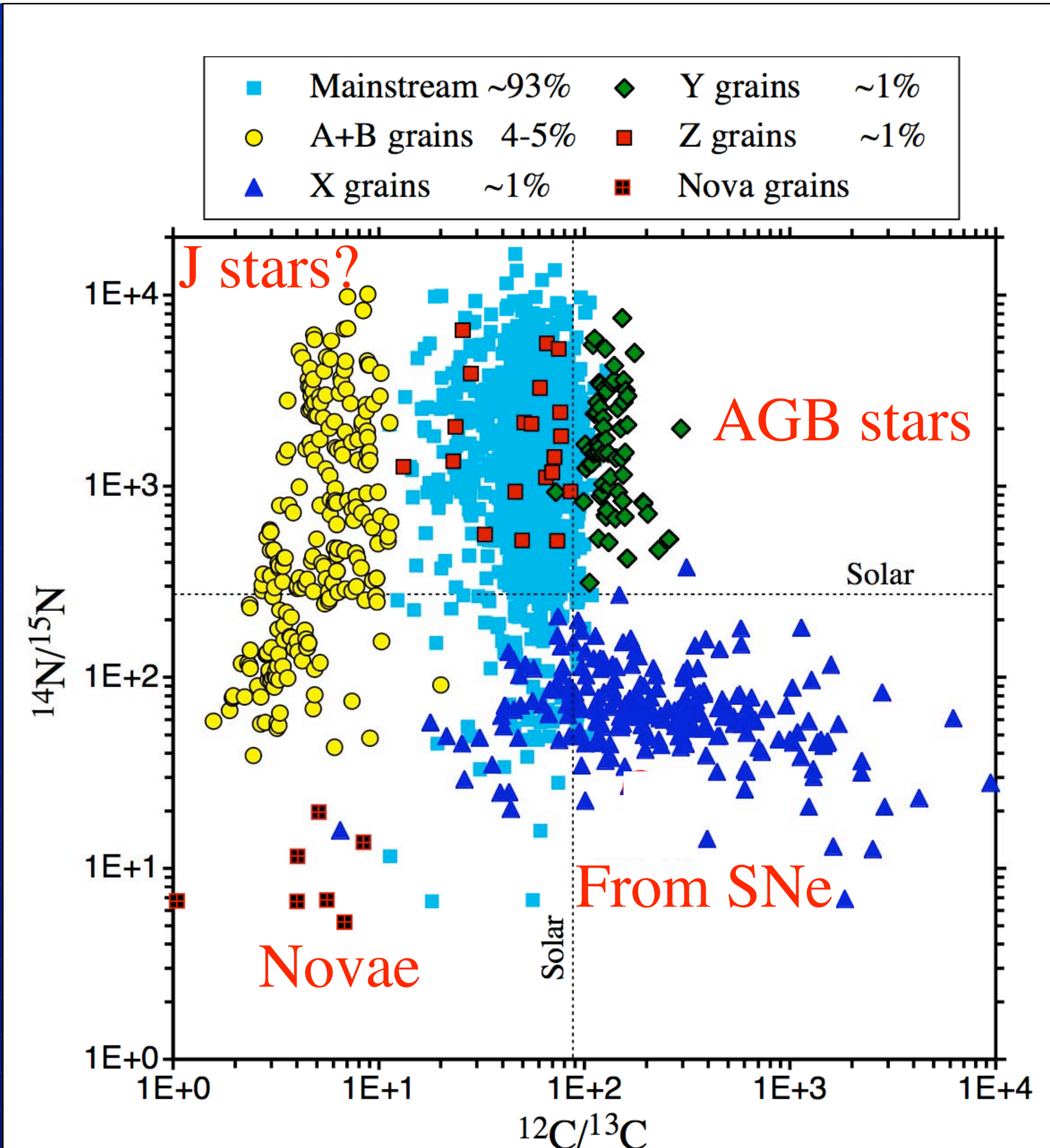

AB grains have low $^{12}C/^{13}C$ ratios.

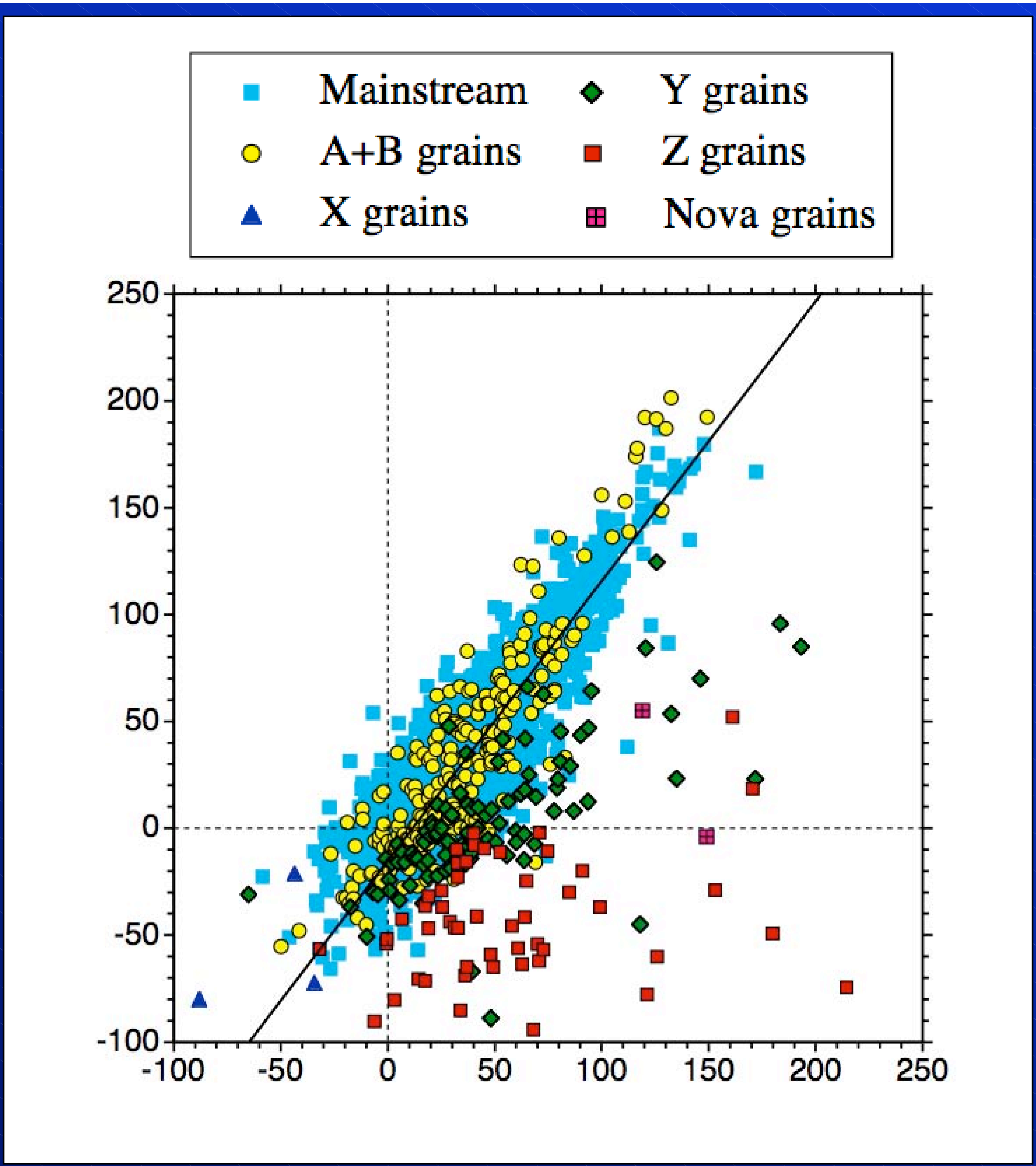

The distribution of the Si isotopic ratios of AB grains is the same as that of mainstream grains.

CARBON STARS

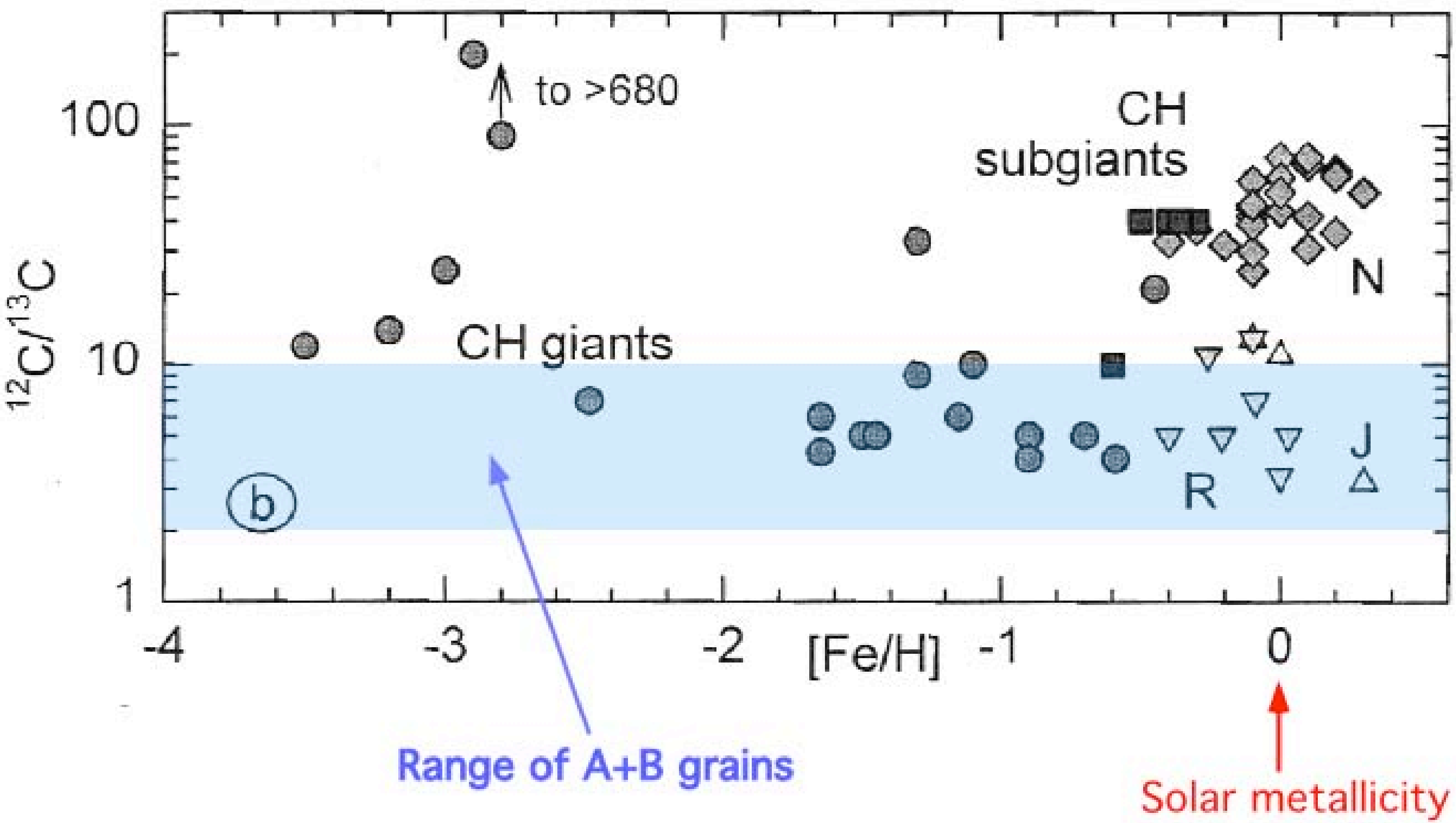

From Lodders and Fegley (1998)

CARBON STARS

1) J and R stars as well as CH giants have low $^{12}C/^{13}C$ ratios
2) CH giants seem to be excluded because they have low metallicities
3) J stars have solar abundances of s-process elements, R stars have hs/Fe>solar. J(N) stars have circumstellar dust shells (with SiC) whereas R stars don't

J-type carbon stars are the most likely parent stars of A+B grains

Born-again AGB stars (Sakurai's object) have also low $^{12}C/^{13}C$ ratios but are expected to show the signature of the s-process.

Oxide grains

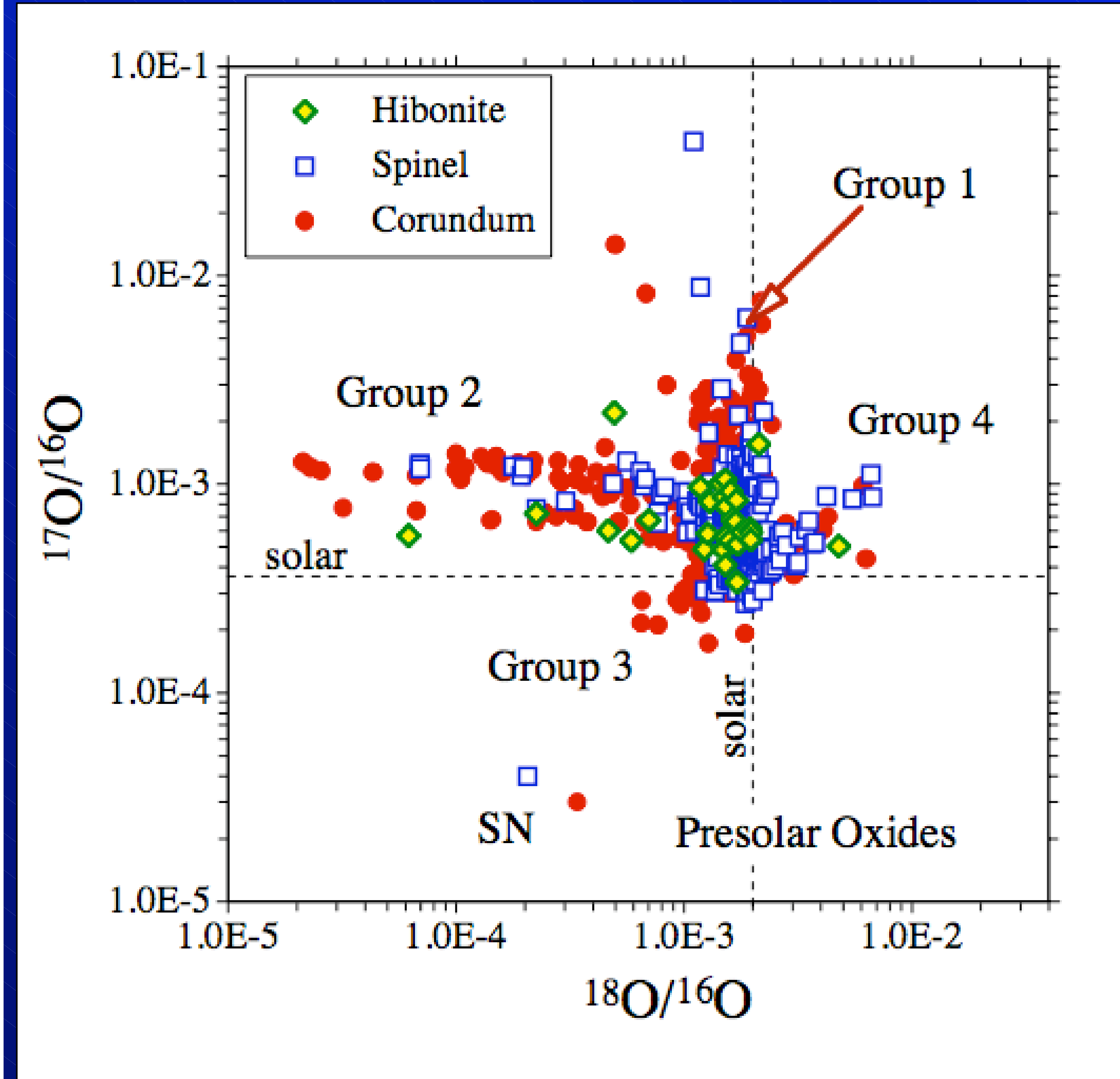

Group 1: RG or AGB stars (1st DUP).
Group 2: stars with CBP
Group 3: low metallicity stars, SNe?
Group 4: high metallicity; SNe

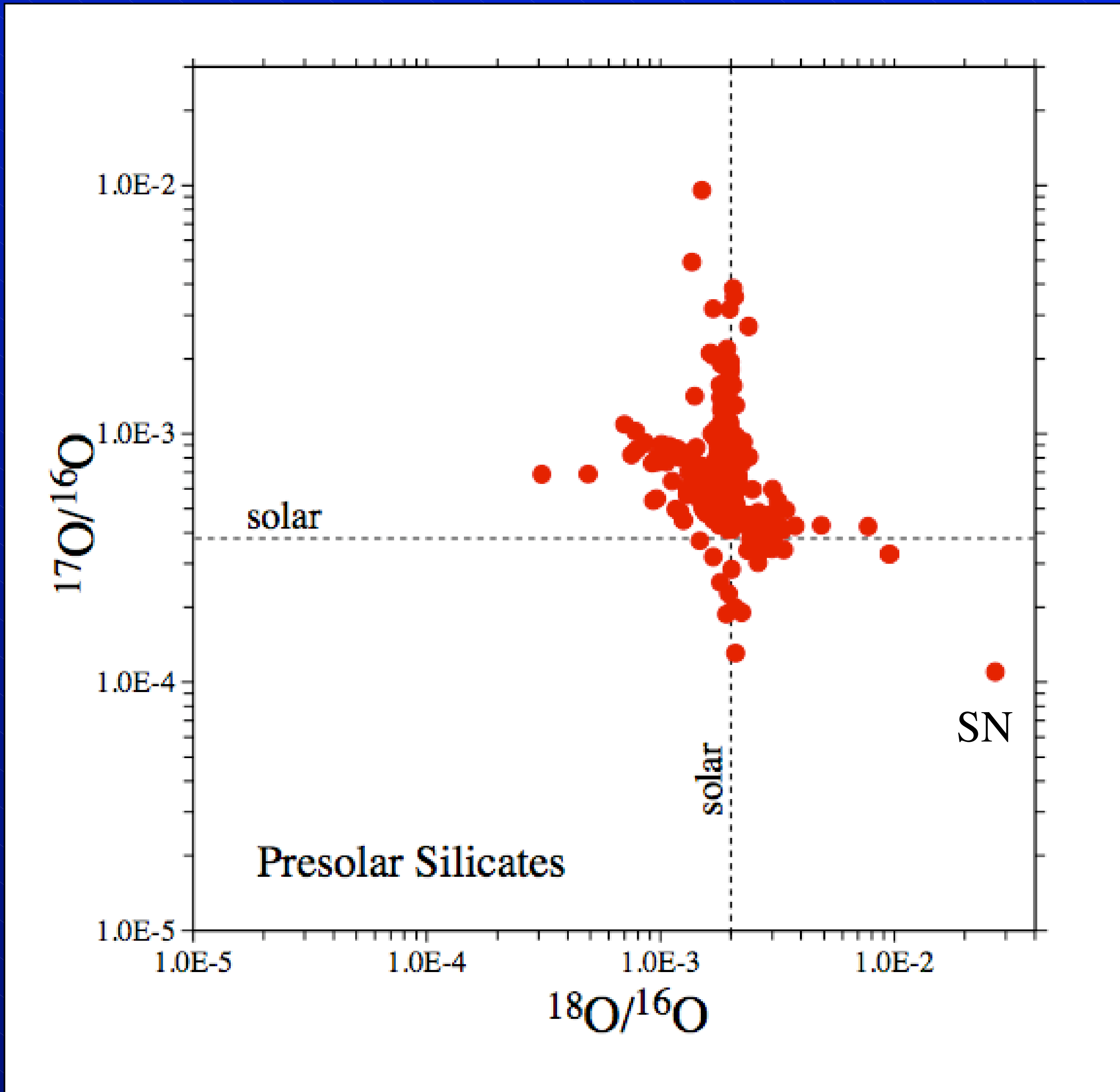

1.0E-2
1.0E-3
1.0E-4
1.0E-5
1.0E-5
1.0E-4
1.0E-3
1.0E-2
$^{17}O/^{16}O$
$^{18}O/^{16}O$
solar
solar
SN
Presolar Silicates

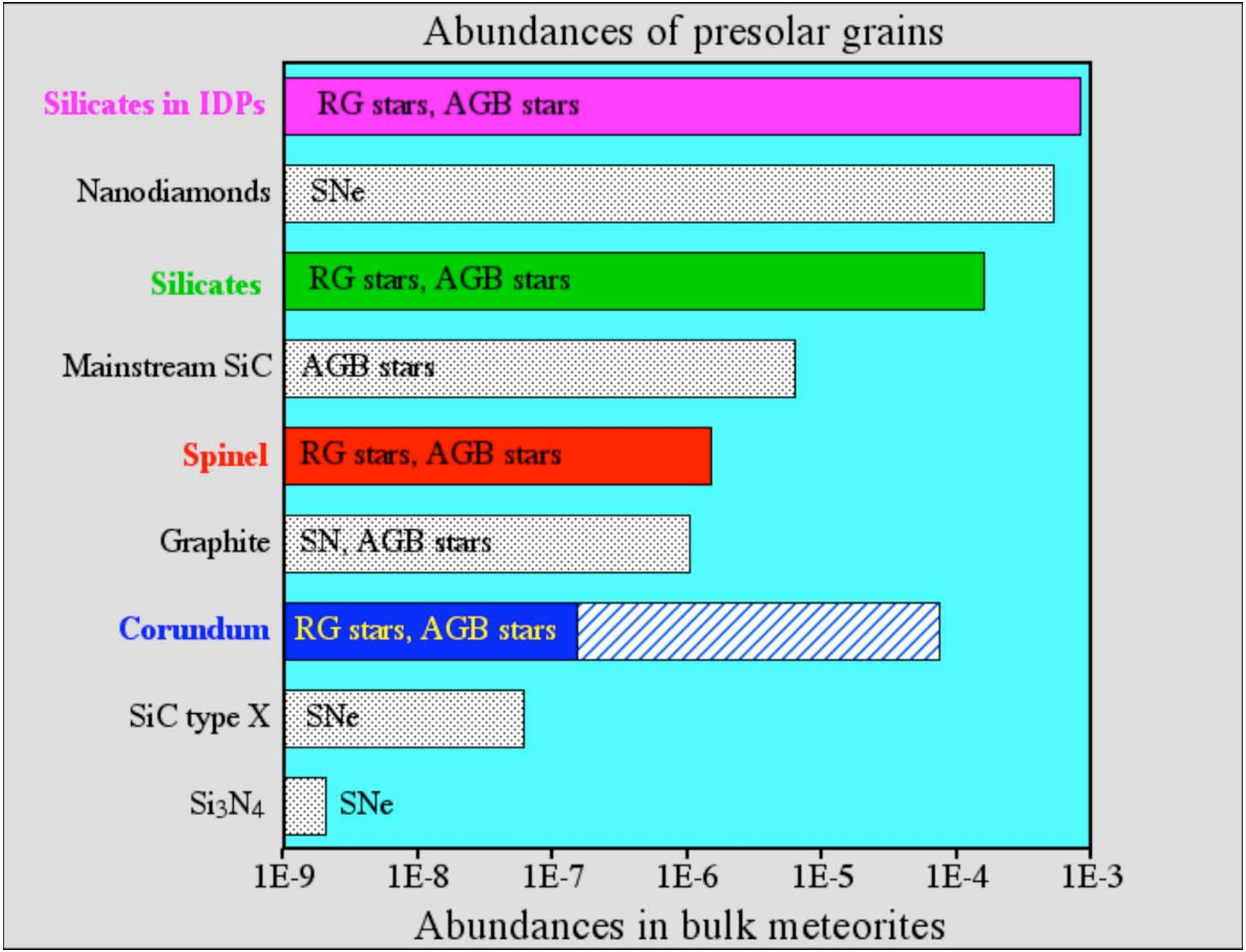

Abundances of presolar grains
Silicates in IDPs
RG stars, AGB stars
Nanodiamonds
SNe
Silicates
RG stars, AGB stars
Mainstream SiC
AGB stars
Spinel
RG stars, AGB stars
Graphite
SN, AGB stars
Corundum
RG stars, AGB stars
SiC type X
SNe
Si3N4
SNe
1E-9
1E-8
1E-7
1E-6
1E-5
1E-4
1E-3
Abundances in bulk meteorites

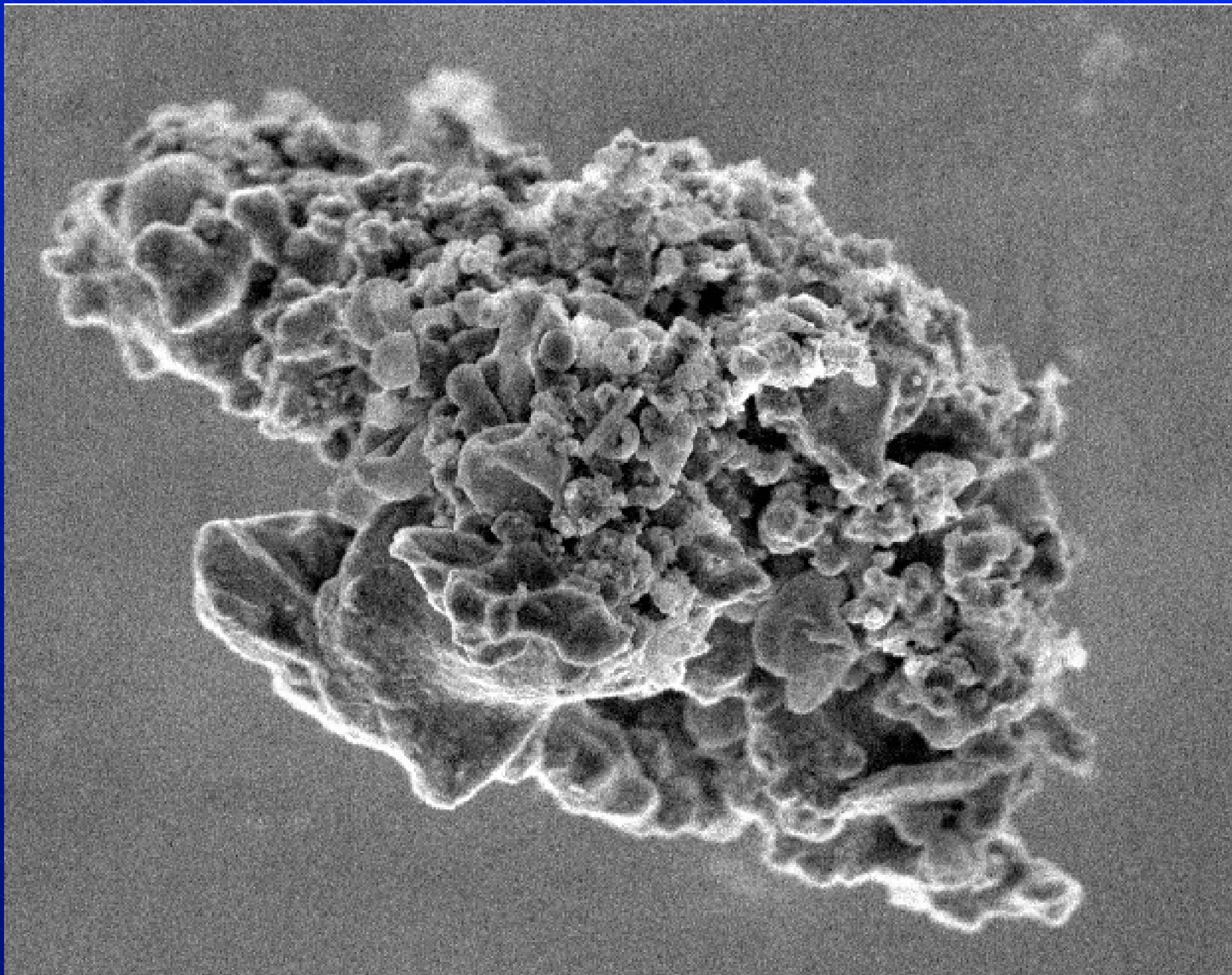

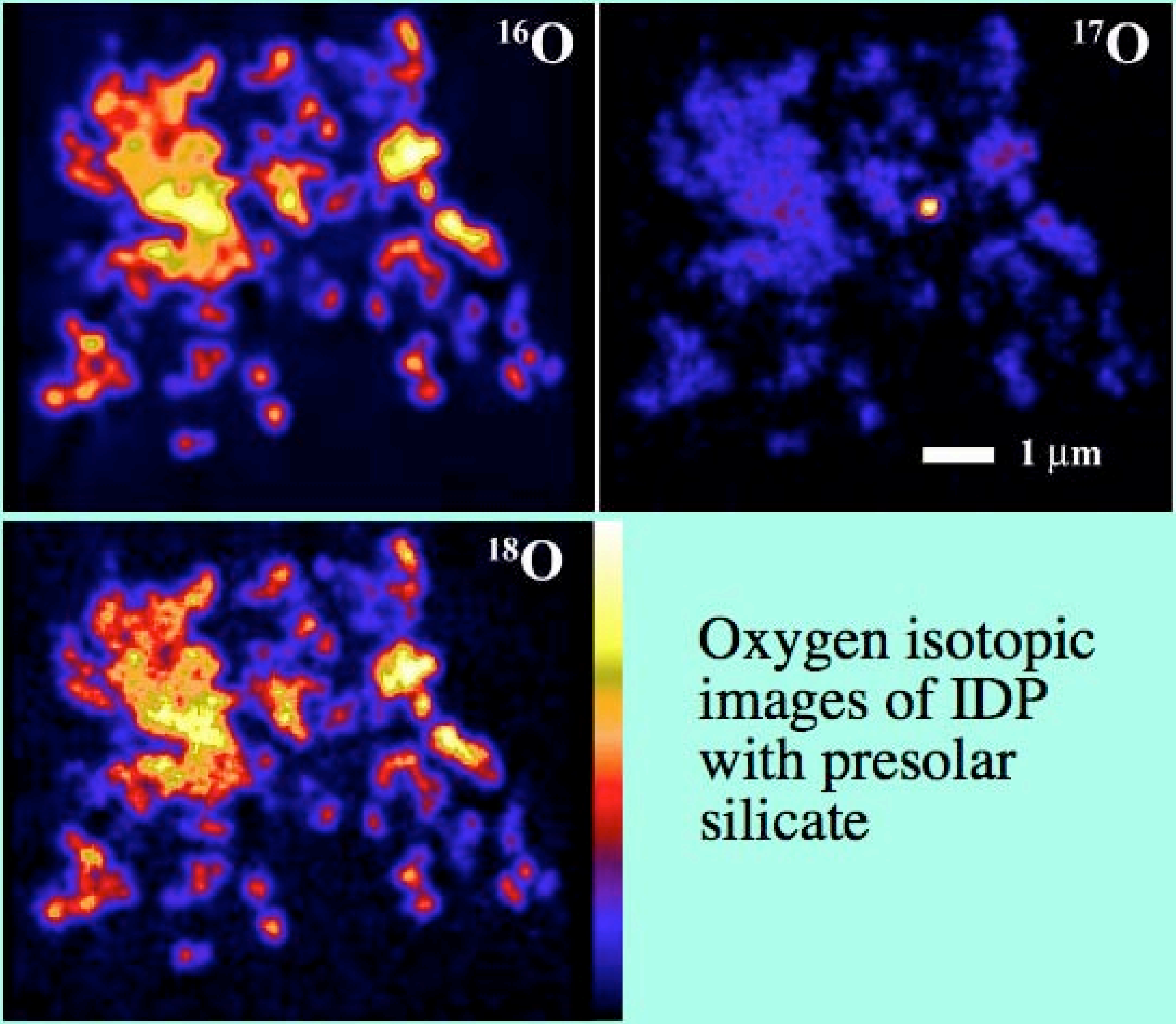

Oxygen isotopic images of IDP with presolar silicate


Presolar Silicate Grains

Presolar Silicates

- newest major addition to presolar grain inventory
- found in most primitive extraterrestrial materials
- large variations in reported abundances:
  - -highest in primitive IDPs: ≥375 ppm

    (e.g., Messenger et al., 2003; Floss et al., 2006; Busemann et al., 2009)
  - -variable in primitive meteorites: up to 220 ppm

    (e.g., Nguyen et al., 2008; Floss and Stadermann, 2009; Vollmer et al., 2009)
- fragile nature of presolar silicates: opportunity to investigate effects of secondary processing

What We Can Learn from Presolar Silicates

- how they formed
  - conditions for grain formation
  - chemical reactions in molecular clouds
  - stellar and galactic evolution
  - nucleosynthesis
- how they evolved
  - processing in interstellar medium (ISM), nebula, or on parent bodies (aqueous alteration, metamorphism)
  - provides information about conditions in these environments
  - terrestrial alteration

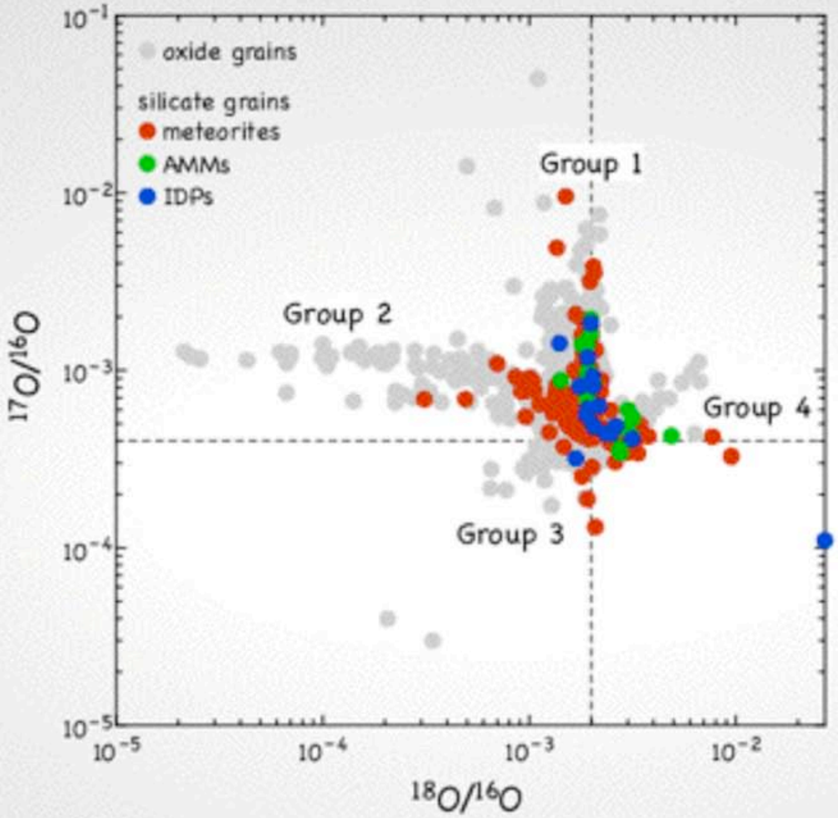

data from Presolar Grain Database (presolar.wustl.edu/~pgd)

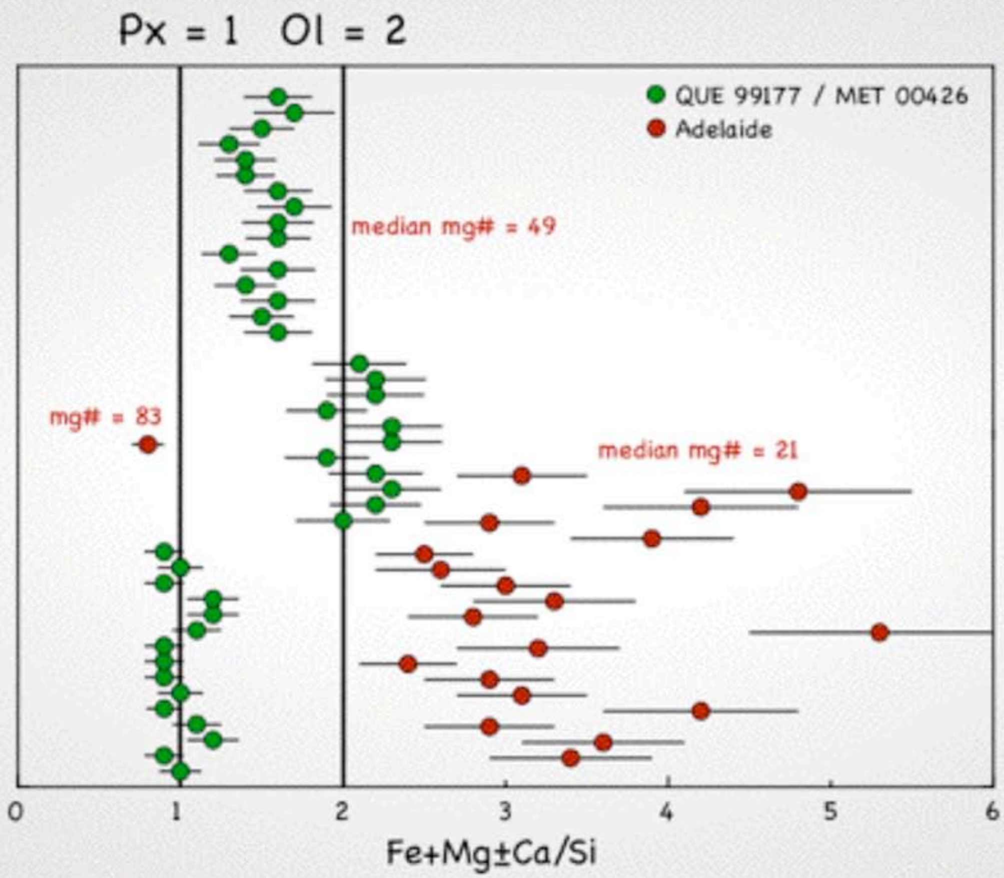

Px = 1 Ol = 2
QUE 99177 / MET 00426
Adelaide
median mg# = 49
mg# = 83
median mg# = 21
0
1
2
3
4
5
6
Fe+Mg±Ca/Si

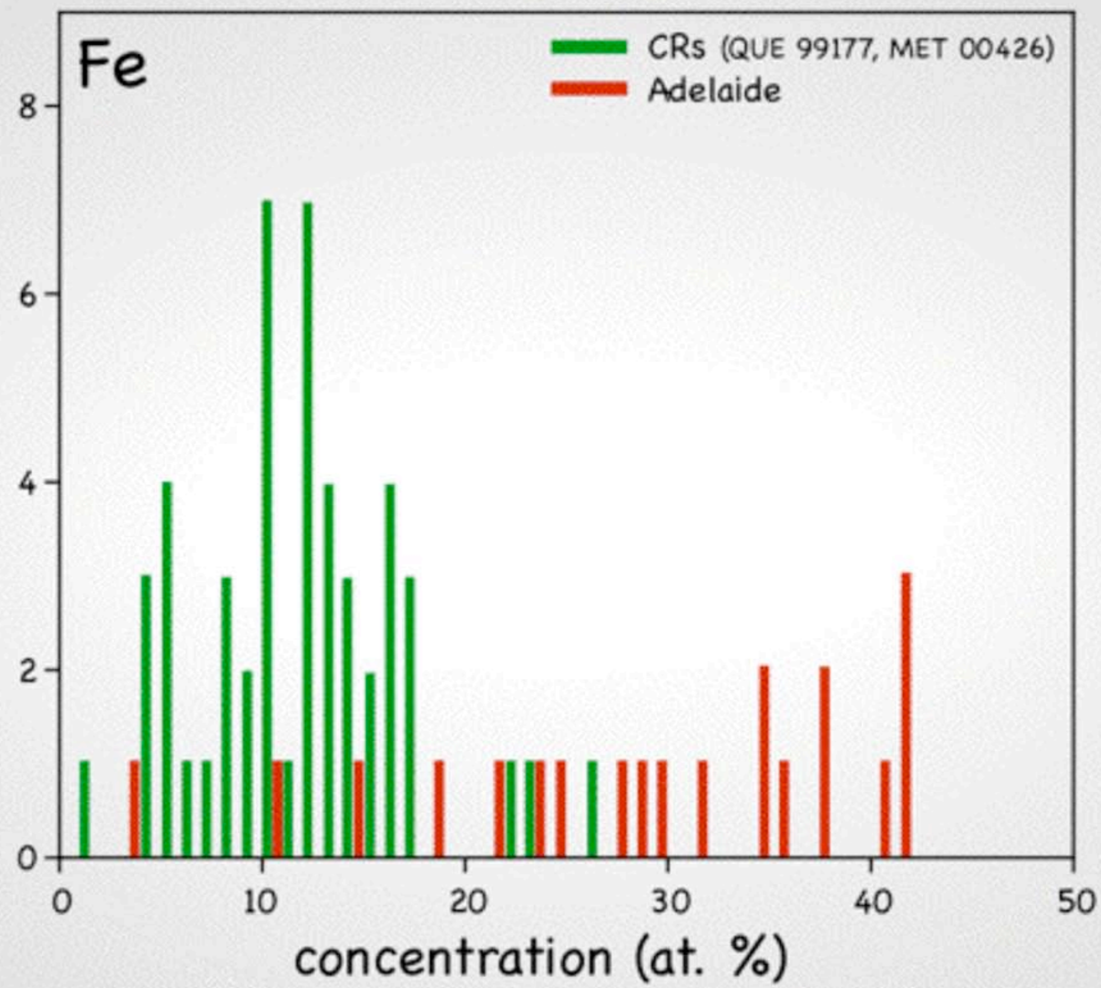

Fe
CRs (QUE 99177, MET 00426)
Adelaide
0
2
4
6
8
0
10
20
30
40
50
concentration (at. %)

Fe-rich Presolar Silicates

- Mg-rich silicates expected
  - equilibrium condensation theory: forsterite, enstatite (Lodders and Fegley, 1999; Ferrarotti and Gail, 2001)
  - astronomical observations: <10% Fe in crystalline silicates (Demyk et al., 2000); mg# >90 in amorphous grains (Min et al., 2007)
- origin of Fe enrichments seen in presolar silicates
  - primary signature vs secondary alteration?
- few Fe isotopic measurements: Acfer 094
  - two presolar silicates with non-solar $^{54}Fe/^{56}Fe$ (Mostefaoui & Hoppe, 2004; Vollmer et al., 2010)
  - grains with solar Fe: difficult measurements; large errors (Bose et al., 2010; Vollmer et al., 2010)

Graphite grains

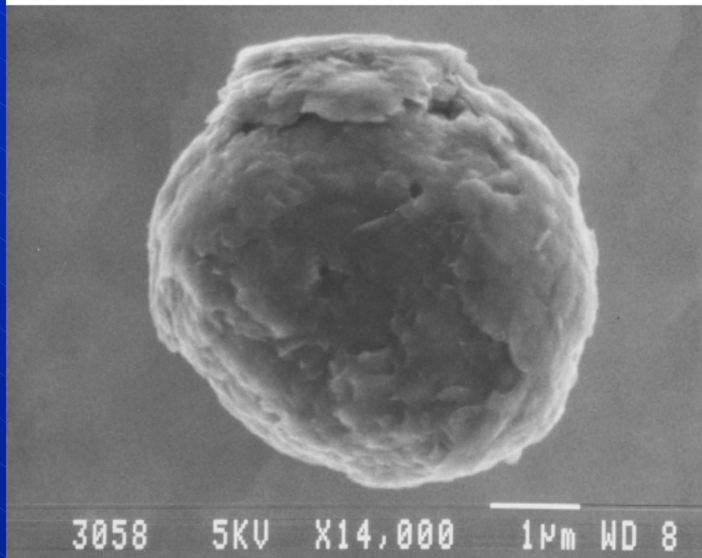

Onion

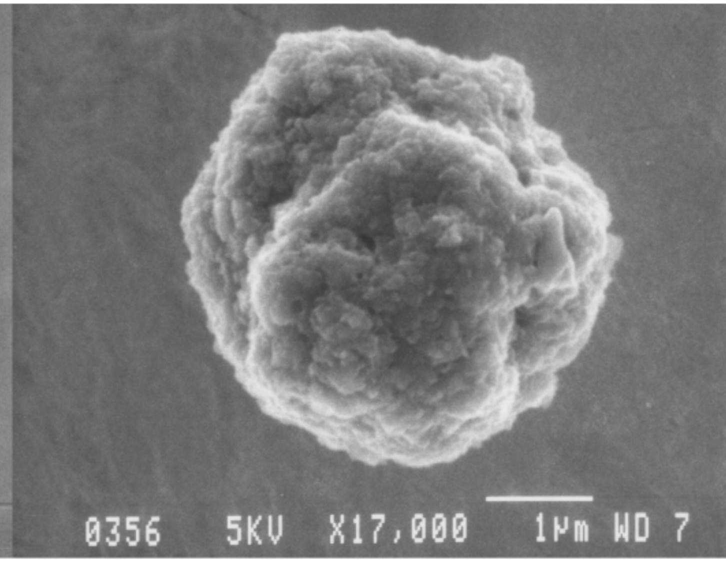

Cauliflower

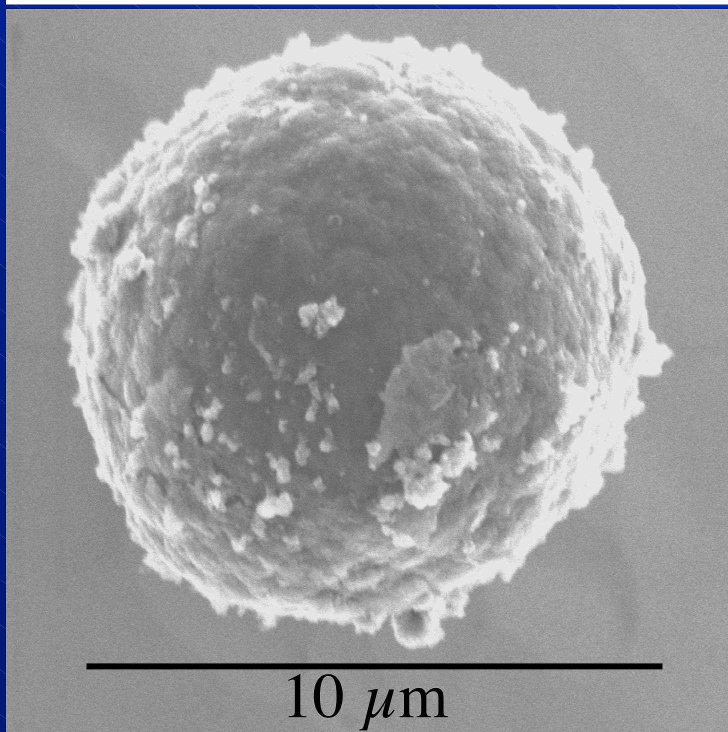

Graphite grains come in different vegetable types. Some of them are huge and provide a lot of material for detailed elemental and isotopic analysis.

Morphological types of presolar graphites

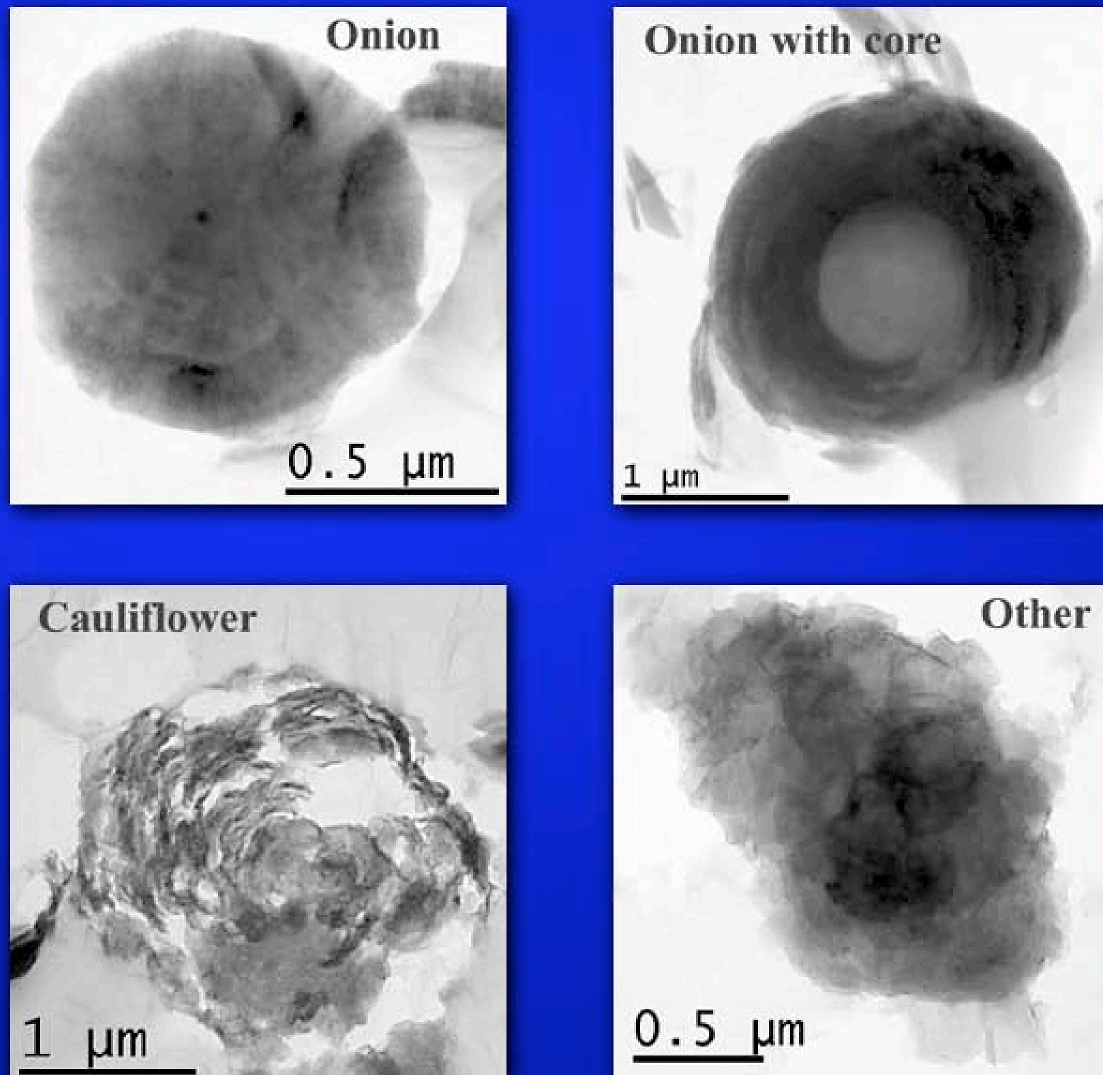

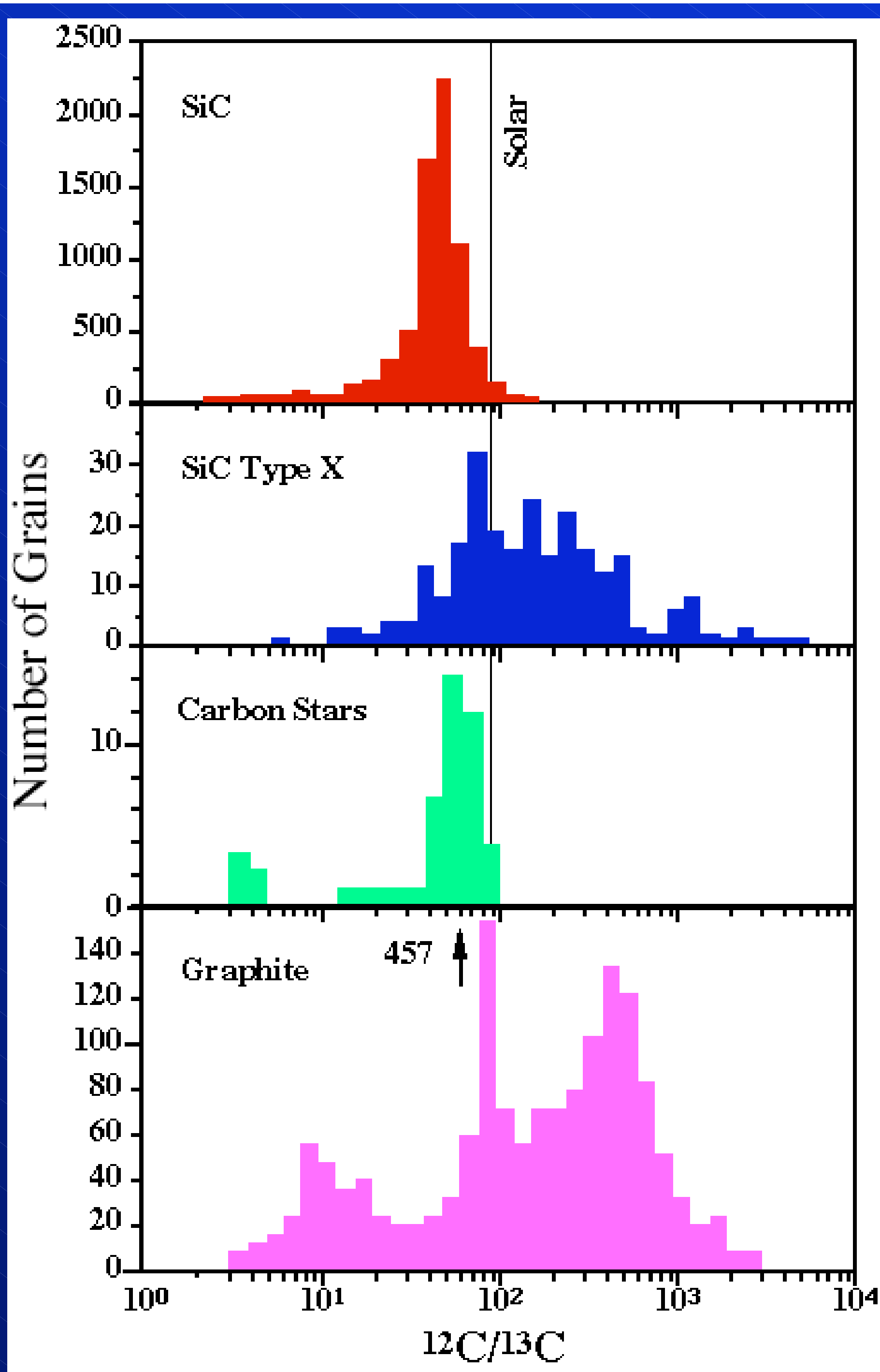

The distribution of carbon isotopic ratios in graphite grains is different from those of mainstream and SN SiC grains, indicating distinct stellar sources.

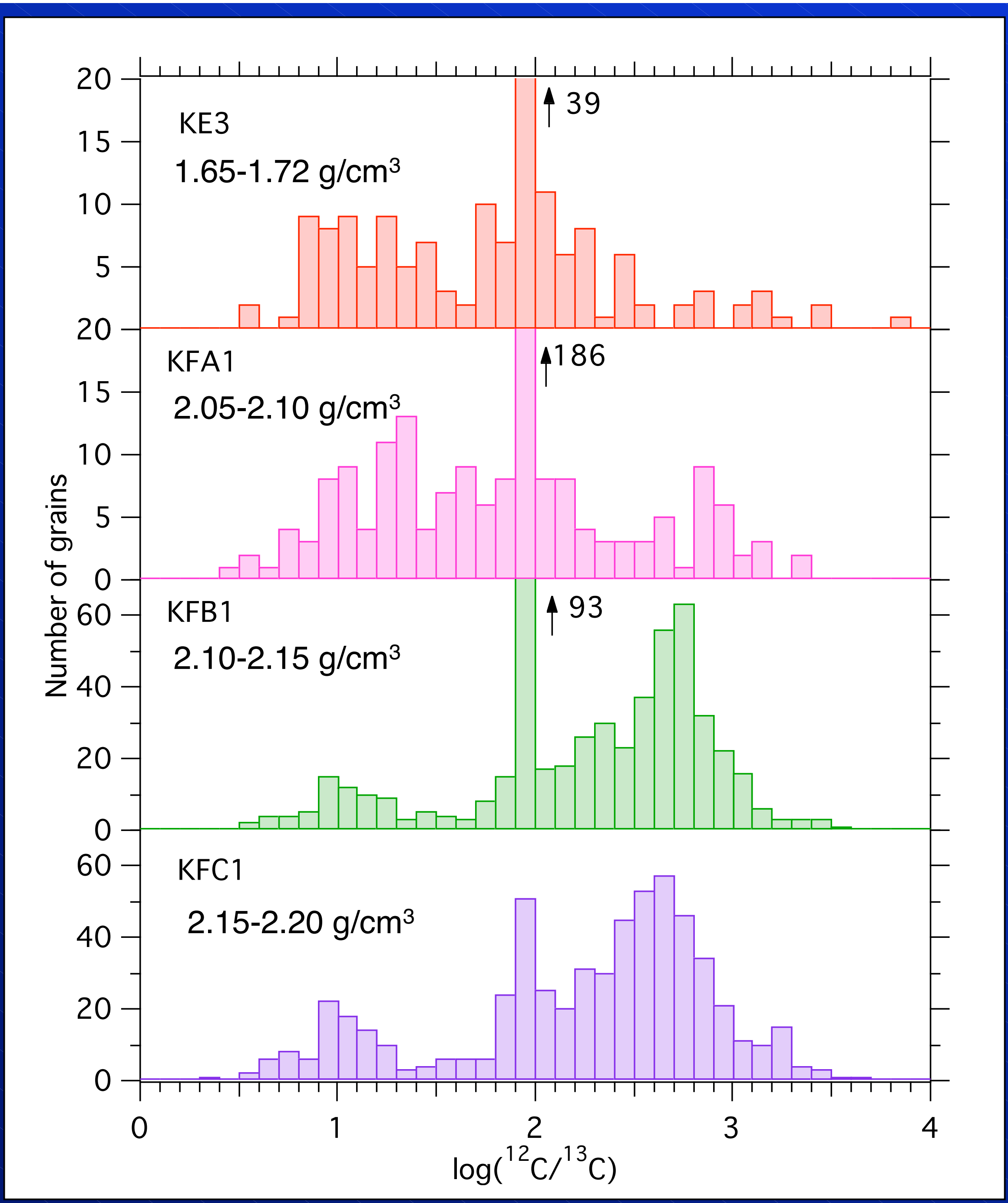

Murchison graphite grains

The isotopic compositions of graphite grains depend on their density.

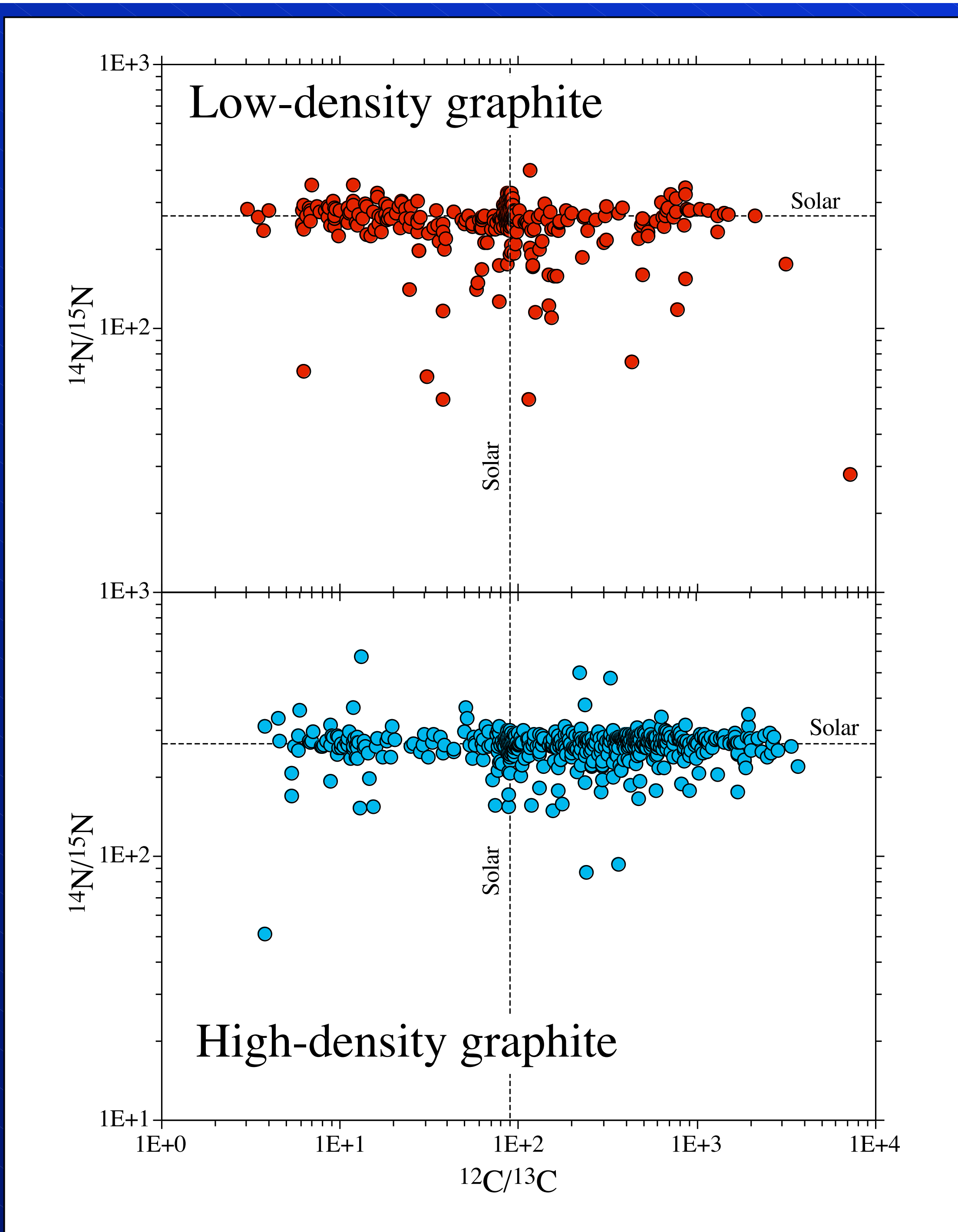

Low-density graphite grains show larger ^{15}N excesses than high-density grains. The normal N isotopic ratios in many grains cannot be indigenous but indicate isotopic equilibration.

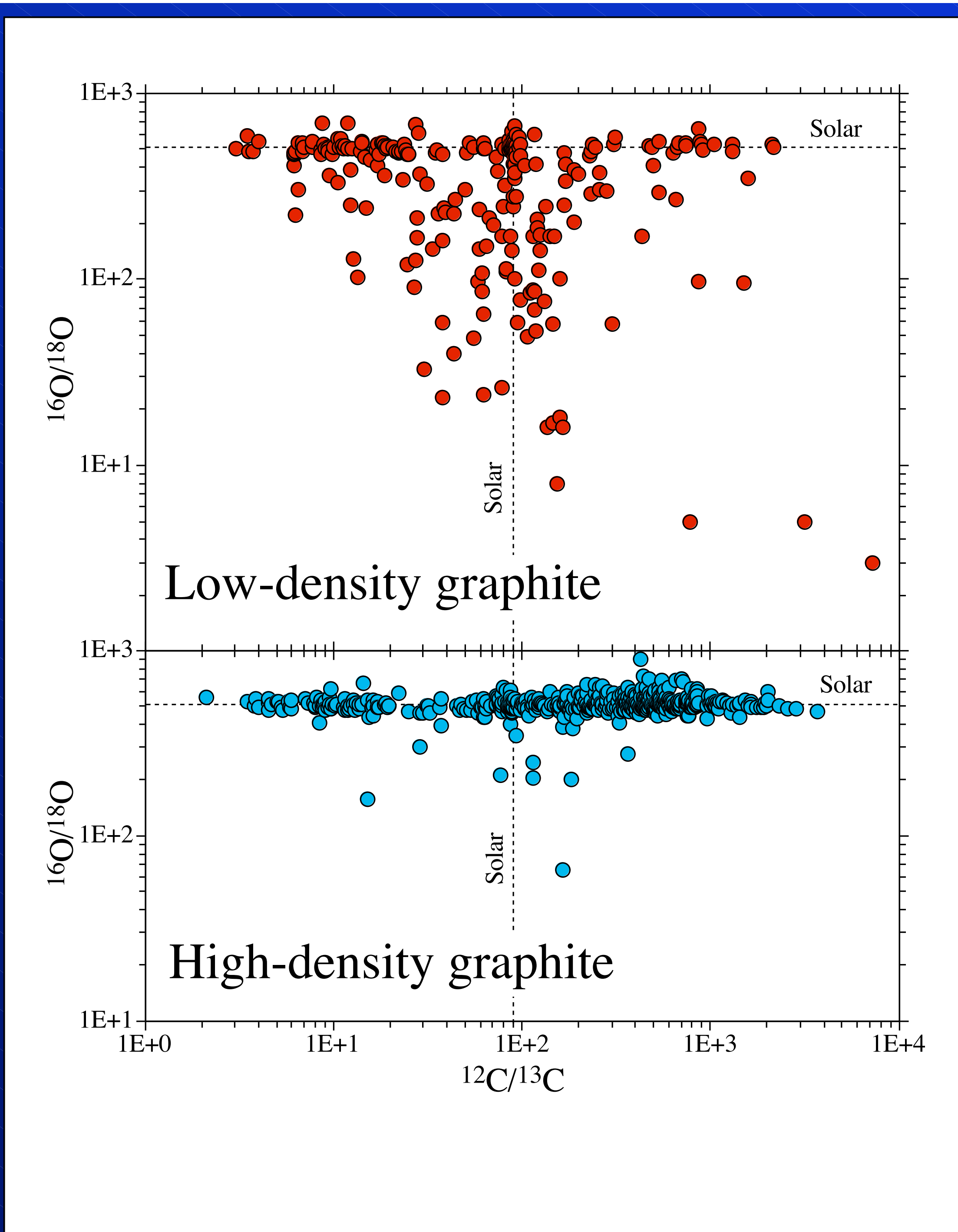

Low-density graphite grains show larger ^{18}O excesses than high-density grains. The normal O isotopic ratios in many grains cannot be indigenous but indicate isotopic equilibration.

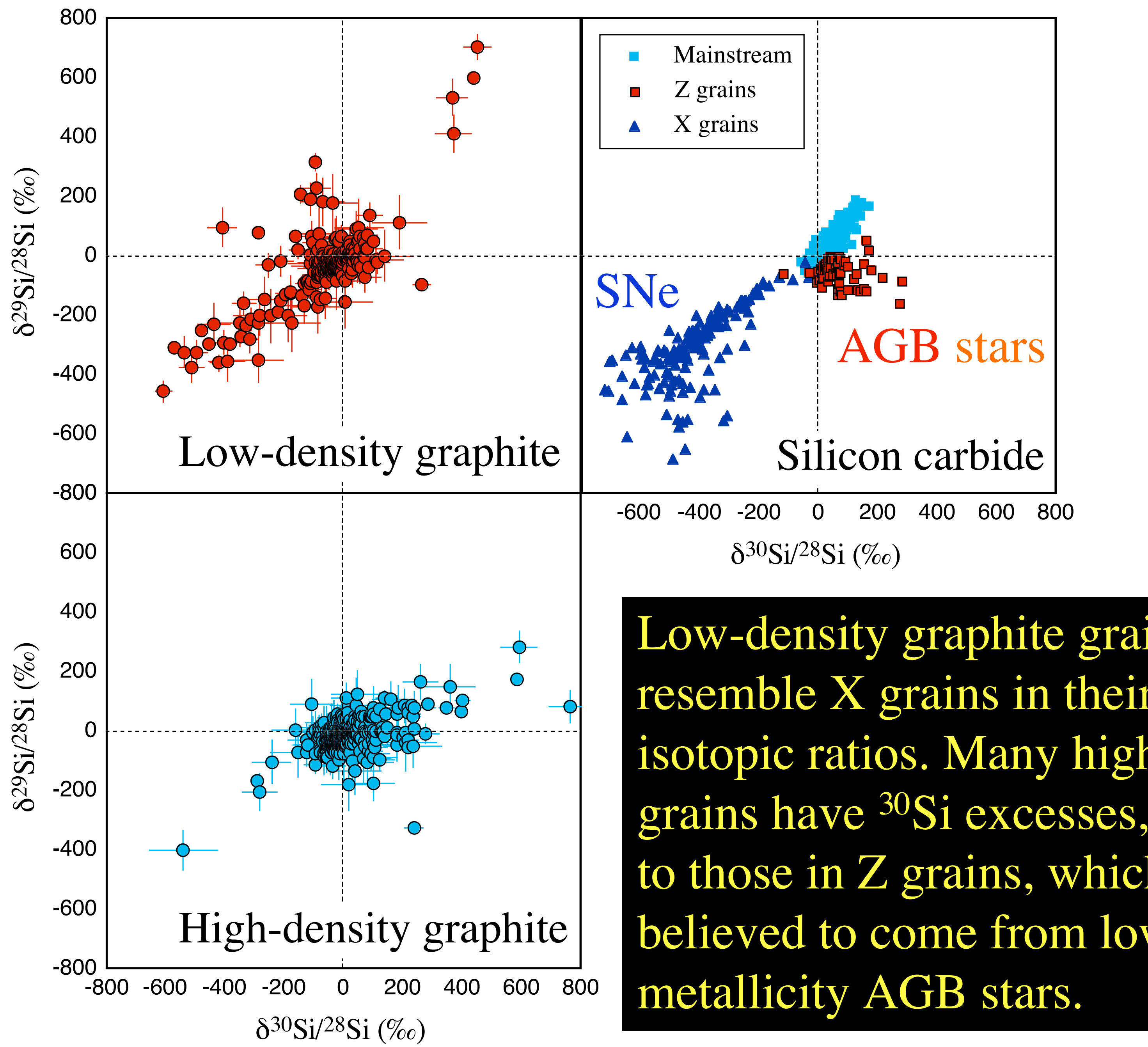

Low-density graphite grains resemble X grains in their Si isotopic ratios. Many high-density grains have ^{30}Si excesses, similar to those in Z grains, which are believed to come from low-metallicity AGB stars.

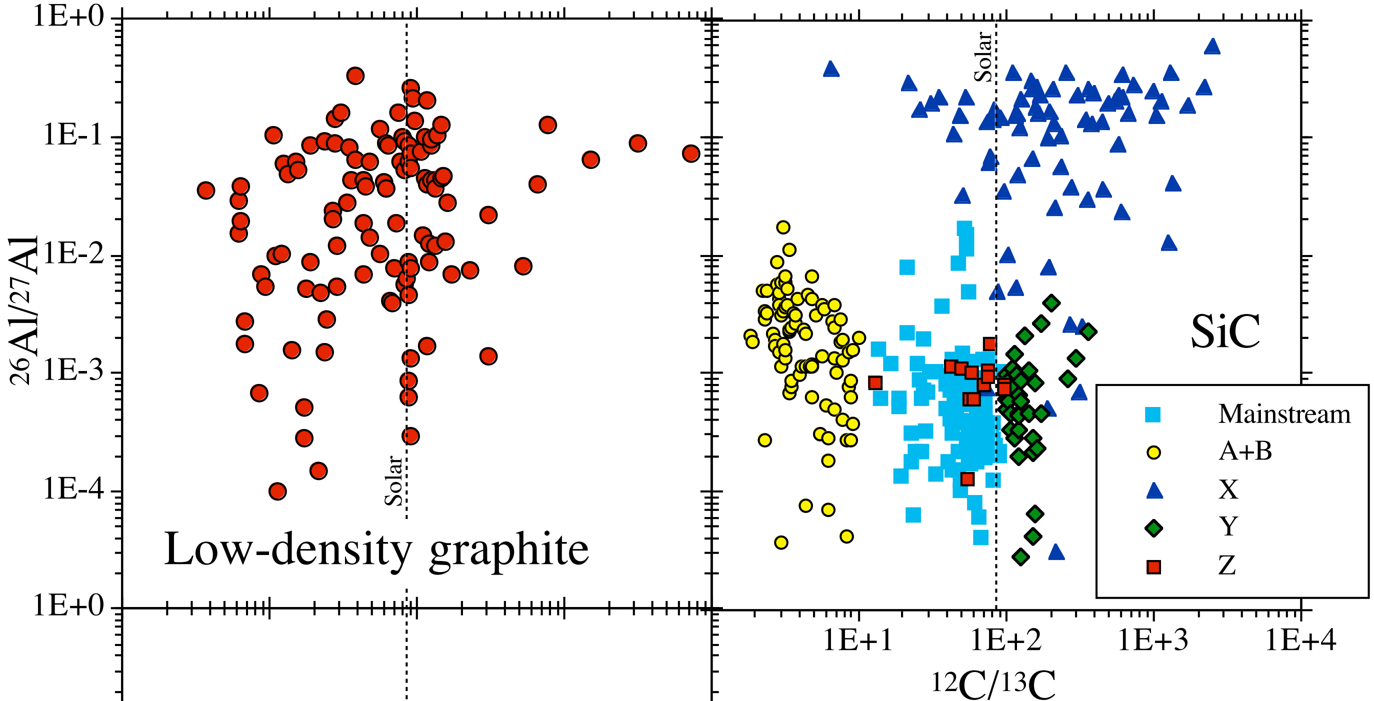

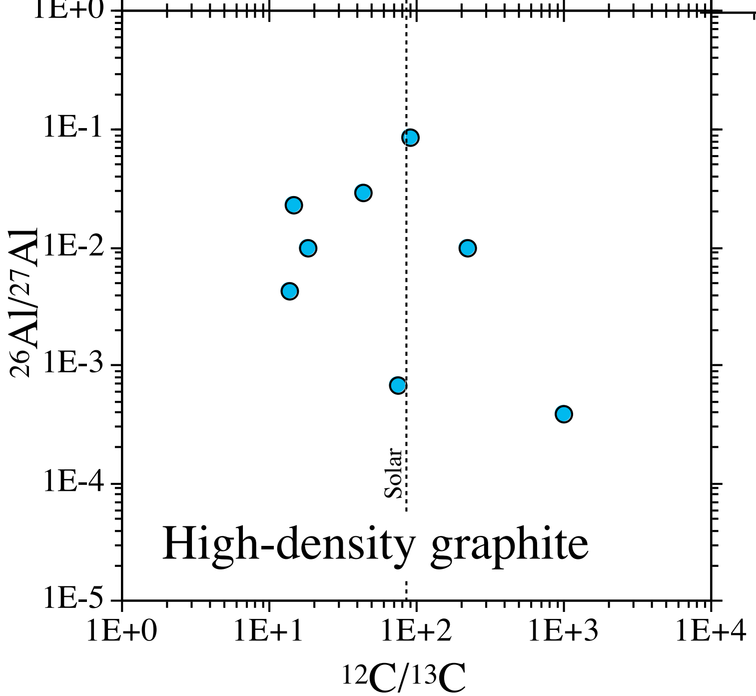

Low-density graphite grains resemble X grains also in their inferred $^{26}Al/^{27}Al$ ratios. There are only few measurements for high-density grains and grains with high ratios have been selected.

Low-density graphite grains are characterized by ^{15}N, ^{18}O, and ^{28}Si excesses (some have ^{29}Si and ^{30}Si excesses), and high inferred $^{26}Al/^{27}Al$ ratios. Some also show evidence for the initial presence of short-lived ^{41}Ca and ^{44}Ti and have ^{49}Ti excesses (possibly from the decay of short-lived ^{49}V). All these signatures indicate an origin in Type II SNe.

The most diagnostic isotopic signatures of high-density graphite grains are high $^{12}C/^{13}C$ ratios and large ^{30}Si excesses. They point to an origin in low-metallicity AGB stars.

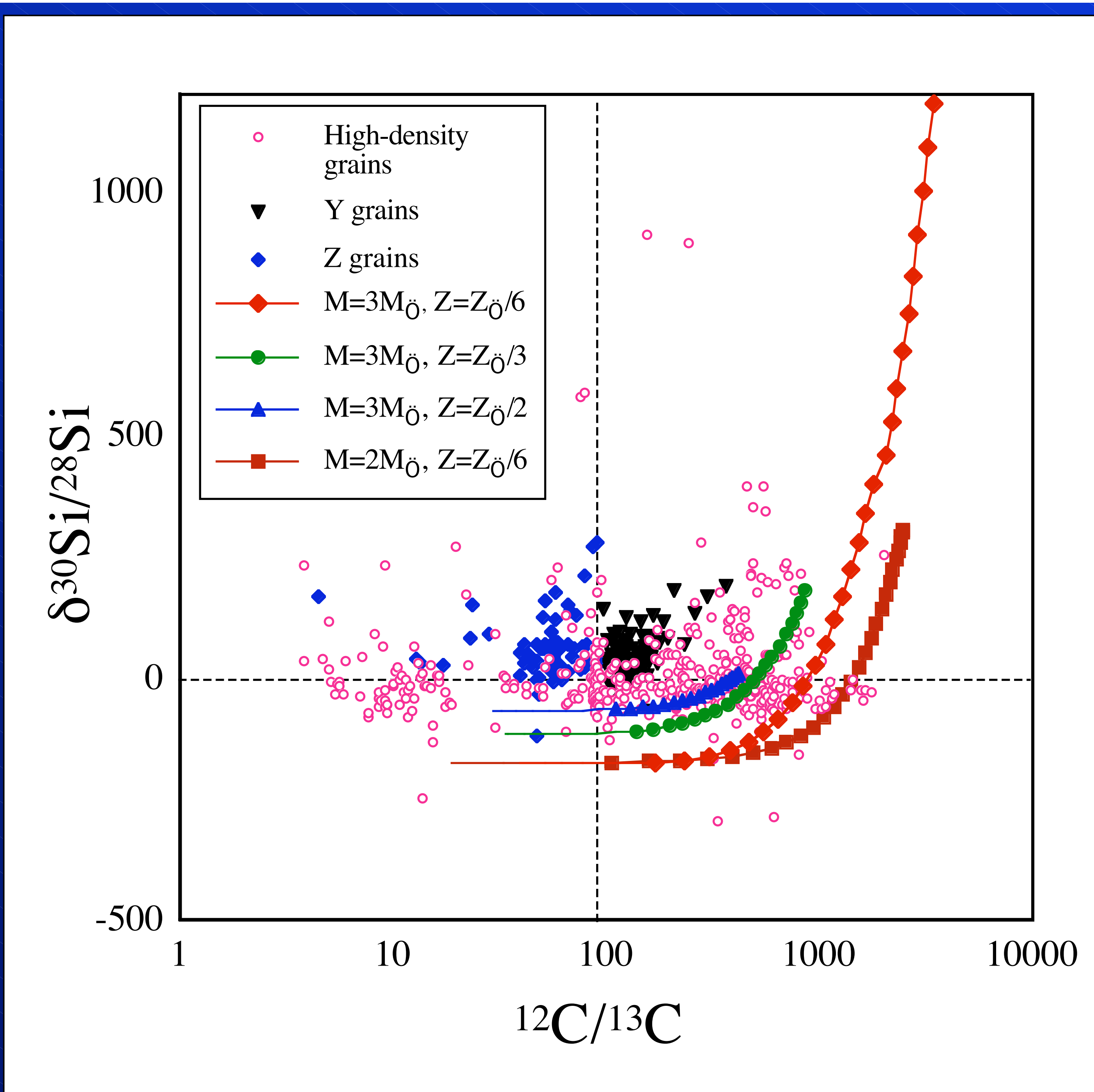

Models for low-metallicity stars give large ^{30}Si excesses, but the $^{12}C/^{13}C$ ratios of the models are too high for large ^{30}Si values.

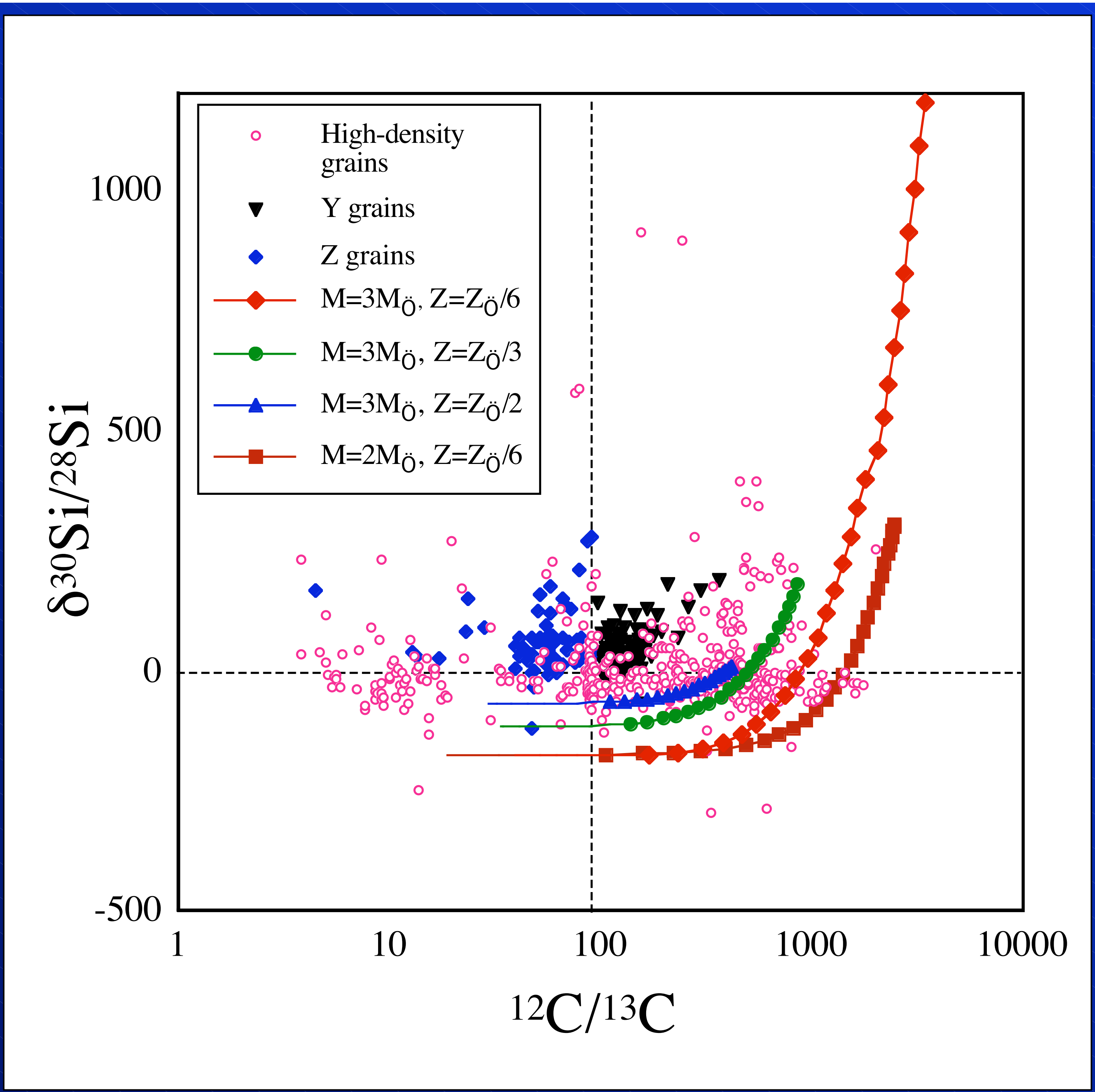

High $^{12}C/^{13}C$ ratios imply high C/O ratios, conditions favoring the formation of graphite instead of SiC.

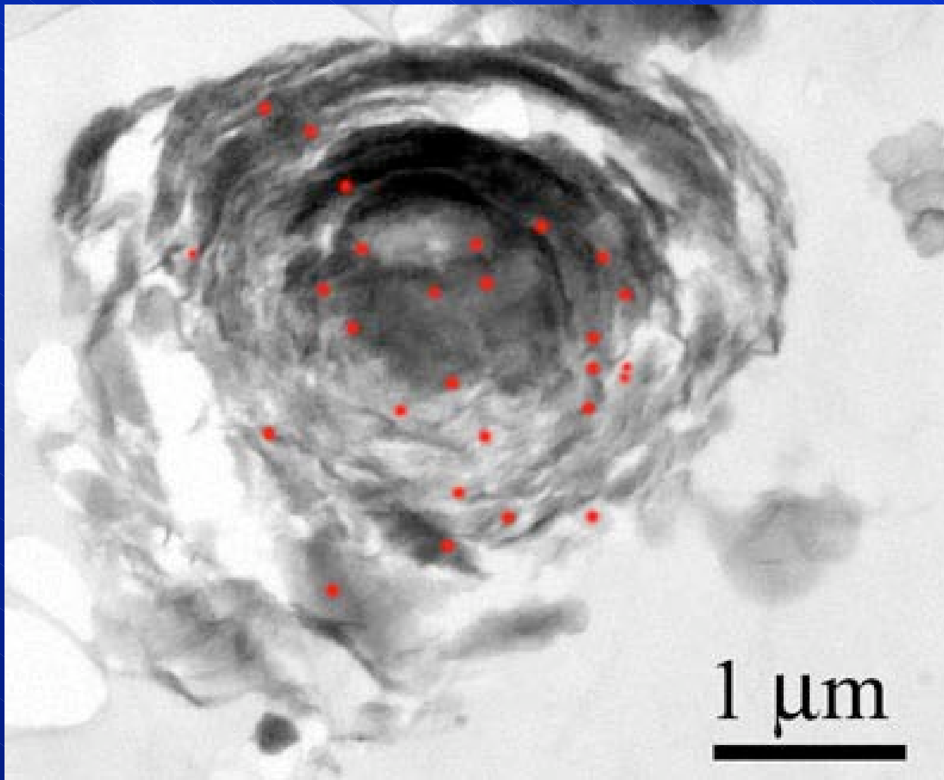

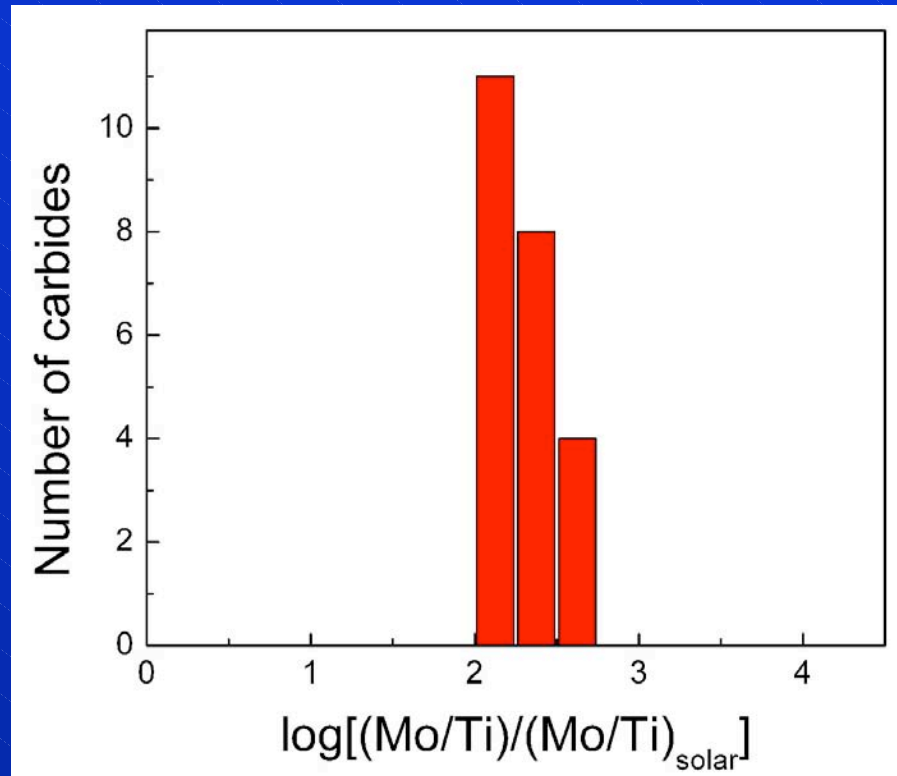

Courtesy of Kevin Croat

Evidence for an AGB star origin of high-density graphite grains comes from internal TiC grains that are highly enriched in the s-process elements Zr, Mo and Ru.